A role for rebinding in the prevalence of on-target side effects of clinically used antipsychotics

David Andrew Sykes, BSc (Hons) MA

Thesis submitted to the University of Nottingham for the degree of Doctor of Philosophy

January 2020

This thesis is entirely the candidates own work. The experiments described in this thesis were performed between 2015 and 2018 in the Cell Signalling Research Group, University of Nottingham. No part of this work has been submitted previously for a degree or any other qualification at any university.

Abstract

One explanation as to why atypical antipsychotic drugs (APDs e.g. clozapine) show reduced extrapyramidal side effects (EPS) involves their rapid dissociation from the dopamine D_2 receptor (D_2R). Their selective regional action in the brain permits an antipsychotic effect through inhibition of mesolimbic dopamine signalling but spares physiological dopamine neurotransmission in the striatum. This hypothesis is based largely on direct kinetic measurements using radiolabelled APDs and achieved under varied conditions and over many years. The alternative, 'serotonin-dopamine hypothesis' of atypicality suggests that antagonism at the 5-HT2A receptor and agonism at the 5-HT1A receptor may account for reduced EPS, due to increased nigrostriatal dopamine release. The strength of this hypothesis is currently limited to a consideration of the relative receptor affinities of APDs for the 5-HT2A and dopamine D_2R, and limited data exploring their 5-HT1A agonist effects.

To further explore these hypotheses, I developed a series of novel higher throughput time-resolved fluorescence resonance energy transfer (TR-FRET) binding assays to measure the kinetic properties of a series of clinically relevant typical and atypical APDs at the dopamine D_2R, the serotonin 5-HT2A and 5-HT1A receptors. Relative 5-HT1AR APD efficacy was estimated using a [^{35}S]-GTPγS assay and through the application of the operational model of agonism. These studies establish a novel mechanism of atypical APD action based on a restricted drug diffusion model, suggesting that for the majority of clinically used APDs association rate and not dissociation rate, better predicts the overall rate of dopamine D_2R reversal in the striatum.

For compounds with negligible affinity for 5-HT2A receptors, EPS is robustly predicted by a D_2R specific rebinding model that integrates D_2R association and dissociation rates, to calculate the net rate of reversal of receptor blockade (k_r). However, I show that for certain compounds (eg sertindole) a combination of high relative 5-HT2A occupancy and rapid dopamine D_2R dissociation (k_{off}), equates to a reduced propensity to cause EPS. Thus, optimizing the binding kinetics of compounds at both the serotonin 5-HT2A and the dopamine D_2R may result in the development of APDs with an improved on-target side-effect profile.

Publications arising from this thesis

Papers

Sykes DA, Jain P, Charlton SJ (2019). Investigating the Influence of Tracer Kinetics on Competition-Kinetic Association Binding Assays: Identifying the Optimal Conditions for Assessing the Kinetics of Low-Affinity Compounds. *Mol Pharmacol.* **96**(3):378-392.

Sykes DA, Lane JR, Szabo M, Capuano B, Javitch JA, Charlton SJ (2018). Reply to 'Antipsychotics with similar association kinetics at dopamine D2 receptors differ in extrapyramidal side-effects'. *Nat Commun*. **9**(1):3568.

Sykes DA, Charlton SJ (2018). Single Step Determination of Unlabeled Compound Kinetics Using a Competition Association Binding Method Employing Time-Resolved FRET. *Methods Mol Biol.* **1824**:177-194.

Sykes DA, Moore H, Stott L, Holliday N, Javitch JA, Lane JR, Charlton SJ (2017). Extrapyramidal side effects of antipsychotics are linked to their association kinetics at dopamine D2 receptors. *Nat Commun.* **8**(1):763.

Klein Herenbrink C, Sykes DA, Donthamsetti P, Canals M, Coudrat T, Shonberg J, Scammells PJ, Capuano B, Sexton PM, Charlton SJ, Javitch JA, Christopoulos A, Lane JR (2016). The role of kinetic context in apparent biased agonism at GPCRs. *Nat Commun.* **7**:10842.

Abstracts

Sykes D, Stott L, Holliday N, Lane RJ, Charlton S. A Role For Association Kinetics In Dictating The On-target Extrapyramidal Side Effects Of Antipsychotic Dopamine D2 Receptor Antagonists. 013P University of Leicester, UK. 6th Focused Meeting on Cell Signalling.

Comfort HM, Charlton SJ, Sykes DA. Functional and kinetic binding analysis of clinical antipsychotics at the 5HT1A receptor. 160P London, UK. Pharmacology 2017.

Sykes D, Charlton S. Investigating the influence of tracer kinetics on competition-kinetic association assays; identifying the optimal conditions for kinetic fragment screening. 240P London, UK. Pharmacology 2016.

Acknowledgements

I would like to thank my supervisors Professor's Steve Hill and Steven Charlton for their support, help and guidance over the past four years. I would also like to thank our external collaborators Rob lane, Carmen Klein-Herenbrink, John Javitch and Holly Moore who have all helped make this a more interesting and balanced piece of work. I should also thank my sponsor BMG Labtech (Robert Mount and Catherine Wark) and Cisbio Bioassays (Nicolas Pierre, Thomas Roux, Louise Affleck, Eric Trinquet and Francois Degorce), who have both provided invaluable support.

I would also like to thank Dr Nicholas Holliday for his supervision of the molecular biology experiments that enabled the creation of the various cell lines described in this thesis. Also, I would like to thank Lisa Stott, Jack Lochray and Hannah Comfort for their contributions and Palash Jain for creating alternative R models to help display the modelling and simulation data.

I would also like to thank the members of COMPARE and Cell Signalling, in particular Prof Dmitry Veprintsev, and my other friends and family who have supported me through this journey. Proof if it was needed that it's never too late to make that journey.

I will now thank and recognise some of the people who have shaped my career in Molecular Pharmacology through their mentorship; Christopher Bowmer (Leeds University), Richard Hoffman (MRC CORU Cambridge), Elaine Harper, Gillian Watt, Carol Austin, Nigel Shankley, and Sir James Black (James Black Foundation). Last but not least, I would like to thank Elisabeth Charbonneau for her continuous encouragement and patience in the pursuit of this 'dream'.

Abbreviations

APD	Antipsychotic drug
AGT	alkylguanine transferase
B_{max}	Maximal level of specific binding
BSA	Bovine serum albumin
CHO	Chinese hamster ovary
CNS	Central nervous system
cpm	Counts per minute
DMSO	Dimethyl sulphoxide
D-PBS	Dulbecco's phosphate buffered saline
D_2R	Dopamine D_2R
EC_{50}	Concentration at which half the maximum response occurs
EPS	Extrapyramidal side effects
FDA	Food and Drug Administration
FRET	Fluorescence resonance energy transfer
GPCR	G protein coupled receptor
HBSS	Hank's balanced salt solution
HEK	Human embryonic kidney
HTRF	Homogeneous time resolved fluorescence
IC_{50}	Concentration at which half maximal inhibition occurs
K_D	Equilibrium dissociation constant or concentration of a drug at which half the available receptors are occupied
k_{obs}	observed rate of association
k_{off}	dissociation rate constant
k_{on}	association rate constant
MARTAS	multi-acting receptor-targeted antipsychotics
OR	Odds ratio
PD	Pharmacodynamics
PET	Positron Emission Tomography
PK	Pharmacokinetics

RPM	Revolutions per minute
SMD	Standard mean difference
SPA	Scintillation proximity assays
SPECT	Single photon emission computed tomography
StaRs	Stabilised receptors
TR-FRET	Time-resolved fluorescence resonance energy transfer
WGA	Wheat germ agglutinin

Glossary of terms

Akathisia	A feeling of restlessness, making it hard to sit down or hold still. Symptoms include tapping your fingers, rocking, and crossing and uncrossing your legs.
Atypical antipsychotics	Also known as second generation antipsychotics. Compounds that has clinical antipsychotic efficacy while producing minimal catalepsy (the behavioural equivalent of extrapyramidal side effects (EPS)) in animal models.
Basal ganglia	Primarily comprising the striatum (dorsal and ventral) plus other structures involved in movement including the substantia nigra.
Dystonia	Involuntarily muscle contraction and contortion, leading to painful positions or movements.
Extrapyramidal side effects	Physical symptoms, associated with improper dosing of or unusual reactions to neuroleptic (antipsychotic) medications including parkinsonism, akathisia, tardive dyskinesia and dystonia.
Hyperprolactinaemia	The presence of abnormally high levels of prolactin in the blood. Prolactin is a peptide hormone produced by the anterior pituitary gland.
Law of mass action	The principle that the rate of a chemical reaction is proportional to the concentrations of the reacting substances.
Meta-analysis	A statistical analysis that combines the results of multiple scientific studies.
Micro-pharmacokinetics	Refers to the study of local drug concentrations in membrane microdomains eg. lipid rafts or within specific membrane structures such as the synapse.
Neuroleptic	The original term used to describe antipsychotics, describing tranquilising action or tendency to reduce nerve function.
Odds ratio	A statistic that quantifies the strength of association between two events eg. EPS OR is

	defined as the ratio of the odds of EPS in the presence or absence of drug.
Parkinsonism	The same symptoms as someone with Parkinson's disease, but caused by medication, not by the disease. These symptoms may include tremor, slower thought processes, slower movements, rigid muscles, difficulty speaking and facial stiffness.
Positron emission tomography	Whole body imaging technique using radioactive tracers.
Schizophrenia	Derived from the Greek 'schizo' (splitting) and 'phren' (mind) with the term first coined by Eugen Bleuler in 1908.
Standardized mean difference	A summary statistic in meta-analysis used when studies assess the same outcome but measure it in a variety of ways. Sandardization to a uniform scale allows results to be combined and compared.
Tardive dyskinesia	Uncontrollable facial movements eg. sucking, chewing, lip smacking, tongue protrusion or blinking repeatedly.
Typical antipsychotics	A class of antipsychotic drugs first developed in the 1950s and used to treat psychosis (in particular, schizophrenia). Also known as first generation antipsychotics their use is characterised by EPS effects eg. Parkinson-like side effects.

Contents

Abstract ... iii
Publications arising from this thesis ... iv
Acknowledgements ... vi
Chapter 1 - General introduction ... 1
1.1 Schizophrenia, the discovery of antipsychotics and the role of the dopamine receptor. ... 2
1.2 Dopamine and dopamine receptors ... 5
1.3 Equilibrium affinity and drug-receptor binding kinetics ... 6
1.4 Understanding receptor kinetics at the molecular level ... 7
1.5 Understanding drug-receptor association and its role in pharmacodynamics ... 8
1.6 Drug-receptor residence time and toxicity ... 9
1.7 A role for kinetics in the on target side effects of antipsychotics ... 10
1.8 How are the kinetics of ADPs traditionally measured? ... 11
1.9 Introducing new chemical starting points for the development of APDs – What are the problems? ... 19
1.10 Aims ... 19
Chapter 2 - Materials and Methods ... 21
2.1 Materials ... 22
2.1.1 Cell culture reagents ... 22
2.1.2 Ligand binding assays ... 22
2.2 Methods ... 23
2.2.1 Cell culture ... 23
2.2.2 Stable transfections ... 24
2.2.3 Dilution Cloning ... 24
2.2.4 Transient transfections ... 25
2.2.5 Terbium labeling of SNAP-tagged cells and membrane preparation ... 26
2.2.6 Determination of tracer binding kinetics and equilibrium affinity ... 26
2.2.7 Competition binding kinetics ... 27
2.2.8 Signal detection and data analysis ... 28
2.2.9 Modelling drug-receptor re-binding ... 33
2.2.10 Comparing binding kinetics and clinical side effect profile ... 34

Chapter 3 - Establishing a dopamine D_2 receptor-specific FRET-based competition association binding assay 35
3.1 Introduction 36
3.2 Materials and Methods 39
3.2.1 Materials 39
3.2.2 Cell culture 39
3.2.3 Terbium labelling of SNAP-tagged D_{2L} and D_{2S} cells 39
3.2.4 Whole cell-based D_2R fluorescent ligand-binding assays and BMG Labtech PHERAstar FS performance tests 40
3.2.5 Membrane-based $D_{2L}R$ fluorescent ligands binding assays 40
3.2.6 Competition binding kinetics 41
3.2.7 Data analysis and signal detection 42
3.2.8 Modelling of tracer competition curves 43
3.3 Results 45
3.3.1 Establishing a dopamine D_2 receptor competition association binding assay 45
3.3.2 Whole cells versus membranes 50
3.3.3 Characterisation of dopamine-d2 binding in HBSS 52
3.3.4 Characterisation of clozapine-Cy5 binding in HBSS 56
3.3.5 Characterisation of PPHT-red binding in a HEPES-based buffer (HEPES-salt) 60
3.3.6 Characterisation of Spiperone-d2 binding in a HEPES based buffer (HEPES-salt) 67
3.3.7 Experimental and modelled IC_{50} curves 76
3.3.8 Residual plots as a means of assessing competition-association fits 80
3.3.9 Determination of kinetics of D_2R specific antagonists and agonists ..82
3.4 Discussion 91
3.4.1 Establishing a dopamine D_2 receptor competition association binding assay 91
3.4.2 Whole cells versus membranes 92
3.4.3 Establishing a D_{2L} membrane-based competition association assay 92
3.4.4 The influence of the chemical and physical properties of a compound on drug-receptor binding parameters 96
3.5 Conclusions 103
Chapter 4 - Investigating the influence of tracer kinetics on competition-kinetic association binding assays; identifying the optimal conditions for assessing the kinetics of low-affinity compounds. 124

4.1 Introduction 125
4.2 Materials and Methods 128
4.2.1 Determining the kinetics of the tracer for use in competition kinetic binding studies 128
4.2.2 Determining the suitability of the tracer for competition kinetic binding studies 131
4.2.3 Monte Carlo simulation data analysis 132
4.2.4 Fluorescent ligand binding assays 133
4.2.5 Data analysis and signal detection 135
4.3 Results 136
4.3.1 Monte Carlo simulations 136
4.3.2 Experimental validation of the Monte Carlo simulation approach 162
4.4 Discussion 167
4.5 Conclusions 171
Chapter 5 - Extrapyramidal side effects of antipsychotics are linked to their association kinetics at the dopamine D_2 receptor 173
5.1 Introduction 174
5.1.1 Antipsychotic drug action and classification 174
5.1.2 Two theories of atypicality the 'fast off' hypothesis and the multi-receptor hypothesis 174
5.1.3 The kinetic basis of atypicality and typicality 176
5.1.4 Challenges to the kinetic hypothesis 177
5.2 Materials and methods 179
5.2.1 Materials 179
5.2.2 Cell culture 179
5.2.3 Terbium labelling of SNAP-tagged D_{2L} cells and membrane preparation 179
5.2.4 [^{3}H]-Spiperone saturation binding assays. 179
5.2.5 Fluorescent ligand-binding assays 180
5.2.6 Signal detection and data analysis. 181
5.2.7 Modelling striatal dopamine D_2R re-binding 182
5.2.8 Relationship between binding kinetics and clinical side effect profile 182
5.3 Results 183
5.3.1 Characterisation of PPHT-red binding from saturation analysis 183
5.3.2 Characterisation of unlabelled D_2R ligands 185

5.3.3 Relationship between dopamine D_2 antagonist kinetics and atypical and typical classification 192
5.3.4 Relationship between Kinetics and Clinical measures of Dopamine D_2 Antagonist Reversibility 194
5.3.5 Modelling the effects of rebinding on APD dissociation rates 199
5.3.6 The relationship between relative drug rebinding and clinical effects 202
5.4 Discussion 204
5.5 Conclusion 211
Chapter 6 - Investigating a role for serotonin 5-HT2A and 5-HT1A receptors in the reduced incidence of EPS of clinically used antipsychotics; the influence of differential receptor target coverage 212
6.1 Introduction 213
6.1.1 Schizophrenia and on-target side effects 'The Dopamine Hypothesis' 213
6.1.2 5-HT2A and 5-HT1A receptors anatomical location and physiology 214
6.1.3 The 'serotonergic-dopamine' theory of atypicality a historical perspective. 215
6.1.4 Rapid dissociation hypothesis and the phenomenon of rebinding 216
6.1.5 Role of 5-HT1A in psychosis/EPS 217
6.2 Materials and Methods 219
6.2.1 Materials 219
6.2.2 Cell culture 219
6.2.3 Terbium labelling of SNAP-tagged cells 219
6.2.4 Fluorescent ligand-binding assays 220
6.2.5 Signal detection and data analysis. 221
6.2.6 5-HT1A [^{35}S]-GTP□S binding 222
6.2.7 Operational modelling and clinical effect 223
6.2.8 5-HT2A calcium assay 224
6.2.9 Rebinding at Dopamine D2 and serotonin 5-HT2A receptors as a cumulative measurement of drug effect 225
6.2.10 Comparing binding kinetics and clinical side effect profile. 225
6.2.11 Structure-property relationships 225
6.3 Results 226
6.3.1 Characterization of 4F4PP oxalate-red binding to the human 5-HT2A receptor 226

6.3.2 Characterization of unlabeled APDs binding to the human 5-HT2A receptor 230
6.3.3 Characterization of NAN190-red binding to the human 5-HT1A receptor 239
6.3.4 Assessing antipsychotic 5-HT1A agonism and its potential to reduce EPS in the clinic 251
6.3.5 Functional consequences of slow dissociation from 5-HT2A receptors 255
6.3.6 Modelling the relative effects of 5-HT2A and dopamine D_2 receptor rebinding 257
6.4 Discussion 262
6.5 Conclusions 272
Chapter 7 - Discussion 274
7.1 Drug target occupancy and the role of rebinding 276
7.2 Formulating competition kinetic binding assays; the unappreciated role of tracer kinetics in successful assay development. 278
7.3 Comparing equilibrium and kinetic binding data with historical data on APDs 282
7.4 Historical kinetic data and the relevance of measured dissociation (k_{off}) rates 285
7.5 Affinity and the contention that association rates (k_{on}) are constant 289
7.6 Role of the 5-HT2A receptor in the reduced incidence of side effects 298
7.7 Functional data supporting the dopamine D_2R kinetic measurements 301
7.8 Cinical data supporting the rebinding hypothesis 304
7.9 Limbic selectivity is rebinding the driver 307
7.10 A role for the 5-HT2C receptor in reduced EPS 311
7.11 Does k_{off} or k_r play a role in limbic selectivity? 313
7.12 PET/SPECT studies exploring clinical D_2R occupancy and EPS 316
7.13 Role of the 5-HT1A receptor in the reduced incidence of side effects 320
7.14 Relevance to the classification of antipsychotics 321
7.15 SKR of dopamine D_2 specific ligands 323
7.16 Conclusions 333
Chapter 8 - Appendices and References 336
8.1 Appendix I – Supplementary data 337
8.2 References 359

Chapter 1 - General introduction

1.1 Schizophrenia, the discovery of antipsychotics and the role of the dopamine receptor.

Schizophrenia is a long-term mental disorder involving a breakdown in the relation between thoughts, emotions, and behaviour. This leads to faulty perception, actions, and feelings, culminating in a breakdown in personal relationships and a withdrawal from reality into fantasy and delusion. The first effective treatment (and first antipsychotic drug (APD)) identified for this disorder was chlorpromazine, discovered in 1951 (López-Muñoz et al., 2005; Ban 2007). Its administration to patients confined to psychiatric hospitals caused a dramatic reduction in the number of patients who required hospitalisation, making it the first real breakthrough in the treatment and understanding of this socially debilitating and chronic disease (López-Muñoz et al., 2005).

Another decade passed before a plausible mechanism of action for chlorpromazine was put forward by Carlsson and Lindqvist who suggested that it may be acting by blocking dopamine D_2 receptors in the brain (Carlsson and Lindqvist 1963). Although efficacious chlorpromazines use is characterised by an unacceptable level of toxicity, which manifests itself in movement disorders some of which remain permanent even when treatment is stopped (Wolf et al., 1993). As such blockade of dopamine D_2 receptor (D_2R) by antipsychotics is on the one hand necessary for their antipsychotic action but if the levels of D_2 receptor occupancy achieved exceed a certain level then the on-target side effects of individual drug treatments predominate (Kapur et al., 2000a).

The neurobiology of schizophrenia is complex and is still not entirely understood. The dopamine hypothesis of schizophrenia implicates an excess of dopamine neurotransmission in the mesolimbic areas and a hypoactivity of dopamine neurotransmission in the nigrostriatal and mesocortical areas of the brain (see Figure 1.1). According to this hypothesis excess dopamine neurotransmission in the mesolimbic areas leads to the positive symptoms of schizophrenia (eg. hallucinations), whilst hypoactivity of dopamine neurotransmission in the mesocortical areas is associated with the negative symptoms of schizophrenia (eg. apathy and poverty of speech). The therapeutic activity of conventional

antipsychotics has been largely correlated with their ability to block dopaminergic D_2R in the mesolimbic system (Davis et al., 1991; Grace et al., 1997; Pilowsky et al., 1997). Recently this hypothesis has been challenged and it has been suggested that dorsal striatal regions may in fact play a central role in the pathophysiology of this disorder (Kegeles et al., 2010; McCutcheon et al., 2019). What is not in any doubt is the finding that blockade of D_2R in the striatum and tuberoinfudibular dopamine tracts leading to the adverse on-target side effects, including extrapyramidal side effects (EPS) and elevated circulating prolactin levels, respectively (Markowitz et al., 1999).

APDs generally fall into one of three classes, so called first generation or typical antipsychotics drugs, the classic example being the highly D_2R selective haloperidol and second generation or atypical antipsychotics and finally third generation partial agonists typified by aripiprazole. The classic definition of atypicality describes a compound that has clinical antipsychotic efficacy while producing minimal catalepsy (the behavioural equivalent of EPS) in animal models, the prototypic atypical antipsychotic being clozapine. This strict definition has gradually evolved and an atypical agent is now generally defined as one that (1) has a decreased or absent propensity to produce EPS or other movement disorders at doses producing antipsychotic effects, (2) does not or only minimally elevates prolactin concentrations, and (3) significantly reduces both positive and negative symptoms of schizophrenia (Markowitz et al., 1999).

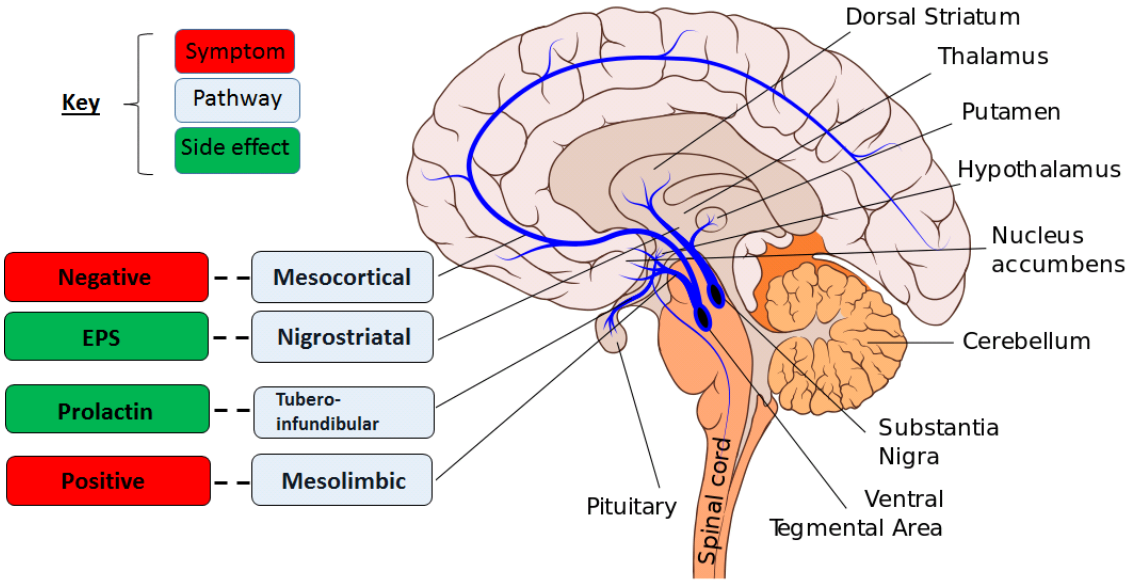


Figure 1.2. The four main dopaminergic pathways of the human brain: These include the mesocortical pathway, involved in the negative symptoms of schizophrenia and which connects the ventral tegmental area (VTA) with the frontal cortex. The mesolimbic pathway, involved in the positive symptoms of schizophrenia connects the VTA with the nucleus accumbens. The nigrostriatal pathway, involved in the prevalence of EPS, connects the substantia nigra with the dorsal striatum and lastly the tuberoinfundibular pathway, involved in prolactin secretion connects the hypothalamus with the pituitary. Figure adapted from the following web link:

https://commons.wikimedia.org/wiki/File:Dopaminergic_pathways.svg

User:Slashme; Patrick J. Lynch; User:Fvasconcellos [CC BY-SA 4.0 (https://creativecommons.org/licenses/by-sa/4.0)]

1.2 Dopamine and dopamine receptors

Dopamine is a catecholamine neurotransmitter implicated in a number of central nervous system (CNS) disorders, including schizophrenia, Parkinson's disease, attention deficit hyperactivity and addiction disorders (Perez de la Mora et al., 2019). Dopamine controls a variety of physiological functions in the brain and periphery mediated by two major subclasses of dopamine GPCR which is based on their signalling preference: the dopamine D1 class which includes D_1R and D_5R and activates G protein Gαs/olf, and the D2 class which includes D_2R, D_3R, and D_4Rs, and couples to the inhibitory G protein Gαi/o signalling pathway. Activation Gαi/o-mediated signalling inhibiting adenylyl cyclase, cyclic adenosine monophosphate (cAMP) production and protein kinase A.

Perhaps the most well studied of these five receptors is the dopamine D_2R of which there are two isoforms, the short form (D_{2S}) and the long form (D_{2L}, 29 amino acid longer), generated by alternative splicing of the same gene (Dal Toso et al., 1989). These two D_2R isoforms have been shown to possess different affinities for inhibitory G-proteins (Montmayeur et al., 1993; Guiramand et al., 1995) and modest differences in affinity (<3 fold) for certain D_2R specific antagonists and agonists (Castro and Strange 1993; Gardner and Strange 1998; Seeman 2013). For example, the atypical antipsychotic clozapine displays a 2-fold higher affinity for the D_{2S} form of the receptor when measured in the presence of sodium ions (Malmberg et al., 1993). Differences in dopamine D_2 isoform receptor coupling suggest that the 29 amino acid insertion in the third cytoplasmic loop of the $D_{2L}R$ plays a key role in the interaction of the receptor with both intracellular effectors (Montmayeur et al., 1993; Senogles 1994; Liu et al., 1996; Senogles 2000; Kim et al., 2004), and receptor trafficking machinery (Kubale et al., 2006), and therefore mediates their differential signalling properties. These two receptor isoforms are also thought to show varied expression in different brain regions eg. $D_{2L}R$ are found mainly in the neurons of the striatum, whilst the D_{2S} isoform predominates in the midbrain and hypothalamus (Khan et al., 1998). Within synaptic structures, the $D_{2S}R$ is thought to exist mainly as a presynaptic autoreceptor, being localized in dopaminergic cell bodies and axons, whilst the $D_{2L}R$ is thought to be located largely postsynaptically (Khan et al., 1998). However, this distinction is not absolute since the long form of

the receptor has itself been shown to act as an effective autoreceptor in mice (Wang et al., 2000). Indeed, the role of each D_2R receptor isoform in the pathogenesis of schizophrenia is currently unknown. Regardless, antipsychotic drugs (APDs) acting at these two receptor isoforms should readily block dopamine stimulated D_2R effector coupling events, and in doing so fine-tune the expression of dopamine-associated behaviours and functions, including so called positive/negative symptoms and on-target side effects. Given their physiological and pharmacological relevance resolving the determinants of drug binding to dopamine D_2R would be extremely valuable both from the perspective of understanding of drug-receptor function but also for the design of new therapeutics targeting these receptors.

1.3 Equilibrium affinity and drug-receptor binding kinetics

The equilibrium dissociation constant (K_d), i.e. the concentration of drug required to occupy 50% of available receptors, is an important pharmacological parameter and is a measure of the 'affinity' of a drug for its receptor and is traditionally considered fundamental to understanding structure/function relationships enabling more efficient drug design. In chemistry, thermodynamic affinity is the driving force of chemical reactions, measured by a change in Gibbs free energy (ΔG) (Holdgate and Ward 2005). Put in simpler terms affinity is the degree to which two or more species are attracted and is dictated by their chemical composition and structure. Intermolecular interactions are electrostatic, and of a specific chemical nature, with different contributions to the overall binding affinity of drugs for their receptors. For example, hydrogen bonds form weak interactions the result of an attraction between a proton in one molecule and an electronegative atom in the other. Van der Waals forces are also weak attractive electrostatic forces between instantaneous and permanent dipoles. Additional types of electrostatic interaction include ionic pairs, the interaction between oppositely charged groups. Hydrophobic interactions also contribute directly to affinity existing as a combination of Van der Waals interactions between nonpolar groups and hydrogen bonds between surrounding water molecules (Claveria-Gimeno et al., 2017).

The proposal that the rate of a chemical reaction is directly proportional to the product of the activities or concentrations of the reactant is linked with the so-called

law of mass action (Guldberg and Waage 1864; Kenakin 2016). In terms of drug-receptor binding, the law of mass action has two important aspects, the composition of the final reaction at equilibrium between receptor and drug, and kinetic aspects concerned with the rate equation for individual reactions which have a forward (k_{on}) and reverse (k_{off}) component. By the law of mass action, K_d is a composite of these two kinetic parameters and is defined as a ratio of the rate constants (k_{off}/k_{on}). In a closed system, such as is the case for simple binding reactions, when the concentration of reactants reaches the point that the forward and reverse (or on and off) reactions are in balance, the system is said to be at equilibrium. While the dissociation rate constant (k_{off}) is independent of ligand concentration (unit of min^{-1}), the observed rate of drug association (k_{obs}) also shares the same units and is highly dependent upon drug concentration, meaning that the association rate constant (k_{on}) has units of both concentration and time (e.g. M^{-1} min^{-1}). The equations which govern binding reactions assume that only a small fraction of added ligand binds to the target so that effectively the added concentration is equal to the free concentration. In situations where a larger fraction of the added ligand is bound then the reaction is said to be subject to depletion. This becomes experimentally significant at levels exceeding 10%, a situation that can lead to serious errors in the estimation of ligand affinity (Carter et al., 2007; Hulme and Trevethick 2010).

1.4 Understanding receptor kinetics at the molecular level

The dissociation rate constant - The dissociation rate constant (k_{off}) describes the dissociation of a single species and is, therefore, a unimolecular (first order) rate constant. k_{off} is independent of the local concentration of free drug and entirely dependent on specific interactions between the drug and its target which in the case of GPCRs is often a binding pocket. The same interaction forces which determine thermodynamic affinity, namely hydrogen bonding, hydrophobic interactions, and van der Waals forces are thought to play a role in determining dissociation rate (Pan et al., 2013). These electrostatic interactions hold the receptor and drug together in a complex and only when all such interactions are broken will the ligand finally dissociate.

Association rate constant - The association rate constant (k_{on}) is a bimolecular (second order) rate constant since it describes the rate at which two molecules bind to each other. Binding reactions may be thought of as either being diffusion-limited (or diffusion-controlled), which describes a process so fast that the reactants need only collide with one another for binding to occur or encounter limited (encounter-controlled) indicating that before a reaction can occur the reactants must undergo some degree of reorganisation, which may be reorientation and/or desolvation i.e. the release of water molecules electrostatically bound to a particle in aqueous solution, prior to reaction (Copeland 2011). As a consequence, k_{on} cannot be greater than the diffusion limit 10^9 M^{-1} sec^{-1} ($6x10^{10}$ M^{-1} min^{-1}) which represents the maximum rate at which two molecules can move through an aqueous environment and eventually collide (Alberty and Hammes, 1958; Pan et al., 2013). When k_{on} approaches the diffusion limit essentially all encounters of the two species involved result in successful binding. The literature is full of examples of compounds with k_{on} values several orders of magnitude lower than the diffusion limit (Gillard and Chatelain 2006; Sykes et al., 2009; Sykes et al., 2012; Sykes and Charlton 2012; Sykes et al., 2016) suggesting that at least for these compounds very few encounters result in a successful binding event demonstrating the inherent specificity of binding interactions. Drug-receptor selectivity for a target is often expressed in terms of differences in equilibrium affinity (Copeland 2016). Kinetic receptor selectivity being described in terms of differences in the dissociation rate of a ligand for two receptors, which may be closely related subtypes (Sykes et al., 2012; Tautermann et al., 2013). However, the association rate can also be the main driver of compound affinity and therefore dictate apparent receptor selectivity as described above. A good example is the association rate-driven selectivity of salmeterol for the β_1 and β_2 adrenergic receptors (Ramos et al., 2018).

1.5 Understanding drug-receptor association and its role in pharmacodynamics

The association process has received much less attention than the dissociation binding step as a factor important in the pharmacodynamics (PD) properties of drugs (Swinney 2004; Swinney 2008; Tummino and Copeland 2008). Pharmacodynamics referring specifically to the study of the biochemical and physiologic effects of drugs.

However, evidence is slowly emerging to suggest that the measured association rate may just be as important as the dissociation rate of a drug in determining the overall PD properties of drugs which are a direct function of receptor occupancy (Vauquelin 2010; Vauquelin 2016; Vauquelin 2018; de Witte et al., 2016). Until recently it was thought that molecules within a chemical series would share very similar association rates (k_{on}) and that affinity (or K_d) changes were driven mainly by changes in the magnitude of k_{off}, the dissociation rate constant (Tummino and Copeland 2008; Nunez et al., 2012). However, there are many examples where relatively minor changes in structure lead to a significant change in the magnitude of k_{on}, and therefore directly to a change in affinity (Sykes et al., 2009; Guo et al., 2012; Sykes et al., 2014). Factors which are thought to affect the association process include diffusion, desolvation, the molecular orientation of the molecule (Copeland et al., 2006; Nunez et al., 2012; Deganutti et al., 2017) and favourable and unfavourable intermolecular interactions (Radić et al., 1997; Schmidtke et al., 2011).

1.6 Drug-receptor residence time and toxicity

There is a growing appreciation that under certain conditions, binding kinetics or the rates of binding and unbinding (k_{on} and k_{off} respectively) may be a better predictor of pharmacological response than the equilibrium constant (Swinney 2004; Copeland et al., 2006; Charlton and Vauquelin 2010; Copeland 2016; Sykes et al., 2016; Bosma et al., 2018). Historically it is the dissociation rate or k_{off} that is considered the key driver of the drug-receptor complex lifetime *in-vivo* (Tummino and Copeland 2008) contributing directly to residence time ($1/k_{off}$). A complete understanding of drug residence time, or the length of time a drug stays bound to its target receptor, can be considered a critical part of compound optimisation, where sustained drug-receptor residence time has been identified as a factor crucial to improved clinical efficacy (Copeland 2016; Sykes et al., 2016). More recently the residence time concept has been openly questioned with an alternative explanation put forward based on a simple receptor occupancy model to explain the extended duration of action of certain drugs (Dahl and Akerud 2013; Folmer 2018; de Witte et al., 2018).

As discussed above the significant effect of prolonged residence time on drug pharmacodynamics (PD) is well documented but there are also examples in the literature where compound kinetics is thought to play a significant role in dictating compound safety or toxicity (Guo et al., 2014). In terms of drug safety profile, there are two major types of drug-induced toxicity, off-target toxicity, and on-target toxicity. Off-target toxicity is generally assessed in terms of the relative difference in affinity for the targets in question (Copeland et al., 2006), toxicity is a function of relative receptor occupancy (Copeland et al., 2006; Copeland 2010). More recently kinetic differences have been proposed to be clinically relevant (Sykes et al., 2012; Tautermann et al., 2013) with dissociation rate thought to dictate the temporal occupancy of a drug for a receptor subtype when a drug shows similar affinities. In contrast, on-target toxicity occurs when side effects result from either extended blockade or over-stimulation of the therapeutic target. Antagonist occupancy in such situations eg. during synaptic transmission, is thought to be largely a function of residence time, dictated by the dissociation rate of a molecule and the concentration of the competing agonist (Vauquelin et al., 2012).

1.7 A role for kinetics in the on target side effects of antipsychotics

The use of APDs provides one of the most enduring theories of on-target toxicity where D_2R antagonist off-rate is thought to play a key role in dictating the clinically observed EPS of antipsychotics and also their degree of hyperprolactinaemia (Kapur and Seeman 2000; Kapur and Seeman 2001). The complex disorders of movement which characterise EPS and the concomitant hyperprolactinaemia which characterise the earliest treatment options for schizophrenia are thought to result from the extended occupancy of dopamine D_2 receptors in the face of physiological dopamine neurotransmission. The implication being that rapid-off compounds should in theory show a reduced incidence of clinically observed side effects (Kapur and Seeman 2001; Dyhring et al., 2010; Langlois et al., 2012; Pompeu et al., 2015), a factor important in dictating clinical efficacy but also compliance (Leucht et al., 2013; Perkins 2002; Kane 2011).

Despite more than 60 years of APD research, the drivers of EPS effects remain difficult to predict, with newer treatments designed with the promise of fewer side effects, showing EPS levels not dissimilar to the agents they were designed to replace (Leucht et al., 2013).

1.8 How are the kinetics of ADPs traditionally measured?

Radioligand binding is a widely employed technique to characterise GPCRs and the ligands which bind to them. Radiolabelling of a drug enables the binding of that drug to its receptor to be studied directly (Sykes et al., 2016). Radioligands can be produced with a variety of different isotopes although classically tritium has proved to be the most useful partly due to its long half-life (12.3 years) and good safety record (Hein et al., 2005). The first radioligand binding assay specifically developed to characterise a GPCR was formulated by Paton and Rang in the mid-1960s in a study of muscarinic receptors (Paton and Rang 1965). Since this initial publication, competition radioligand binding assays have formed the mainstay of many successful drug discovery programs (Carpenter et al., 2002). Binding assays are classically described as either equilibrium or kinetic. Equilibrium studies represent the point at which the concentration ligand-bound receptor and each reactant; tracer, competitor and receptor remains constant and no longer changes. Kinetic (i.e. association and dissociation) studies are essential to determine both equilibrium (e.g. K_d) and tracer kinetic binding parameters (e.g. k_{on} and k_{off}), but also to define the optimal assay conditions for the determination of the equilibrium affinity (and kinetics parameters) of any unlabelled competitor which is in direct competition with it for the receptor of interest (Sykes et al., 2010; Hulme and Trevethick 2010).

Traditionally the dissociation kinetics of APDs have been studied using radiolabelled forms of the compounds (Urwyler and Coward 1987; Lepiku et al., 1997a; Lepiku et al., 1997b; Kapur and Seeman 2000; Seeman 2005; Langlois et al., 2012). In such experiments, membranes containing the D_2 receptor are pre-incubated with radioligand and the dissociation phase is initiated by adding an excess of an unlabelled competitor or through the process of dilution. Preincubation of radioligand allows an equilibrium between tracer and receptor binding to be established. It must be emphasised that equilibrium is dynamic, in other words, the

tracer will still undergo the process of association and dissociation but without a net change in overall specific binding (i.e. ligand-bound receptor remains constant). Hence following the addition of an excess of an unlabelled competitor only the process of tracer dissociation will be observed as the unlabelled ligand replaces the tracer on the receptor. For the dilution method to be successful, the free tracer concentration must drop immediately to a level at which no re-binding should occur (eg 1000-fold below the tracer's K_d). These experiments are likely to produce the most direct information about a drug's dissociation rate however they are not without their problems especially when we consider the relatively low reported affinities of the atypical APDs such as clozapine and quetiapine (82 and 155 nM respectively) which will likely contribute to relatively small windows of specific binding due to increased levels of non-specific binding to biological membranes and the filters used to capture them (Kapur and Seeman 2000; Auberson et al., 2016).

Another problem with the above procedures is that every compound must be custom synthesised and radiolabelled which is prohibitive and restricts the number of compounds that can be readily tested. An alternative low-throughput method is to use a single radioligand with high affinity and selectivity for the receptor and utilise the equations provided by Motulsky and Mahan (1984) allowing the kinetics of an unlabelled ligand in competition with the radioligand to be measured. Here the interaction of the tracer and unlabelled competitor with receptor are described by two differential equations which when solved yield a single equation describing the binding of the tracer as a function of time. One of the assumptions being that the tracer and competitor bind to the same site on the protein of interest. Following the quantification of tracer kinetic parameters, the application of this model allows the determination of the kinetic parameters of the unlabelled compound.

This method has been applied successfully to determine the kinetics of both antagonists (Gillard and Chatelain 2006; Dowling and Charlton 2006; Slack et al., 2011; Sykes et al., 2014) and agonists (Sykes et al., 2009; Sykes et al., 2012; Guo et al., 2012) acting at a variety of aminergic GPCRs (eg. M3 muscarinic, β_2-adrenergic and histamine H1 receptors). Lipid receptors (eg. cannabinoid CB2 and prostanoid CRTH2), nucleotide receptors (eg. adenosine A2a) and peptide receptors (eg. Corticotropin-releasing hormone receptor 1) have also been studied

(Martella et al., 2017; Sykes et al., 2016, Guo et al., 2012; Fleck et al., 2012), and even a non-GPCR target, the HERG channel (Yu et al., 2015). Others have successfully employed the competition association technique to study relatively small numbers of D_2 antagonists (Carboni et al., 2012). The limitations of this technique have largely remained unexplored, with only very limited treatments of its applicability (Motulsky and Mahan 1984; Contreras et al., 1986). Ultimately success is largely determined by the availability of a suitable tracer capable of discriminating the kinetics of the most rapidly dissociating compounds. Depending on the kinetic properties of the tracer used compounds with very rapid off-rates may become practically indistinguishable from each other or even unmeasurable (Klein-Herenbrink et al., 2016). A solution employed in the past is to reduce the assay temperature (Guo et al, 2012; Contreras et al., 1986), which effectively slows the whole process of binding down allowing these drug-receptor interactions at early time points to be very accurately defined.

Alternatively, multistep washout experiments (see Vauquelin et al., 2012 for a comprehensive review) have been employed to compare the dissociation rates of unlabelled APDs (Leysen and Gommeren 1984; Tresadern et al., 2011). However, although these techniques show increased throughput they only allow relative differences in dissociation rates to be approximated. The principle of these filtration receptor-capture washout assays assumes that the faster an unlabelled compound dissociates from any given receptor, the faster the tracer eg [^{3}H]-spiperone, will bind to that receptor.

Radioactive based methods to assess kinetics in a low throughput way - Despite their undoubtedly high sensitivity, with only pM levels of a receptor required, the use of radioactive ligands as tracers in competition association binding assays presents several challenges. Classic radiotracer binding assays cannot be performed in a homogeneous format and the radioligand itself will not just bind to the intended target (specific binding) but will also bind to the membranes/cells which house the receptors but also to the filter/cell plates which trap the receptors (Non-specific binding, NSB). This necessitates multiple washing steps to separate bound and free radioligand to indirectly observe the level of specific binding (Specific binding = total binding - NSB) of the tracer following scintillation counting. This step

brings added complexity to the procedure and makes these assays more difficult to perform in High Throughput Screening (HTS) mode and therefore less attractive from the perspective of testing all available clinical antipsychotics. More importantly the wash steps prevent any possibility of carrying out kinetics experiments on a single sample, since each well represents a single time point and prohibits the use of very rapidly dissociating (and usually low affinity) ligands whose specific binding signal is likely to be lost or reduced in the wash step which itself takes time to complete. More recently scintillation proximity assays (SPA) have been developed to explore the kinetics of ligand binding (Heise et al., 2007; Xia et al., 2016). These assays rely on the excitation of scintillation fluid impregnated into so-called scintillation beads. Excitation occurs when radio-labelled molecules interact and bind to the surface of the bead. Receptor specific binding signals are enhanced in the presence of membranes or cells which specifically bind to specially coated bead surfaces eg. wheat germ agglutinin (WGA) and the radioligand itself. These interactions triggering the bead to emit light, which can be detected using a photometer eg TopCount^{TM} PerkinElmer. Such assays can be performed homogeneously but they suffer from the problems of bead settling which can lead to inaccurate estimates of binding at the very early time points, these being critical for accurate estimations of unlabelled compound kinetic parameters (Xia et al., 2016). Another major drawback with radioactive probes is their hazardous nature which can be restrictive in terms of radioactive waste disposal and delimitation of working areas. Fortunately, other techniques have emerged which seemingly negate the need for radioactive probes.

Fluorescence-based methods to assess kinetics in a medium-throughput way **-** The emergence of fluorescence-based methods offers an alternative to radioactive binding assays and represent a potentially higher-throughput method to assess unlabelled ligand kinetics (Briddon et al., 2011; Sridharan et al., 2014; Stoddart et al., 2018). The fluorescent probes themselves are safer making assays easier to implement, plus the costs associated with waste disposal compared to radiometric assays are minimal. Potent fluorescent tracers have now been designed and synthesized for numerous receptors and are now readily available from an ever-increasing number of commercial suppliers (Vernall et al., 2014; Stoddart et al., 2015; Stoddart et al., 2018). It is important to note that the addition of a fluorescent

probe to a ligand will likely affect its physicochemical properties (e.g. hydrophobicity) and potentially increase steric hindrance resulting in significantly altered pharmacological properties potentially reducing its affinity to the point it becomes useless as a pharmacological tool (Middleton and Kellam 2005; Baker et al., 2010; Briddon et al., 2011; Iliopoulos-Tsoutsouvas et al., 2018). However, a modest reduction in affinity need not reduce the effectiveness of the ligand for binding studies provided it remains specific for the intended target site. In fact, such reductions in affinity may actually result in a more viable tracer for HTS kinetic studies which ultimately rely on miniaturisation if they are to be successful and as a consequence a lower affinity ligand avoids the possibility of encountering tracer depletion a potential problem in the smaller assay volumes routinely employed in a 384 well format (Carter et al., 2007).

A fluorescence-based method to measure GPCR binding kinetics of unlabelled ligands has been previously described involving the use of time-resolved fluorescence resonance energy transfer (TR-FRET) and a SNAP-tagged receptor (Schiele et al., 2015, see Figure 2.1A). SNAP-tag is a ~20 kDa protein derived from the DNA repair enzyme alkylguanine transferase (AGT) which is inserted at the N-terminal of the GPCR. This enzyme contains a reactive cysteine that binds to the oxygen of a benzylguanine substrate carrying a lanthanide cryptate, such as terbium forming an irreversible covalent bond and in doing so it creates a fluorescent donor capable of exciting a fluorescent ligand on binding (the acceptor). Terbium is an example of a lanthanide which when excited produces a long-lived fluorescent emission, which facilitates the efficiency of the time-resolved fluorescence resonance energy transfer process (Figure 2.1B). The cryptate forms a cage, acting not just as a terbium carrier but serves two other important functions. Lanthanides exhibit very weak absorbance and so the cryptate serves as an antenna, absorbing the excitation energy and transferring it directly to the terbium. Also, the cryptate cage protects the terbium from quenching by water molecules (Selvin, 2002).

TR-FRET detection itself involves the transfer of energy from the donor, eg. terbium to an acceptor fluorophore, usually, a fluorescent ligand when they are in close proximity (≤10 nm) (see Cottet et al., 2012). TR-FRET includes a time delay (or lag time) from the initial donor stimulation to the point of detection, usually 60 μs. This

time delay from stimulation to detection, allows the decay of background fluorescence, ensuring that the signal recorded is specific for the binding event between the labelled ligand and the protein (Figure 2.1B). Therefore, separation of the bound and unbound fluorescent ligand is no longer necessary and thus this homogeneous assay format enables higher throughput (Emami-Nemini et al., 2013). In addition to its time-resolved qualities which reduces background emission following stimulation, terbium cryptate has excellent spectral properties in terms of its fluorophore compatibility, with four useful emission peaks (490, 548, 587, and 621 nm), allowing different fluorescent acceptors to be utilised as acceptors in the formulation of these binding assays (Cottet et al., 2012). The overall approach of Schiele et al (2015) was similar to the classic competitive association radioligand binding methodology described above except a modified Motulsky and Mahan competitive binding model was employed to take into account apparent bleaching of the fluorophore. The modification being the incorporation of a simple decay function.

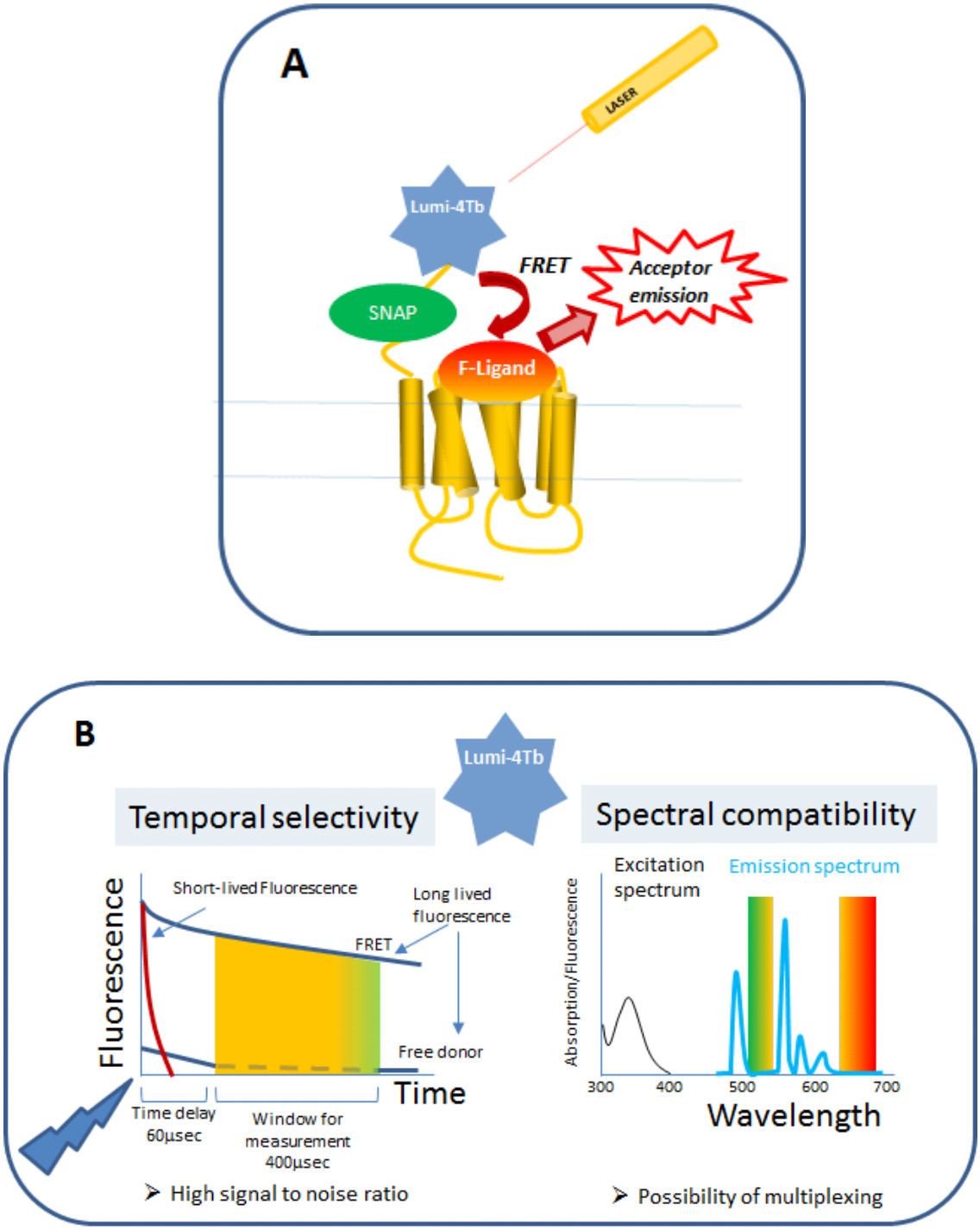


Figure 2.1. The principles behind homogenous TR-FRET between a terbium cryptate labelled GPCR and a fluorescent ligand. (A) Excitation of a terbium cryptate (donor) labelled receptor by either laser (as shown) or lamp (BMG PHERAstar FS or FSx) allows excitation of a receptor-bound fluorescent ligand which in turn emits at a wavelength-dependent on its fluorescent properties (Figure modified from Ward and Milligan 2014). **(B)** Terbium cryptate has two distinct properties which make it a perfect donor for formulating homogenous TR-FRET

assays; temporal selectivity allowing for short-lived fluorescence to rapidly decay and spectral compatibility which allows for excitation of both green (emission 495-570nm) and red (emission 620-720nm) fluorescent acceptors (Figure modified from Cottet et al., 2012).

1.9 Introducing new chemical starting points for the development of APDs – What are the problems?

APD research has yet to provide an effective and risk-free treatment for schizophrenia a condition that has been estimated to affect up to 1% of the population (Cunningham and Peters 2014). For example, although the atypical antipsychotic clozapine is effective at treating the symptoms of schizophrenia it also comes with the risk of agranulocytosis, a potentially life-threatening condition necessitating prophylactic blood monitoring, which has considerable cost implications (Wiciński and Węclewicz 2018). Agranulocytosis is thought to be an off-target effect, potentially the result of histamine H4 receptor activation (Goto et al., 2016). Therefore, the opportunity exists for the development of an alternative molecule with an optimised kinetic profile and overall reduced side effects. The ideal molecule being one that blocks the pathological effects of raised dopamine levels in the brain but preserves normal synaptic signalling preventing serious side effects eg EPS and prolactin release. Thus, identifying a suitable assay format for the high throughput kinetic profiling of unlabelled molecules would be highly advantageous. The main limitation with such an approach at present is our ability to assess the kinetics of the most rapidly dissociating 'hits' with affinities likely to be in the high nM-μM range.

1.10 Aims

The overriding aim of this study is to determine the kinetic and equilibrium properties of a large number of clinically used APDs at their primary target the dopamine D_2R, and in doing so, explore the distinction between atypical and typical APDs in terms of on-target side effect profile, both from a kinetic and occupancy perspective. The existing kinetic data on clinical atypical and typical APDs is from a variety of groups using an assortment of different methods, species and measured over a considerable period of time (Leysen and Gommeren 1984; Urwyler and Coward 1987; Lepiku et al., 1997a, Lepiku et al., 1997b; Kapur and Seeman 2000; Seeman 2005; Tresadern et al., 2011; Carboni et al., 2012; Langlois et al., 2012; Sahlholm et al., 2014; Sahlholm et al., 2016). Another key aim of this study was to kinetically profile the current clinically favoured APDs against other disease-relevant receptors

such as the serotonin 5-HT1A and 5-HT2A receptors for which there is little or no data available and determine the influence of these receptors on the prevalence of reported on target side effects.

Chapter 2 - Materials and Methods

2.1 Materials

2.1.1 Cell culture reagents

Cell culture plasticware was purchased from Scientific Laboratory Supplies Limited (Nottingham, UK). Dulbecco's modified Eagle's medium: Ham F12 (DMEM: F12) containing 2mM glutamine, Dulbecco's phosphate buffered saline (D-PBS, minus Mg^{2+} and Ca^{2+}) and heat-inactivated Foetal Calf Serum (FCS) was purchased from Sigma-Aldrich, Poole, UK. Trypsin-EDTA solution (10x) and Enzyme-free Hank's-based cell dissociation solution was purchased from Sigma-Aldrich (Poole, UK). Recovery™ Cell Culture Freezing Medium and the selection reagents zeocin and geneticin (G418) were purchased from Thermo Fisher Scientific (Paisley UK).

2.1.2 Ligand binding assays

96-well polypropylene plates (Corning) were purchased from Fisher Scientific UK (Loughborough, UK) and 384-well Optiplates plates were purchased from Perkin Elmer (Beaconsfield, UK). Hanks Balanced Salt Solution (HBSS, components 1mM calcium chloride, 0.8mM magnesium sulphate, 5mM potassium chloride, 0.4mM potassium phosphate monobasic, 137mM sodium chloride, 0.3mM sodium phosphate dibasic and 5mM D-glucose), HEPES solution (1M), Pluronic acid (Pluronic F-127), DMSO, 5'-Guanylyl imidodiphosphate (GppNHp), risperidone, chlorpromazine hydrochloride, quetiapine hemifumarate, ziprasidone hydrochloride monohydrate, zotepine, sertindole, thioridazine hydrochloride, fluphenazine dihydrochloride, molindone hydrochloride, loxapine succinate, perphenazine, trifluoperazine dihydrochloride, (-)sulpiride, droperidol, (+)butaclamol, spiperone, dopamine, (−)-quinpirole hydrochloride, aripiprazole, R-propylnorapomorphine (RNPA), R (+)-3-(3-Hydroxyophenyl)-N-propylpiperidone HCl ((+)3PPP), S (-)-3-(3-Hydroxyophenyl)-N propylpiperidone HCl ((-)3PPP), R-(-)-apomorphine HCl hemihydrate, sumanirole maleate, and rotigotine hydrochloride used in competition assays were obtained from Sigma-Aldrich (Poole, UK). Paliperidone, olanzapine, nemonapride, paliperidone, amisulpride, clozapine, asenapine maleate, remoxipride hydrochloride, flupenthixol dihydrochloride, melperone hydrochloride, raclopride, domperidone haloperidol hydrochloride, bromocriptine mesylate, cabergoline, GSK 789472 hydrochloride, B-HT 920, dihydroergocristine (DHEC), 7-

OH DPAT ((±)-7-Hydroxy-2-(di-n-propylamino)tetralin hydrobromide), pergolide, lisuride maleate and desmethylclozapine used for competition assays were obtained from Tocris Bioscience (Avonmouth, Bristol UK). Lurasidone hydrochloride and iloperidone were obtained from Selleckchem (Munich, Germany). Droperidol, pardoprunox, ropinirole, cariprazine, brexpiperazole, and bifeprunox were generous gifts from Dr. Rob Lane (Monash, Australia). The plasmids pSNAP-5HT1A, pSNAP-5HT2A and Tag-lite® labeling reagents, including the labelling medium (LABMED) and SNAP-Lumi4-Tb was obtained from Cisbio Bioassays (Bagnols-sur-Cèze, France).

2.2 Methods

2.2.1 Cell culture

CHO-K1 cells expressing the receptor of interest were maintained in Dulbecco's modified Eagle's medium: Ham F12 (DMEM: F12) containing 2mM glutamine and supplemented with 10% heat-inactivated fetal calf serum. Cells were routinely passaged during the log phase (~70-80 % confluence) every 3-4 days. Selection pressure was applied to stably expressing cells to maintain receptor expression. CHO-D_{2L} cells were maintained in Dulbecco's modified Eagle's medium: Ham F12 (DMEM: F12) containing 2mM glutamine and supplemented with 10% fetal calf serum and 20 μg/mL zeocin to maintain receptor expression. CHO-D_{2S} cells were obtained from Cisbio Bioassays (Bagnols-sur-Cèze, France). Stable CHO-5-HT1A, CHO-5-HT2A cells and CHO cells transiently expressing the human 5-HT2A receptor were prepared from plasmids provided by Cisbio Bioassays (Bagnols-sur-Cèze, France). CHO-$D_{2S,}$ CHO-5-HT1A, and CHO-5-HT2A cells were maintained in Dulbecco's modified Eagle's medium: Ham F12 (DMEM: F12) containing 2mM glutamine and supplemented with 10% fetal calf serum and 200 μg/mL geneticin (or G418) to maintain receptor expression in the stable cell lines. Frozen cell stocks were prepared using Recovery™ Cell Culture Freezing Medium and stored in liquid nitrogen.

2.2.2 Stable transfections

Wild type CHO-K1 cells (t75cm^{2}flask) were trypinised and resuspended in 5 ml medium. Cells were seeded in t25cm^2 flasks, aiming for 80 % confluence on the day of transfection. A lipofectamine: DNA mix (eg. pSNAP-5HT1A and pSNAP-5HT2A) was prepared by first mixing 2 µg total DNA with 200 µl OptiMEM (Invitrogen) in a 1.5mL Eppendorf. In a separate Eppendorf tube, a single lipofectamine / OptiMEM mix was prepared, at the ratio of 18 µl lipofectamine: 200 µl OptiMEM per transfection. The final lipofectamine: DNA mix was prepared by add 215 µl lipofectamine / OptiMEM to each DNA containing tube, mixing gently by pipetting up and down 5- 10 times. A DNA: lipofectamine complex is formed after 20min at room temperature. The medium on each t25cm^2 flask was replaced with 1.2 ml OptiMEM and flasks left in incubator to warm to 37°C.

At the end of the lipofectamine: DNA complex incubation period, 800 µl OptiMEM was added to each tube and mixed gently. 1.2 ml of DNA: lipofectamine mix was added to each labelled t25cm^2 flask and left in the incubator for 18 - 24 h. 3 days post transfection transfected cells were split (~ 1:10 split ratio) into experimental and control cells into t75cm^2 flasks, in antibiotic free DMEM/F12 medium. The following day medium was replaced with complete medium containing appropriate selection antibiotic (pCDNA3.1neo 0.8 mg ml^{-1} G418). Media containing selection antibiotic was replaced every 3 - 4 days, until clear resistant colonies developed. Resistant colonies were split after 10 - 14 days, into 2x t75cm^2, and the selection antibiotics reduced to maintenance concentration for dilution cloning (25 % of above, e.g. 0.2 mg ml^{-1} G418). 1x t75cm^2 was frozen as a mixed population and the remaining t75cm^2 was used for the dilution cloning step.

2.2.3 Dilution Cloning

Single clones were identified by limited dilution and expansion as follows. Polyclonal cells were plated from the selection step described above at a density of 10 cell/mL and 1 cells/ml in 2x 96-well tissue culture plates by adding 100 µL per well (i.e., 1 and 0.1 cell per well). The number of cells per well was assessed after 24-72 hours noting the wells with only one cell/well. Each colony was assumed to be clonal. Wells with 1 colony per well were considered monoclonal. Colony number was

verified every week until the well had reached high confluence. Finally, clones were transferred, and receptor expression assessed. Selected single-colony wells in the 96-well tissue culture plate, grown to high confluence, were expanded by transferring to a 24-well tissue culture plate (2mL volume). A small portion of the cells (100μL) were transferred to a black clear bottom 96 well imaging plate (Greiner 655090) to assess the expression of the target protein. SNAP positive clones were assessed by labelling with 2μM SNAP-surface AF647 for 30mins at 37ºC/5% CO_2. Cells were then washed carefully in PBS (100μL) and fixed by adding 3% PFA in PBS for 15min at room temperature. To remove the PFA cells were washed in PBS (100μL). Finally Hoechst 33342 nuclear stain was added for 15mins (1μM final in PBS, 100μL) and the plate washed x2 with PBS (100μL then 200μL) and then replaced with 100μl PBS, finally plates were imaged on the ImageXpress Ultra plate reader to confirm that the cells were expressing the receptor of interest. AF647 was excited using a 633 nm laser with emission collected through a 640-685 nm bandpass filter. Negative clones were discarded, and the positive 48-well tissue culture plate clones were expanded by passage to a t25cm^2 culture plate. High medium and low expressing clones were identified and frozen down for further profiling.

2.2.4 Transient transfections

The recommended FuGENE®HD (Promega): DNA complex ratio for CHO-K1 cells is 3:1. CHO-K1 cells were plated into a t175cm^2 flask, in complete growth medium DMEM: F12 containing 10% Fetal Bovine Serum and grown to 70% confluency. A FuGENE®HD: DNA complex (eg. pSNAP-5HT2A) was prepared by adding DNA at a concentration of 0.020 μg/μL to OptiMEM 1,175μL total volume (i.e. 25 μg of plasmid DNA in total or 1 μg/mL). 75 μL of FuGENE® HD reagent was then added, and the solution mixed by briefly vortexing. The complex was then incubated for 10 minutes at room temperature. The media on the cells was exchanged and replaced with precisely 23,750 μL of complete media and finally 1250 μL of 3:1 FuGENE®HD: DNA complex was added to the cells and mixed thoroughly. Cells were grown for a further 48 hrs before SNAP labelling.

2.2.5 Terbium labeling of SNAP-tagged cells and membrane preparation

Cell culture medium was removed from the t175cm^2 flasks containing confluent adherent cells. Cells were washed 2x in D-PBS (10mL) and 1x in LABMED (5mL). 10-12 mL of Tag-lite labeling medium containing 100 nM of SNAP-Lumi4-Tb was added to the flask and incubated for 1 h at 37 °C under 5% CO_2. Cells were washed 2x in D-PBS to remove the excess of cell impermeable unreacted SNAP-Lumi4-Tb and then detached using 5 mL of enzyme-free Hank's-based cell dissociation solution and collected in a vial containing 5mL of DMEM: F12 containing 2mM glutamine and supplemented with 10% fetal calf serum. Cells were pelleted by centrifugation (5 min at 1500 rpm) and the pellets were frozen to −80 °C. To prepare membranes homogenisation steps were conducted at 4°C (to avoid receptor degradation). Specifically, 20 ml per t175-cm^2 flask of wash buffer (10 mM HEPES and 10 mM EDTA, pH 7.4) was added to the pellet. This was homogenized using an electrical homogenizer Ultra-Turrax (Ika-Werk GmbH & Co. KG, Staufen, Germany) (position 6, 4 x 5-s bursts) and subsequently centrifuged at 48,000*g* at 4°C (Beckman Avanti J-251 Ultracentrifuge; Beckman Coulter, Fullerton, CA) for 30 min. The supernatant was discarded, and the pellet was re-homogenized and centrifuged as described above in the wash buffer. The final pellet was suspended in ice-cold 10 mM HEPES and 0.1 mM EDTA, pH 7.4, at a concentration of 5 to 10 mg/ml. Protein concentration was determined using the bicinchoninic acid assay kit (Sigma-Aldrich), using BSA as a standard with membrane aliquots maintained at −80°C until required.

2.2.6 Determination of tracer binding kinetics and equilibrium affinity

The competition association method of Motulsky and Mahan (1984) requires an accurate assessment of the kinetic properties of the tracer before the association and dissociation rates of any unlabelled competitor in competition with it can be determined. To accurately determine the fluorescent ligand association rate (k_{on}) and dissociation rate (k_{off}) values, the observed rate of association (k_{obs}) was calculated using six different concentrations. The appropriate concentrations of fluorescent ligand were incubated with cell membranes in assay binding buffer (final assay volume, 40μL). Experiments were conducted in white 384-well Optiplate

plates, in assay binding buffer with GppNHp included to remove the G protein-coupled population of receptors that can result in two distinct populations of binding sites in membrane preparations. This is necessary since the Motulsky–Mahan model (1984) is only appropriate for ligands competing at a single site. Prior to insertion of 384-well plates into the plate reader optical plate seals were applied to the top of the plates to prevent evaporation of the samples. The degree of fluorescent ligand bound to the receptor was assessed at multiple time points by HTRF detection to allow the construction of association kinetic curves. Total and NSB binding was also assessed at equilibrium allowing construction of saturation plots for determination of tracer affinity. Saturation binding data were analysed by non-linear regression according to a one-site model. Fitting the total and NSB data sets simultaneously to Equation 2.1 described in Chapter 2 section 2.2.8 Signal detection and data analysis, provides one best-fit value for both the affinity (K_d) and the maximal level of specific binding (B_{max}) of a fluorescent tracer. Specific binding, obtained by subtracting non-specific binding from total binding, was fitted to Equation 2.2, described in Chapter 2 section 2.2.8 Signal detection and data analysis, a one-site binding model that describes a rectangular hyperbola or binding isotherm.

Data were globally fitted using (Equation 2.5, described in Chapter 2 section 2.2.8 Signal detection and data analysis) to simultaneously calculate k_{on} and k_{off} of the tracer. In addition, tracer association data were analysed using non-linear regression to fit the specific binding data to a one-phase exponential association equation, see Equation 2.6, described in Chapter 2 section 2.2.8 Signal detection and data analysis. Where tracer binding follows a simple law of mass action model, k_{obs} increases linearly as a function of tracer concentration. The slope of the resulting line fitted using linear regression equates to the association rate (k_{on}), and extrapolation of the plot to y = 0 yields the dissociation rate (k_{off}) (Sykes et al., 2010).

2.2.7 Competition binding kinetics

To determine the association and dissociation rates of unlabelled ligands, I used the competition kinetic binding approach first described by Motulsky and Mahan (1984). In the experiments described the degree of fluorescent tracer ligand [L] bound to the receptor was assessed at multiple time points by HTRF detection. Non-specific

binding was determined as the amount of HTRF signal detected in the presence of a high concentration of antagonist [B] and was subtracted from each time point, meaning that t = 0 was always equal to zero. Each time point was conducted on the same 384 well plate incubated at 37°C with orbital mixing (1sec of 100 RPM/cycle). Multiple concentrations of unlabeled competitors were tested, for the determination of rate parameters. Data were globally fitted using (Equation 2.7, Chapter 2, section 2.2.8 Signal detection and data analysis) to simultaneously calculate k_{on} and k_{off} of unlabelled compounds.

2.2.8 Signal detection and data analysis

Signal detection was performed on a PHERAstar FS (BMG Labtech, Offenburg, Germany) using standard HTRF filter settings (dual emission). The terbium donor was always excited with 3 laser flashes at a wavelength of 337 nm at intervals of 20 seconds. Emission (A) of the red acceptor at a wavelength of 665nm and the donor (B) at 620nm was collected using an integration time of 400μs and a delay time of 60μs. HTRF ratios were obtained by dividing the acceptor signal in this case from the fluorescent ligands (i.e. 665 nm, the red spectral region) by the donor signal (i.e. 620 nm from excitation of the terbium labelled receptor) and multiplying this value by 10,000. Specific binding was determined by subtracting the non-specific HTRF ratio from the total HTRF ratio.

All experiments were analyzed by non-regression using Prism 6.0 (GraphPad Software, San Diego, U.S.A.). Saturation binding data were analysed by non-linear regression according to a one-site equation:

Total binding = Specific+NSB = (B_{max}*[L])/(K_d+[L])+(*slope**[L])+Background)

NSB=slope*[L]+Background Equation 2.1

Fitting the total and NSB data sets globally (simultaneously), sharing the value of slope, provides one best-fit value for both the K_d and the B_{max} of a fluorescent tracer. Where B_{max} is the maximal level of specific binding, [L] is the concentration of fluorescent ligand in nM, K_D is the equilibrium dissociation constant in nM, *slope* is

the slope of the linear non-specific binding component, and Background is the *Y*-axis intercept.

Specific binding, obtained by subtracting non-specific binding from total binding, was fitted to a one-site binding model that describes a rectangular hyperbola or binding isotherm:

$$\text{Specific binding} = B_{max}*[L]/(K_d + [L]) \qquad \text{Equation 2.2}$$

Where B_{max} is the maximal level of specific binding, [L] is the concentration of fluorescent ligand in nM, K_d is the equilibrium dissociation constant in nM.

Competition displacement binding data were fitted to sigmoidal (variable slope) curves using a "four-parameter logistic equation":

$$Y = \frac{\text{Bottom}+(\text{Top}-\text{Bottom})}{(1+10^{(\text{logIC50}-X)\text{HillSlope}})} \qquad \text{Equation 2.3}$$

Bottom is the specific binding (Y) value at the bottom plateau (i.e. 0%), Top is the specific binding (Y) value at the top plateau (i.e. 100%). LogIC50 (inhibitory concentration, 50%) is the X value when the specific binding is halfway between Bottom and Top (i.e. 50%). The HillSlope (Hill slope) describes the steepness of the curve. A standard sigmoid inhibitory concentration-response curve has a Hill Slope of -1.0.

IC_{50} values obtained from the inhibition curves were converted to K_i values using the method of Cheng and Prusoff (1973).

$$K_i = \frac{IC_{50}}{1+\frac{[L]}{K_d}} \qquad \text{Equation 2.4}$$

Where, IC_{50} (M) is the concentration of competing compound required to produce 50% inhibition of tracer binding, L (M) is the concentration of tracer added and K_d (M) is a measure of the affinity of the radioligand for the receptor.

Most binding models follow the law of mass action (see DeBlasi et al., 1989) and assume that all the molecules in a binding reaction are equally free to bind receptors

and that binding is readily reversible. The relationship between free tracer (L), the receptor (R) and the tracer-receptor complex (LR) is shown in reaction Scheme 2.1. In a closed system (eg. a reaction vessel) when the concentration of reactants reaches the point that the forward and reverse (or on and off) reactions are in balance, the system is said to be at equilibrium. However, before equilibrium is reached, the rate of [LR] formation, or the observed rate of association (or k_{obs}) is dependent on the concentration of tracer added and its own on and off rates.

$$[L] + [R] \underset{koff}{\overset{kon}{\rightleftharpoons}} [LR] \qquad \text{(Scheme 2.1)}$$

It is worth noting that the calculations performed normally assumes that no ligand depletion occurs and that the free ligand concentration [L] remains unchanged throughout the course of binding.

Fluorescent ligand (tracer) association data were fitted as follows to a global fitting model using GraphPad Prism 6.0 to simultaneously calculate k_{on} and k_{off} using the following equation, where k_{obs} equals the observed rate of association:

$$k_{obs} = [\text{Tracer}]*k_{on} + k_{off}$$

$$Y = Y_{max}*(1-\exp(-1*k_{obs}*X)) \qquad \text{Equation 2.5}$$

In this globally fitted model of tracer binding, tracer concentrations [L] are fixed, k_{on} and k_{off} are shared parameters and independent of tracer concentration. Here, Y is the level of receptor-bound tracer, Y_{max} is the level of tracer binding at equilibrium, X is in units of time (eg. min) and k_{obs} (min^{-1}) is the rate at which equilibrium is approached.

In addition, tracer association data were analysed using non-linear regression to fit the specific binding data to a one-phase exponential association equation.

$$Y = Y_{max}*(1-\exp(-k_{obs}*X)) \qquad \text{Equation 2.6}$$

Where X is time (min) and k_{obs} is the observed rate of association (min^{-1}). Where tracer binding follows a simple law of mass action model, k_{obs} increases linearly as

a function of tracer concentration. The slope of the resulting line fitted using linear regression equates to the association rate (k_{on}), and extrapolation of the plot to y = 0 yields the dissociation rate (k_{off}) (Sykes et al., 2010).

The association and dissociation rates for unlabeled antagonists were calculated using a method first described by Motulsky and Mahan (1984). This approach involves the simultaneous addition of a fixed concentration of tracer (eg. fluorescent ligand or [A]) and varying concentrations of competitor [B] to the receptor preparation so that at t = 0 all receptors are unoccupied. As the binding reaction proceeds two independent receptor complexes are formed [AR] and [BR], with the labelled ligand able to occupy a certain proportion of free receptors [R], over time. The rate of tracer occupation being dependent upon the kinetic properties of the competing ligand [B], its own kinetic properties and the concentration of the competing ligand added. At equilibrium the unlabelled ligand will displace a certain amount of tracer added. The degree of tracer displacement will depend on its own affinity, the affinity of the unlabelled ligand and the relative concentrations added (see reaction Scheme 2.2).

$$[A] + [R] + [B] \underset{\leftarrow}{\overset{\rightarrow}{}} [AR] + [BR] \qquad \text{(Scheme 2.2)}$$

Association and dissociation rates for unlabeled antagonists were calculated using the following equations first described by Motulsky and Mahan (1984):

$$K_A = k_1[L] + k_2$$

$$K_B = k_3[I] + k_4$$

$$S = \sqrt{((K_A - K_A)^2 + 4 \cdot k_1 \cdot k_3 \cdot L \cdot I \cdot 10^{-18})}$$

$$K_F = 0.5 * (K_A + K_B + S)$$

$$K_S = 0.5 * (K_A + K_B - S)$$

$$Q = \frac{B_{max} * K_1 * L * 10^{-9}}{K_F - K_S}$$

$$Y = Q \cdot \left(\frac{k_4 \cdot (K_F - K_S)}{K_F \cdot K_S} + \frac{k_4 - K_F}{K_F} exp^{(-K_F \cdot X)} - \frac{k_4 \quad K_S}{K_S} exp^{(-K_S \cdot X)}\right) \qquad \text{Equation 2.7}$$

Where: X = Time (min), Y = Specific binding (eg. CPM or HTRF units eg. HTRF ratio 665nm/620nm*10,000), k_1 = k_{on} tracer (M^{-1} min^{-1}), k_2 = k_{off} tracer (min^{-1}), L = Concentration of tracer used (nM), I = Concentration unlabeled ligand (nM). Fixing the above parameters allows the following to be calculated: k_3 = Association-rate constant of unlabeled ligand (M^{-1} min^{-1}), k_4 = Dissociation-rate constant of unlabeled ligand (min^{-1}), B_{max} = Maximal specific binding of the system at equilibrium binding (eg CPM or HTRF units e.g. HTRF ratio 665nm/620nm*10,000).

The fluorescent ligand or tracer dissociation rates were analyzed by displacement of the tracer with a large excess of an unlabeled ligand known to bind to the same site with similar or higher affinity. Dissociation of fluorescent ligand was fitted to a one-phase mono-exponential decay function to estimate the dissociation rate of the tracer directly:

$$Y = (Y_0\text{-}NS)*\exp(-K*X) + NS \qquad \text{Equation 2.8}$$

Where Y_0 is specific binding at time zero (equal to 100%). NS is the binding (non-specific) at an infinite time in the units of the Y-axis. *K* is the rate constant in inverse units of the X-axis (min). The half-life equals the natural logarithm of 2 or 0.693 divided by *K* (*K* being equivalent to k_{off}). The dissociation half-life ($t_{1/2}$) is therefore defined as the time (min) required for exactly half of the receptor-ligand complexes to decay.

Statistical differences were determined by one-way ANOVA with individual differences between test groups tested by Bonferroni t-test or using a simple unpaired Students t-test. Differences were considered significant at $P< 0.05$. All statistical analyses were performed using GraphPad Prism 6.0.

2.2.9 Modelling drug-receptor re-binding

Rebinding describes the ability of a drug molecule to bind to multiple receptors within a compartment before diffusing away into bulk, the overall effect being extended target-receptor occupancy (Vauquelin 2010; Vauquelin and Charlton 2010). To examine this, we utilized a model of an immunological synapse with a compartment volume of 0.176 μm^3, which is within the range described for the dopamine synapse (Coombs and Goldstein 2004). To calculate k_r we must first convert the standard units of k_{on} (M^{-1} min^{-1}) to (cm^3/sec), this is because the original units are based on the diffusion of a single ligand molecule to a receptor. To change the units of calculated k_{on} we divide by Avogadro's number (6.02 $x10^{23}$) and convert M^{-1} to cm^3/mole by multiplying by 1000. This is because a 1 molar solution = 1mole/L and there are 1000cm^3 in 1L. Finally, we divide by 60 to give cm^3/sec. In this model, the overall macroscopic reversal rate (k_r) is described by the following equation.

$$k_r = k_{off}/(1+ k_{on} *R/k-) \qquad \text{Equation 2.9}$$

where; k_{off} = dissociation rate from the receptor (sec), k_{on} = association rate onto the receptor (cm^3/sec), R = surface receptor density (cm^{-2}), and k- = the diffusion rate out of the synaptic compartment into bulk aqueous (cm/sec). Dopamine and 5-HT2A synaptic surface receptor density values are based on gold particle surface receptor density estimates and fixed at $1x10^{11}$ cm^{-2} for D_2R calculations and $3x10^{11}$ cm^{-2} for 5-HT2A receptor calculations (Nusser et al., 1997; Tanaka et al, 2005). Human and animal studies indicate that 5-HT2A receptor numbers are at least 2-3 times greater in the (prefrontal) cortex relative to D_2R in the striatum (Joyce et al., 1991; Muguruza et al., 2013; Muguruza et al., 2014; Jafari et al., 2013). k- the diffusion rate out of the synaptic compartment into bulk aqueous is written in the form k- = (D/a)g2(d/a). The value of k- chosen is based on the immunological synapse (Coombs and Goldstein 2004). k- = 1.2 x 10^{-5} cm/sec and is calculated based on a diffusion coefficient of 1 $x10^{-6}$ cm^2/sec where g2(d/a) is a dimensionless function of the immunological synapse with a radius (a) = 2 μm and the distance between synaptic surfaces (d) = 14 nm, such that g2 = 2.6 x 10^{-3}, values taken from Coombs and Goldstein (2004). The diffusion coefficient of dopamine (D) in the rat

striatum is estimated to be in the order of 1 $x10^{-6}cm^2$/sec (Nicholson and Rice, 1991).

2.2.10 Comparing binding kinetics and clinical side effect profile

To explore the role of kinetics in determining the on-target side effect liability we correlated the kinetic values determined in this study with published clinical schizophrenia treatment data taken from a comprehensive meta-analysis of clinically used APDs performed by Leucht et al., (2013). Unless otherwise stated correlation analyses were performed using a two-tailed Spearman rank correlation allowing the calculation of the correlation coefficient, r_s. Although this analysis does not assume a linear relationship, a simple trend line has been added to illustrate the positive or negative association between the two variables. Differences were considered significant at $P< 0.05$. All analyses were performed using GraphPad Prism 6.0.

Chapter 3 - Establishing a dopamine D_2 receptor-specific FRET-based competition association binding assay

3.1 Introduction

The competition association binding approach first described by Motulsky and Mahan was formulated over thirty years ago and involves the use of a previously characterised tracer to determine the kinetics of unlabelled compounds (Motulsky and Mahan 1984). This method has been central to our ability to accurately quantify the kinetics of unlabelled compounds, contributing to our overall understanding of drug action at GPCRs. Until quite recently quantifying the competition between unlabelled compounds and tracer, has largely been achieved using two methods that employ radiometric detection. Filtration binding, a non-homogeneous format (Dowling and Charlton 2006; Sykes et al., 2009; Sykes et al., 2010, Guo et al., 2012) and scintillation proximity binding, a homogeneous format allowing multiple reads from a single well (Xia et al., 2016). Although a convenient format from an assay-throughput perspective scintillation bead-based approaches suffer from several limitations. These include the need to capture membrane-associated receptors onto the surface of the scintillation bead which has a limited surface area. Therefore, signal detection can be an issue if both receptor expression levels and the specific activity of the radioligand are low. Scintillation proximity bead settling can also be a problem during signal detection and instrument constraints can also limit the temperature at which assays are performed (Xia et al., 2016). In the main filtration binding mostly, applied to membrane preparations, has been the method of choice due to reduced assay costs, temperature control and improved detection efficiency.

A homogeneous competition association method for the determination of unlabelled compounds using a fluorescent tracer was first demonstrated in whole cells expressing a terbium-labelled SNAP-tagged receptor by Schiele and colleagues using a modified competition association binding equation designed to account for signal drift due to photobleaching (Schiele et al., 2015). Whole-cell binding by its very nature may involve multiple cellular compartments which can lead to complications and ultimately inaccuracies in the interpretation of competition association binding data. The original equations which describe the competition kinetic model formulated by Motulsky and Mahan are dependent on several important factors (Motulsky and Mahan 1984). These include the presence of a single and constant receptor population and the requirement for tracer and

unlabelled compound concentrations to compete for the same binding site on the receptor and for their concentrations to remain unaltered as the reaction proceeds (Motulsky et al., 1985). A single receptor population is usually achieved by the addition of a high concentration of guanine nucleotide which uncouples the G protein from its associated receptor (Lefkowitz et al., 1976). In the whole-cell environment, it can be argued that the high intracellular concentration of GTP (~200μM, Traut (1994)) largely achieves the same outcome. Sodium ions in the binding buffer will also affect the receptor conformation that the tracer and unlabelled compound interact with via the allosteric sodium site (Neve et al., 1991) and consequently, this will also dictate the kinetic rate constants measured.

In this chapter, I will demonstrate that the kinetics of unlabelled compounds can be determined accurately and efficiently using a time-resolved FRET-based (TR-FRET) method employing terbium labelled, SNAP-tagged receptors and a fluorescent ligand with appropriate kinetic binding properties. Labelling is irreversible with a covalent bond forming a stable thioether bond between a reactive cysteine residue in the tag and the probe (terbium cryptate or Lumi4-Tb) (Gautier et al., 2008). Importantly this simple membrane-based approach makes use of the original competition association binding equations, which describe the binding of a fully reversible ligand to receptors contained within a single compartment (Motulsky and Mahan 1984).

Traditionally the first step in the competition association approach involves the accurate quantification of the tracers association and dissociation rates (or on and off-rates). This is achieved by monitoring the association of binding of increasing concentrations of the tracer and then fitting the data directly to a global association equation (Equation 2.5, Chapter 2) or through linear transformation of the observed rate of association (Equation 2.6, Chapter 2) where the slope of the resulting line is equal to the on-rate and the Y-intercept is equal to the off-rate (Motulsky and Neubig 2002). The second step involves the direct competition between a fixed concentration of the tracer and increasing concentrations of the unlabelled competitor. Using the new HTRF method described herein these two steps are effectively combined and by employing a traditional screening format (10-point curves) we can determine the association and dissociation rates and equilibrium

affinity estimates of the fluorescent tracer and the unlabelled compounds in a single step. The reliability of this method appears to be largely dependent on the kinetic properties of the tracer (and potentially the concentration of tracer employed in the binding assay). Thus, provided a tracer with suitable kinetic properties is available, up to 28 compounds can be tested on a single 384-well plate using this methodology.

3.2 Materials and Methods

3.2.1 Materials

PPHT((±)-2-(n-phenethyl-n-propyl)amino-5-hydroxytetralin hydrochloride; 1-Naphthalenol, 5,6,7,8-tetrahydro-6-[(2-phenylethyl)propylamino]) derivative labelled with a red fluorescent probe (PPHT-red) and spiperone-d2, a spiperone derivative labeled with a red emitting HTRF fluorescent probe were obtained from Cisbio Bioassays (Bagnols-sur- Cèze, France). The fluorescent ligand clozapine-Cy5 was a generous gift from Dr Rob Lane (Monash, Australia). Saponin was obtained from Sigma-Aldrich (Poole, UK). The sources of other materials used in the experiments described in the following sections are detailed in Chapter 2, section 2.1 Materials.

3.2.2 Cell culture

The host Chinese hamster ovary (CHO) K1 cell line was provided by Prof. J. Baker, University of Nottingham (ATCC #CCL-61). This was transfected with the cDNA encoding a SNAP-tagged human dopamine D_{2L} receptor (Genbank ref.: NM_000795), and a stable dilution-cloned cell line (CHO-D_{2L}) was established by zeocin resistance (200μg/mL) encoded by the plasmid vector (pcDNA3.1zeo+, Invitrogen, Paisley UK). This stable cell line expressing the SNAP-tagged human dopamine D_{2L} receptor was provided by Dr. Nicholas Holliday. Cells were maintained as detailed in Chapter 2, section 2.2.1 Cell culture.

3.2.3 Terbium labelling of SNAP-tagged D_{2L} and D_{2S} cells

Cell culture medium was removed from the t175 cm^2 flasks containing confluent adherent CHO-D_{2S} or CHO–D_{2L} cells. Cells were labelled with SNAP-Lumi4-Tb as detailed in Chapter 2, section 2.2.5 Terbium labeling of SNAP-tagged cells and membrane preparation. Before their use, SNAP-Lumi4-Tb labeled cells and membranes were thawed and resuspended in the assay buffer at a concentration of 1 million cells ml^{-1} and 0.2 mg ml^{-1} respectively.

3.2.4 Whole cell-based D_2R fluorescent ligand-binding assays and BMG Labtech PHERAstar FS performance tests

CHO-D_{2S} cells (10,000 per well) were incubated in Tag-lite® labeling medium (LABMED buffer) containing 0.02% pluronic acid in a total volume of 40μL in a white Optiplate. LABMED buffer is phosphate-based and the preferred solution to rapidly and efficiently label SNAP-tagged proteins with Lumi4Tb. This is a propriety formulation buffer its exact composition is currently unknown. Increasing concentrations of spiperone-d2 (0.056-36nM) were added to the wells in duplicate. FRET measurements were made on a BMG PHERAstar FS using the laser excitation function (1 flash per well) and specific binding of spiperone-d2 to the human dopamine $D_{2S}R$ in whole cells was observed. In addition, a series of measurements were performed on a whole-cell preparation at equilibrium comparing the lamp and laser excitation function on the BMG PHERAstar FS. Different frequencies of lamp and laser excitation were compared with excitation function assessed as the degree of error associated with each measurement (i.e. %CV was calculated). Also, the time to read 48 wells at each flash level of the lamp or laser was determined plus the relative level of donor and acceptor signal produced by the laser or lamp. Binding reactions were performed in the absence of GppNHp with non-specific-binding levels determined by the inclusion of spiperone (1 μM). Spiperone-d2 dissociation following the addition of an excess of unlabelled spiperone (1 μM) was also performed on whole cells containing a fixed concentration of spiperone-d2. The cell permeabilizing agent saponin (100 μg/mL) was added to cells in the absence and presence of an excess concentration of spiperone (1 μM) to test both the access and the reversibility of binding in this whole cell preparation.

3.2.5 Membrane-based $D_{2L}R$ fluorescent ligands binding assays

Fluorescent binding experiments using spiperone-d2, clozapine-Cy5 and PPHT-red were conducted in white 384-well Optiplate plates at physiological temperature (37°C). GppNHp (0.1 mM) was included to remove the G protein-coupled population of receptors that can result in two distinct populations of binding sites in membrane preparations since the Motulsky–Mahan model is only appropriate for ligands competing at a single site. Unless otherwise stated experiments were conducted in

two different assay buffer types; 20mM HEPES, 138mM NaCl, 6mM $MgCl_2$, 1mM EGTA, 1 mM EDTA pH 7.4, containing 1% DMSO, 0.02% pluronic acid, and 0.1% ascorbic acid (HEPES-salt buffer) or Hanks Balanced Salt Solution (HBSS, full composition see Chapter 2 section 2.1.2 Ligand binding assays) containing 5mM HEPES, 1% DMSO and 0.02% pluronic acid pH 7.4. In all cases, non-specific binding was determined in the presence of 10 μM haloperidol.

To accurately determine association-rate (k_{on}) and dissociation-rate (k_{off}) values, the observed rate of association (k_{obs}) was calculated using at least four different concentrations of either spiperone-d2, clozapine-Cy5, and PPHT-red. The appropriate concentration of fluorescent ligand was incubated with human dopamine D_{2L} CHO cell membranes (2 μg per well) in assay binding buffer (final assay volume, 40 μL) in either the absence or presence of haloperidol (10μM). The levels of specific fluorescent ligand bound to the receptor were assessed at multiple time points by HTRF detection to allow the construction of association kinetic curves. The resulting data were globally fitted to the association kinetic model (Equation 2.5, Chapter 2) to derive a single best-fit estimate for k_{on} and k_{off} as described in Chapter 2, section 2.2.8 Signal detection and data analysis. Also, data were fitted to a one-phase exponential association model (Equation 2.6, Chapter 2) to derive an estimate of k_{on} and k_{off} from plotting tracer concentration versus observed association (k_{obs}) as described in Chapter 2, section 2.2.8 Signal detection and data analysis.

3.2.6 Competition binding kinetics

To determine the association and dissociation rates of D_2R specific ligands, we used a competition-association binding assay (Motulsky and Mahan, 1984). This approach involves the simultaneous addition of both fluorescent ligand and competitor to the receptor preparation so that at t = 0 all receptors are unoccupied. To achieve this aim CHO cell membranes containing the human dopamine D_{2L} receptor (2 μg per well) were added to wells containing 12.5 nM PPHT-red (~1x K_d), a concentration which avoids ligand depletion in this assay volume, (see Carter *et al*., 2007) and different concentrations (10 in total) of unlabeled compound in a total assay volume of 40 μL. The degree of PPHT-red bound to the receptor was assessed at multiple time points by HTRF detection. In contrast, spiperone-d2 was added at concentrations of ~3-10x K_d concentrations chosen to avoid ligand

depletion in the 40 µL assay volume. Clozapine-Cy5 was added at a concentration of 50nM, significantly less than its own K_d, but a concentration intended to avoid complete association in the time taken from initial membrane addition (t=0) to the point of the first read on the PHERAstar FS. The kinetic parameters of spiperone-d2, clozapine-Cy5, and PPHT-red, plus those of unlabeled compounds were determined using a start time of ~30sec and an interval time of 20sec. Non-specific binding was determined as the amount of HTRF signal detected in the presence of haloperidol (10 µM) and was subtracted from each time point, meaning that t = 0 was always equal to zero. Each time point was conducted on the same 384-well plate incubated at 37ºC with orbital mixing (1sec of 100 RPM/cycle).

Multiple concentrations of unlabeled competitors were tested, for the determination of rate parameters. Data were globally fitted using (Equation 2.7, Chapter 2) to simultaneously calculate k_{on} and k_{off} of unlabelled compounds. Different ligand concentration ranges were chosen, as compounds with a long residence time equilibrate more slowly, so a higher relative concentration is required to ensure the experiments reach equilibrium within a reasonable time frame, while still maintaining a good signal-to-noise.

3.2.7 Data analysis and signal detection

For the binding experiments described, signal detection was performed on a PHERAstar FS (BMG Labtech, Offenburg, Germany) using standard HTRF settings (dual emission), as described in Chapter 2, section 2.2.8 Signal detection and data analysis. HTRF ratios and specific binding were calculated as describes in Chapter 2, section 2.2.8 Signal detection and data analysis.

All experiments were analyzed using GraphPad Prism 6.0. Saturation binding data were analysed by non-linear regression according to a one-site model. Fitting the total and NSB data sets simultaneously to Equation 2.1 described in Chapter 2, provides one best-fit value for both the K_d and the B_{max} of a fluorescent tracer. For presentation purposes specific binding, obtained by subtracting non-specific binding from total binding, was fitted to Equation 2.2 Chapter 2, a one-site binding model that describes a rectangular hyperbola or binding isotherm.

Competition displacement binding data were fitted to sigmoidal (variable slope) curves using a “four-parameter logistic equation”, see Equation 2.3, Chapter 2. IC_{50}

values obtained from the inhibition curves at equilibrium were converted to K_i values using the method of Cheng and Prusoff (1984), see Equation 2.4, Chapter 2.

Fluorescent-ligand association data were fitted as follows to a global fitting model using GraphPad Prism 6.0 to simultaneously calculate k_{on} and k_{off} using Equation 2.5, Chapter 2. In addition, tracer association data were analysed using non-linear regression to fit the specific binding data to a one-phase exponential association equation, see Equation 2.6, Chapter 2. Where tracer binding follows a simple law of mass action model, k_{obs} increases linearly as a function of tracer concentration. The slope of the resulting line fitted using linear regression equates to the association rate (k_{on}), and extrapolation of the plot to y = 0 yields the dissociation rate (k_{off}) (Sykes et al., 2010).

Association and dissociation rates for unlabeled antagonists were calculated using the equations described by Motulsky and Mahan (1984), see Equation 2.7, Chapter 2. Probe dissociation rates were determined by the displacement of the tracer with a large excess of an unlabeled ligand known to bind to the same site with similar or higher affinity. Dissociation of fluorescent ligand (or tracer) was fitted to Equation 2.8, Chapter 2. Outliers in a kinetic data set were identified using a two-sided Grubbs' test in GraphPad Prism 6.0. which can detect a value much larger or value much smaller than the rest (Grubbs α = 0.0001). Experimental variation was calculated as % coefficient of variance (CV) values i.e. (standard deviation/mean)*100.

3.2.8 Modelling of tracer competition curves

To simulate the change in IC_{50} data for a rapidly and slowly dissociating compound over time the kinetic parameters obtained for the appropriate tracer (Equation 2.5, Chapter 2) and unlabelled compound, derived from the Motulsky-Mahan model fits (Equation 2.7, Chapter 2) were used to reconstruct competition binding data. Kinetic parameters (k_{1-4}) were fixed to those determined in individual experiments for each tracer and the appropriate unlabelled antagonist and then the expected IC_{50} curves were recreated. Tracer binding was simulated every 20sec in the presence of various concentrations of the unlabelled compound at the indicated time points. Families of IC_{50} curves were analysed in GraphPad Prism 6.0, as described above to provide simulated IC_{50} values. IC_{50} values were derived for selected compounds from experimental data in the presence of the various tracers under different

experimental conditions. Comparisons were made of simulated IC_{50} values with measured IC_{50} values for selected compounds. IC_{50} value comparisons of measured and modelled behaviour were more easily visualised as residual plots with the residuals calculated as the difference between measured IC_{50} and modelled IC_{50} values.

3.3 Results

3.3.1 Establishing a dopamine D_2 receptor competition association binding assay

BMG PHERAstar FS settings. TR-FRET based dopamine D_2 receptor-specific binding was achieved in TagLite labelling medium (LABMED) using the high-affinity tracer spiperone-d2 (the acceptor) and whole cells expressing the dopamine D_{2S} receptor labelled with the lanthanide terbium cryptate (the donor). Once specific binding of the tracer was established a series of characterisation experiments were performed focused on the functionality of the BMG PHERAstar FS itself. Characterisation started with a series of measurements performed on whole CHO-D_{2S} cells following the addition of increasing concentrations of spiperone-d2 (i.e. a saturation experiment taken to equilibrium) comparing the lamp versus the laser excitation function on the BMG PHERAstar FS (Figure 3.1A and C).

Figure 3.1B and D illustrates the effect of increasing energy input at 337nm (i.e. increasing flashes from either lamp or laser) on the level of the signal output from the 665nm channel (acceptor emission from the fluorescent ligand). Signal output at spiperone-d2 (20nM) from both lamp and laser were linear, however, the absolute values obtained for equivalent excitation inputs (i.e. the number of flashes) are much greater (by a factor of 10) using the laser compared to the lamp.

The relative HTRF ratios (665nm/620nm *10,000) at each level of laser or lamp input would appear to be largely equivalent, however, the relative error associated with each measurement increases noticeably with the lamp at the lower flash levels (i.e. those below 8, Figure 3.1E and F).

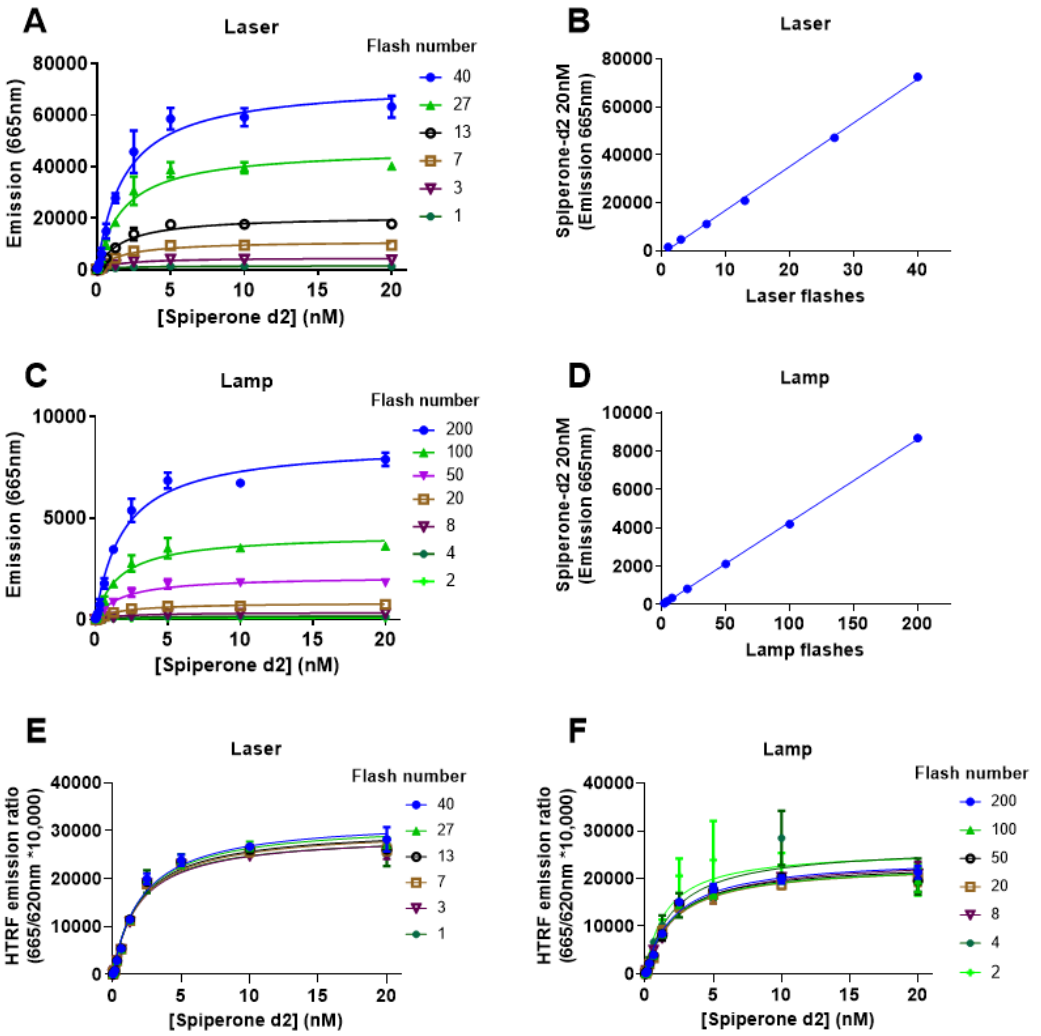


Figure 3.1. BMG Labtech PHERAstar FS performance tests comparing the lamp and laser excitation function. A series of measurements were performed on a whole CHO-D_{2S} cell preparation (10,000 cells per well) incubated with increasing concentrations of spiperone-d2 (saturation experiment) at equilibrium comparing excitation using the laser **(A)** and **(B)**, and the lamp **(C)** and **(D)**. Acceptor emission (665nm) with increasing flashes of the laser **(B)** or lamp **(D)** at a saturating concentration on spiperone-d2 (20nM) was linear. Relative HTRF ratios (665nm/620nm *10,000) at each level of laser **(E)** or lamp **(F)** flash input. The degree of error associated with each measurement at increasing concentrations of spiperone-d2 on both the laser and lamp are shown for comparison**.** Data are from a single experiment presented as mean ± range from duplicate determinations.

The manufacturer's (BMG LabTech) suggested lamp/laser input equivalency seems to be based on the time to read rather than the relative level of acceptor signal produced by the laser or lamp. For example, BMG Labtech's 40 laser flash suggested equivalent = 200 lamp flashes (Figure 3.2A and B). The levels of acceptor signal measured from the lamp or laser flash input appears to be an indicator of the level of relative error of measurements (i.e. mean %CV, measured at each concentration of tracer examined in the saturation analysis), and likely reflects the different contribution of specific versus background signal, with the latter increasing at lower levels of excitation. In the case of the laser, this level of error seems to reach a lower plateau, with increasing excitation input producing no further reduction in the mean %CV (Figure 3.3A and B). At the point of plateau, any differences in measurements likely reflect the errors associated with pipetting rather than any imperfections in detection capability.

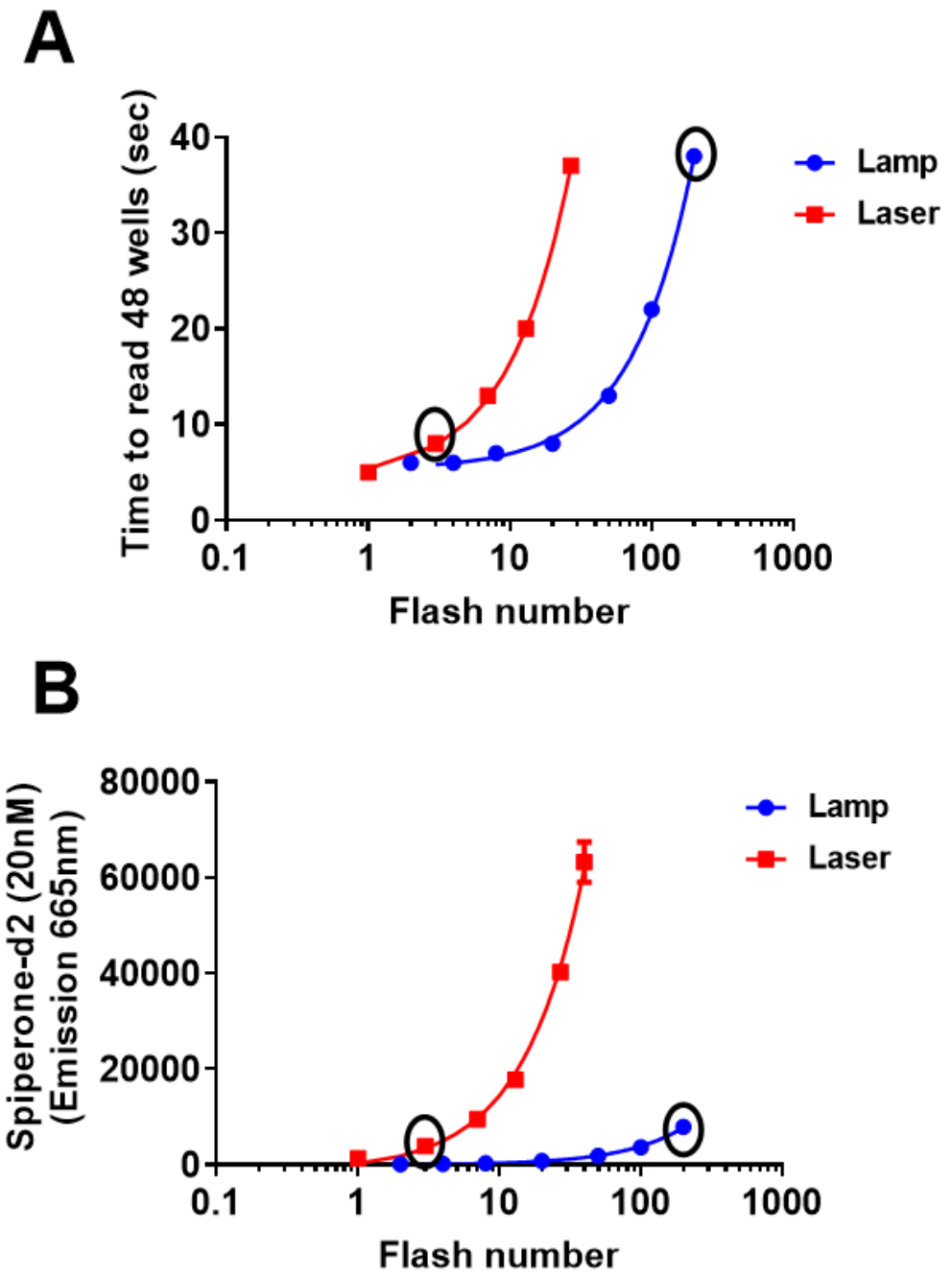


Figure 3.2. BMG Labtech PHERAstar FS performance tests comparing the lamp and laser excitation function. Comparing BMG's suggested lamp/laser input equivalency based on **(A)** time to read and **(B)** the relative level of acceptor signal produced by the laser or lamp. Data for B are taken from Figure 3.1B and D. The circles in Figure 3.2A represent the lamp and laser flash levels which produce similar acceptor emission signals, and which translates into similar measurement variabilities as judged by % CV, see Figure 3.3.

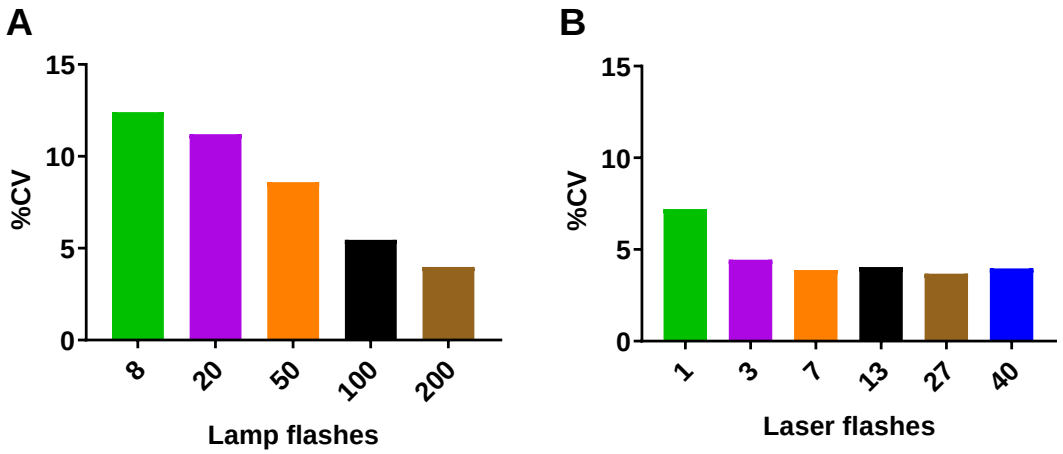


Figure 3.3. BMG Labtech PHERAstar FS performance tests comparing the lamp and laser excitation function. A series of HTRF emission ratio measurements were performed on a whole CHO-D_{2S} cell preparation incubated with increasing concentrations of spiperone-d2 (saturation experiment) at equilibrium (see Figure 3.2 E and F. Mean %CV measured across the full spiperone-d2 concentration range using the lamp **(A)** was compared to the laser **(B)**. In the case of the laser, the level of error reaches a lower plateau, with increasing excitation input producing no further reduction in the mean %CV.

3.3.2 Whole cells versus membranes

In another series of experiments, we explored the possibility of collecting kinetic data in whole CHO-D_{2S} cells at room temperature. Spiperone-d2 association curves are shown in Figure 3.4A. The corresponding relationship between tracer concentration and k_{obs} is shown in Figure 3.4B. A linear relationship between k_{obs} and spiperone-d2 was readily detected however surprisingly spiperone-d2 could not be fully dissociated using an excess of unlabelled spiperone (1 μM), see Figure 3.4C. To understand this phenomenon further we added the cell permeabilizing agent saponin (100 μg/mL) to the cells in the presence of the excess concentration of spiperone (Figure 3.4D). Under these conditions, we observed the complete displacement of the tracer. Whereas in the absence of spiperone (1 μM), the level of binding remains largely constant, suggesting that all receptors are fully accessible to the fluorescent ligand. In contrast, it is only when the cell and internal organelles are permeabilised that this allows the unlabelled spiperone to fully compete with the prebound tracer. Similar results were obtained in CHO-D_{2L} cells.

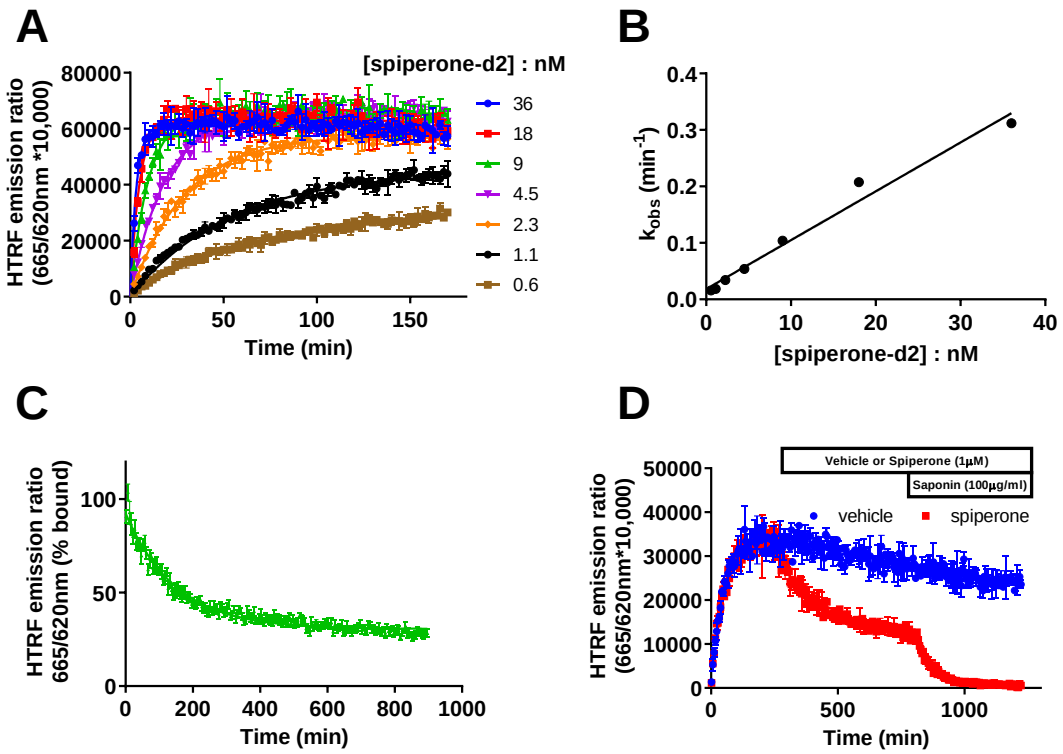


Figure 3.4. Determination of spiperone-d2 equilibrium and kinetic binding parameters in whole cells. (A) The observed association of spiperone-d2 binding to the human dopamine receptor in whole CHO-D_{2S} cells. Data are presented as a mean ± SEM, from a single experiment, with 3 replicates. **(B)** Corresponding plot of spiperone-d2 concentration versus k_{obs}. Binding appears to follow a simple law of mass action model, k_{obs} increasing linearly with fluorescent ligand concentration. Data are presented as an average from three replicates from a single experiment. Binding reactions were performed in the absence of GppNHp with non-specific-binding levels determined by the inclusion of spiperone (1 μM). Spiperone-d2 dissociation **(C)** following the addition of an excess of unlabelled spiperone (1 μM), data from a single representative experiment, with 8 replicates. **(D)** Addition of a cell permeabilizing agent, saponin (100 μg/mL) to cells in the absence and presence of an excess concentration of spiperone (1 μM), data are from a single representative experiment performed in duplicate.

3.3.3 Characterisation of dopamine-d2 binding in HBSS

Specific binding of the fluorescent antagonist spiperone-d2 to human D_{2L} receptor ($hD_{2L}R$) expressed in CHO cell membranes was fitted to a one-site model. Fitting the total and NSB data sets simultaneously to Equation 2.1 described in Chapter 2 section 2.2.8 Signal detection and data analysis, provides one best-fit value for both the K_d and the B_{max} of a fluorescent tracer. Specific binding was saturable, whilst non-specific binding was linear and represented only a small fraction (<10%) of total binding (Figure 3.5A). From these HTRF-based binding studies, the equilibrium dissociation constant (K_d) of the fluorescent ligand spiperone-d2 was determined to be 0.23 ± 0.09 nM, n=4. For presentation purposes specific binding, obtained by subtracting non-specific binding from total binding, was fitted to Equation 2.2, described in Chapter 2 section 2.2.8 Signal detection and data analysis, a one-site binding model that describes a rectangular hyperbola or binding isotherm.

The binding kinetics of the tracer spiperone-d2 were characterized by monitoring the observed association rates (k_{obs}) at six different concentrations (Figure 3.5B). The resulting association data were fitted to Equation 2.5, Chapter 2. The observed rate of association was linearly related to spiperone-d2 concentration (Figure 3.5C), the slope of this line being equal to its association rate constant (k_{on}) and the Y-intercept its dissociation rate constant (k_{off}). Kinetic rate parameters for spiperone-d2 used in the competition-association binding analysis were calculated by globally fitting the association time course, resulting in a mean k_{on} (k1) of 1.93 ± 0.49 $\times 10^8 M^{-1}$ min^{-1} and a mean k_{off} (k2) of 0.029 ± 0.006 min^{-1}, n=4. The resulting kinetic K_d (k_{off} / k_{on}) of 0.22 ± 0.09 nM was identical to that obtained from the equilibrium studies, n=4. Kinetic off-rates and equilibrium affinity parameters obtained from the linear fit of k_{obs} versus spiperone-d2 concentration differed significantly from those obtained from the global fitting of the association time courses. Equilibrium and kinetic binding parameters for spiperone-d2 binding to the $hD_{2L}R$ in HBSS are summarised in Table 3.1.

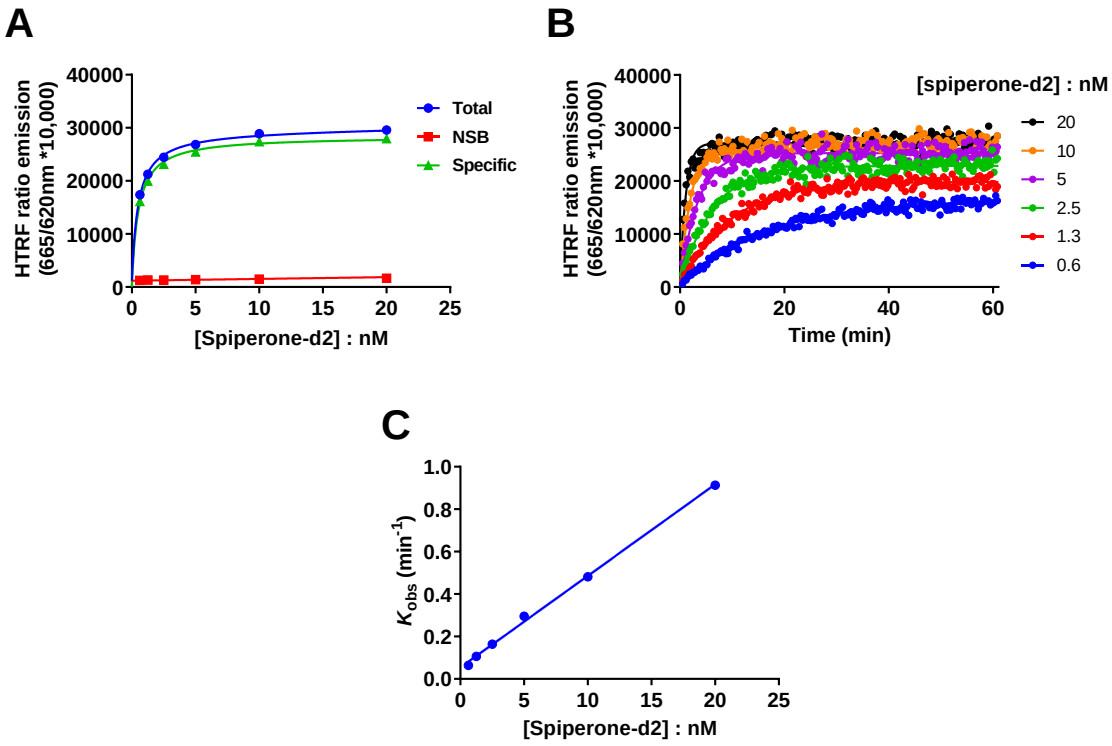


Figure 3.5. Determination of spiperone-d2 equilibrium and kinetic binding parameters. (A) Saturation analysis showing the binding of spiperone-d2 to the human dopamine $D_{2L}R$. CHO–$D_{2L}R$ cell membranes (2 µg per well) were incubated in HBSS buffer for 60 min with gentle agitation with increasing concentrations of spiperone-d2. Data are presented in singlet form from a representative of 4 experiments. **(B)** The observed association of spiperone-d2 binding to the human dopamine $D_{2L}R$. Data are presented in singlet form from a representative of 4 experiments. **(C)** A plot of spiperone-d2 concentration versus k_{obs}. Binding followed a simple law of mass action model, k_{obs} increasing linearly with fluorescent ligand concentration. All binding data are presented in singlet form from a representative of 4 experiments. Binding reactions were performed in HBSS containing 5mM HEPES, 1% DMSO and 0.02% pluronic acid pH 7.4 in the presence of GppNHp (0.1mM) with non-specific-binding levels determined by the inclusion of haloperidol (10µM).

The binding affinity of a range of ligands with rapid off-rates from the $hD_{2L}R$ was measured at 37 °C in HBSS buffer containing 5′-guanylyl imidodiphosphate (GppNHp) (0.1 mM) to ensure that antagonist binding only occurred to the G protein-uncoupled form of the receptor. Binding affinities (K_i values) for the ligands studied are summarized in Table 3.2, and representative competition curves are presented in Figure 3.6A.

Representative spiperone-d2 competition association curves for selected D_2R ligands are shown in Figure 3.6B to D. Progression curves for spiperone-d2 alone and in the presence of competitor were globally fitted to Equation 2.7, Chapter 2 which in the case of paliperidone enabled the calculation of both k_{on} (k3) and k_{off} (k4) as reported in Table 3.2. In all other instances, the model fitting proved unreliable with a large proportion of fits proving to be ambiguous or with unrealistic estimates in the off and on-rates which varied widely. Ambiguous fits are those for which confidence intervals are extremely wide and therefore not reported by Prism 6.0.

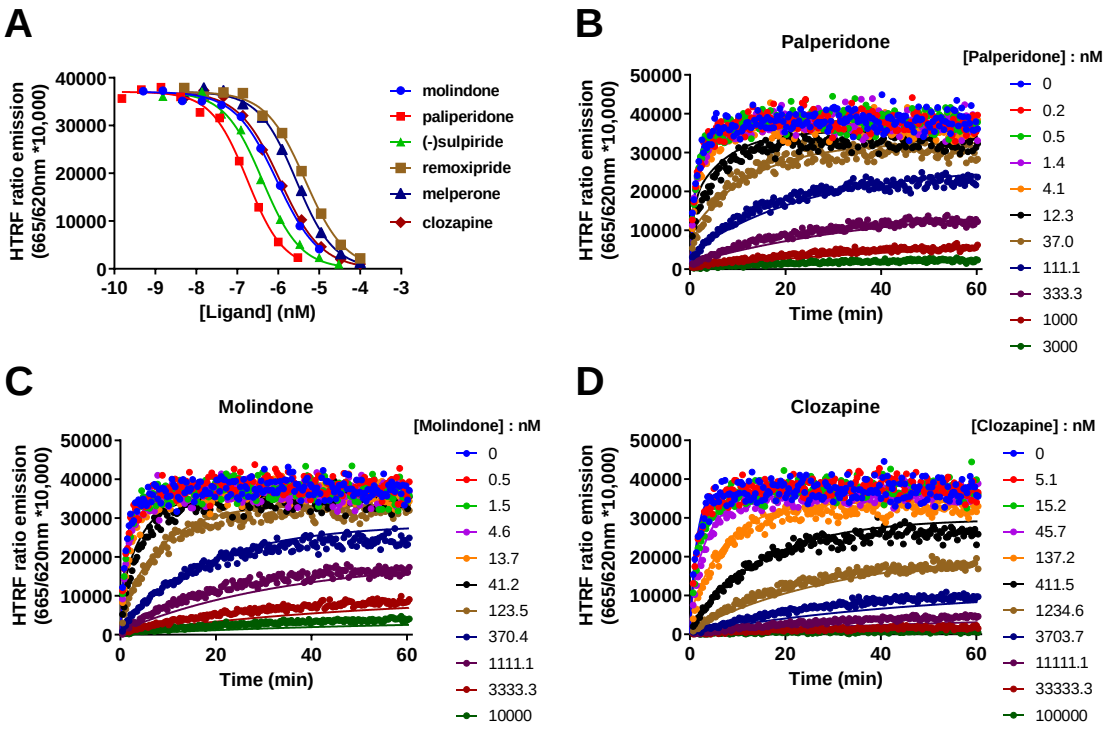


Figure 3.6. Equilibrium and competition association binding in HBSS buffer. **(A)** Competition between spiperone-d2 (2 nM) and increasing concentrations of representative atypical and typical APDs molindone, paliperidone, (−)sulpiride, remoxipride, melperone and clozapine for the human dopamine $D_{2L}R$. Spiperone-d2 competition association curves in the presence of **(B)** paliperidone, **(C)** molindone, and **(D)** clozapine. All binding reactions were performed in HBSS containing 5mM HEPES, 1% DMSO and 0.02% pluronic acid pH 7.4 in the presence of GppNHp (0.1mM) with non-specific-binding levels determined by the inclusion of haloperidol (10 μM). Equilibrium data were fitted to Equation 2.3, Chapter 2 described in Methods section to calculate K_i values using the Cheng-Prusoff correction (Equation 2.4, Chapter 2) and kinetic association data to Equation 2.7, Chapter 2 to calculate K_d, and k_{on} and k_{off} values for the unlabeled ligands; these are summarized in Table 3.2. Data are presented as singlet values from a representative of three separate experiments. All data used in these plots are summarised in Table 3.1 and 3.2.

3.3.4 Characterisation of clozapine-Cy5 binding in HBSS

The fluorescent antagonist clozapine-Cy5 produced concentration-dependent increases in specific binding to the $hD_{2L}R$ expressed in CHO membranes however full saturation was not achieved (Figure 3.7A). Non-specific binding was linear representing ~20% of total binding. From these studies, the equilibrium dissociation constant (K_d) of clozapine-Cy5 was determined to be 431 ± 125 nM, n=5.

The binding kinetics of clozapine-Cy5 were characterized by monitoring the observed association rates for six different ligand concentrations (Figure 3.7B). The observed rate of association was related to clozapine-Cy5 concentration in a linear fashion (Figure 3.7C), allowing an estimation of k_{on} (slope) and k_{off} (Y-intercept). Kinetic rate parameters for clozapine-Cy5 used in the competition-association binding studies were calculated by globally fitting the association time courses, resulting in a k_{on} (k1) of 2.53 ± 0.71 $\times 10^6 M^{-1}$ min^{-1} and a k_{off} (k2) of 0.78 ± 0.07 min^{-1}, n=5. The resulting K_d (k_{off} / k_{on}) of 295 ± 60 nM was similar to that obtained from the equilibrium studies. The kinetic parameters obtained from the linear fit of k_{obs} versus clozapine-Cy5 concentration proved to be almost identical to those obtained from the global fitting of clozapine-Cy5 association curves. Equilibrium and kinetic binding parameters for clozapine-Cy5 binding to the $hD_{2L}R$ in HBSS are summarised in Table 3.3.

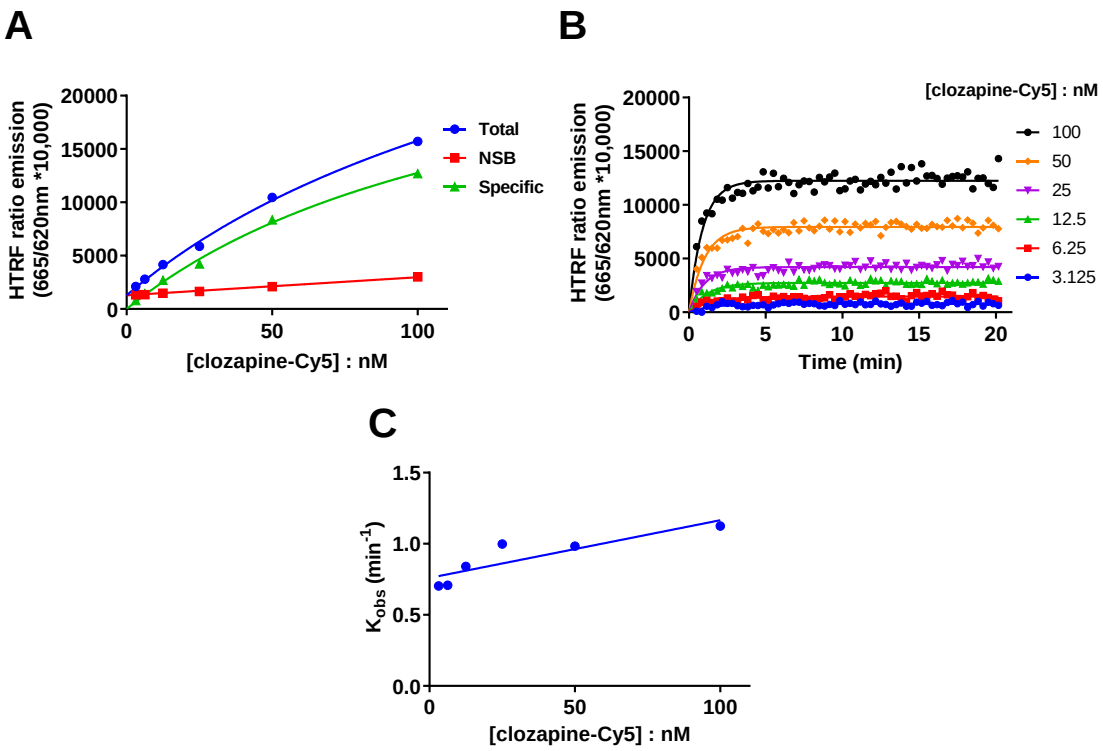


Figure 3.7. Determination of clozapine-Cy5 equilibrium and kinetic binding parameters. (A) Saturation analysis showing the binding of clozapine-Cy5 to the human dopamine $D_{2L}R$. CHO-$D_{2L}R$ cell membranes (2 µg per well) were incubated for up to 60 min with gentle agitation with increasing concentrations of clozapine-Cy5 in assay buffer HBSS. Data are presented in singlet form from a representative of 5 experiments. **(B)** The observed association of clozapine-Cy5 binding to the human dopamine $D_{2L}R$. Data are presented in singlet form from a representative of 5 experiments. **(C)** A plot of clozapine-Cy5 concentration versus k_{obs}. Binding followed a simple law of mass action model, k_{obs} increasing linearly with fluorescent ligand concentration. All binding data are presented in singlet form from a representative of 5 experiments. Binding reactions were performed in HBSS containing 5mM HEPES, 1% DMSO and 0.02% pluronic acid pH 7.4 in the presence of GppNHp (0.1mM) with non-specific-binding levels determined by the inclusion of haloperidol (10 µM). All data used in these plots are summarised in Table 3.3.

As previously described for spiperone-d2 binding the binding affinities of ligands with rapid off-rates from the human $D_{2L}R$ were measured at 37 °C in HBSS containing GppNHp (0.1 mM). Binding affinities (reported as K_i values) for the ligands studied are summarized in Table 3.4, and representative competition curves are presented in Figure 3.8A.

Representative clozapine-Cy5 competition association curves for selected dopamine D_2R specific ligands are shown in Figure 3.8B to D. Progression curves for clozapine-Cy5 alone and in the presence of competitor were globally fitted to Equation 2.7, Chapter 2 which enabled the calculation of both k_{on} (k3) and k_{off} (k4) as reported in Table 3.4. In the majority of instances, fitting proved to be reliable however some curve fits removed or rejected due to ambiguity in the fit. Ambiguous fits are those for which confidence intervals are extremely wide and therefore not reported by Prism 6.0. For molindone only two out of the four curve fits attempted proved reliable. From a high throughput perspective this and the overall average rate of fit failure (~1 in 4) is still problematic leading us to a search for an alternative tracer.

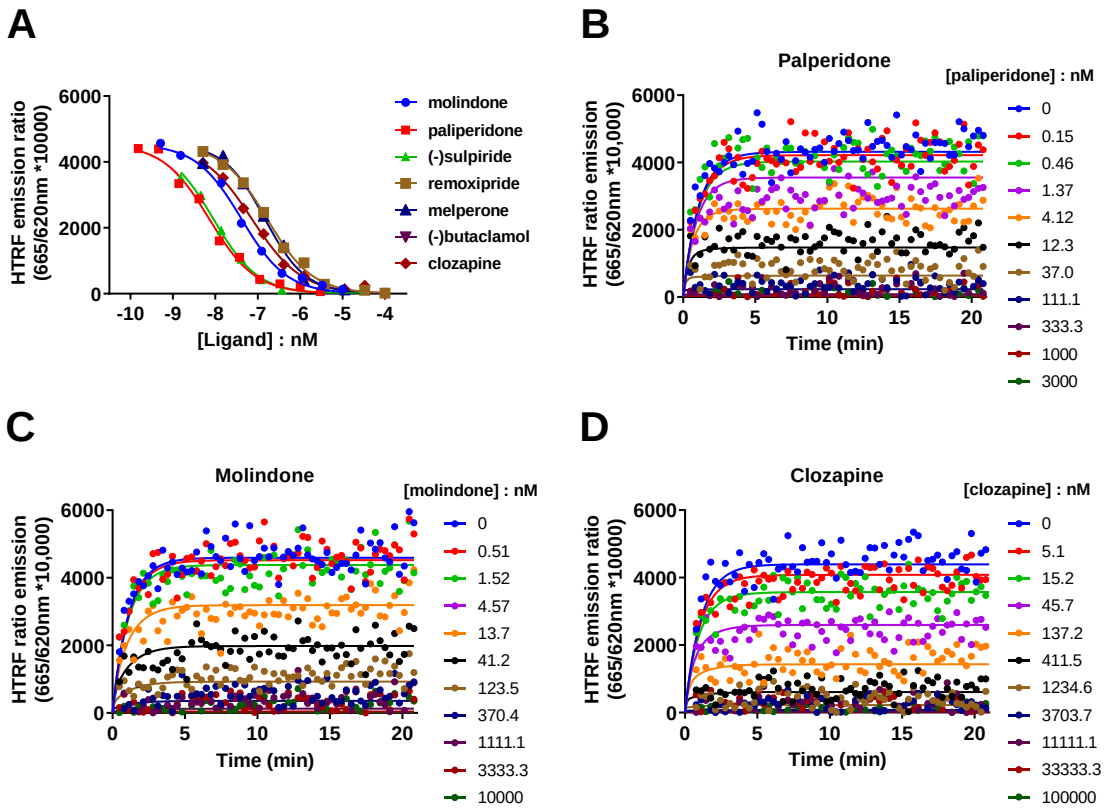


Figure 3.8. Equilibrium and competition association binding in HBSS buffer. **(A)** Competition between clozapine-Cy5 (~50 nM) and increasing concentrations of representative APDs molindone, paliperidone, (−)sulipride, remoxipride, melperone and clozapine for the human dopamine $D_{2L}R$. Clozapine-Cy5 competition association curves in the presence of **(B)** paliperidone, **(C)** molindone, and **(D)** clozapine. All binding reactions were performed in HBSS containing 5mM HEPES, 1% DMSO and 0.02% pluronic acid pH 7.4 in the presence of GppNHp (0.1mM) with non-specific-binding levels determined by the inclusion of haloperidol (10 μM). Equilibrium data were fitted Equation 2.3 and 2.4, Chapter 2 described in the Methods section to calculate K_i, and clozapine-Cy5 competition association binding data to Equation 2.7, Chapter 2 to calculate K_d and k_{on} and k_{off} values for the unlabeled ligands; these are summarized in Table 3.4. Data are presented as singlet values and representative of four separate experiments. All data used in these plots are summarised in Table 3.3 and 3.4.

3.3.5 Characterisation of PPHT-red binding in a HEPES-based buffer (HEPES-salt)

The availability of the PPHT-red provided by CisBio gave us another opportunity to assess the kinetics of a range of rapidly and slowly dissociating dopamine D_2R specific ligands. Also in view of the poor fits achieved with fluorescent spiperone and clozapine in HBSS buffer I swapped to a HEPES-based buffer recommended by Klein-Herenbrink (personal communication) but increased the sodium chloride levels to a value identical to that contained in the more physiological buffer HBSS, 138mM.

Specific binding of the fluorescent antagonist PPHT-red to the $hD_{2L}R$ expressed in CHO membranes was saturable with non-specific binding representing <25% of total binding (Figure 3.9A). From these studies, the equilibrium dissociation constant (K_d) of PPHT-red was determined to be 21.9 ± 4.1 nM, n=6.

The binding kinetics of PPHT-red were characterized by monitoring the observed association rates at six different ligand concentrations (Figure 3.9B). The observed rate of association was related to PPHT-red concentration in a linear fashion (Figure 3.9C), allowing an estimation of on and off-rates. Kinetic rate parameters for PPHT-red used in competition association studies were calculated by globally fitting the association time courses, resulting in a k_{on} (k1) of 2.1 ± 0.3 $\times 10^7 M^{-1}$ min^{-1} and a k_{off} (k2) of 0.35 ± 0.02 min^{-1}. The resulting K_d (k_{off} / k_{on}) of 18.3 ± 0.2 nM was similar to that obtained from the equilibrium studies described above. PPHT-red dissociation estimated directly through the addition of an excess of haloperidol revealed a k_{off} value of 0.52 ± 0.04 min^{-1}, which was in good agreement with the value estimated from the global association time course described above. Equilibrium and kinetic binding parameters for PPHT-red binding to the $hD_{2L}R$ in a HEPES-salt buffer, containing 138mM sodium chloride are summarised in Table 3.5.

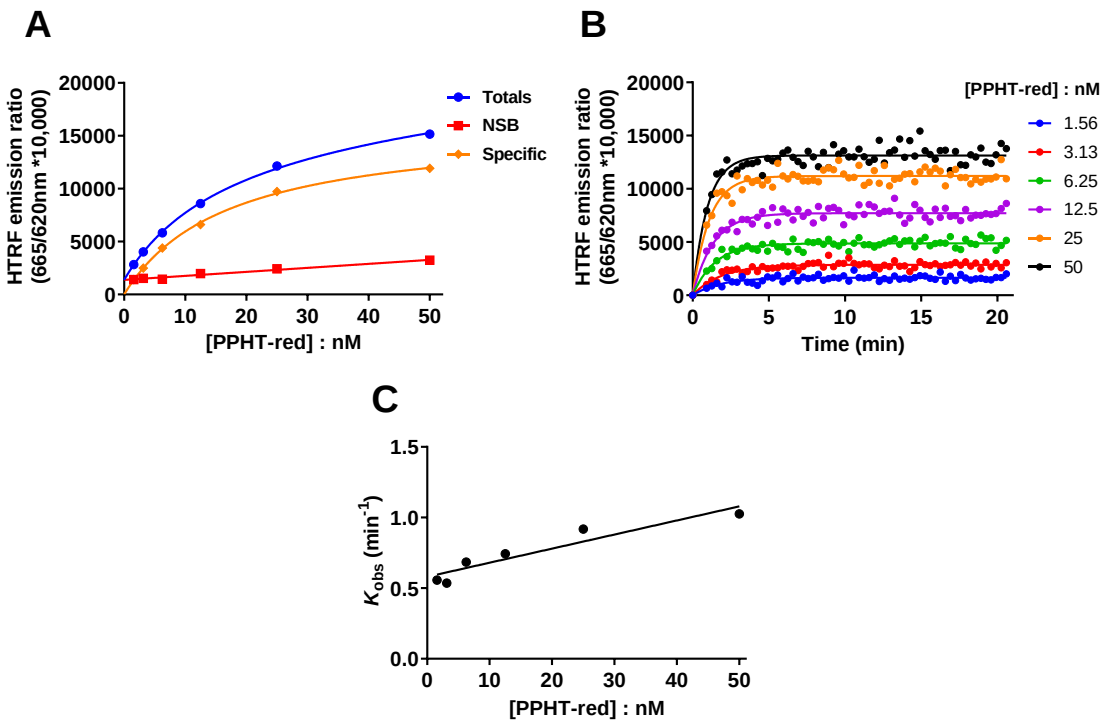


Figure 3.9. Determination of PPHT-red equilibrium and kinetic binding parameters. (A) Saturation analysis showing the binding of PPHT-red to the human dopamine $D_{2L}R$. CHO–$D_{2L}R$ cell membranes (2 µg per well) were incubated for up to 120 min with gentle agitation with increasing concentrations of PPHT-red. Data are presented in singlet form from a representative of 6 experiments. **(B)** The observed association of PPHT-red binding to the human dopamine $D_{2L}R$. Data are presented in singlet form representative of 6 experiments. **(C)** A plot of PPHT-red concentration versus k_{obs}. Binding followed a simple law of mass action model, k_{obs} increasing linearly with fluorescent ligand concentration. All binding data are presented in singlet form representative of 6 experiments. Binding reactions were performed in a HEPES-based binding buffer (HEPES-salt buffer containing 138mM sodium chloride), in the presence of GppNHp (0.1mM) with non-specific-binding levels determined by the inclusion of haloperidol (10 µM). All data used in these plots are summarised in Table 3.5.

Representative PPHT-red competition association binding curves for selected D_2R specific ligands are shown in Figure 3.10A to G. Progression curves for PPHT-red alone and in the presence of competitor were globally fitted to Equation 2.7, Chapter 2 which enabled the calculation of both k_{on} (k3) and k_{off} (k4) as reported in Table 3.6. In all instances, fitting proved to be extremely reliable.

When the dissociation rate constant of the competing ligand is slower than that of the tracer ligand (k4<k2), it is the dissociation rate constant of the competing ligand (k4) that determines the rate of approach to equilibrium. Such cases are characterised by an overshoot in tracer binding as was observed for domperidone, lisuride, nemonapride, and bromocriptine, see Figure 3.10D-G. When k4>k2 it is the dissociation rate of the tracer which largely determines the time to equilibrium, see Figure 3.10A-C. Equilibrium being the point at which the concentration of receptor bound tracer remains constant and no longer changes.

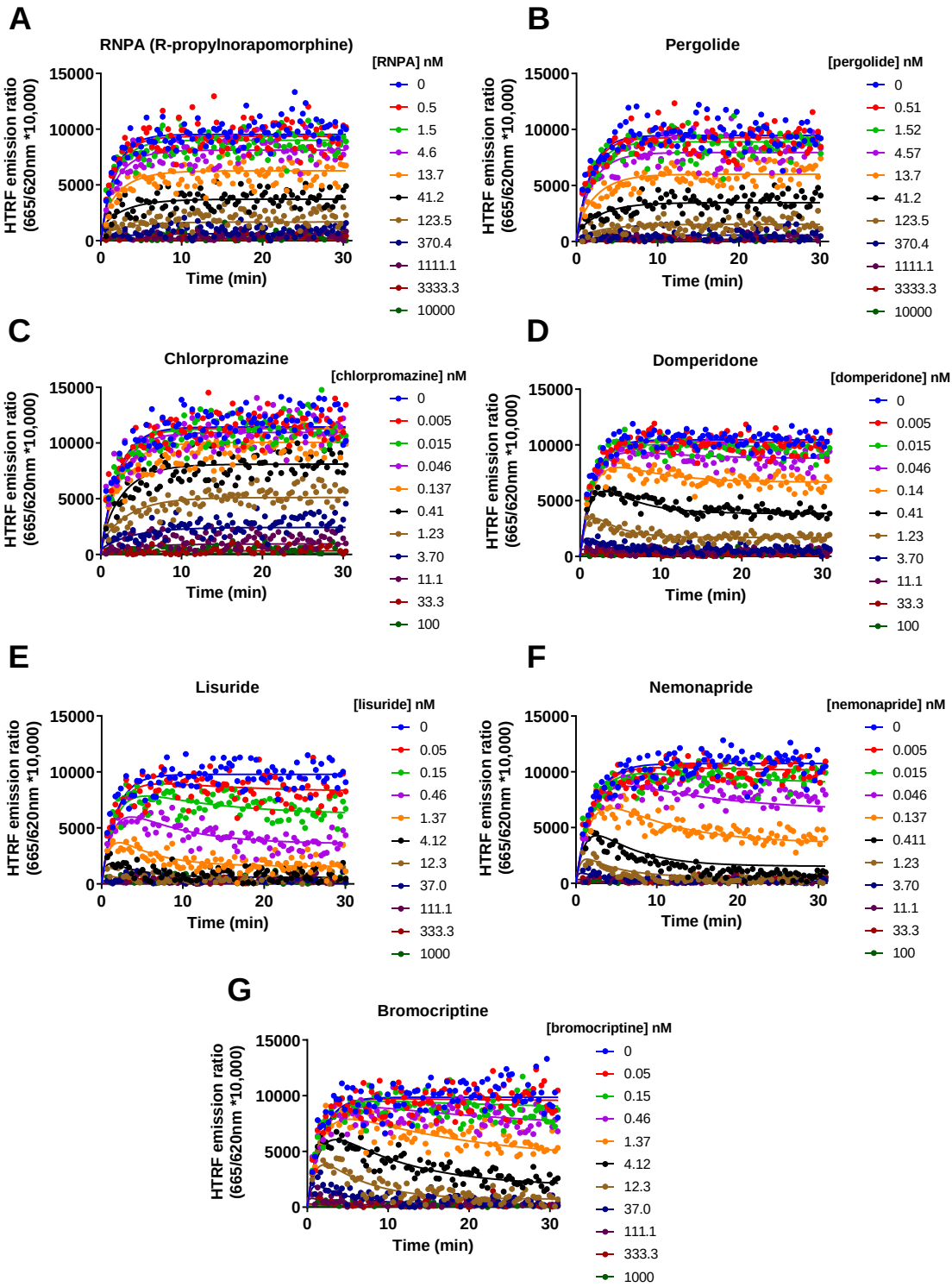


Figure 3.10. PPHT-red competition association binding to the human dopamine D_2 receptor. Competition between PPHT-red (~12.5 nM) and increasing concentrations of **(A)** RNPA, **(B)** pergolide, **(C)** chlorpromazine, **(D)** domperidone, **(E)** lisuride, **(F)** nemonapride, **(G)** bromocriptine, for the human dopamine $D_{2L}R$. All binding reactions were performed in a HEPES-based binding buffer (HEPES-salt

buffer containing 138mM sodium chloride) in the presence of GppNHp (0.1mM) with non-specific-binding levels determined by the inclusion of haloperidol (10 μM). Equilibrium data were fitted Equation 2.3 and 2.4 described in Chapter 2 to calculate K_i, and PPHT-red competition association binding data to Equation 2.7 to calculate K_d and k_{on} and k_{off} values for the unlabeled ligands; these are summarized in Table 3.6. Data are presented as singlet values from a representative of 4-6 experiments. All data used in these plots are summarised in Table 3.5 and 3.6.

In addition to obtaining equilibrium competition IC_{50} measurements at equilibrium (120min), IC_{50} estimates were also determined at 1 min following the addition of membranes so that the relative change in competitor IC_{50} could be calculated for each ligand under test. The IC_{50} fits obtained for a rapidly dissociating and a slowly dissociating compound in competition with the tracer PPHT-red changes are shown in Figure 3.11A.

The IC_{50} values determined from these inhibitory binding curves obtained with the slowly dissociating compound bromocriptine in the presence of the more rapidly dissociating tracer PPHT-red changes dramatically with time, from the first min of the binding reaction to a point at equilibrium. Each of these time points essentially represents a snapshot of a phase of competition between the unlabelled drug and the labeled tracer for the $hD_{2L}R$ as they compete for free receptors on their approach to equilibrium. In this instance, bromocriptine slowly binds to the free dopamine receptors and so it appears to be less potent at the earliest time points. However, as the binding reaction proceeds the unlabelled compound effectively starts to 'outcompete' the tracer, the speed at which this occurs is partly dependent on its off-rate and the concentration of tracer added.

In contrast, the IC_{50} of the more rapidly dissociating compound pergolide remains almost constant over the time course of the binding reaction, from the first min to a point at equilibrium. In this instance, the rapidly dissociating compound effectively binds to the D_2R at a rate similar to the tracer and so it appears to be equally potent at the very earlist time point (1min) as it is at the point when equilibrium is been established (120min). There is a small rightward shift of the pergolide IC_{50} curve at the 120min time point indicative of the fact that pergolide is more rapidly dissociating than the tracer.

For each compound shown in Figure 3.10, the relative difference in IC_{50} values obtained at 1 and 120min and expressed as a ratio were plotted against the kinetic off-rates measured. A seemingly linear relationship was observed demonstrating the reliability of this method as a useful predictor of the relative off-rates of unlabelled compounds (Figure 3.11B).

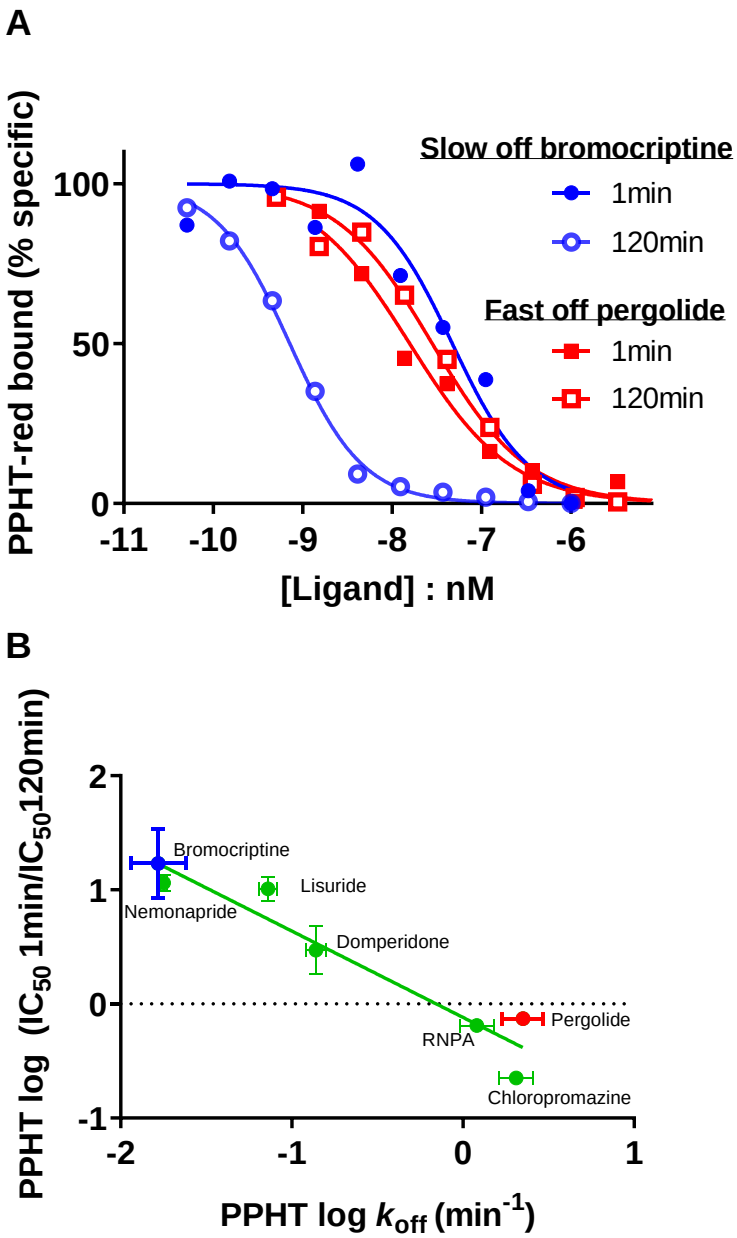


Figure 3.11. Competitive displacement of PPHT-red binding to the dopamine D_2 receptor. (A) Representative concentration-inhibition curves for pergolide and bromocriptine at 1 min and 120min. Each assay was performed in singlet and normalized to 0% and 100% specific PPHT-red D_2R binding. **(B)** Ratio of the unlabelled compound IC_{50} values determined at 1 min divided by the IC_{50} value determined at 120 min plotted against their measured k_{off} values determined in the competition association assay. Data are presented as mean values from a representative of 4-6. All kinetic data used in these plots are detailed in Table 3.6.

3.3.6 Characterisation of Spiperone-d2 binding in a HEPES based buffer (HEPES-salt)

Following our success with PPHT-red in the HEPES based buffer we decided to re-test spiperone-d2 in this same buffer to reassess its potential to quantify the kinetics of rapidly and slowly dissociating dopamine D_2R specific ligands. Specific binding of the antagonist spiperone-d2 to the $hD_{2L}R$ expressed in CHO membranes was saturable (Figure 3.12A), with non-specific binding representing less than 15 % of total binding. From these studies, the equilibrium dissociation constant (K_d) of spiperone-d2 was determined to be 0.64 ± 0.18 nM, n=6.

The binding kinetics of spiperone-d2 was characterized by monitoring the observed association rates at six different ligand concentrations (Figure 3.12B). Kinetic rate parameters for spiperone-d2 were calculated by globally fitting the association time courses, resulting in a k_{on} (k1) of 1.33 ± 0.20 $\times 10^8$ M^{-1} min^{-1} and a k_{off} (k2) of 0.074 ± 0.013 min^{-1}. The resulting K_d (k_{off} / k_{on}) of 0.68 ± 0.19 nM was similar to that obtained from the equilibrium studies. The observed rate of association was linearly related to the spiperone-d2 concentration (Figure 3.12C) however the kinetic off-rate estimated was almost 3-fold faster than predicted from the global association analysis described above resulting in an apparent underestimation of spiperone-d2's affinity for the receptor. Ligand dissociation estimated directly through the addition of an excess of haloperidol revealed a k_{off} value of 0.09 ± 0.01 min^{-1}, which was in good agreement with the value estimated from the global association time course described above (Figure 3.12D). Equilibrium and kinetic binding parameters for spiperone-d2 binding to the $hD_{2L}R$ in a HEPES-salt, 138mM sodium chloride are summarised in Table 3.7.

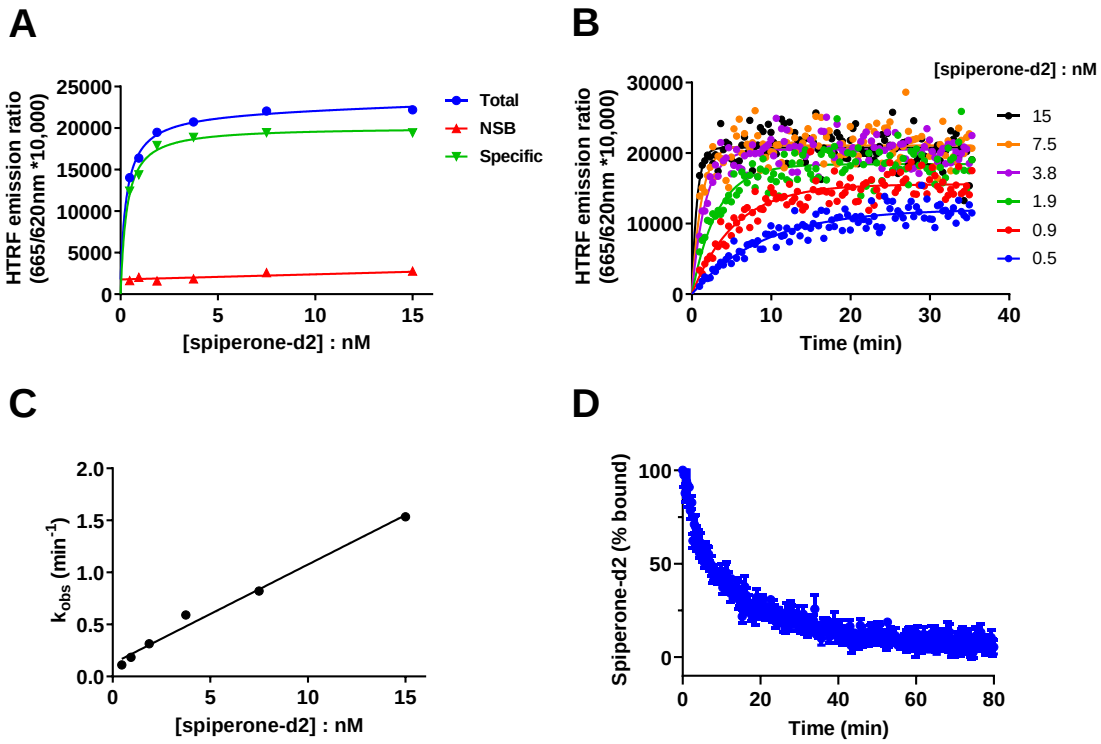


Figure 3.12. Determination of spiperone-d2 equilibrium and kinetic binding parameters. (A) Saturation analysis showing the binding of spiperone-d2 to the human dopamine $D_{2L}R$ determined in a HEPES-based binding buffer (HEPES-salt, 138mM sodium chloride). CHO-$D_{2L}R$ cell membranes (2 µg per well) were incubated for up to 120 min with gentle agitation with increasing concentrations of spiperone-d2. Data are presented in singlet form from a representative of 6 experiments. **(B)** The observed association of spiperone-d2 binding to the human dopamine $D_{2L}R$. Data are presented in singlet form from a representative of 6 experiments. **(C)** A plot of spiperone-d2 concentration versus k_{obs}. Binding followed a simple law of mass action model, k_{obs} increasing linearly with fluorescent ligand concentration. **(D)** Spiperone-d2 dissociation following the addition of haloperidol (10 µM). Data are presented as mean ± S.E.M. from a total of 6 experiments. All binding reactions were performed in the presence of GppNHp (0.1mM) with non-specific-binding levels determined by the inclusion of haloperidol (10 µM).

As described for PPHT-red binding the binding affinity of the same collection of ligands with both rapid and slow off-rates from the $hD_{2L}R$ was measured at equilibrium at 37 °C in a HEPES-based buffer (HEPES-salt, 138mM sodium chloride) containing GppNHp (0.1 mM). Binding affinities (expressed as K_i values) for the ligands studied are summarized in Table 3.8.

Representative spiperone-d2 competition association binding curves for selected D_2R specific ligands are shown in Figure 3.13A to G. Progression curves for spiperone-d2 alone and in the presence of competitor were globally fitted to Equation 2.7, Chapter 2 which enabled the calculation of both k_{on} (k3) and k_{off} (k4) as reported in Table 3.8. k1 and k2 were fixed according to the global association model of tracer binding. In the majority of instances, fitting proved to be reliable with only a single curve removed due to ambiguity in the fit. However, there was a noticeable and consistent difference in the kinetic on-rates of the unlabelled compounds tested compared to those obtained using PPHT-red (and therefore in the predicted the affinities of these compounds).

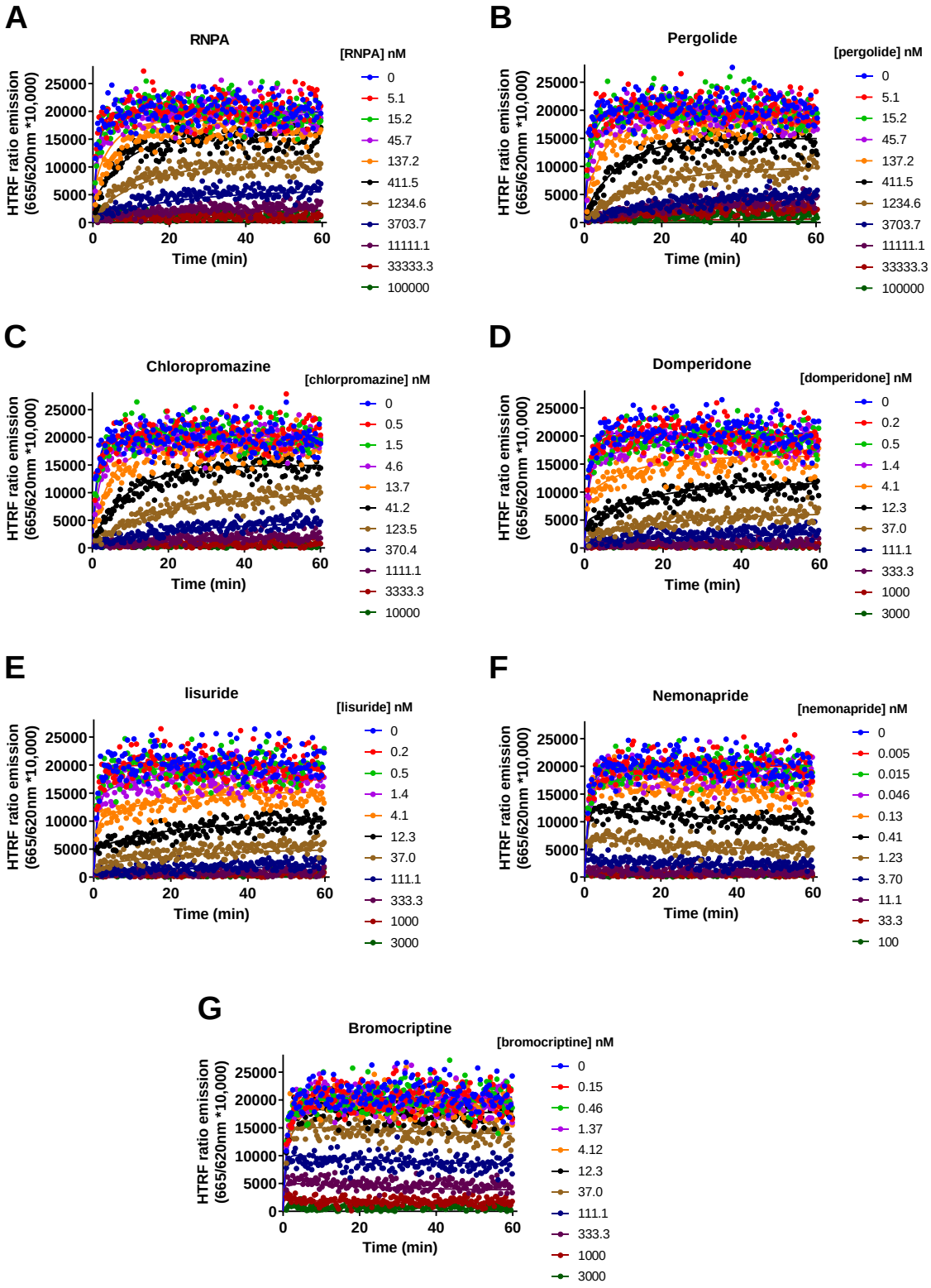


Figure 3.13. Spiperone-d2 competition association binding to the human dopamine D_2 receptor. Competition between spiperone-d2 (~5 nM) and increasing concentrations of **(A)** RNPA, **(B)** pergolide, **(C)** chlorpromazine, **(D)** domperidone, **(E)** lisuride, **(F)** nemonapride, **(G)** bromocriptine, for the human dopamine $D_{2L}R$. All

binding reactions were performed in HEPES-based binding buffer (HEPES-salt buffer containing 138mM sodium chloride), in the presence of GppNHp (0.1mM) with non-specific-binding levels determined by the inclusion of haloperidol (10 μM). Equilibrium data were fitted Equation 2.3 and 2.4 described in Chapter 2 to calculate K_i, and kinetic association data to Equation 2.7 to calculate K_d and k_{on} and k_{off} values for the unlabeled ligands; these are summarized in Table 3.8. Data are presented as singlet values from a representative of 3-6 experiments. All data used in these plots are detailed in Table 3.7 and 3.8.

As described previously following the addition of membranes, IC_{50} measurements for each test ligand in competition with the slowly dissociating tracer spiperone-d2 were obtained under both non-equilibrium (1min) and equilibrium conditions (120min). The IC_{50} fits obtained for a rapidly dissociating and a slowly dissociating compound in competition with spiperone-d2 are shown in Figure 3.14.

The IC_{50s} values estimated from the inhibitory binding curves obtained with the rapidly dissociating compound pergolide in the presence of a slowly dissociating tracer change dramatically over the time-course of the binding reaction from the first min to a point of equilibrium (120min). In this instance, the rapidly dissociating compound binds first to the free dopamine receptors and so it appears to be more potent at this very early time point (1min), but then the concentration-inhibition curve gradually shifts to the right. This is because as the binding reaction proceeds, the tracer effectively starts to 'outcompete' the unlabelled compound, the speed at which this occurs is partly dependent on its off-rate and, the concentration of tracer added.

In contrast, the IC_{50} values of the more slowly dissociating compound bromocriptine remain almost constant over the time-course of the binding reaction from the first min to a point at equilibrium (120 min). In this instance, the slowly dissociating compound binds slowly to the D_2R and at a rate similar to that of the tracer and so it appears to be equally potent at early time points (min) and at the point when equilibrium is established (hours later).

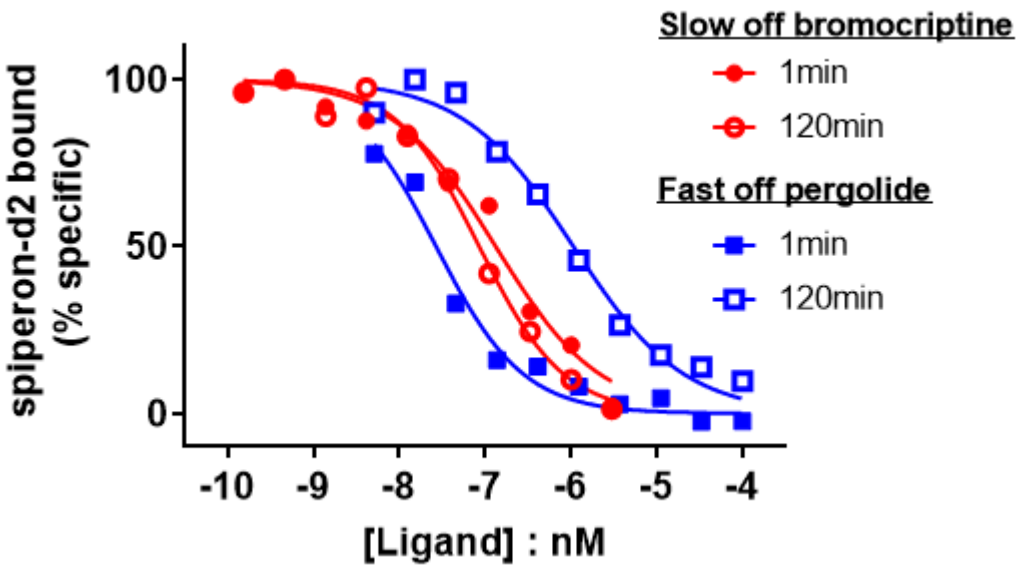


Figure 3.14. Competitive displacement of spiperone-d2 binding to the dopamine D_2 receptor. Representative concentration-inhibition curves for pergolide and bromocriptine at 1 min and 120min. Each assay was performed in singlet and normalized to 0% and 100% specific spiperone-d2 D_2R binding.

Changes in compound IC_{50} are plotted against measured kinetic off-rates for the tracer spiperone-d2 (Figure 3.15A). Finally, the compound off-rates obtained with the antagonist spiperone-d2 and the agonist PPHT-red are plotted against each other as measured k_{off} values (Figure 3.15B) and as the relative changes in competitor IC_{50} values calculated from measurements taken at 1 and 120mins (Figure 3.15C).

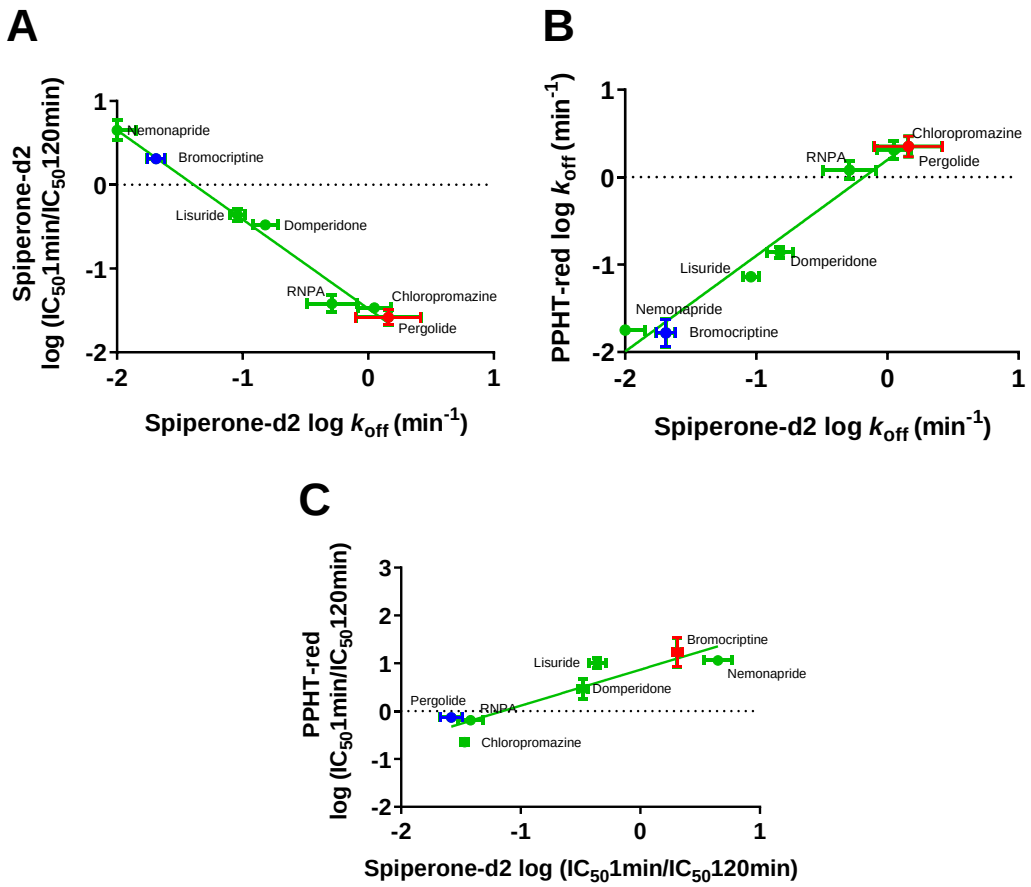


Figure 3.15. Correlating kinetic measurements made using the rapidly dissociating tracer PPHT-red and the slowly dissociating tracer spiperone-d2. (**A)** Measured compound k_{off} values determined in the competition association assay using spiperone-d2 as the tracer versus the ratio of the unlabelled compound IC_{50} values determined at 1 min and 120 min. **(B)** Measured compound k_{off} values determined in the competition association assay using the slowly dissociating spiperone-d2 versus those determined using PPHT-red. **(C)** Ratio of the unlabelled compound IC_{50} values determined at 1 min and 120 min using spiperone-d2 versus those determined by PPHT-red. Data are presented as mean values from a representative of 4-6 experiments. All kinetic data used in these plots are detailed in Table 3.6 and 3.8.

3.3.7 Experimental and modelled IC_{50} curves

The competition association model fits for the slowly dissociating tracer spiperone-d2 obtained in HBSS in the presence of the rapidly dissociating competitor molindone did not produce modelled IC_{50} values matching measured IC_{50} estimates, see Figure 3.16A, mismatches being most apparent at the very earliest time points. This perhaps emphasises the imprecise nature of the competition association fits with respect to the competition association data itself. Indeed, the measured IC_{50} estimates for molindone appear to be still changing as time advances, indicating that the binding reaction has failed to reach a true equilibrium. This demonstrates that the 60min data collection period was likely insufficient to allow an accurate assessment of the kinetics of molindone even though the approach to equilibrium had been established. Longer kinetic incubation periods were not possible due to time-dependent reductions in HTRF signal likely the result of receptor or probe instability.

In contrast, the competition association fits of spiperone-d2 binding obtained in HBSS in the presence of the more slowly dissociating paliperidone, produced modelled IC_{50} fits which more closely approximate measured IC_{50s} estimates, a sign of the improved goodness of fit in the competition association model see Figure 3.16B.

The competition association fits of spiperone-d2 binding in a HEPES-based buffer (HEPES-salt, 138mM sodium chloride) obtained in the presence of the rapidly dissociating compound pergolide produced modelled IC_{50} values that closely approximate measured IC_{50} estimates, see Figure 3.16C. Again, this illustrates the improved precision of the competition association fit. Similarly, competition association fits of spiperone-d2 obtained in a HEPES-based buffer (HEPES-salt, 138mM sodium chloride) in the presence of the very slowly dissociating bromocriptine produces modelled IC_{50} fits which appear to closely match the measured IC_{50s} again emphasising the good fit of the competition association model, see Figure 3.16D.

Similarly, the competition association fits of PPHT-red binding obtained in a HEPES-based buffer (HEPES-salt, 138mM sodium chloride) in the presence of the rapidly

dissociating compound pergolide produced IC_{50} values that more precisely match the measured IC_{50} estimates, see Figure 3.16E. Thus helping to explain the major improvement in the competition association fits. Similarly, competition association fits of PPHT-red obtained in HEPES-salt in the presence of the very slowly dissociating bromocriptine, produced IC_{50} fits which closely match measured IC_{50s} values emphasising the improved fit of the competition association model when PPHT-red is employed as the tracer, see Figure 3.16F.

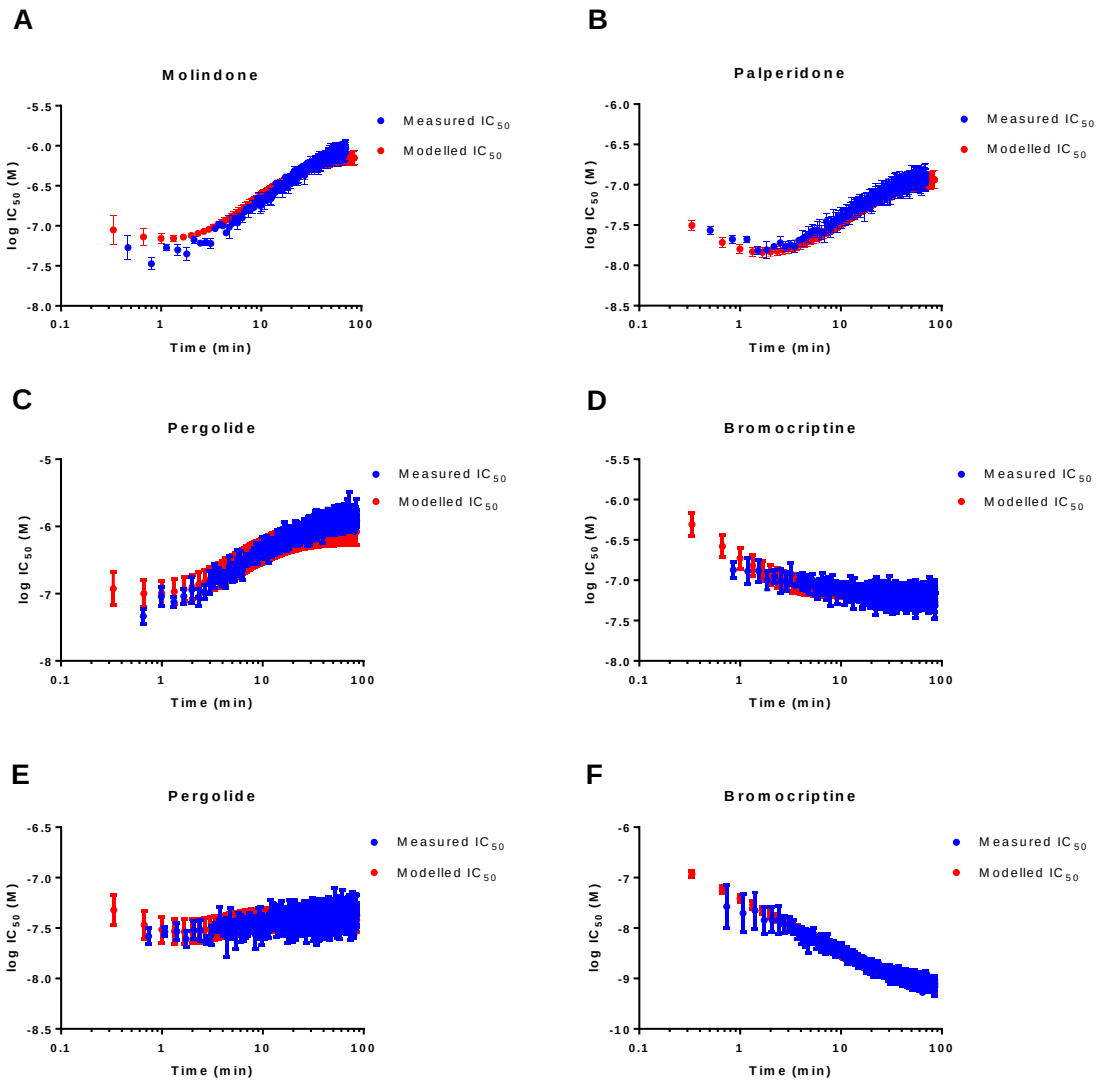


Figure 3.16. Simulated and experimental IC_{50} values for rapidly and slowly dissociating dopamine D_2 ligands obtained using different tracers under various experimental conditions. Relationship between measured and simulated IC_{50} values plotted over time for **(A)** molindone and **(B)** paliperidone with experimental competition association data obtained in HBSS using spiperone-d2. Relationship between measured and simulated IC_{50} plotted over time for **(C)** pergolide and **(D)** bromocriptine with experimental competition association data obtained in HEPES-salt, using spiperone-d2. Relationship between measured and simulated IC_{50} plotted over time for **(E)** pergolide and **(F)** bromocriptine with experimental competition association data obtained in HEPES-salt using PPHT-red. Simulated data were generated in GraphPad Prism 6.0 using Equation 2.7, Chapter 2 as detailed in the methods. The kinetic parameters ($k_{1\text{-}4}$) were fixed to those

determined experimentally for each tracer and the appropriate unlabelled antagonist. The binding of each tracer was simulated in the presence of different concentrations of the unlabelled antagonist at the indicated time points. Families of IC_{50} curves were analysed using GraphPad Prism 6.0, to provide simulated competition binding curves from which IC_{50} values were obtained. Data are presented as mean ± S.E.M. values from 3-6 separate experiments.

3.3.8 Residual plots as a means of assessing competition-association fits

Modelled and measured IC_{50} data can be readily transformed into residual plots to help visualise tracer and competitor behaviour i.e. Modelled IC_{50} – measured IC_{50} = residual IC_{50} value. Residual plots allow an assessment of observed error which if a particular model predicts observed behaviour should be stochastic or in other words subject only to random error. Random errors are assumed to produce residuals that are normally distributed. Therefore, the residuals should fall in a symmetrical pattern and have a constant spread centred on zero throughout the range (Lin et al., 2002). If met, this criterion is an indication that the model is correct on average for all fitted values. If the points have a pattern this indicates that the prediction equation used (the model) is not a good fit for the data. If the model is systematically incorrect (i.e. non-symmetrical), it suggests that the model can be improved.

IC_{50} residuals plotted against time are shown in Figure 3.17 and represent the difference between modelled and expected tracer binding in the presence of different competitors with different kinetic signatures performed in two different buffers. The competition kinetic data for the unlabelled compound molindone in competition with the slowly dissociating tracer spiperone-d2 failed to reliably fit the Motulsky-Mahan model and this is clearly illustrated in the residual plot Figure 3.17A. The fits deviate from zero at the very early (and late) time points. In the same plot, residual data for the more slowly dissociating paliperidone exhibits more random behaviour, although not completely centred around zero. In contrast, the data obtained with molindone competing against the same tracer, but in HEPES-salt buffer produces a residual plot closer to stochastic behaviour Figure 3.17B. This situation is further improved by using PPHT-red, indicating strongly that this tracer is the most suited for determining the kinetics of the most rapidly dissociating compounds Figure 3.17C. Bromocriptine's behaviour is adequately described by either tracer in HEPES-salt buffer demonstrating that the more slowly dissociating compounds are more readily fitted to the Motulsky-Mahan model by tracers with very divergent kinetic properties Figure 3.17B and C.

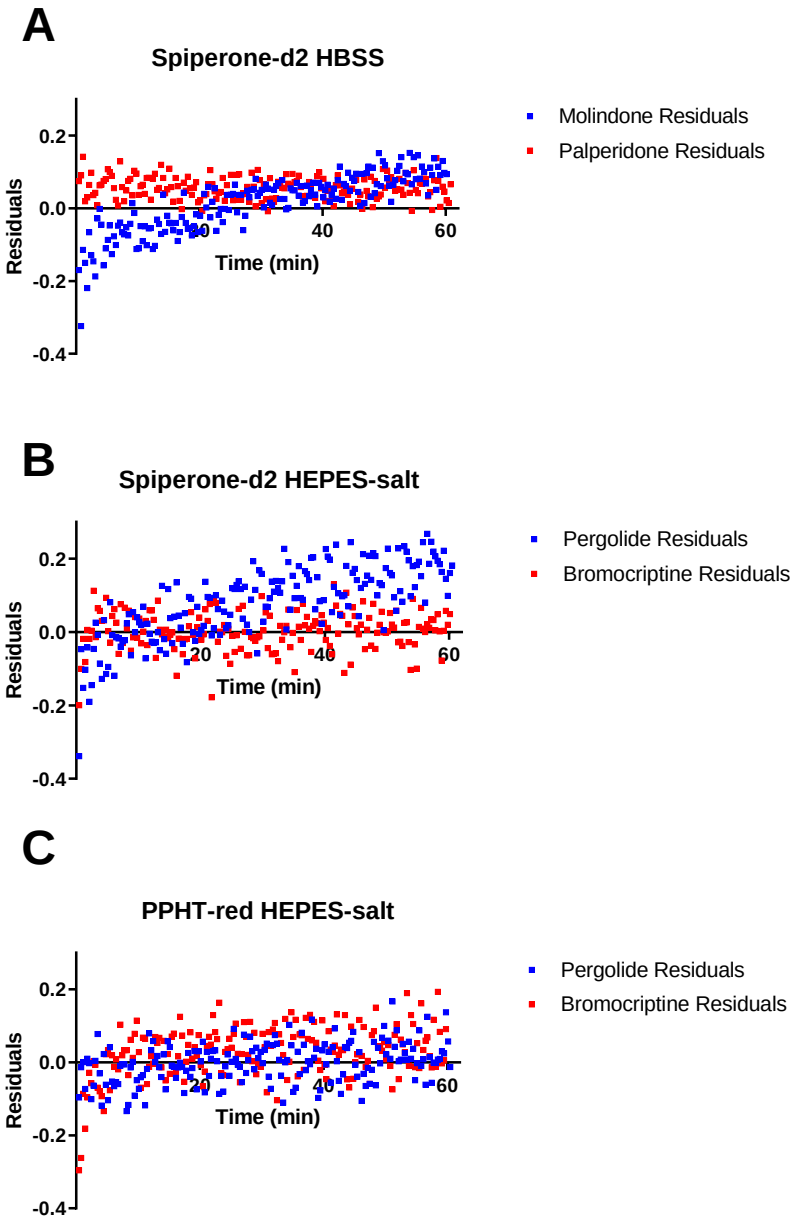
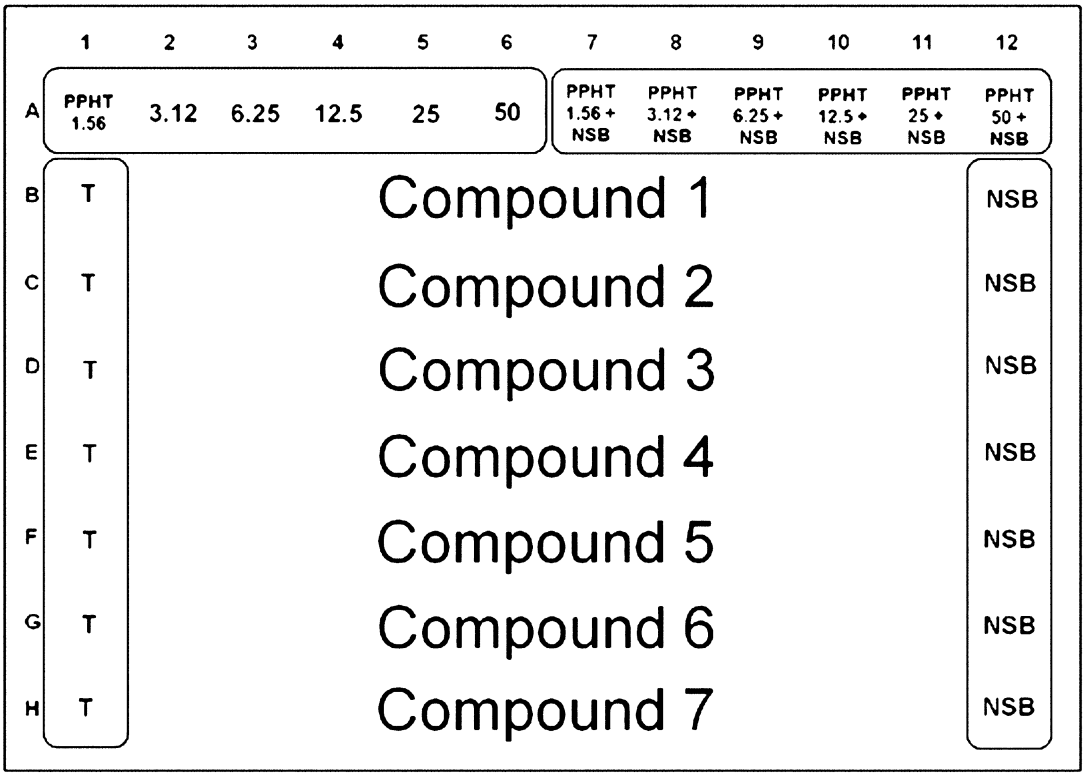


Figure 3.17. A plot of residuals versus time for IC_{50} data derived from competition association binding experiments performed with different tracers under different experimental conditions. **(A)** Spiperone-d2 binding in HBSS buffer in the presence of molindone and paliperidone. **(B)** Spiperone-d2 binding in HEPES-salt buffer in the presence of molindone and bromocriptine and **(C)** PPHT-red binding in HEPES-salt buffer in the presence of molindone and bromocriptine. Data are presented as mean values from 3-6 separate experiments.

3.3.9 Determination of kinetics of D_2R specific antagonists and agonists

The experiments outlined above established PPHT-red as the most suitable tracer to determine the kinetics of dopamine receptor agonists and antagonists, which based on the early literature, we expected to exhibit a wide range of kinetic parameters from slowly dissociating high affinity ligands to rapidly dissociating fragment-like compounds such as dopamine itself (Kapur and Seeman 2001).

The kinetic off-rates of a collection of dopamine D_2 receptor-specific agonists and antagonists are detailed in Table 3.9 and 3.10 respectively. These values were obtained using the tracer PPHT-red and a standard plate format detailed in Figure 3.18. To validate the rate constants, the kinetically derived dissociation constant (K_d) values (k_{off}/k_{on}) were compared with the dissociation constant (K_d) obtained from equilibrium competition binding experiments (see Figure 3.19). There was a very good correlation between these two values for all dopamine D_2R specific antagonists and agonists tested (two-tailed Pearson's correlations $r^2 = 0.99$, $P < 0.0001$ and $r^2 = 0.99$, $P < 0.0001$ respectively) indicating the kinetic parameters obtained with PPHT-red were consistent with equilibrium affinity values. A more complete discussion of these results with regards to APD clinical use and their differential propensity to produce side effects can be found in Chapter 5.



Key: Total = total binding (absence of competitor); Compound = D_2 ligands at various concentrations based on estimated K_i; NSB = haloperidol (10μM) defines non-specific binding

Figure 3.18 Standard competition association plate layout.

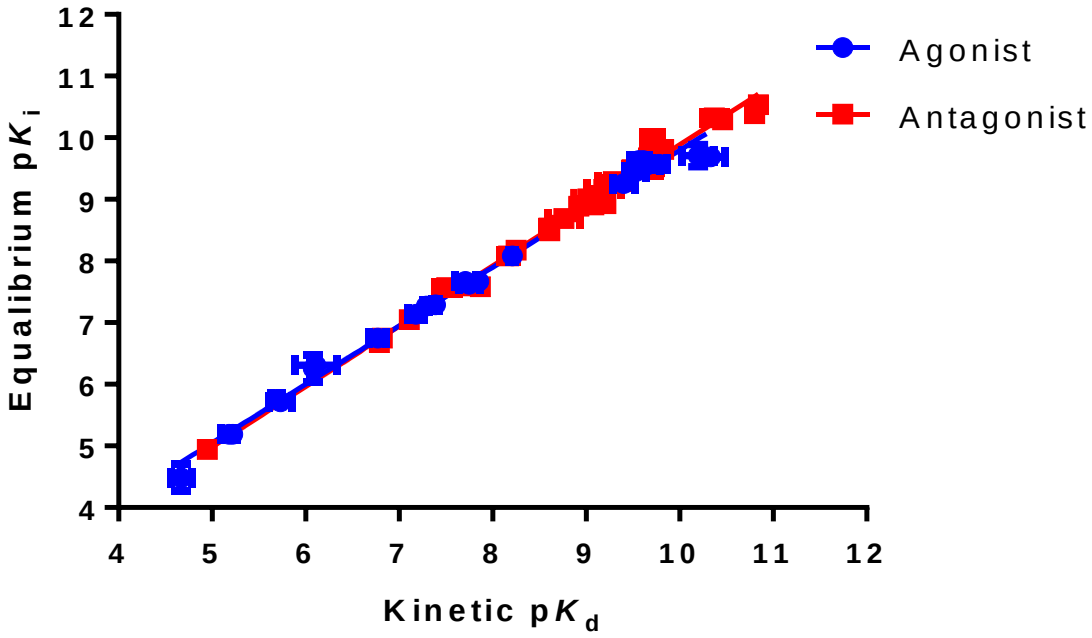


Figure 3.19. Validation of kinetic rate constants, the kinetically derived equilibrium dissociation constant (pK_d = -log k_{off}/k_{on}) compared with the equilibrium dissociation constant (pK_i) obtained from competition binding experiments. Dopamine D_2 receptor-specific agonists and antagonists kinetic and equilibrium values are detailed in Tables 3.9 and 3.10 respectively.

Table 3.1. Equilibrium and kinetic binding parameters of spiperone-d2 for human dopamine D_{2L} receptors performed in HBSS at 37°C. Data are mean ± S.E.M. from 4 experiments performed in singlet. Global kinetic and linear plot k_{obs} versus tracer concentration derived dissociation rates and affinity constants for spiperone-d2 were compared using an unpaired Student's t-tests **P < 0.05.

Analysis	***k_{off} (min^{-1})***	***k_{on} ($M^{-1}min^{-1}$)***	***K_d (nM)***	***Dissociation $t_{1/2}$ (min)***	***HTRF ratio (665/620nm*10,000)***	***n***
Saturation	ND	ND	0.23 ± 0.09	ND	24469 ± 4927	4
Global kinetic association	0.029 ± 0.006	1.93 ± 0.49 $x10^8$	0.22 ± 0.09	23.9	24982 ± 4208	4
Linear plot k_{obs} versus [tracer]	0.11 ± 0.02**	1.42 ± 0.39 $x10^8$	0.94 ± 0.14**	6.3	ND	4

Table 3.2. Equilibrium and kinetic binding parameters of unlabelled dopamine D_2 antagonists for human dopamine D_{2L} receptors obtained using the rapidly dissociating tracer spiperone-d2 performed in HBSS at 37°C. Data are mean ± S.E.M. from 3 experiments performed in singlet.

D_2 antagonists	***k_{off} (min^{-1})***	***k_{on} ($M^{-1}min^{-1}$)***	***Kinetic pK_d***	***Dissociation $t_{1/2}$ (min)***	***Kinetic n***	***Equilibrium pK_i***	***n***
Molindone**	0.63	2.65 $x10^7$	7.62	1.1	1	7.27 ± 0.05	3
Paliperidone	1.10 ± 0.20	1.72 ± 0.24 $x10^8$	8.20 ± 0.10	0.63	3	8.13 ± 0.08	3
Sulpride*	2.59	1.51 $x10^8$	7.79	0.27	2	7.57 ± 0.05	3
Remoxipride	4.17 $x10^8$	1.29 $x10^{15}$	6.66 ± 0.11	1.66e-9	3	6.57 ± 0.06	3
Melperone***	4.18	3.25 $x10^7$	6.91	0.17	2	6.80 ± 0.05	3
Clozapine*	4.75 $x10^7$	5.23 $x10^{14}$	7.23	1.46e-8	2	7.14 ± 0.06	3

* single ambiguous fit, ** two ambiguous fits and *** single outlier removed from kinetic data fits.

Table 3.3. Equilibrium and kinetic binding parameters of clozapine-Cy5 for human dopamine D_{2L} receptors performed in HBSS at 37°C. Data are mean ± S.E.M. from 5 experiments performed in singlet.

Analysis	***k_{off} (min^{-1})***	***k_{on} ($M^{-1}min^{-1}$)***	***K_d (nM)***	***Dissociation $t_{1/2}$ (min)***	***HTRF ratio (665/620nm*10,000)***	***n***
Saturation	ND	ND	431 ± 125	ND	59061 ± 9812	5
Global kinetic association	0.78 ± 0.07	2.53 ± 0.71 x10^6	295 ± 60	0.89	65355 ± 22277	5
Linear plot k_{obs} versus [tracer]	0.78 ± 0.16	7.51 ± 2.82 x10^6	223 ± 89	0.89	ND	5

Table 3.4. Kinetic binding parameters of unlabelled dopamine D_2 antagonists for human dopamine D_{2L} receptors obtained using the rapidly dissociating tracer clozapine-Cy5 performed in HBSS at 37°C. Data are mean ± S.E.M. from 2-4 experiments performed in singlet.

D_2 antagonists	***k_{off} (min^{-1})***	***k_{on} ($M^{-1}min^{-1}$)***	***Kinetic pK_d***	***Dissociation $t_{1/2}$ (min)***	***Kinetic n***	***Equilibrium pK_i***	***n***
Molindone	3.95 ± 0.72	1.37 ± 0.22 x10^8	7.54 ± 0.02	0.18	4	7.44 ± 0.02	4
Paliperidone	1.05 ± 0.15	1.49 ± 0.30 x10^8	8.15 ± 0.07	0.66	4	8.15 ± 0.09	4
Sulpride***	2.77 ± 0.60	1.77 ± 0.13 x10^8	7.84 ± 0.10	0.25	3	7.79 ± 0.11	4
Remoxipride***	2.70 ± 0.20	1.56 ± 0.20 x10^7	6.75 ± 0.07	0.26	3	6.66 ± 0.05	4
Melperone*/***	1.84	1.38 x10^7	6.89	0.38	2	6.83 ± 0.04	4
Clozapine*	4.45 ± 1.76	1.38 ± 0.60 x10^8	7.43 ± 0.09	0.16	4	7.32 ± 0.07	4

* single ambiguous fit and *** single outlier removed from kinetic data fits.

Table 3.5. Equilibrium and kinetic binding parameters of PPHT-red for human dopamine D_{2L} receptors performed in a HEPES based buffer containing physiological levels of sodium chloride (HEPES-salt buffer) at 37ºC. Data are mean ± S.E.M. from 4-6 experiments performed in singlet.

Analysis	***k_{off} (min^{-1})***	***k_{on} ($M^{-1}min^{-1}$)***	***K_d (nM)***	***Dissociation $t_{1/2}$ (min)***	***HTRF ratio (665/620nm*10,000)***	***n***
Saturation	ND	ND	21.9 ± 4.1	ND	21444 ± 4436.8	6
Global kinetic association	0.35 ± 0.02	2.1 ± 0.3 x10^7	18.3 ± 0.2	2.0	15007 ± 3025	6
Linear plot k_{obs} versus [tracer]	0.49 ± 0.06	2.2 ± 1.3 x10^7	58.4 ± 16.6	1.4	ND	6
Dissociation	0.52 ± 0.04	ND	ND	1.3	ND	4

Table 3.6. Kinetic binding parameters of unlabelled dopamine D_2 antagonists for human dopamine D_{2L} receptors obtained using the rapidly dissociating tracer PPHT-red performed in HEPES-salt buffer at 37ºC. Data are mean ± S.E.M. from 4-6 experiments performed in singlet.

D_2 antagonists	***k_{off} (min^{-1})***	***k_{on} ($M^{-1}min^{-1}$)***	***Kinetic pK_d***	***Dissociation $t_{1/2}$ (min)***	***Equilibrium pK_i***	***n***
RNPA	1.49 ± 0.22	7.97 ± 2.82 x10^7	7.67 ± 0.12	0.47	7.73 ± 0.11	6
Pergolide	2.08 ± 0.56	1.27 ± 0.50 x10^8	7.71 ± 0.11	0.33	7.59 ± 0.07	5
Molindone	1.62 ± 0.29	6.49 ± 2.16 x10^7	7.51 ± 0.13	0.43	7.48 ± 0.10	6
Chlorpromazine	1.99 ± 0.34	2.74 ± 7.87 x10^8	9.02 ± 0.15	0.35	8.85 ± 0.12	6
Domperidone	0.15 ± 0.02	7.75 ± 1.63 x10^8	9.66 ± 0.11	4.62	9.66 ± 0.11	6

Liseride	0.074 ± 0.009	4.49 ± 0.66 x10^8	9.78 ± 0.08	9.36	9.57 ± 0.05	4
Nemonopride	0.025 ± 0.004	1.51 ± 0.13 x10^9	10.80 ± 0.07	27.72	10.59 ±0.13	5
Bromocriptine	0.020 ± 0.007	4.28 ± 0.52 x10^7	9.40 ± 0.12	34.65	9.26 ± 0.05	4

Table 3.7. Equilibrium and kinetic binding parameters of spiperone-d2 for human dopamine D_{2L} receptors performed in a HEPES based buffer containing physiological levels of sodium chloride (HEPES-salt buffer) at 37ºC. Data are mean ± S.E.M. from 6 experiments performed in singlet.

Analysis	***k_{off} (min^{-1})***	***k_{on} ($M^{-1}min^{-1}$)***	***K_d (nM)***	***Dissociation $t_{1/2}$ (min)***	***HTRF ratio (665/620nm*10,000)***	***n***
Saturation	ND	ND	0.64 ± 0.18	ND	14701 ± 2135	6
Global kinetic association	0.074 ± 0.013	1.33 ± 0.20 x10^8	0.68 ± 0.19	9.36	15845 ± 2491	6
Linear plot k_{obs} versus [tracer]	0.20 ± 0.05	7.55 ± 1.71 x10^7	3.81 ± 1.43	3.47	ND	6
Dissociation	0.09 ± 0.01	ND	ND	7.70	ND	6

Table 3.8. Kinetic binding parameters of unlabelled dopamine D_2 antagonists for human dopamine D_{2L} receptors obtained using the rapidly dissociating tracer spiperone-d2 performed in HEPES-salt buffer at 37ºC. Data are mean ± S.E.M. from 3-6 experiments performed in singlet.

D_2 antagonists	***k_{off} (min^{-1})***	***k_{on} ($M^{-1}min^{-1}$)***	***Kinetic pK_d***	***Dissociation $t_{1/2}$ (min)***	***Equilibrium pK_i***	***n***
RNPA	1.21 ± 0.35	1.57 ± 0.18 x10^7	7.16 ± 0.09	0.57	7.05 ± 0.10	6
Pergolide	3.37 ± 0.83	5.65 ± 2.16 x10^7	7.08 ± 0.13	0.21	6.98 ± 0.09	6
Molindone	2.63 ± 0.90	5.10 ± 2.16x10^7	7.19 ± 0.16	0.26	7.03 ± 0.02	3
Chlorpromazine*	3.01 ± 0.73	7.35 ± 1.24 x10^8	8.40 ± 0.09	0.23	8.13 ± 0.08	5
Domperidone	0.35 ± 0.06	3.48 ± 0.48 x10^8	9.01 ± 0.09	1.98	8.96 ± 0.11	6

Liseride	0.18 ± 0.02	2.85 ± 0.33 x10^8	9.21 ± 0.09	3.85	9.03 ± 0.10	4
Nemonopride	0.039 ± 0.007	1.29 ± 0.19 x10^9	10.54 ± 0.13	17.77	10.56 ± 0.11	6
Bromocriptine	0.040 ± 0.005	1.51 ± 0.48 x10^7	8.52 ± 0.18	17.33	8.81 ± 0.25	4

* single ambiguous fit removed from kinetic data fits.

3.4 Discussion

3.4.1 Establishing a dopamine D_2 receptor competition association binding assay

BMG PHERAstar FS settings. Initial attempts to establish a TR-FRET based dopamine D_2 receptor-specific competition association binding assay were performed in LABMED buffer concentrating on the high-affinity fluorescent tracer dopamine-d2 and whole cells expressing the dopamine D_{2S} receptor labelled with the lanthanide terbium cryptate. Once specific binding of the tracer had been established a series of characterisation experiments were performed focused initially on the functionality of the BMG PHERAstar FS itself. To establish higher throughput homogenous kinetics assays measurements must be taken with sufficient frequency that the association of the tracer and its competition with the unlabelled ligand can be readily and reliably quantified.

In a series of measurements performed on whole CHO-D_{2S} cells following the addition of saturating concentrations of spiperone-d2 I compared the lamp versus the laser excitation function on the BMG PHERAstar FS. Signal output (donor emission at 620nm and acceptor emission at 665nm) with increasing flash number, at a saturating concentration of spiperone-d2 (20nM) from both lamp and laser was linear, however the absolute values obtained for equivalent excitation inputs (i.e. number of flashes) is greater (by a factor of 10) using the laser versus the lamp. This presumably results from the increased energy provided by the laser at equivalent flash input levels.

Another interesting aspect of this analysis relevant to high throughput screening is concerned with the manufacturer's suggested lamp/laser input equivalency which would seem to be based on the time to read rather than the relative level of donor signal produced by the laser or lamp (See Figure 3.2A and B). The level of the signal from lamp or laser appears to be an indicator of the level of relative error of measurements and likely reflects the different contributions of specific versus background signal, with the latter increasing at lower levels of excitation. In the case of the laser, this level of error seems to reach a lower plateau, with increasing

excitation input producing no further reduction in the mean %CV (Figure 3.3A and B).

3.4.2 Whole cells versus membranes

Whole cells perhaps represent the most relevant model system in which to collect kinetic data (Vauquelin et al., 2015) and was the initial driver behind our desire to formulate a FRET-based competition association binding assay. Initial experiments were focused around the possibility of collecting kinetic data in whole CHO-D_{2S} cells at room temperature. The expected linear relationship between k_{obs} and spiperone-d2 was readily detected in whole cells (Figure 3.4B), however surprisingly spiperone-d2 could not be fully dissociated using an excess of unlabelled spiperone (1 μM) see Figure 3.4C. To understand this phenomenon further we added a cell permeabilizing agent saponin (100 μg/mL) to the cells in the presence of the excess concentration of spiperone Figure 3.4D. The full displacement of the tracer was observed only in the presence of the cell permeabilizing agent saponin (100 μg/mL). Whereas following its addition in the absence of spiperone the level of binding remained constant suggesting that all the D_2R receptors are fully accessible to the fluorescent ligand, spiperone-d2. Only when the cell and the internal organelles are permeabilised is the unlabelled spiperone fully able to compete with the prebound tracer.

It can be argued that the presence of whole cells effectively represents a two-compartment model a situation which violates a fundamental assertion implicit in the equations which describe the competition kinetic model formulated by Motulsky and Mahan, namely that all the receptors are accessible to all ligands and that binding of tracer and competitor are fully reversible (Motulsky et al., 1985). Having observed this unexpected and confounding phenomenon it was decided to concentrate efforts around establishing a kinetic binding assay in membranes at physiological temperature (37^{o}C).

3.4.3 Establishing a D_{2L} membrane-based competition association assay

Having established that membranes represent a more appropriate experimental model situation for the study of D_{2L} receptor binding kinetics we performed a series

of experiments utilising different buffers and employing different fluorescent tracers with ranging kinetic properties to develop an assay sensitive enough to measure the kinetics of slowly and rapidly dissociating dopamine D_2 receptor-specific ligands.

A critical assessment of the kinetic association data achieved with spiperone-d2 in HBSS suggests that the global association fit produced the most accurate estimation of tracer kinetic parameters (Table 3.1). The K_d of spiperone-d2 estimated from the global association analysis matching the K_d from the saturation analysis with B_{max} values in the same range. In contrast, the K_d obtained from the linear plot of k_{obs} versus tracer concentration appeared to underestimate the affinity of the tracer. Correspondingly the kinetic off-rate of the tracer appeared to be much more rapidly dissociating than that suggested by the global fit hence the global association fit was chosen for estimating the kinetic rate constants of the unlabelled compounds.

Initial experiments were performed with spiperone-d2 in HBSS on a series of compounds we predicted would show relatively rapid rates of dissociation from the D_2R (see Table 3.2). Only the kinetics of paliperidone could be quantified with any degree of reliability as judged by a lack of ambiguity in fits and the absence of any outliers (Grubbs $\alpha = 0.0001$). Interestingly this particular compound proved to have the slowest kinetic dissociation rate of the 6 compounds tested as judged in subsequent experiments performed with the rapidly dissociating tracer clozapine-Cy5 indicating that a limit of detection for this particular tracer had been unwittingly established.

Clozapine-Cy5 proved to be a more reliable tracer for determining the kinetics of unlabelled compounds based on the number of observations producing a reliable fit relative to spiperone-d2 (contrast data in Table 3.2 and Table 3.4). This increase in reliability is potentially due to an increase in tracer kinetic resolution observed when the kinetics of the tracer approaches that of the unlabelled compound. This phenomenon will be discussed in more detail in Chapter 4 of this thesis.

Reassuringly in the case of clozapine-Cy5 the global kinetic association derived kinetic off-rate estimation was very much in line with that estimated from the linear fit of tracer concentration versus k_{obs}. Additionally, in the case of clozapine-Cy5, the

K_d estimates from equilibrium and kinetic association experiments were within 2-fold of each other indicating that the overall assessment of tracer properties was relatively robust. However, there were still several examples where the competition data collected failed to reliably fit the Motulsky-Mahan model with either outliers or ambiguous fits contributing to these failures. One possible explanation for the relatively high number (1 in 4) of failures is the low concentration of tracer employed relative to its own affinity. This limitation was imposed largely based on the quantity of tracer available but also its own relatively rapid rate of observed association following offline addition. Again, this phenomenon will be discussed in more detail in Chapter 4 of this thesis.

This relatively high rate of competition association fit failure with clozapine-Cy5 led us to seek an alternative tracer. Details of a medium affinity fluorescent tracer used to characterise the dopamine D_2 receptors have been published previously (Bakthavachalam et al., 1991; Albizu et al., 2010) and this ligand was sourced from CisBio. At this point we switched to a similar HEPES-based buffer containing physiological levels of sodium chloride (HEPES-salt 138mM sodium chloride) which had been previously used to formulate $D_{2L}R$ radioligand binding kinetic experiments with some success (Klein-Herenbrink personal communication).

In the case of PPHT-red, the kinetic properties were relatively easily estimated using the off-line addition protocol and the rates of observed association were not so fast that their accurate quantification proved to be a problem. Details of the PPHT-red equilibrium and kinetic parameters are shown in Table 3.5. Table 3.6 details the kinetic parameters of a selection of unlabelled compounds estimated using fluorescent PPHT-red. Compounds were selected with a range of kinetic off-rates allowing us to make direct comparisons with the more slowly dissociating tracer spiperone-d2. In this case the kinetics of both rapidly and slowly dissociating compounds (agonists and antagonists) could be estimated with a high degree of accuracy with no exclusions due to fit ambiguity or outlier exclusion.

In contrast to the situation observed with spiperone-d2 in HBSS we were able to obtain a relatively reliable estimation of the competitor kinetic parameters using this same tracer in the HEPES-salt buffer. The reasons for this are not completely clear but they most likely relate to the relatively faster off-rate of the tracer obtained in

HEPES-salt buffer relative to HBSS (23.9 vs 9.36 min^{-1}) and the relative off-rates of the compounds selected for testing. The importance of tracer concentration (relative to its own affinity), dissociation rate and its consequences for accurate compounds kinetics will be discussed in more detail in Chapter 4.

Reassuringly a good correlation was obtained between the off-rates obtained with PPHT-red (agonist) and spiperone-d2 (antagonist) suggesting that off-rates can be accurately estimated independently of the type of probe used provided GppNHp is used to uncouple any prebound G proteins. Surprisingly spiperone-d2 appeared to underestimate the on-rates and the corresponding affinity of these compounds under test, this could be related to some inaccuracy in the estimation of its kinetic on-rate (and therefore affinity) which may result from its tendency to stick to plastic or potentially points to probe-dependant on-rate estimations (compare values in Table 3.6 and 3.8). Probe-dependent affinity estimations have been suggested previously for discrepancies in affinity for ligands binding the D_2R (Seeman et al., 1997a). However, this seems very unlikely since the same probe was able to estimate the affinities of compounds in the buffer HBSS with values largely matching those obtained with clozapine-Cy5 in the same buffer and PPHT-red obtained in HEPES-salt buffer (compare values in Table 3.2, 3.4 and 3.6).

It has been well documented that competition between an unlabelled competitor and tracer slows the time to equilibrium (Rang, 1966; Motulsky and Mahan, 1984; Hulme and Birdsall, 1992; Dowling and Charlton 2006 and Hulme and Trevethick 2010). Consequently, the IC_{50} curve of a competitor compound changes with time as the binding reaction proceeds towards the point of equilibrium following addition of the membranes. This pattern of change is very much dependent on the kinetic properties of both the competitor and the relative concentrations of competitor and tracer employed (Motulsky and Mahan, 1984).

Interestingly we were able to use IC_{50} estimates as another way of assessing the relative off-rates of the compounds profiled in these competition association studies. This technique has been used in the past to estimate the relative off rates of a series of GnRH antagonists using a SPA-based radioligand binding assay (Heise *et al*., 2007). Figure 3.15A and C shows the excellent correlations between k_{off} estimates and IC_{50} shifts obtained with spiperone-d2 and PPHT-red at 1 and 120 min for the

compounds detailed in Table 3.6 and 3.8. Correspondingly the correlation between off rates obtained with these two tracers is shown in Figure 3.15B. This type of analysis which requires no knowledge of the tracer kinetics could prove useful to investigators when the kinetics of the tracer prove unsuitable to determine the kinetics of compounds with any degree of reliability or when only a non-homogenous radioligand binding assay with limited throughput is available for the determination of relative kinetic off-rates.

3.4.4 The influence of the chemical and physical properties of a compound on drug-receptor binding parameters

One aspect of GPCR kinetics which is not well understood is the influence of the chemical and physical properties of a compound on drug-receptor kinetic binding parameters. One advantage of collecting such a large kinetic data set for both dopamine agonists and antagonists is that we can make useful correlations and determine the influence of any number of physicochemical properties. The chemical and physical properties of the D_2R agonists and antagonists are detailed in Table 3.11 and 3.12 respectively.

Previous analysis of dopamine D_2 physicochemical and kinetic properties revealed that more rapidly dissociating dopamine receptor antagonists tend to have lower molecular weights and lower lipophilicities (Trasadern et al., 2011). Lipophilicity is defined as the ability of a molecule to mix with an oily phase (usually octanol) rather than with water and is often expressed as a partition coefficient, P, between these two phases. Specifically, log P is defined as the ratio of the un-ionized drug distributed between the octanol and water phases at equilibrium with larger values indicating greater lipophilicity. The influence of log P (or lipophilicity) on drug-receptor affinity is well documented, with increasing drug lipophilicity shown to increase in line with changes in drug receptor potency (Parker et al., 2008). Such ideas go back as far as the late 1800s and early 1900s when anaesthetic potency was shown to correlate strongly with lipid solubility the basis of the Meyer-Overton hypothesis (Janoff et al., 1981).

Figure 3.20A-C shows the correlation of dopamine D_2 agonist and antagonist receptor affinity (kinetic pK_d), association rate (or k_{on}) and dissociation rate (or k_{off})

with calculated logP or clogP. As one might predict dopamine D_2 agonist and antagonist receptor affinity (pK_d), increases with increasing lipophilicity (clogP), Figure 3.20A**.** Interestingly it would appear that this increase in receptor affinity accompanying the increase in drug lipophilicity for both agonists and antagonists is largely driven by changes in the kinetic on-rates of these compounds. The magnitude of agonist and antagonist k_{on} values increasing significantly with lipophilicity and its measure clogP (Figure 3.20B). In contrast, no such correlation with clogP and measured dissociation rates was observed for these compounds, Figure 3.20C. These findings contrast somewhat with the findings of Trasadern and colleagues since reduced drug lipophilicity does not appear to be a prerequisite for rapid dissociation. However, it is fair to say that the range of lipophilicities of more rapid dissociating compounds will be wider than those of more slowly dissociating compounds, which tend to be more lipophilic.

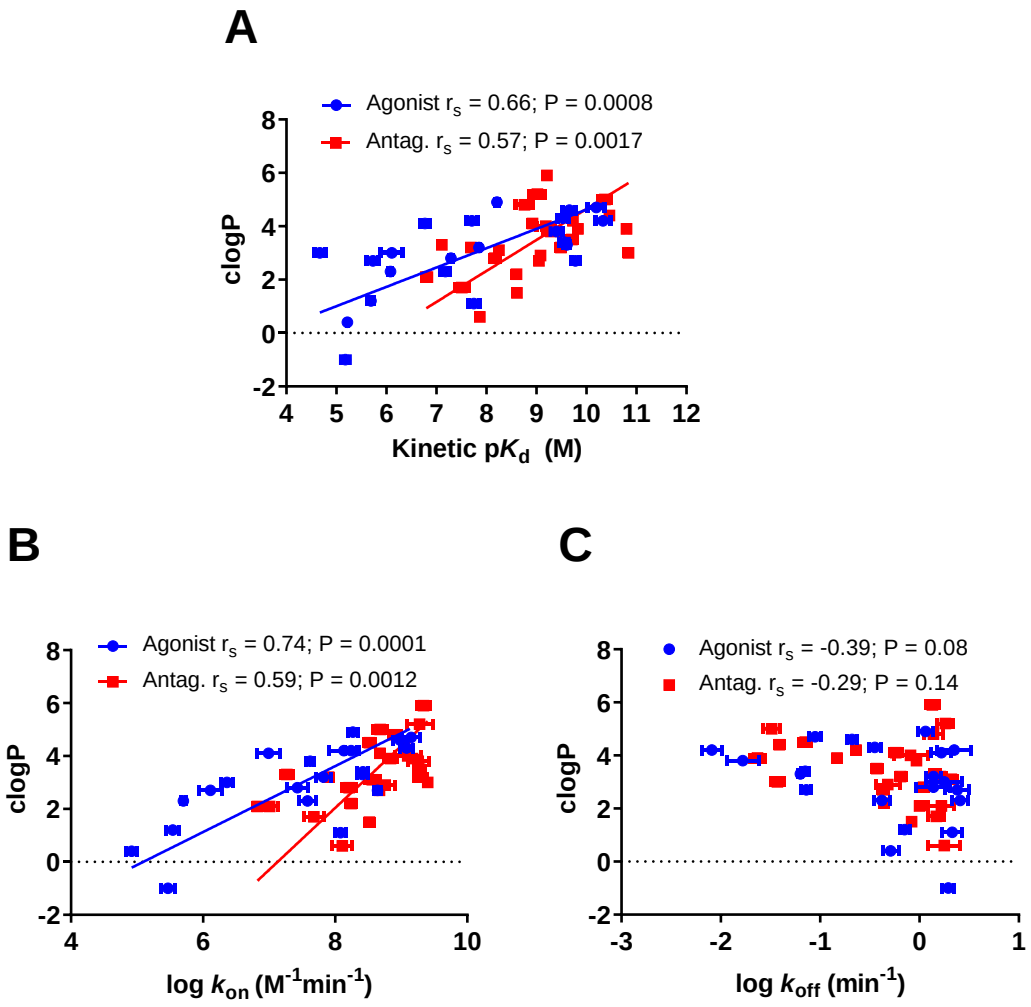


Figure 3.20. Correlating dopamine D_2 ligand physiochemical parameters with kinetic parameters derived from competition association studies. Correlation plot showing the relationship between **(A)** pK_d and clogP, **(B)** logk_{on} and clogP and **(C)** logk_{off} and clogP. All data used in these plots are detailed in Tables 3.9 to 3.12. Kinetic data are presented as mean ± S.E.M. from three or more experiments.

Ligand-receptor binding results from intermolecular forces, such as ionic bonds, hydrogen bonds and Van der Waals forces, and as a consequence as molecular weight increases so drug-receptor binding affinity tends to increase. Figure 3.21A-C shows the correlation of dopamine D_2 agonist and antagonist receptor affinity (kinetic pK_d), association rate (or k_{on}) and dissociation rate (or k_{off}) with compound molecular weight. Predictably dopamine D_2 agonist and antagonist receptor binding affinity increases with increasing molecular weight Figure 3.21A. For both agonists and antagonists, the kinetic dissociation rate (plotted as log k_{off}) is negatively correlated with increases in molecular weight (or mass) Figure 3.21C. This finding perhaps reflects the nature of the interactions which govern binding affinity as described above, with slower off-rates resulting from an increase in specific drug-receptor interactions. Interestingly for antagonists only the kinetic parameter k_{off} (and not k_{on}) is correlated with increases in molecular weight (or mass) see Figure 3.21B and C.

No correlation was observed between antagonist association rate and molecular weight Figure 3.21B, this contrasts directly with the lipophilicity measure clogP in the situation described above. However, the agonist association rate was significantly correlated with drug molecular weight (as it was to clogP) Figure 3.21B. Interestingly D_2R agonist clogP and molecular weight are correlated whereas in contrast antagonist drug molecular weight and clogP are not Figure 3.21D. This implies that at least for dopamine antagonists it is the lipophilic nature of these molecules which drives their association rate rather than any increase in molecular weight since these two parameters are readily separated (not linked).

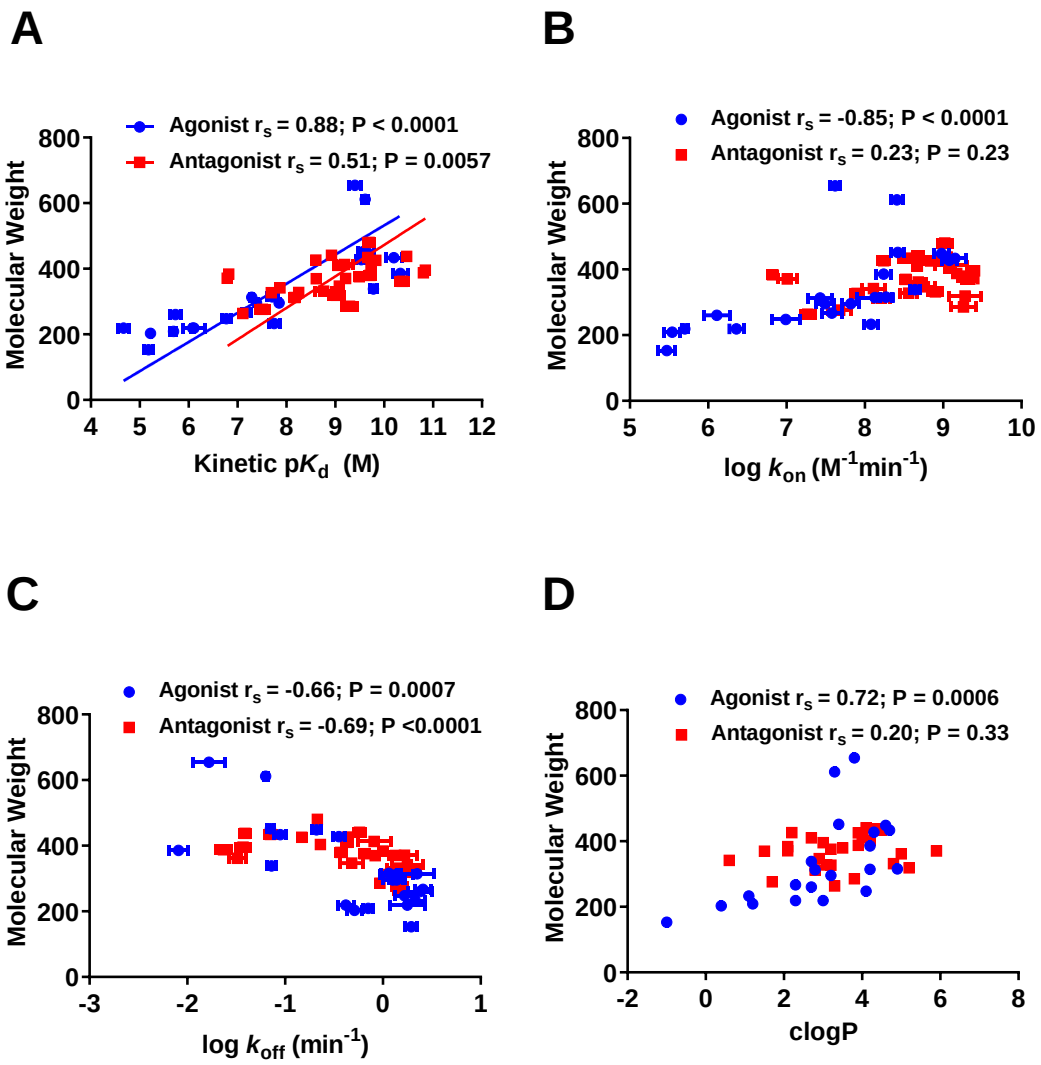


Figure 3.21. Correlating dopamine D_2 ligand physiochemical parameters with kinetically derived parameters. Correlation plot showing the relationship between dopamine agonist and antagonist **(A)** pK_d and molecular weight (Mwt), **(B)** logk_{on} and Mwt and **(C)** logk_{off} and Mwt. Correlation plot showing the relationship between dopamine agonist and antagonist **(D)** clogP and Mwt. All data used in these plots are detailed in Tables 3.9 to 3.12. Kinetic data are presented as mean ± S.E.M. from three or more experiments.

Like molecular weight, heavy atom count (HAC) is another useful measure of the physicochemical properties of a compound and has been advocated as a means of improving ligand efficiency (i.e. potency/size) (Reynolds et al., 2008). Figure 3.22A-C shows the correlation of dopamine D_2 agonist and antagonist receptor affinity (kinetic pK_d), association rate (or k_{on}) and dissociation rate (or k_{off}) with drug HAC.

As might be expected as HAC increased so does the binding affinity of the dopamine agonist and antagonists for the D_2 receptor. Agonist and antagonist correlations of HAC and drug -receptor binding affinity were minor improvements over molecular weight although differences were modest. Similarly, k_{off} and k_{on} correlations with HAC largely reflected those seen with molecular weight reflecting the strong correlation of molecular weight with HAC (Figure 3.22D).

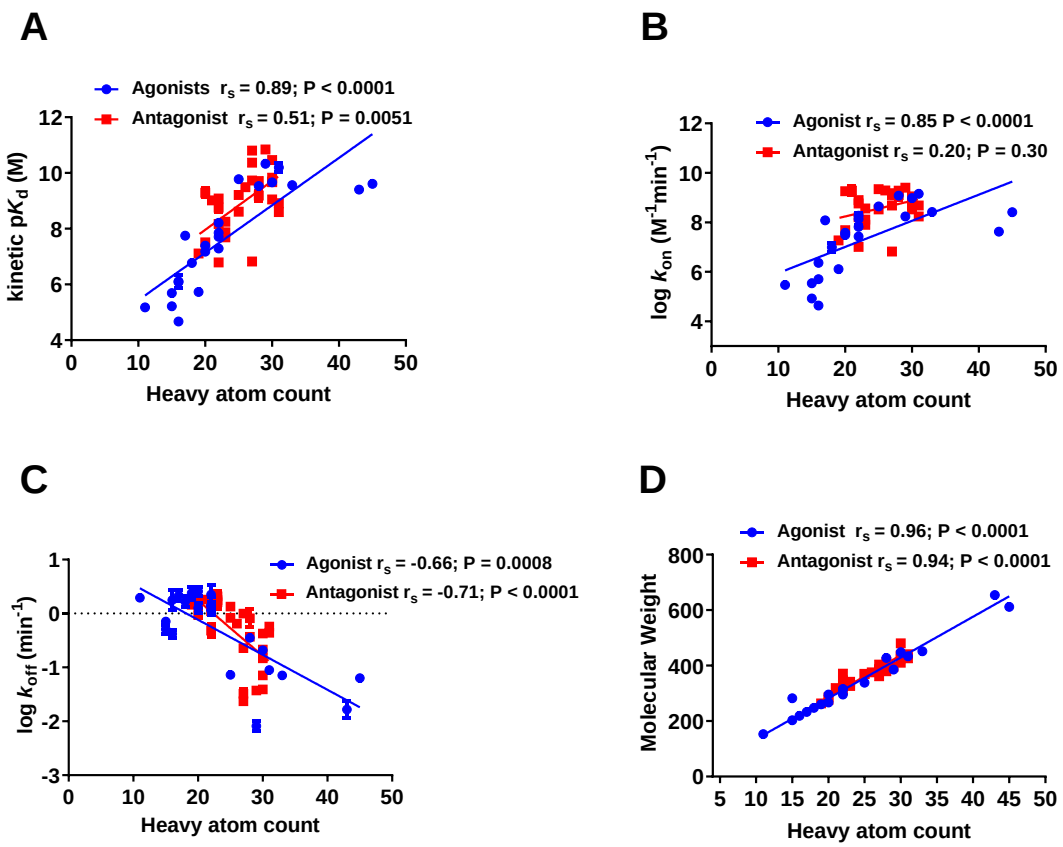


Figure 3.22. Correlating dopamine D_2 ligand physiochemical parameters with kinetically derived parameters and with each other. Correlation plot showing the relationship between dopamine agonist and antagonist **(A)** pK_d and heavy atom count (HAC), **(B)** logk_{on} and HAC and **(C)** logk_{off} and HAC. Correlation plot showing the relationship between dopamine agonist and antagonist **(D)** HAC and Mwt. All data used in these plots are detailed in Tables 3.9 to 3.12. Kinetic data are presented as mean ± S.E.M. from three or more experiments.

3.5 Conclusions

The BMG PHERAstar FS is a multimode plate reader capable of measuring FRET between a fluorescently labelled receptor (eg. terbium the donor) and a fluorescent tracer (eg spiperone-d2 the acceptor). We have demonstrated that a careful optimisation of excitation parameters enables higher throughput determinations of both labelled and unlabelled compound kinetic parameters.

Initially, we were intent on developing a whole cell FRET-based kinetic binding assay however whole-cell binding proved to be problematic. Whole-cell binding by its very nature may involve multiple cellular compartments which can lead to complications and ultimately inaccuracies in the interpretation of competition association binding data (Motulsky et al., 1985). This is highlighted by the incomplete reversal of spiperone-d2 binding from the dopamine D_{2S} receptor expressed in intact CHO-cells following the addition of a vast excess of competitor intended to reverse the binding of this high-affinity fluorescent tracer. This incomplete reversal of binding can be overcome by adding a cell permeabilising agent such as saponin (Verheijen et al., 2004). However practically it makes more sense to study the binding of compounds in membrane preparations prepared from broken cells given that the aim of this study was to accurately determine accurate D_2R drug-receptor kinetic binding parameters.

Using a terbium labelled dopamine $D_{2L}R$ membrane preparation and a selection of tracers with varied kinetic properties we were able to identify a suitable tracer (PPHT-red) to assess the kinetics and equilibrium affinity of a variety of unlabelled compounds with off-rates ranging from very slow (eg. nemonapride) to very rapid (eg chlorpromazine). Relative measures of off rates were also determined simply by measuring the ratio of IC_{50} values obtained at the beginning (~1min post-membrane addition) and the very end of the competition association binding experiment. Plotting changes in IC_{50} values over time for rapidly and slowly dissociating compounds proved to be a useful way of understanding discrepancies between fitted and modelled competition association data. Further examination through residual (measured – modelled IC_{50}) plots versus time confirmed these

inadequacies in the model fitting and established PPHT-red as the most suitable tracer for determination of unlabelled compound kinetic parameters.

By determining the kinetic parameters of a series of dopamine D_2 receptor-specific agonist and antagonist compounds we were able to assess the physical and chemical drivers of ligand affinity and relate these back to their measured kinetic parameters. Increasing HAC appears to be one factor driving the slow off-rates of these compounds and likely reflects the promotion of specific complementary interactions between drug and receptor. In contrast, kinetic on-rate appears to be driven largely by increases in drug lipophilicity a property which may reflect both increases in local drug concentration (Sykes et al., 2014; Gherbi et al., 2018) and the promotion of specific low-affinity drug-receptor interactions which drive macroscopic measured association rates.

Table 3.9. Kinetic binding parameters of unlabeled agonists for human D_{2L} receptors. Data are mean ± S.E.M. for the number of observations (n) stated, each performed in singlet.

D_2 *agonist*	***k_{off} (min^{-1})***	***k_{on} ($M^{-1}min^{-1}$)***	***Dissociation $t_{1/2}$ (min)***	***Kinetic pK_d***	***Equilibrium pK_i***	***n***
Bromocriptine	0.020 ± 0.007	4.28 ± 0.52 x10^7	34.3	9.40 ± 0.12	9.26 ± 0.05	4
R-propylnorapomorphine	1.49 ± 0.22	7.97 ± 2.82 x10^7	0.46	7.85 ± 0.02	7.67 ± 0.12	6
Lisuride	0.074 ± 0.009	4.49 ± 0.66 x10^8	9.35	9.78 ± 0.08	9.57 ± 0.05	4
Pergolide	2.08 ± 0.56	1.27 ± 0.50 x10^8	0.33	7.71 ± 0.11	7.67 ± 0.07	5
(+)3PPP	0.95 ± 0.10	4.87 ± 1.25 x10^4	0.73	4.67 ± 0.11	4.48 ± 0.22	4
Apomorphine	2.68 ± 0.42	4.31 ± 1.11 x10^7	0.26	7.18 ± 0.09	7.14 ± 0.08	4
Cabergoline	0.072 ± 0.007	2.73 ± 0.48 x10^8	9.61	9.56 ± 0.09	9.63 ± 0.03	4
Rotigotine	1.20 ± 0.21	1.97 ± 0.34 x10^8	0.58	8.21 ± 0.03	8.08 ± 0.10	4
GSK789472	1.38 ± 0.33	3.50 ± 1.07 x10^7	0.50	7.39 ± 0.04	7.29 ± 0.03	4
DHEC	0.064 ± 0.003	2.70 ± 0.44 x10^7	10.84	9.61 ± 0.06	9.63 ± 0.03	4
7-OH DPAT	1.79 ± 0.40	1.23 ± 0.42 x10^7	0.39	6.77 ± 0.09	6.75 ± 0.10	4
(-)Quinpirole	0.43 ± 0.07	5.03 ± 0.46 x10^5	1.61	6.08 ± 0.03	6.26 ± 0.23	3
Sumanirole	0.53 ± 0.09	8.82 ± 1.46 x10^4	1.30	5.22 ± 0.00	5.19 ± 0.03	4
Desmethylclozapine	1.78 ± 0.83	3.33 ± 1.43 x10^7	0.39	7.29 ± 0.03	7.27 ± 0.06	4
B-HT 920	0.72 ± 0.08	3.72 ± 0.79 x10^5	0.97	5.69 ± 0.06	5.76 ± 0.07	4
Brexpiperazole	0.09 ± 0.01	1.60 ± 0.37 x10^9	7.62	10.20 ± 0.17	9.71 ± 0.18	4

Bifeprunox	0.009 ± 0.002	1.84 ± 0.39 x10^{8}	80.30	10.33 ± 0.15	9.69 ± 0.11	3
Aripiprazole*	0.21 ± 0.03	1.01 ± 0.23 x10^{9}	3.25	9.66 ± 0.13	9.56 ± 0.11	3
Cariprazine*	0.36 ± 0.05	1.27 ± 0.30 x10^{9}	1.91	9.53 ± 0.11	9.45 ± 0.09	3
Pardoprunox*	2.28 ± 0.56	1.25 ± 0.24 x10^{8}	0.30	7.75 ± 0.11	7.62 ± 0.11	3
(-)3PPP*	1.51 ± 0.35	3.25 ± 0.90 x10^{6}	0.46	6.11 ± 0.22	6.31 ± 0.10	3
Ropinirole*	2.60 ± 0.75	1.46 ± 0.46 x10^{6}	0.27	5.73 ± 0.12	5.72 ± 0.07	3
Dopamine*	2.00 ± 0.30	3.14 ± 0.73 x10^{5}	0.35	5.18 ± 0.09	5.19 ± 0.06	3

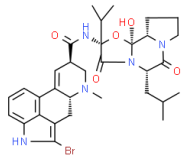
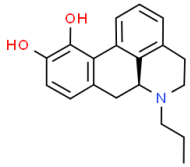
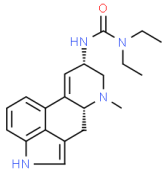
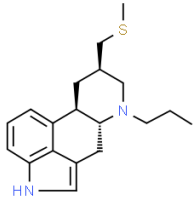
*Experiments were conducted in 20mM HEPES,100mM NaCl, 6mM $MgCl_2$, 1mM EGTA, 1 mM EDTA pH 7.4, containing 1% DMSO, 0.02% pluronic acid, and 0.1% ascorbic acid (HEPES-salt buffer) all other tests were made in the same buffer but containing 138mM NaCl.

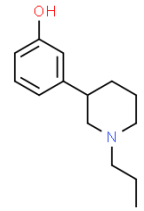
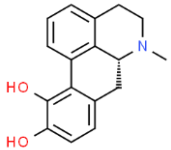
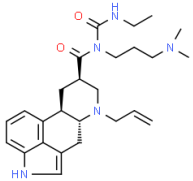
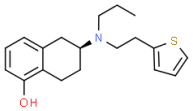
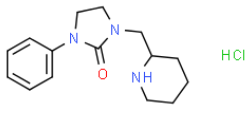
Table 3.10. Kinetic binding parameters of dopamine D_2 antagonists for human dopamine D_{2L} receptors. Data are mean ± S.E.M. for three or more experiments performed in singlet.

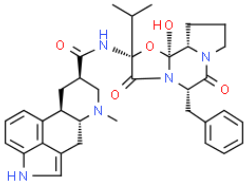
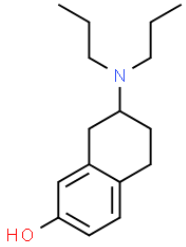
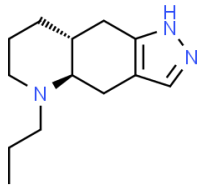
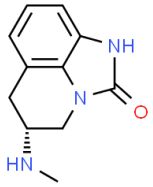
D_2 antagonists	***k_{off} (min^{-1})***	***k_{on} ($M^{-1}min^{-1}$)***	***Dissociation $t_{1/2}$ (min)***	***Kinetic pK_d***	***Equilibrium pK_i***	***n***
Paliperidone	0.44 ± 0.04	1.80 ± 0.29 x10^8	1.57	8.60 ± 0.07	8.54 ± 0.07	4
(-)Sulpiride	2.23 ± 0.93	1.60 ± 0.67 x10^8	0.31	7.87 ± 0.06	7.58 ± 0.10	4
Remoxipride	1.90 ± 0.55	1.16 ± 0.37 x10^7	0.37	6.79 ± 0.04	6.68 ± 0.07	4
Melperone	1.48 ± 0.18	1.99 ± 0.41 x10^7	0.47	7.11 ± 0.04	7.05 ± 0.03	4
Clozapine	1.67 ± 0.25	8.23 ± 1.42 x10^7	0.42	7.69 ± 0.02	7.60 ± 0.02	4
Amisulpride	0.83 ± 0.05	3.44 ± 0.50 x10^8	0.83	8.61 ± 0.06	8.49 ± 0.07	4
Ziprasidone	1.07 ± 0.52	1.61 ± 0.50 x10^9	0.65	9.19 ± 0.18	9.16 ± 0.19	4
Risperidone	0.43 ± 0.05	4.83 ± 0.52 x10^8	1.60	9.05 ± 0.01	8.93 ± 0.05	4
Zotepine	1.41 ± 0.34	9.15 ± 1.63 x10^8	0.49	8.76 ± 0.17	8.69 ± 0.11	5
Sertindole	0.59 ± 0.07	4.91 ± 0.82 x10^8	1.18	8.92 ± 0.07	8.89 ± 0.03	4
Quetiapine	1.01 ± 0.09	6.57 ± 0.85 x10^6	0.69	6.82 ± 0.02	6.75 ± 0.07	4
Olanzapine	1.12 ± 0.12	1.79 ± 0.44 x10^8	0.62	8.17 ± 0.09	8.08 ± 0.11	4
Asenapine	0.93 ± 0.06	2.17 ± 0.65 x10^9	0.74	9.29 ± 0.16	9.29 ± 0.12	4
Loxapine	2.14 ± 0.33	4.04 ± 1.04 x10^8	0.32	8.25 ± 0.05	8.18 ± 0.05	4
Molindone	1.62 ± 0.29	6.49 ± 2.16 x10^7	0.43	7.51 ± 0.13	7.57 ± 0.12	6
(+)Butaclamol	0.036 ± 0.007	5.67 ± 1.71 x10^8	19.25	10.37 ± 0.12	10.32 ± 0.13	6

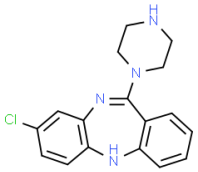
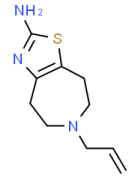
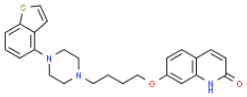
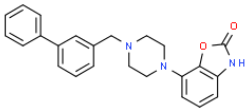
Flupenthixol	0.072 ± 0.010	3.50 ± 0.73 x10^8	9.60	9.67 ± 0.07	9.68 ± 0.10	4
Haloperidol	0.65 ± 0.07	2.13 ± 0.52 x10^9	1.06	9.49 ± 0.08	9.48 ± 0.08	4
Fluphenazine	0.040 ± 0.004	1.13 ± 0.10 x10^9	17.52	10.46 ± 0.06	10.29 ± 0.04	4
Chlorpromazine	1.99 ± 0.34	2.74 ± 0.79 x10^9	0.35	9.02 ± 0.15	9.01 ± 0.11	6
Thioridazine	1.41 ± 0.25	2.37 ± 0.61 x10^9	0.49	9.21 ± 0.03	8.93 ± 0.05	4
Perphenazine	0.23 ± 0.02	1.29 ± 0.17 x10^9	3.02	9.73 ± 0.06	9.53 ± 0.04	4
Trifluoperazine	0.22 ± 0.01	1.10 ± 0.20 x10^9	3.22	9.69 ± 0.10	9.48 ± 0.04	4
Spiperone	0.038 ± 0.006	2.55 ± 0.19 x10^9	18.12	10.84 ± 0.07	10.54 ± 0.04	4
Nemonapride	0.025 ± 0.005	1.51 ± 0.13 x10^9	27.6	10.80 ± 0.07	10.39 ± 0.04	5
Droperidol	0.38 ± 0.04	2.01 ± 0.38 x10^9	1.84	9.71 ± 0.10	9.99 ± 0.10	4
Raclopride	0.53 ± 0.14	6.69 ± 2.04 x10^8	1.31	9.08 ± 0.04	8.91 ± 0.08	4
Domperidone	0.15 ± 0.02	7.75 ± 1.63 x10^8	4.53	9.83 ± 0.07	9.81 ± 0.09	6

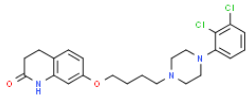
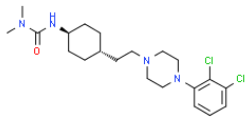
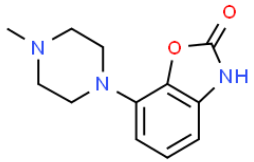
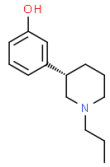
Table 3.11. Physicochemical properties of dopamine D_2 receptor agonists. Data from the National Center for Biotechnology Information. PubChem Compound Database; https://pubchem.ncbi.nlm.nih.gov/compound/

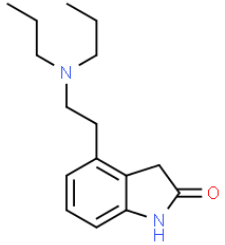
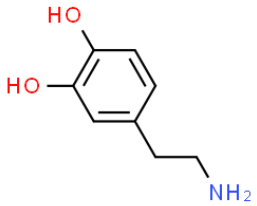
D_2 *agonist*	**Structure**	***Molecular Weight (g/mol)***	***XLogP3-AA**	***Heavy Atom Count***	**Topological Polar Surface Area A^2**
Bromocriptine		654.606	3.8	43	118
R-propylnorapomorphine		295.382	3.2	22	43.7
Lisuride		338.455	2.7	25	51.4
Pergolide		314.491	4.2	22	44.3

(+)3PPP		219.32	3	16	23.5
Apomorphine		267.328	2.3	20	43.7
Cabergoline		451.615	3.4	33	71.7
Rotigotine		315.475	4.9	22	51.7
GSK789472		295.808	ND	20	35.6

DHEC		611.743	3.3	45	118
7-OH DPAT		247.38	4.1	18	23.5
(-)Quinpirole		219.332	2.3	16	31.9
Sumanirole		203.245	0.4	15	44.4

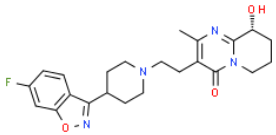
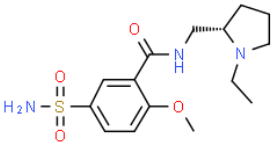
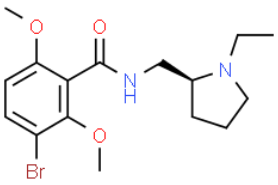
Desmethylclozapine		312.801	2.8	22	39.7
B-HT 920		209.311	**1.2	15	70.4
Brexpiprazole		433.57	4.7	31	73
Bifeprunox		385.467	4.2	29	44.8

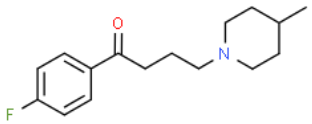
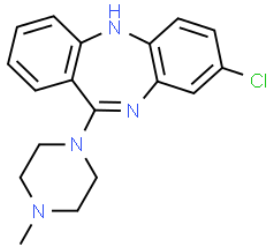
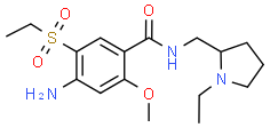
Aripiprazole		448.388	4.6	30	44.8
Cariprazine		427.414	4.3	28	38.8
Pardoprunox		233.271	1.1	17	44.8
(-)3PPP		219.32	3	17	ND

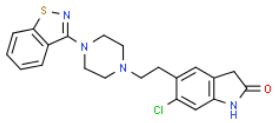
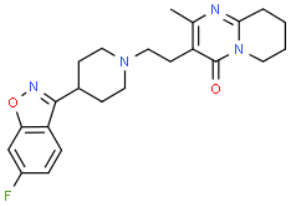
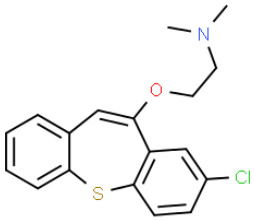
Ropinirole		260.381	2.7	19	32.3
Dopamine		153.181	-1	11	66.5

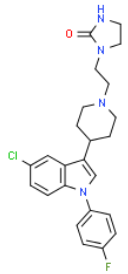
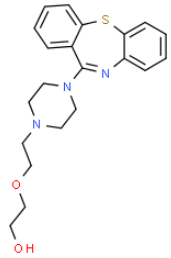
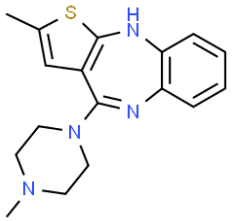
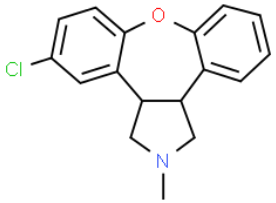
*clogP was calculated using an enhanced atomic approach. Atomic logP considers that each atom has a contribution to the logP, with contributions purely additive. Enhanced atomic takes into account the atom type eg. nitrogen of an amide is different to a nitrogen in an amine or pyridine. **Predicted data generated using the ACD/Labs Percepta Platform - PhysChem Module. ND = no data.

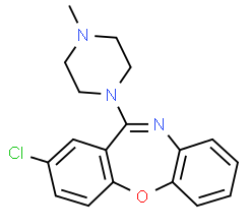
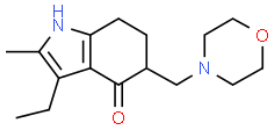
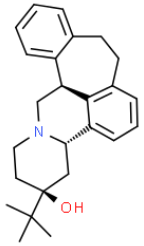
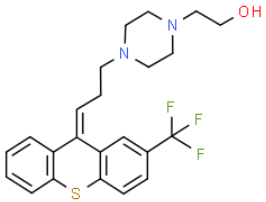
Table 3.12. Physicochemical properties of dopamine D_2 receptor antagonists. Data from the National Center for Biotechnology Information. PubChem Compound Database; https://pubchem.ncbi.nlm.nih.gov/compound/

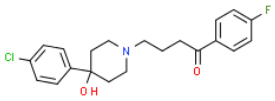
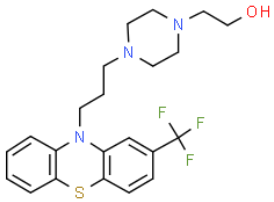
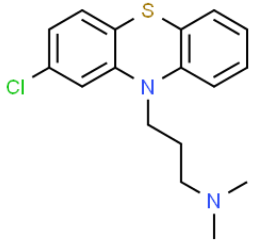
D_2 antagonists	**Structure**	***Molecular Weight (g/mol)***	***XLogP3-AA**	***Heavy Atom Count***	**Topological Polar Surface Area A^2**
Paliperidone		426.492	2.2	31	82.2
(-)Sulpiride		341.426	0.6	23	110
Remoxipride		371.275	2.1	22	50.8

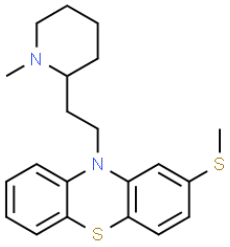
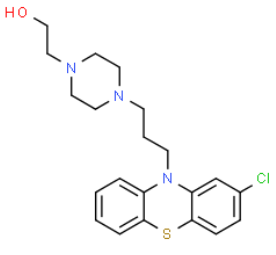
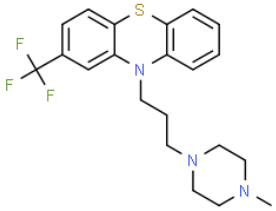
Melperone		263.356	3.3	19	20.3
Clozapine		326.828	3.2	23	30.9
Amisulpride		369.48	1.5	25	110

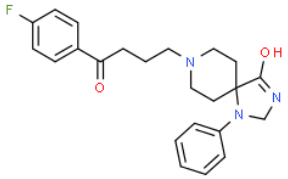
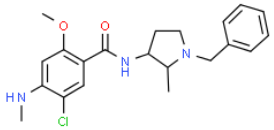
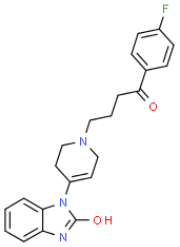
Ziprasidone		412.936	4	28	76.7
Risperidone		410.493	2.7	30	61.9
Zotepine		331.858	4.8	22	37.8

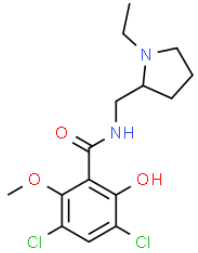
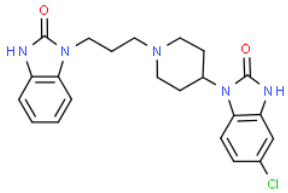
Sertindole		440.947	4.1	31	40.5
Quetiapine		383.51	2.1	27	73.6
Olanzapine		312.435	2.8	22	56.2
Asenapine		285.771	3.8	20	12.5

Loxapine		327.812	3.1	23	28.1
Molindone		276.38	1.7	20	45.3
(+)Butaclamol		361.529	5	27	23.5
Flupenthixol		434.521	4.5	30	52

Haloperidol		375.868	3.2	26	40.5
Fluphenazine		437.525	4.4	30	55.2
Chlorpromazine		318.863	5.2	21	31.8

Thioridazine		370.573	5.9	25	57.1
Perphenazine		403.969	4.2	27	55.2
Trifluoperazine		480.415	ND	30	35

Spiperone		395.478	3	29	52.6
Nemonapride		387.908	3.9	27	53.6
Droperidol		379.435	3.5	28	52.6

Raclopride		347.236	2.9	22	61.8
Domperidone		425.917	3.9	30	67.9

*clogP was calculated using an enhanced atomic approach. Atomic logP considers that each atom has a contribution to the logP, with contributions purely additive. Enhanced atomic considers the atom type eg. nitrogen of an amide is different to a nitrogen in an amine or pyridine. ND = no data.

Chapter 4 - Investigating the influence of tracer kinetics on competition-kinetic association binding assays; identifying the optimal conditions for assessing the kinetics of low-affinity compounds.

4.1 Introduction

Historically most drug discovery programs have relied upon equilibrium dissociation constant measurements when assessing the potential of future lead-drug candidates, rather than the kinetic parameters that comprise it (K_d = k_{off} / k_{on}). However, it is becoming more widely appreciated that optimising the kinetics of drug binding (k_{off} and k_{on}) can enhance both compound efficacy and duration of action (Sykes et al., 2009; Guo et al., 2012; Vauquelin, 2016; Copeland, 2016). This has resulted in the introduction of novel methods to assess ligand binding kinetics at earlier stages in the drug discovery process, allowing the development of structure-kinetic relationships (SKR) (Schmidtke et al., 2011; Georgi et al., 2018). A commonly applied method to assess the kinetics of unlabeled compounds is surface plasmon resonance (SPR) spectroscopy, but this is still not widely utilized for membrane proteins due to issues with protein purification and stability (Patching 2014). To overcome this competition-association kinetic binding assays using radioactive probes have been employed successfully to determine the kinetic values for both antagonists (Gillard and Chatelain 2006; Slack et al., 2011; Fleck et al., 2012; Sykes et al., 2014; Sykes et al, 2016) and agonists (Sykes et al., 2009; Sykes and Charlton 2012) acting at a variety of G protein-coupled receptors (GPCRs) at physiological temperature, and even more recently at non-GPCR targets (Yu *et al*., 2015).

Despite their undoubtedly high sensitivity, the use of radioactive probes as tracers in competition association binding assays presents several challenges. Classic radioactive binding requires the need for multiple washing steps to separate bound and free radioligand, adding complexity to the procedure and reducing throughput. Importantly the wash step requirement also prevents any possibility of multiple single sample reads. More recently scintillation proximity assays (SPA) have been formulated which can be performed in homogeneous conditions, but signal-drift due to bead settling can complicate interpretation at early time points (Xia et al., 2016).

The emergence of time-resolved fluorescent resonance energy transfer (TR-FRET)-based methods (Schiele et al., 2015; Klein-Herenbrink et al., 2016) and bioluminescence-based methods (Stoddart et al., 2018; Bouzo-Lorenzo et al., 2019) offers an alternative to radioactive binding assays and represent higher throughput

methods to assess unlabelled ligand kinetics. With the separation of bound and unbound-label no longer necessary multiple reads can be made from the same well (Emami-Nemini et al., 2013; Stoddart et al., 2015). Using the simple technique of TR-FRET we successfully characterised the binding of a series of dopamine D_2 specific agonists and clinically used antipsychotics employing a SNAP-tagged receptor labelled with terbium and a fluorescent tracer (Klein-Herenbrink et al., 2016; Sykes et al, 2017).

A key observation made during these studies was that the kinetic characteristics of the tracer had a profound effect on the reliability of the estimated kinetic parameters of unlabelled competitors (Klein-Herenbrink et al., 2016). This was most evident when using a slowly dissociating tracer to assess rapidly dissociating, low-affinity ligands. This represents a potential barrier to successfully introducing kinetic assays earlier in the drug discovery process (e.g. hit identification/validation) as tracers need to be capable of determining the kinetics of low affinity "hits" (in the μM range). Thus, the current study aimed to use a modeling and simulation approach to identify the optimal tracer characteristics for determining the kinetics of a variety of unlabeled ligands typically encountered during different stages of a drug discovery program (i.e. low affinity "hits" through to high affinity "candidates").

Using Monte Carlo simulations, we have assessed the ability of the global association method to accurately determine the kinetics of different model tracers. The global association method is a way of simultaneously fitting multiple tracer association curves (eg. different tracer concentrations) to find best fit k_{off} and k_{on} parameters across the whole dataset. Additionally using Monte Carlo simulations, we have explored the utility of these model tracers to predict the kinetic parameters of unlabeled ligands in competition-association binding mode. Furthermore, we have explored the influence of experimental design on the accuracy of kinetic parameter estimation, testing the impact of increasing tracer concentrations, and investigating different plate reader configurations, particularly the influence of read frequency time and on-line (direct reagent injection into sample wells) versus off-line (reagent addition into plate prior to insertion into reader) reagent addition.

Finally, we test the validity of this modelling approach through the detailed characterisation of two dopamine D_2R specific fluorescent tracers; spiperone-d2 and PPHT-red. Assessing their ability to determine the kinetics of D_2R specific ligands with very varied kinetic characteristics, from the rapidly dissociating chlorpromazine to the very slowly dissociating butaclamol.

The analysis presented has important implications for the design of competition-kinetic approaches to assess unlabelled compound kinetics, providing a framework for the identification and testing of suitable tracers. In particular, we have identified the optimal tracer characteristics and experimental design for assessing low-affinity competitors, enabling the utilisation of kinetics assays much earlier in the drug discovery process.

.

4.2 Materials and Methods

4.2.1 Determining the kinetics of the tracer for use in competition kinetic binding studies

Monte Carlo simulations are useful to investigate the behaviour of a system under controlled situations and may be thought of as statistical experiments. They provide an estimation of variance for complex models, which ultimately helps researchers with experimental design and provides confidence in a particular experimental approach before testing. The underlying principle is to take a simulated dataset that is based on a set of 'ideal' model parameters, add random error to the 'dataset' and then recreate the resulting dataset many times to obtain the parameters of interest. In this case, the 'dataset' comprises an XY table where X is time and Y is % specific binding of the tracer. This process allows a frequency distribution to be built from the resulting parameter estimates allowing an understanding of the associated error of each parameter estimate under the conditions employed (Christopoulos 2001).

The competition association assay model (Motulsky and Mahan, 1984) relies on an accurate assessment of the kinetic properties of the labelled tracer, both the association rate constant (k_{on} *or* $k1$) and the dissociation rate constant (k_{off} *or* $k2$). Since the introduction of fitting software, such as GraphPad Prism, a popular experimental procedure to estimate the kinetics of the tracer is to monitor the binding of two or more different concentrations of tracer over time until equilibrium is reached, in doing so it is possible to calculate the k_{on} and k_{off} values of the tracer by simultaneously fitting all curves to generate global estimates for these rate parameters (Motulsky and Neubig 2010; Sykes et al., 2010).

For this study tracer association was simulated at multiple ligand concentrations [L] using GraphPad Prism 6.0, employing Equation 2.5 as described in Chapter 2, section 2.2.8 Signal detection and data analysis.

Tracer binding simulations were performed to assess the effect of on-line and off-line reagent addition on our ability to accurately estimate the kinetics of a variety of model tracers with varied kinetics parameters, consistent with the properties of compounds discovered in the various phases of the drug discovery cascade, the

details of which are provided in Table 4.1. Tracer Monte Carlo simulations were performed using the following parameters; the k_{on} and k_{off} of each model tracer studied were allowed to vary, whilst the concentrations of tracer (L) employed were fixed at various multiples of the tracer's affinity, specifically 30, 10, 3, 1, 0.3, 0.1 xK_d. Unless otherwise stated the assay start time was fixed at either 1 sec to mimic on-line addition of reagents via plate reader injectors or 30 sec to mimic the delay in the time to read following off-line addition of membranes before insertion of the assay plate into the plate reader. Read frequency (i.e. the time between each well-read) was varied at 1, 5, 10, 20 & 60 seconds. Random error was added to the generated y values by taking each theoretical (i.e. 'correct') value and adding to it a random number taken from a uniformly distributed population with a standard deviation equal to one. The random error chosen for simulation was Gaussian absolute to directly reflect the pattern of error observed in our experimental data. The resulting simulated data sets were individually fit to the association kinetic model equation (two or more concentration of hot, GraphPad Prism 6.0) and 'Global (shared) parameters' including tracer k_{off} and k_{on} values were tabulated. In total 200 simulations were performed per test condition.

Table 4.1. Tracer equilibrium affinity and kinetic properties typical of the kinetic parameters of compounds discovered at all phases of the drug discovery screening cascade. These tracer properties were used to construct Figure 4.1 to 4.14 and Supplementary Figures 8.1 and 8.2, see Chapter 8, 8.1 Appendix I – Supplementary data.

Tracer K_D (nM)	**Tracer k_{off} (min^{-1})**	**Tracer k_{on} (M^{-1} min^{-1})**	**Characteristic of tracer**
0.01	0.01	$1x10^9$	Very high affinity candidate, very slow off
1	0.1	$1x10^8$	High affinity candidate, slow off
100	1	$1x10^7$	Lead-like, fast off
300	10	$3x10^7$	Hit-like, very fast off

4.2.2 Determining the suitability of the tracer for competition kinetic binding studies

The interactions of the tracer and unlabelled competitor with the receptor are described by two differential equations which when solved yield a single equation describing the binding of the tracer as a function of time (Motulsky and Mahan, 1984). This model was used to simulate competition association curves to a variety of unlabelled compounds with different association rate constants (k_{on} *or* $k3$) and dissociation rate constants (k_{off} *or* $k4$), according to Equation 2.7 as described in Chapter 2, section 2.2.8 Signal detection and data analysis.

All competition kinetic association simulations were performed using the model tracers described in Table 4.1. These Monte Carlo simulation studies were designed to assess the effect of tracer kinetics on the ability of the Motulsky-Mahan model to distinguish compounds typically encountered in a drug discovery program with a wide range of kinetic off-rates ranging from the more rapidly dissociating (e.g. k_{off} = 100min^{-1} representative of low affinity fragments) to the more slowly dissociating (e.g. k_{off} = 0.01min^{-1} representative of a lead candidate compound).

Unless otherwise stated, the concentration of tracer (L) employed was fixed at 3x K_d. The concentration of unlabelled competitor (I) was routinely fixed at various multiples of its affinity, specifically 100, 30, 10, 3, 1x K_d. Also taken into consideration was on-line versus off-line addition protocols and their effect on our ability to accurately estimate the kinetics of unlabeled compounds with varied kinetics parameters. Start time was fixed at either 1 second (to mimic on-line addition) or 30 seconds (to mimic off-line addition) and the read frequency was varied using either 1, 5, 10, 20 & 60 seconds unless otherwise stated.

Random error was added to the generated y values by taking each theoretical (i.e. ‘correct’) value and adding to it a random number taken from a uniformly distributed population with a standard deviation equal to one. The random error chosen for simulation was Gaussian absolute to directly reflect the pattern of error observed in our experimental data. The resulting simulated data sets were individually fit to the competition association model equation (Kinetics of competitive binding, GraphPad

Prism 6.0) and 'Global (shared) parameters' including tracer k_{off} and k_{on} values were tabulated. In total 200 simulations were performed per test condition.

To test the effect of tracer concentration on our ability to estimate the kinetic parameters of unlabelled compounds we performed a further series of simulations but this time we employed tracer concentrations (L) at 1x, 10x and 30x K_d. The concentrations of unlabelled competitor (I) was varied accordingly. This allowed us to test the effect of decreasing and increasing tracer competition on the accuracy of unlabelled compound kinetic determinations.

In another series of competition kinetic association simulations, the ability of a rapidly dissociating tracer to assess the kinetics of low affinity (1-1000 μM) unlabelled fragments was explored in both double and single concentration screening modes. All Monte Carlo simulations were performed using the following parameters; the k_{on} and k_{off} of the model tracer studied was fixed at $3x10^7$ M^{-1} min^{-1} and 10 min^{-1} respectively, with the concentration of tracer (L) employed fixed at 3x K_d whilst the concentrations of the fragments were fixed specifically at 10 and 100 μM (typical of a fragment screen where affinity of the fragments is unknown). Start time was fixed at 1 second (to mimic on-line addition) and a standard read frequency of 5 seconds was employed. The resulting simulated data sets were individually fit to the competition association model and 'Global (shared) parameters' including competitor k_{off} and k_{on} values were tabulated. In total 200 simulations were performed per test condition. All the experiments described above assume that the law of mass action are obeyed, and that ligand depletion does not occur under any of the conditions of tracer and competitor binding explored (Carter et al., 2007).

4.2.3 Monte Carlo simulation data analysis

All Monte Carlo simulations were performed in Prism 6.0. In total 200 simulations were performed per test condition using an associated error equivalent to a standard deviation of one. 'Global (shared) parameters' associated with Equations 2.5 and 2.7 as described in Chapter 2 section 2.2.8 Signal detection and data analysis, were recorded and an outlier test (using an iterative Grubb's test, α=0.0001) was performed on reported k_{on} and k_{off} values for tracers and unlabelled competitors. Outliers and ambiguous fits (those for which confidence intervals were extremely

wide) were removed from the analysis before calculation of mean and % coefficient of variance (CV) values (i.e. (standard deviation/mean)*100), which are indications of accuracy and variation around the expected input value. Mean fitting values were considered a reliably "good fit" if >90% of fits (i.e. >180//200) were returned without being judged as either outlier and/or ambiguous fits. Ambiguous fits are those for which confidence intervals are extremely wide and therefore not reported (see GraphPad Prism 7.0 online guide). Graphical representation of Monte Carlo data was also performed using R and competition association data were fitted in Prism 6.0.

4.2.4 Fluorescent ligand binding assays

Materials

PPHT ((±)-2-(n-phenethyl-n-propyl)amino-5-hydroxytetralin hydrochloride;1-Naphthalenol, 5,6,7,8-tetrahydro-6-[(2-phenylethyl)propylamino]) derivative labeled with a red fluorescent probe (PPHT-red) and spiperone-d2 was obtained from Cisbio Bioassays (Bagnols-sur-Cèze, France). Ninety-six-well polypropylene plates (Corning) were purchased from Fisher Scientific UK (Loughborough, UK) and 384-well Optiplates were purchased from PerkinElmer (Beaconsfield, UK). GppNHp, chlorpromazine hydrochloride and (+)-butaclamol used in competition assays were obtained from Sigma-Aldrich (Poole, UK). Domperidone, and haloperidol hydrochloride used for competition assays were obtained from Tocris Bioscience (Avonmouth, Bristol). Pergolide and ropinirole were kind gifts from Dr Robert Lane (Monash University), whilst bromocriptine was a kind gift of Dr Nicholas Holliday (Nottingham University).

Cell culture

The host Chinese hamster ovary (CHO) K1 cell line was provided by Prof. J. Baker, University of Nottingham (ATCC #CCL-61) and established as described in Chapter 3, section 3.2.2 Cell culture. CHO-hD_{2L} cells were maintained as described in Chapter 2, section 2.2.1 Cell culture.

Determination of D_2R fluorescent ligand binding kinetics.

All fluorescent binding experiments using PPHT-red and spiperone-d2 were conducted in white 384-well Optiplate plates, in assay binding buffer, HBSS containing 5mM HEPES, 1% DMSO and 0.02% pluronic acid pH 7.4, 0.1mM GppNHp. GppNHp was included to remove the G protein-coupled population of receptors that can result in two distinct populations of binding sites in membrane preparations since the Motulsky–Mahan model is only appropriate for ligands competing at a single site. In all cases, non-specific binding was determined in the presence of 10 μM haloperidol.

To accurately determine the association rate (k_{on}) and dissociation rate (k_{off}) values, the observed rate of association (k_{obs}) was calculated using at least four different concentrations of either PPHT-red or spiperone-d2. SNAP-tagged terbium labelled human dopamine D_{2L} receptors expressed in CHO cell membranes (2 μg per well) were injected into wells containing six different concentrations of the fluorescent tracers PPHT-red (50-1.56 nM) or spiperone-d2 (10-0.3 nM) in a final assay volume of 40 μL. A detailed description of the terbium labelling procedure and membrane preparation can be found in Chapter 2 section 2.2.5 Terbium labeling of SNAP-tagged cells and membrane preparation.

The degree of PPHT-red or spiperone-d2 bound to the receptor was assessed at multiple time points by HTRF detection to allow construction of association kinetic curves. The resulting data were globally fitted to the association kinetic model (Equation 2.5 as described in Chapter 2 section 2.2.8 Signal detection and data analysis) to derive a single best-fit estimate for k_{on} and k_{off}.

Competition binding kinetics.

To determine the association and dissociation-rates of D_2R ligands, we used a competition kinetic binding assay we recently described to profile the kinetics of a series of D_2R agonists (Klein-Herenbrink *et al*., 2016). This approach involves the addition of a receptor preparation to wells containing fluorescent ligand and competitor so that at t = 0 all receptors are unoccupied.

12.5 nM PPHT-red (~1x K_d) or 5 nM spiperone-d2 (~10x K_d), concentrations which avoid ligand depletion in this assay volume, (see Carter *et al*., 2007) were added simultaneously with the unlabeled compound (at t = 0) to CHO cell membranes containing the human dopamine D_{2L} receptor (2 µg per well) in 40 µL of assay buffer.

Online addition is best achieved by injecting an equal volume of the receptor (20 µL membranes) to the assay plate containing the ligands of interest (e.g. tracer and/or competitor 20 µL) to ensure complete and adequate mixing of all reagents. The degree of PPHT-red bound to the receptor was assessed at multiple time points by HTRF detection. The kinetic parameters of PPHT-red and spiperone-d2 plus those of unlabeled compounds were determined using a start time of ~1sec and a read frequency of 5sec.

Non-specific binding was determined as the amount of HTRF signal detected in the presence of haloperidol (10 µM) and was subtracted from each time point, meaning that t = 0 was always equal to zero. Each time point was conducted on the same 384-well plate incubated at room temperature with orbital mixing (1sec of 100 RPM/cycle).

Data were globally fitted using Equation 2.7 section 2.2.8 Signal detection and data analysis, to simultaneously calculate k_{on} and k_{off} of the unlabeled compounds. Different competitor concentration ranges were chosen, as compounds with a long residence time equilibrate more slowly, so a higher relative concentration is required to ensure the experiments reach equilibrium within a reasonable time frame (20 minutes), while still maintaining a good signal-to-noise.

4.2.5 Data analysis and signal detection

For the binding experiments described, signal detection was performed on a PHERAstar FS (BMG Labtech, Offenburg, Germany) using standard HTRF settings. The terbium donor was always excited with up to 6 laser flashes at a wavelength of 337 nm. Kinetic TR-FRET signals were collected at 5 seconds when using red acceptor. HTRF ratios were obtained by dividing the acceptor signal (665 nm) by the donor signal (620 nm) and multiplying this value by 10,000.

4.3 Results

4.3.1 Monte Carlo simulations

Accurate determination of model tracer kinetic parameters

To accurately calculate the kinetic association (k_{on}) and dissociation rates (k_{off}) of unlabelled competitor compounds the kinetic parameters of the tracer used must first be determined by fitting tracer association data to a global kinetic model (see Equation 2.5 Chapter 2 section 2.2.8 Signal detection and data analysis). Simulations were performed for four model tracers whose rates of dissociation differed up to 1000-fold (see Table 4.1).

For each tracer tested a family of association kinetic curves were constructed using 6 concentrations of each tracer, ranging from ~30 to 0.1x K_d with each association curve being monitored to the point of equilibrium; such that Y_{max} is reached allowing for the most accurate estimation of tracer kinetic parameters, k_{on} and k_{off} (see Figure 4.1A and C).

To construct Figure 4.1A and C using Monte Carlo simulations the k_{on} input value for the very rapidly dissociating tracer was fixed at 3 x10^7 M^{-1} min^{-1} and k_{off} input value at 10 min^{-1}. Figure 4.1A and C differ only in their initial start time 1 sec (representative of on-line injection) and 30 sec (representative of off-line addition) respectively with the read frequency fixed every 10 sec thereafter. What is immediately apparent under these simulation conditions is that the equilibrium between a very rapidly dissociating tracer (k_{off} 10min^{-1}) and the receptor is reached rapidly within the first 30 sec and as a consequence, an accurate determination of tracer association is improbable with a 30 sec start time. This is reflected in the graphical plots, Figure 4.1B and D showing the relationship between input tracer k_{off} and output k_{off} and read frequency, following an online injection and offline addition protocol. With a start time of 1 sec tracer kinetic determinations (data fits) are on the whole extremely reliable, with a 'good fit' achieved on > 90% of the 200 fits. In contrast reliable determinations of tracer kinetics, as judged through off-rate monitoring, following a 30 sec start time representative of off-line addition, is only possible when the off-rate of the tracer is less than 1min^{-1}.

Also apparent is the effect of read frequency on the variation in reported k_{off} values with shorter read frequencies resulting in an improved quality of fit as highlighted by a reduction in the variability of the estimated output of tracer off-rate values. The results of Monte Carlo simulations using the kinetic association model equations are summarized in Chapter 8, Supplementary Table 8.1. It must be emphasized that although our analysis focuses on the kinetic parameter k_{off}, the variability of k_{on} is also documented in these Supplementary Tables.

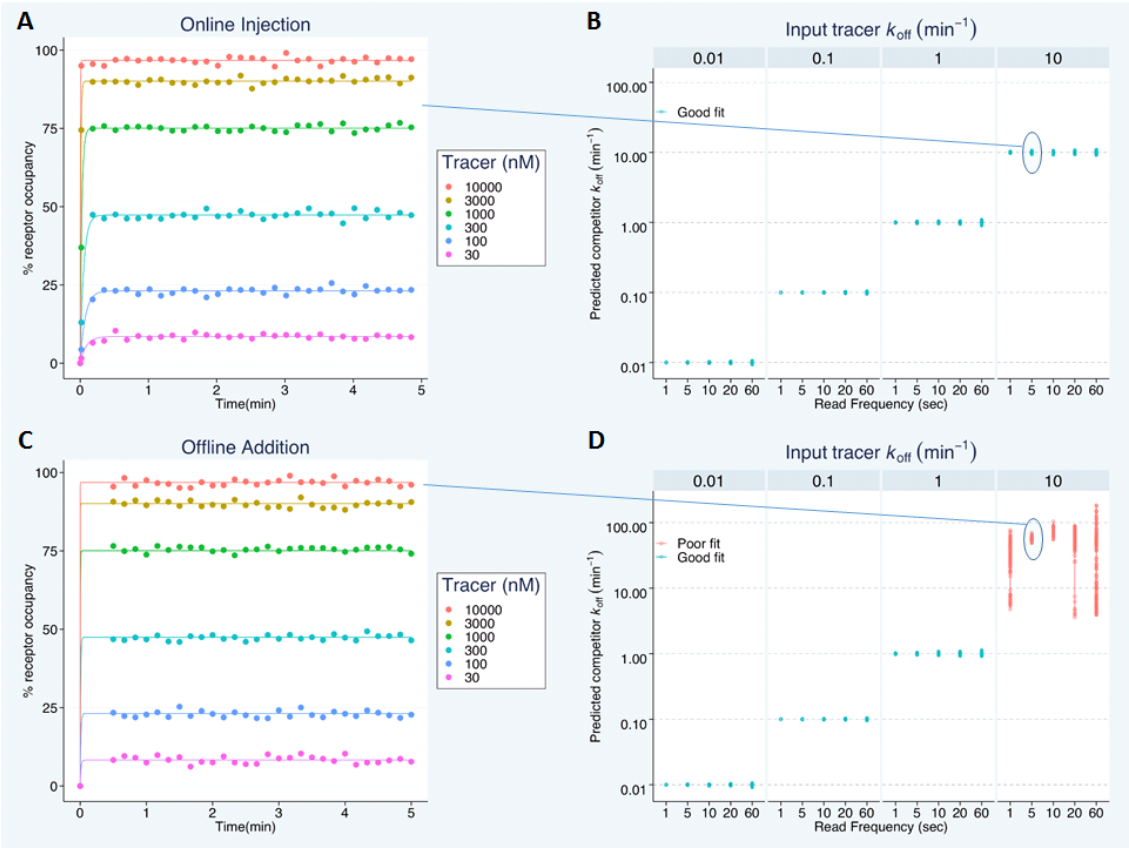


Figure 4.1. Monte-Carlo simulation results exploring the effect of sample time on the determination of tracer kinetic parameters. **(A)** Association with time (1sec start; 10sec interval) of various concentrations of a very rapidly dissociating tracer with the following kinetic parameters; k_{off} of $10min^{-1}$, k_{on} of $3x10^7$ M^{-1} min^{-1} representative of 200 simulations. In this globally fitted model (see Equation 2.5, Chapter 2 section 2.2.8 Signal detection and data analysis) of tracer binding, tracer concentrations [L] are fixed, k_{on} and k_{off} are shared parameters to be determined. **(B)** Effect of read frequency on the output k_{off} (or predicted competitor k_{off}) of a series of experimental tracers (L) with varied kinetics, absolute values are the average of 200 simulations. In this instance, tracer simulations were performed with an initial start time of 1sec representative of injection of receptor to a reaction containing tracer only. Blue open symbols represent conditions which returned >90% reliable fits. Red open symbols represent conditions which returned <90% reliable fits. **(C)** Association with time (30sec start; 10sec interval) of various concentrations of a very rapidly dissociating tracer with the following kinetic parameters; k_{off} of $10min^{-1}$, k_{on} of $3x10^7$ M^{-1} min^{-1}, representative of 200 simulations. **(D)** Effect of read frequency on the output k_{off} of a series of experimental tracers (L) with varied kinetics. In this instance tracer simulations were performed with an initial start time of 30 sec representative of off-line

addition of receptor to a reaction containing tracer only, absolute values are the average of 200 simulations. Line-circles indicate the position of example simulations **(A)** and **(C)** and represent a small fraction of the total number of simulations shown in the plots **(B)** and **(D)**.

Competition kinetic binding between tracer and unlabelled competitor mimicking an off-line addition protocol

To accurately determine the kinetics of unlabelled competitor compounds it is conventional to construct a family of association kinetic curves using a fixed tracer concentration (~3x K_d) and varying concentrations of the unlabelled compound with each association curve being monitored until equilibrium (see Figure 4.2A and B). In the case, of the most slowly dissociating tracer, association curves were monitored for 180 min to reflect practical limitations. The resulting data were then fitted to the Motulsky–Mahan model which describes the interaction between an unlabelled compound and a labelled tracer and allows us to calculate the k_{on} and k_{off} of the unlabelled compound (see Equation 2.7 Chapter 2 section 2.2.8 Signal detection and data analysis).

Example results of Monte Carlo simulations using the Motulsky-Mahan model equation are shown in Figure 4.2A and B. In each case the very rapidly dissociating tracer was employed; with input values of k_{on} for the tracer fixed at 3 x10^7 M^{-1} min^{-1} and k_{off} fixed at 10 min^{-1}. Figure 4.2A and B differ only in respect of the kinetic properties of the unlabelled compound in competition with the tracer, with initial start times fixed at 1 sec and with read frequency fixed every 10 sec thereafter. Under these simulation conditions and in the presence of a rapidly dissociating unlabelled compound (with kinetic parameters; k_{off} of 10 min^{-1}, k_{on} of 1x10^6 M^{-1} min^{-1}), the equilibrium between the rapidly dissociating tracer, competitor compound and receptor is reached rapidly within the first 30 sec (see Figure 4.2A).

In direct contrast in the presence of a more slowly dissociating competitor (with kinetic parameters; k_{off} of 1min^{-1}, k_{on} of 1x10^7 M^{-1} min^{-1}) then the time to equilibrium is markedly increased with a characteristic 'overshoot' in the initial binding of the tracer (see Figure 4.2B). The data contained in Figure 4.2 represents a single simulation and is illustrative of the whole data set which is summarized in Figure 4.3.

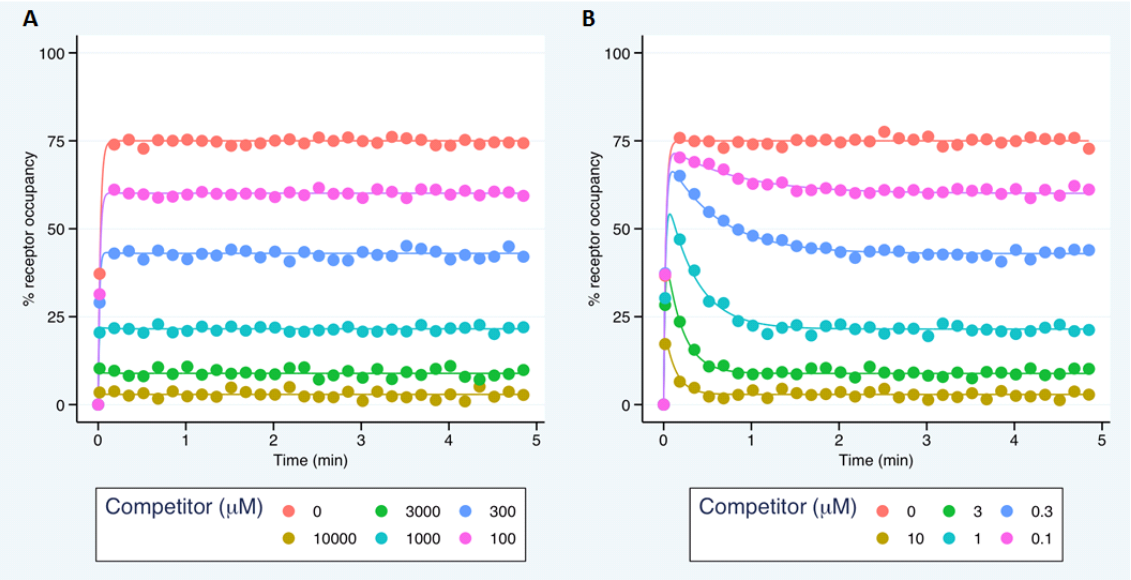


Figure 4.2. Monte-Carlo simulation results exploring the effect of competitor off-rate on the competition profile observed with a rapidly dissociating tracer. **(A)** Competition between a fixed concentration (3x K_d) of a very rapidly dissociating tracer; k_{off} of 10 min^{-1}, k_{on} of $3x10^7$ M^{-1} min^{-1} and a rapidly dissociating competitor with the following kinetic parameters; k_{off} of $10min^{-1}$, k_{on} of $1x10^6$ M^{-1} min^{-1}, data shown are representative of 200 simulations. **(B)** Competition between a fixed concentration (3x K_d) of a very rapidly dissociating tracer and a slowly dissociating competitor with the following kinetic parameters; k_{off} of $1min^{-1}$, k_{on} of $1x10^7$ M^{-1} min^{-1}, data shown are representative of 200 simulations. In all cases, tracer and competitor binding simulations were performed with an initial start time of 1sec (representative of injection of receptor to a reaction containing tracer) and a read frequency of 10sec.

State of the art radioligand-based competition association binding assays are routinely formulated using only 12 time points (Sykes et al., 2010) employing either a single concentration of competitor (Sykes et al., 2014; Martella et al., 2017) or up to three concentrations of competitor (Sykes et al., 2009; Sykes et al., 2010) and a tracer concentration in the range of 1-10x its own K_d. Current knowledge of FRET-based competition association binding assays is based on a small number of studies which in general have employed an offline addition protocol to improve experimental throughput but also to allow greater temperature control during the initial mixing step (Klein-Herenbrink et al., 2016; Sykes et al., 2017; Sykes and Charlton 2018).

Figure 4.3A-D shows summary off-rate data from the Motulsky-Mahan fits of the Monte-Carlo kinetic simulations exploring the effect of sample time and tracer kinetics on our ability to accurately determine competitor kinetic parameters (k_{off} range from 100 to 0.01 min^{-1}) and is representative of an off-line addition protocol with a 30 sec start time. In all cases, tracers were employed at a concentration 3x their own K_d value. These results demonstrate that even the very rapidly dissociating tracer examined (k_{off} = 10 min^{-1}) is not able to accurately determine the kinetics of unlabeled compounds with off-rates ranging from 100 – 10 min^{-1} (see Figure 4.3A). This represents a limitation in the kinetic quantification of unlabelled compounds using the competition association method where reagents are added offline from the plate reader.

Also apparent was the influence of read frequency on our ability to accurately predict the kinetics of unlabeled competitor compounds with slower dissociation rates, i.e. those in the range of 0.01 min^{-1}, reflecting the imprecise fitting of the tracer 'overshoot'. Interestingly, a tracer with a k_{off} of 1 min^{-1} under the conditions explored could not accurately fit the kinetics of unlabeled compounds with a k_{off} of 100 min^{-1} and is only suitable to unambiguously and accurately quantify the kinetics of unlabeled compounds with a k_{off} in the range of 10 min^{-1} if the read frequency remains at 1 sec (see Figure 4.3B). Almost identical patterns were observed for tracers with k_{off} values of 0.1 and 0.01min^{-1} (see Figure 4.3C and D). The results of Monte Carlo simulations using the Motulsky-Mahan model equation are summarized in Chapter 8, Supplementary Tables 8.2 to 8.5.

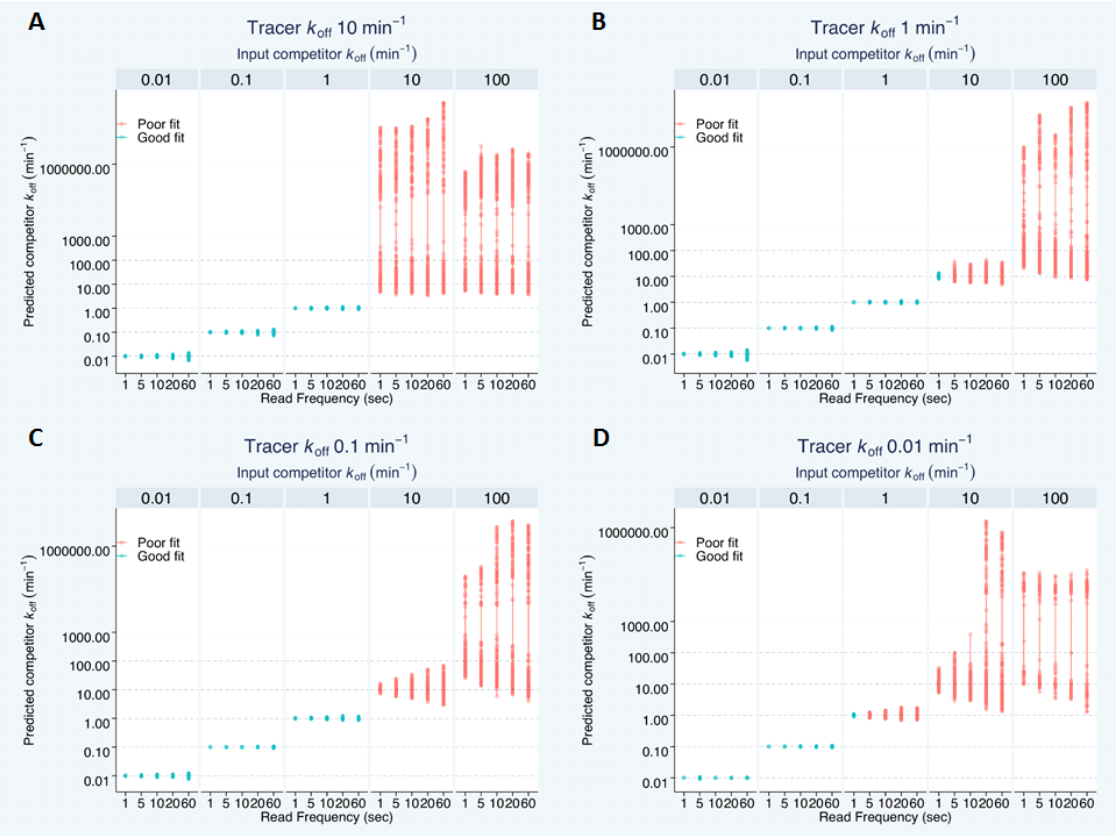


Figure 4.3. Monte-Carlo simulation results exploring the effect of sample time and tracer kinetics on the accurate determination of competitor k_{off} representative of an off-line addition protocol. Individual figures show the effect of assay read frequency-time on the measured k_{off} of unlabelled competitor compounds with varied kinetics in competition with a fixed concentration (3x K_d) of; **(A)** a very rapidly dissociating tracer with the following kinetic parameters; k_{off} of 10min^{-1}, k_{on} of 3x10^7 M^{-1} min^{-1}, **(B)** a rapidly dissociating tracer with the following kinetic parameters; k_{off} of 1min^{-1}, k_{on} of 1x10^7 M^{-1} min^{-1}, **(C)** a slowly dissociating tracer with kinetic parameters; k_{off} of 0.1min^{-1}, k_{on} of 1x10^8 M^{-1} min^{-1}, and **(D)** a very slowly dissociating tracer with kinetic parameters; k_{off} of 0.01min^{-1}, k_{on} of 1x10^9 M^{-1} min^{-1}. Blue open symbols represent conditions which returned >90% reliable fits. Red open symbols represent conditions which returned <90% reliable fits. In all cases tracer simulations were performed with an initial start time of 30sec representative of off-line addition of receptor to a reaction containing free tracer (L) and unlabelled competitor (I), absolute values are the average of 200 simulations.

Competition kinetic binding between tracer and unlabelled competitor mimicking an on-line injection protocol

Having established the limitation of the off-line injection protocol we decided to explore the potential of utilising on-board plate reader injectors and the increased resolution at very early time points to improve the goodness of fit (fit quality). Figure 4.4A-D shows summary dissociation rate estimates obtained by fitting Monte-Carlo simulations that explore the effect of read frequency and tracer kinetics on our ability to accurately determine competitor kinetic parameters (k_{off} range from 100 to 0.01 min^{-1}) and is representative of an injection protocol with a 1 sec start time. In all cases, tracers were employed at a concentration 3x their K_d value. These simulations demonstrate that the very rapidly dissociating tracer examined (k_{off} = 10 min^{-1}) can accurately determine the kinetics of unlabeled compounds with off-rates ranging from 100 – 0.01 min^{-1} (see Figure 4.4A). Interestingly under these tracer conditions employed the range of dissociation rate estimates markedly increases for the most rapidly dissociating unlabeled compounds examined (10-100 min^{-1}) representing the limit of kinetic detection for this type of competition kinetic binding approach (See Chapter 8, Supplementary Table 8.2). Also apparent was the influence of increasing read frequency on our ability to accurately predict the kinetics of unlabeled compounds with slower dissociation rates in the range of 0.01 min^{-1}. Increased variation likely reflects the imprecise fitting of the tracer 'overshoot' which is reliant on early time points for accuracy. In contrast, a tracer with a k_{off} of 1 min^{-1} is seemingly suitable for the determination of off-rates in the range of ~10 min^{-1}, but increasing variation in the mean is observed as the read frequency is increased from 1 to 60 seconds (see Figure 4.4B). Practically this wider degree of variation in the mean will become especially apparent if the number of observations for a particular compound is kept low (i.e. n ≤ 4). A different pattern is observed for a tracer with a k_{off} value equal to 0.1 min^{-1}, as shown in Figure 4.4C for compounds with rapid off-rates between 10-100 min^{-1} the number of ambiguous fits is very high (see Chapter 8, Supplementary Table 8.4), and only compounds with k_{off} value of ≤ 1 min^{-1} that can be measured without ambiguity at this concentration of tracer employed (i.e. 3x K_d). Interestingly the appearance of ambiguity in fitting estimates precedes any inaccuracies in the fitting estimates themselves. Finally a kinetic tracer with a k_{off} of 0.01min^{-1} employed at a concentration of 3x K_d, is only able to unambiguously (and

accurately) determine the kinetics of compounds with $k_{off} \leq 1 min^{-1}$ when the read frequency is shortened to 1 sec (see Figure 4.4D) and as a consequence is of limited value as a tracer for kinetic determinations of more rapidly dissociating compounds.

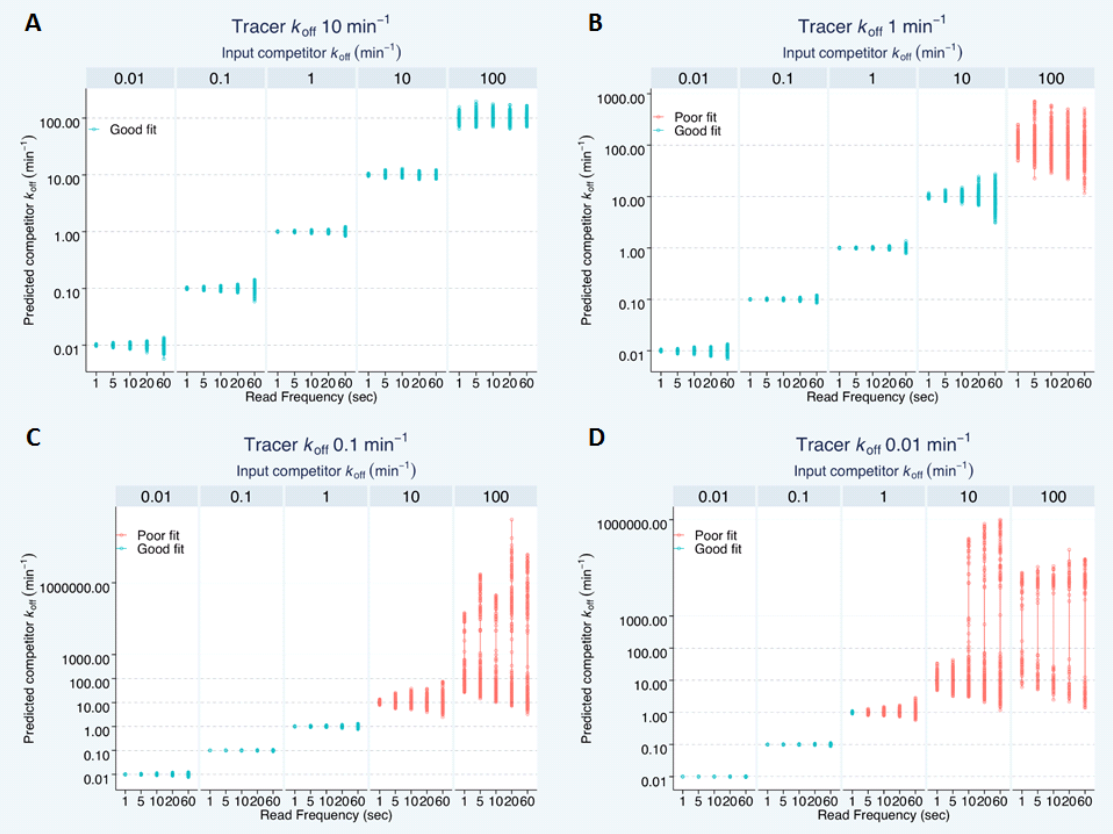


Figure 4.4. Monte-Carlo simulation results exploring the effect of tracer kinetics and sample time on the accurate determination of competitor k_{off} representative of an injection protocol. Individual figures show the effect of assay read frequency on the measured k_{off} of unlabelled competitor compounds with varied kinetics in competition with a fixed concentration (3x K_d) of; **(A)** a very rapidly dissociating tracer with the following kinetic parameters; k_{off} of 10min^{-1}, k_{on} of 3x10^7 M^{-1} min^{-1}, **(B)** a rapidly dissociating tracer with kinetic parameters; k_{off} of 1min^{-1}, k_{on} of 1x10^7 M^{-1} min^{-1}, **(C)** a slowly dissociating tracer with kinetic parameters; k_{off} of 0.1 min^{-1}, k_{on} of 1x10^8 M^{-1} min^{-1}, and **(D)** a very slowly dissociating tracer with kinetic parameters; k_{off} of 0.01min^{-1}, k_{on} of 1x10^9 M^{-1} min^{-1}. Blue open symbols represent conditions which returned >90% reliable fits. Red open symbols represent conditions which returned <90% reliable fits. In all cases, tracer simulations were performed with an initial start time of 1sec representative of injection of receptor to a reaction containing free tracer (L) and unlabelled competitor (I), absolute values are the average of 200 simulations. k_{obs} $t_{1/2}$ values (0.693/k_{obs}) for the tracers with dissociation rates of 10, 1, 0.1, and 0.01 min^{-1} were 1.1 sec, 10.4 sec, 1.7 min and 17.3 min respectively.

The figures which are derived from these Monte-Carlo simulations are useful guides to enable investigators interested in compound kinetics and associated SAR to set up kinetic screens and choose appropriate tracers to profile the properties of unlabeled compounds. To illustrate some key points, Monte-Carlo simulation results reproducing the experimentally observed effect of competitor off-rate on the competition profile observed with a rapidly dissociating tracer and a slowly dissociating tracer with varying start time are depicted in Figure 5A-D. Figure 5A shows competition between a fixed concentration (3x K_d) of a very slowly dissociating tracer (k_{off} of 0.01 min^{-1}, k_{on} of $1x10^9$ M^{-1} min^{-1}) and unlabeled competitors with varying dissociation-rates. What becomes apparent is that despite the variation in the unlabeled compound off-rate (0.01- 100 min^{-1}) the tracer association curves in the presence of the compounds with a k_{off} > 0.01 become bunched to the point they become practically indistinguishable. Figure 5C was obtained under identical conditions apart from a 30 sec delay in start time, representative of off-line addition. The increased start time has little effect on the ability to discriminate between the kinetic off-rates of these compounds primarily as the tracer itself is slow to reach equilibrium with the receptor.

Figure 5B shows competition between a fixed concentration (3x K_d) of a rapidly dissociating tracer (k_{off} of 10 min^{-1}, k_{on} of $3x10^7$ M^{-1} min^{-1}) and unlabeled competitors with varying dissociation-rates (0.01- 100 min^{-1}), and demonstrates how it is possible to accurately determine the dissociation-rates of the more rapidly dissociating competitors using the injection protocol (k_{off} range 0.01–10 min^{-1}, assay start time 1 sec). Figure 5D was obtained under identical conditions apart from a 30 sec delay in start time representative of off-line addition. This time the increased start time has a major effect on the ability of this tracer to discriminate between the kinetic off-rates of these compounds primarily as the tracer itself very rapidly reaches equilibrium with the receptor. Interestingly this loss of early time points in the case of an unlabeled competitor with a k_{off} of 10 min^{-1} results in an apparent underestimation of the k_{off} of the unlabeled competitor as demonstrated by the apparent tracer ‘overshoot’. This highlights the key importance of early time points for accurate competitor characterization.

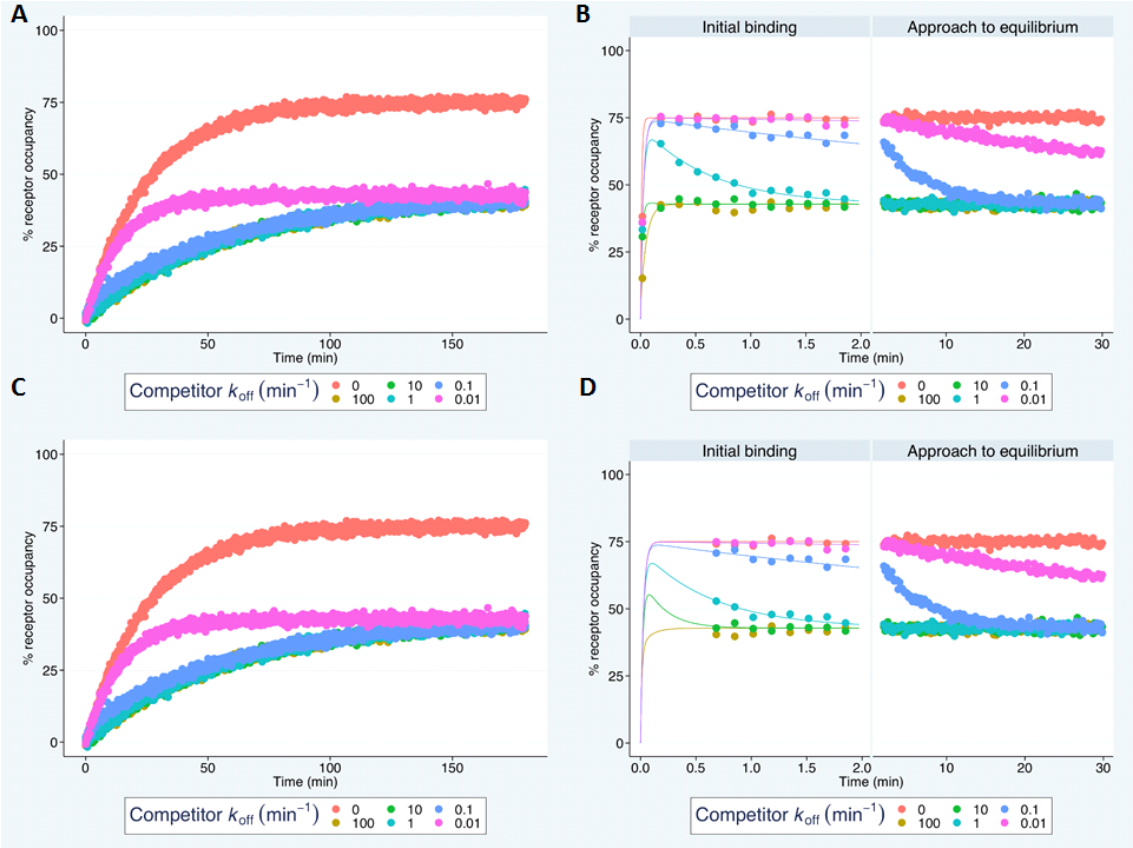


Figure 4.5. Monte-Carlo simulation results reproducing the experimentally observed effect of competitor off-rate on the competition profile observed with a rapidly dissociating tracer and a slowly dissociating tracer at varying start times. **(A)** and **(C)** show competition between a fixed concentration (3x K_d) of a very slowly dissociating tracer with the following kinetic parameters; k_{off} of 0.01min^{-1}, k_{on} of 1x10^{9} M^{-1} min^{-1}, and competitors with varying dissociation-rates. **(B)** and **(D)** show competition between a fixed concentration (3x K_d) of a rapidly dissociating tracer with the following kinetic parameters; k_{off} of 10min^{-1}, k_{on} of 3x10^{7} M^{-1} min^{-1}, and competitors with varying dissociation-rates. In the case of **(A)** and **(B)** tracer and competitor binding simulations were performed with an initial start time of 1sec (representative of on-line injection of receptor to a reaction containing tracer and competitor) whereas **(C)** and **(D)** were performed with a start time of 30 sec (representative of off-line addition of receptor). All simulations have a read frequency of 10 sec. and the data shown are representative of 200 simulations.

In line with previous kinetic studies (Klein-Herenbrink et al., 2016) the k_{off} of unlabeled compounds was poorly estimated when the tracer k_{off} is substantially slower than that of the unlabeled ligand. Increasing the k_{off} of the tracer from 0.1 to 10 vastly improved the precision with which the values of k_{on} and k_{off} were estimated for the more rapidly dissociating compounds (as documented in Chapter 8, Supplementary Tables 8.2 to 8.5). In contrast, k_{on} had no impact on the accuracy of the parameter estimate reflective of the fact that changes in k_{on} are completely compensated for by changes in the ligand concentration (data not shown) i.e. no change in k_{obs}.

Effect of tracer concentration on kinetic determination

The effect of tracer concentration on the accuracy of kinetic determinations was explored in a further series of Monte Carlo simulations. Tracer concentration was both lowered to 1x K_d and increased to 10 and 30x K_d. We chose to highlight a tracer with kinetic properties commonly encountered in drug-receptor screening campaigns; high affinity (1nM), fast on $1x10^8$ M^{-1} min^{-1} and slow off $0.1min^{-1}$. The results obtained with this tracer in competition with compounds with kinetic off-rates ranging from 100 to 0.01 min^{-1} following an on-line addition protocol are shown in Figure 4.6.

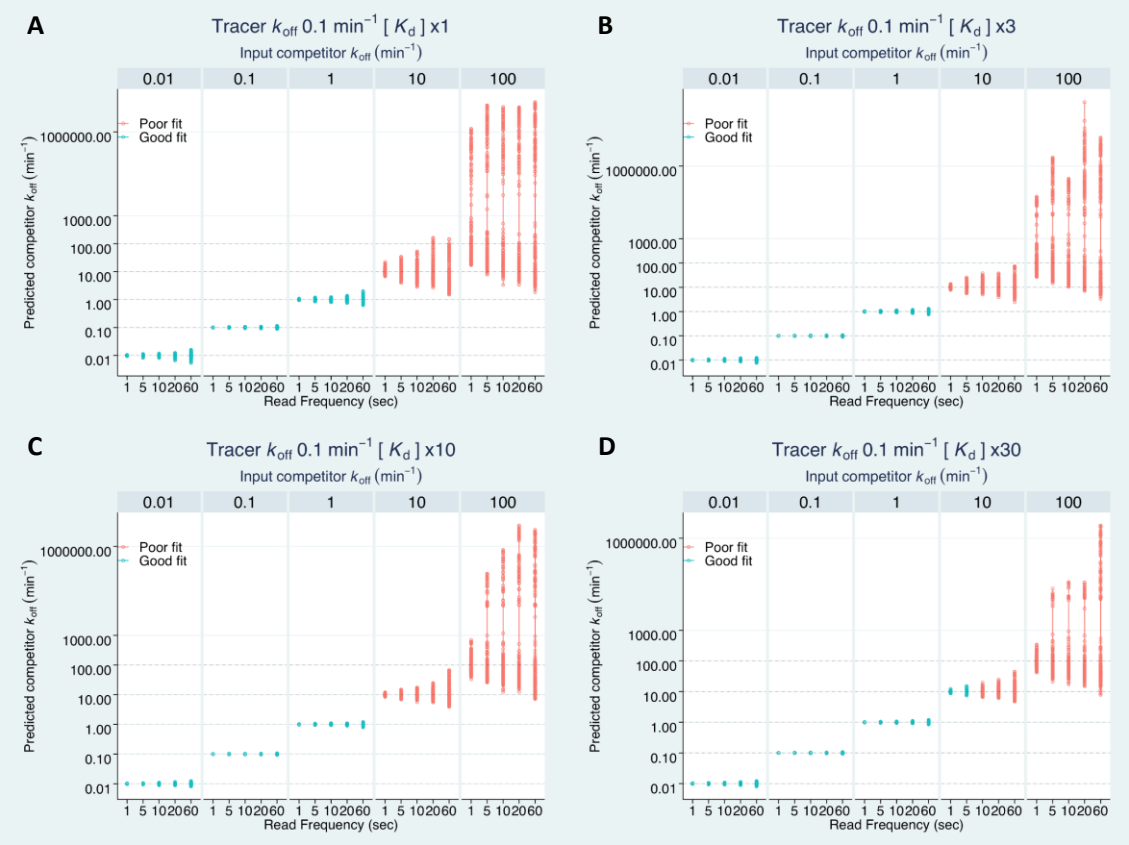


Figure 4.6. Monte-Carlo simulation results exploring the effect of tracer concentration and sample time on the accurate determination of competitor k_{off} representative of an injection protocol. Effect of assay read frequency on measured k_{off} of unlabelled competitor compounds with varied kinetics in competition with different concentrations of a slowly dissociating tracer with kinetic parameters; k_{off} of 0.1min^{-1}, k_{on} of 1x10^{8} M^{-1} min^{-1}. Tracer concentrations were **(A)** 1x K_d, **(B)** 3x K_d, **(C)** 10x K_d and **(D)** 30x K_d. Blue open symbols represent conditions which returned >90% reliable fits. Red open symbols represent conditions which returned <90% reliable fits. In all cases, tracer simulations were performed with an initial start time of 1sec representative of injection of receptor to a reaction containing free tracer (L) and unlabelled competitor (I), absolute values are the average of 200 simulations. k_{obs} $t_{1/2}$ values (0.693/k_{obs}) for a tracer with a dissociation rate of 0.1 min^{-1}, with increasing concentration of tracer 1, 3, 10 and 30x K_d were 3.5, 1.7, 0.6 and 0.2 min respectively.

Simulations varying concentration following an on-line addition protocol were also performed for tracers with off-rates of 10, 1 and 0.01 as shown in Figures 4.7, 4.8 and 4.9. k_{obs} $t_{1/2}$ values ($0.693/k_{obs}$) for the tracers with dissociation rates of 10, 1, 0.1, and 0.01 min^{-1} were 1.1 sec, 10.4 sec, 1.7 min and 17.3 min respectively at tracer concentrations 3x their respective K_d.

As a generality, an increase in ligand concentration was associated with an improvement in both the accuracy of kinetic determinations but also the number of fits deemed unambiguous and, in some cases, effectively rescued the ability of a tracer to determine the kinetics of a more rapidly dissociating competitor. For example, a competitor with an off-rate of 10 min^{-1} competing with a tracer with an off rate of 0.1min^{-1} could be readily resolved when the tracer concentration was increased from 3x K_d (Figure 4.7B) to 30x K_d (Figure 4.7D). k_{obs} $t_{1/2}$ values for a tracer with a dissociation rate of 0.1 min^{-1} ranged from 3.5 to 0.2 min, at concentrations of tracer, 1 to 30x K_d respectively. Data for a competitor with a very rapid off-rate of 10 min^{-1} competing with different concentrations of tracers with off-rates ranging from 0.01-10 min^{-1} are summarized in Figure 4.10.

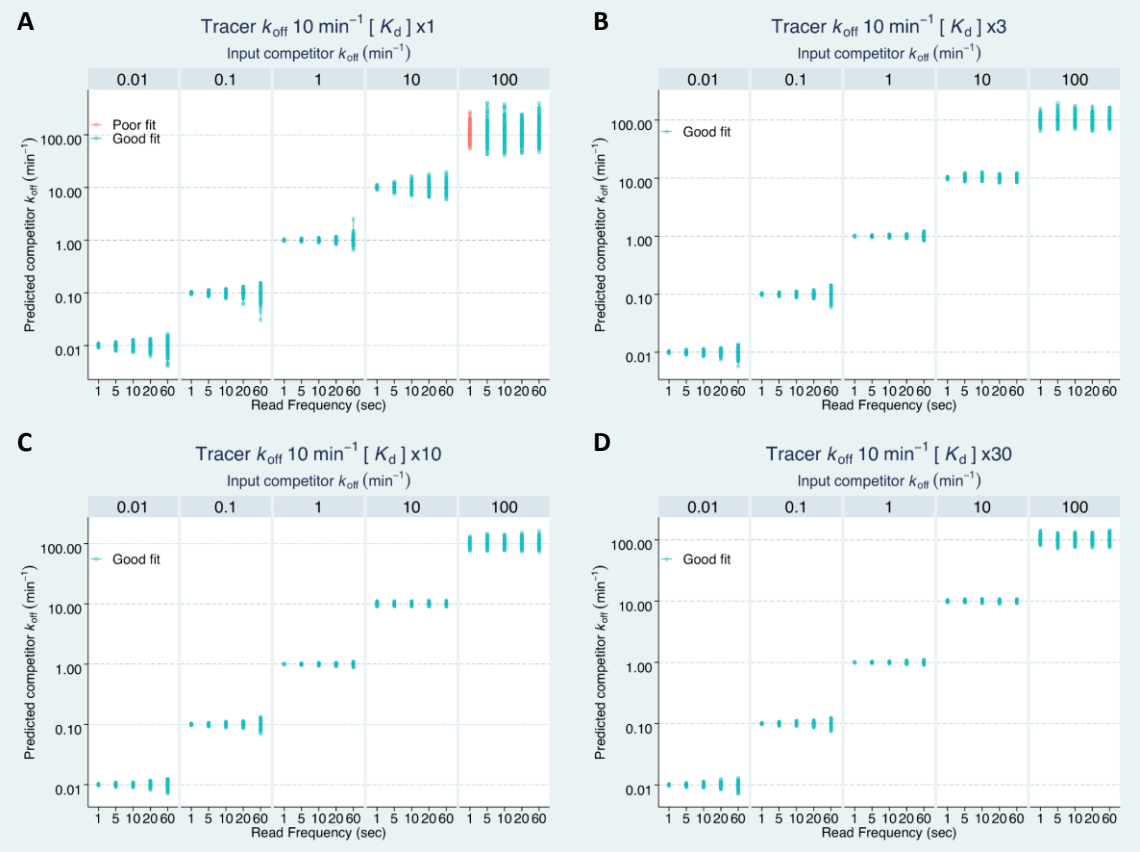


Figure 4.7. Monte-Carlo simulation results exploring the effect of tracer concentration and sample time on the accurate determination of competitor k_{off} representative of an injection protocol. Effect of assay read frequency on measured k_{off} of unlabelled competitor compounds with varied kinetics in competition with different concentrations of a very rapidly dissociating tracer with kinetic parameters; k_{off} of 10min^{-1}, k_{on} of 3x10^{7} M^{-1} min^{-1}. Tracer concentrations were **(A)** 1x $K_{d,}$ **(B)** 3x $K_{d,}$ **(C)** 10x K_d and **(D)** 30x K_d. Blue open symbols represent conditions which returned >90% reliable fits. Red open symbols represent conditions which returned <90% reliable fits. In all cases, tracer simulations were performed with an initial start time of 1sec representative of injection of receptor to a reaction containing free tracer (L) and unlabelled competitor (I), absolute values are the average of 200 simulations.

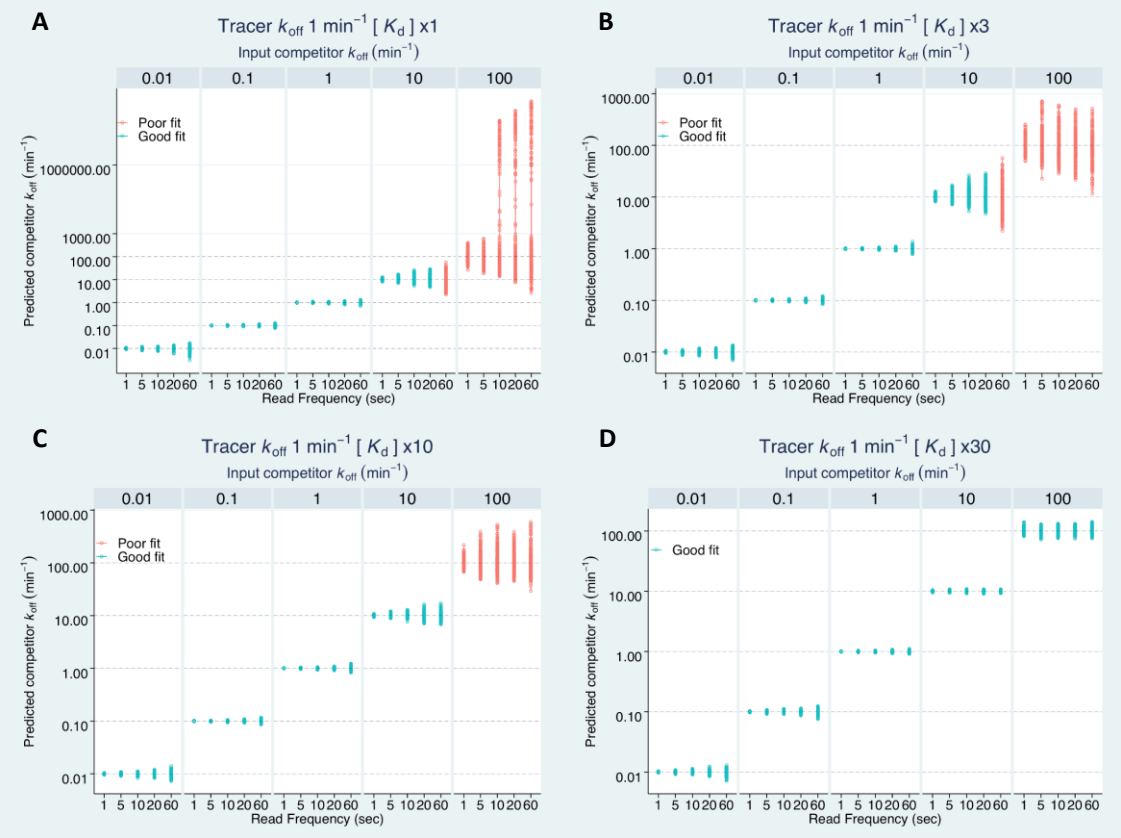


Figure 4.8. Monte-Carlo simulation results exploring the effect of tracer concentration and sample time on the accurate determination of competitor k_{off} representative of an injection protocol. Effect of assay read frequency on measured k_{off} of unlabelled competitor compounds with varied kinetics in competition with different concentrations of a rapidly dissociating tracer with kinetic parameters; k_{off} of 1min^{-1}, k_{on} of 1x10^{7} M^{-1} min^{-1}. Tracer concentrations were **(A)** 1x K_d, **(B)** 3x K_d, **(C)** 10x K_d and **(D)** 30x K_d. Blue open symbols represent conditions which returned >90% reliable fits. Red open symbols represent conditions which returned <90% reliable fits. In all cases, tracer simulations were performed with an initial start time of 1sec representative of injection of receptor to a reaction containing free tracer (L) and unlabelled competitor (I), absolute values are the average of 200 simulations.

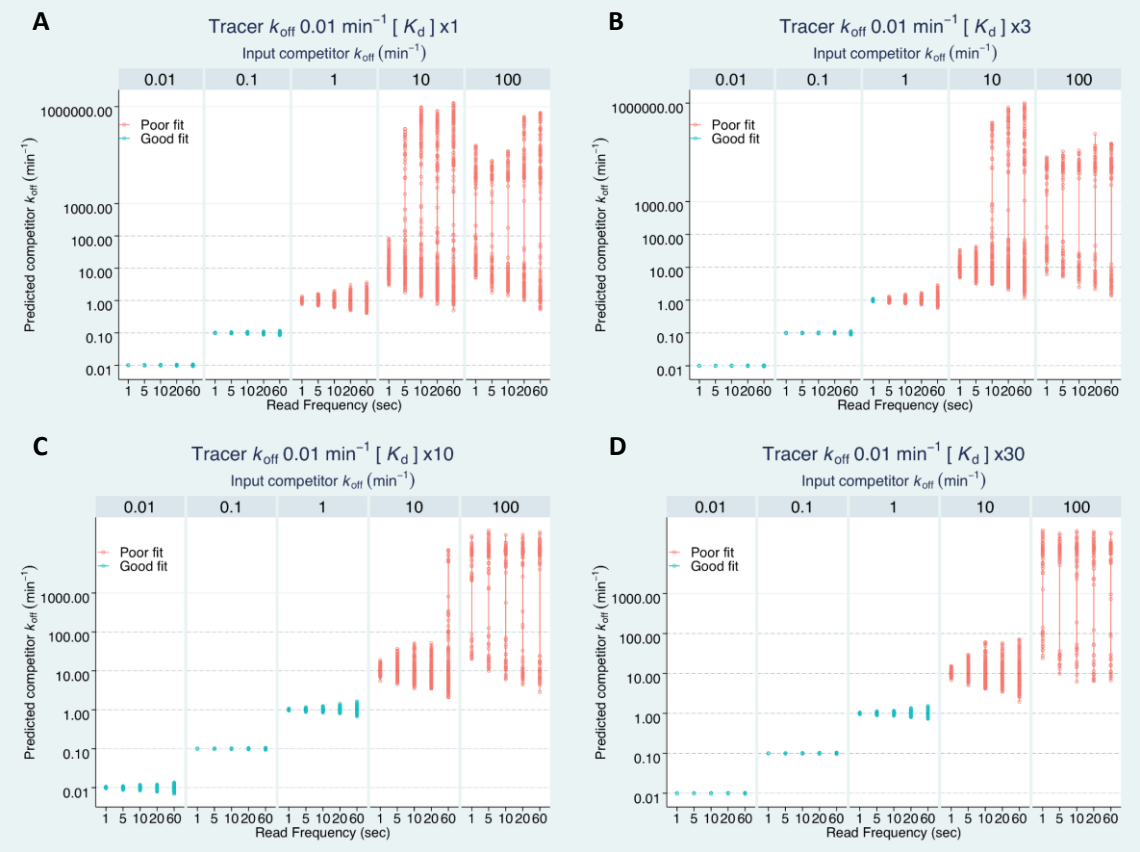


Figure 4.9. Monte-Carlo simulation results exploring the effect of tracer concentration and sample time on the accurate determination of competitor k_{off} representative of an injection protocol. Effect of assay read frequency on measured k_{off} of unlabelled competitor compounds with varied kinetics in competition with different concentrations of a very slowly dissociating tracer with kinetic parameters; k_{off} of 0.01min^{-1}, k_{on} of 1x10^{9} M^{-1} min^{-1}. Tracer concentrations were **(A)** 1x K_d, **(B)** 3x K_d, **(C)** 10x K_d and **(D)** 30x K_d. Blue open symbols represent conditions which returned >90% reliable fits. Red open symbols represent conditions which returned <90% reliable fits. In all cases tracer simulations were performed with an initial start time of 1sec representative of injection of receptor to a reaction containing free tracer (L) and unlabelled competitor (I), absolute values are the average of 200 simulations.

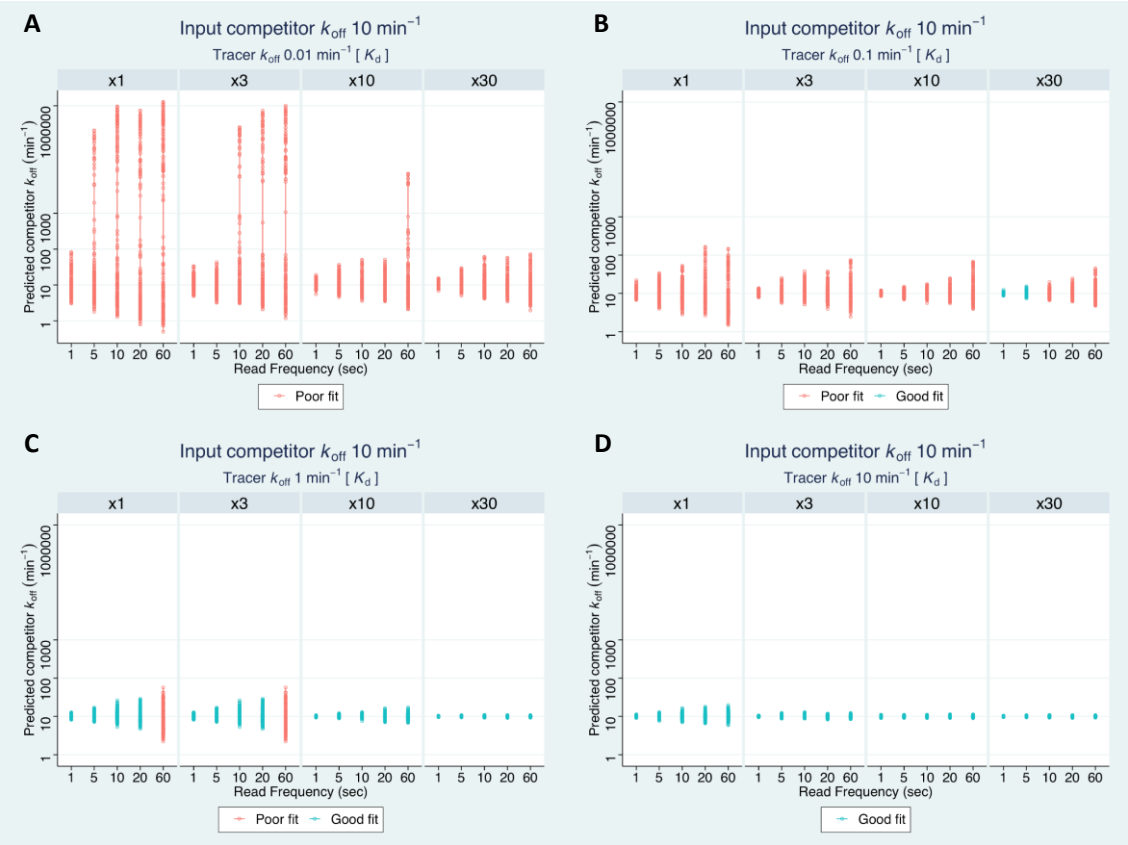


Figure 4.10. Monte-Carlo simulation results exploring the effect of tracer kinetics, concentration and sample time on the accurate determination of k_{off} of a rapidly dissociating competitor representative of an injection protocol. Effect of tracer concentration (1-30*K_d) and read frequency (1-60 sec) on the measured k_{off} of an unlabelled competitor compound with a k_{off} of 10 min^{-1} in competition with different concentrations of tracers with varied kinetic k_{off} rates ranging from 0.01 min^{-1},- 10 min^{-1}. Tracer off-rates were **(A)** 0.01 min^{-1}, **(B)** 0.1 min^{-1}, **(C)** 1 min^{-1}and **(D)** 10 min^{-1}. Blue open symbols represent conditions which returned >90% reliable fits. Red open symbols represent conditions which returned <90% reliable fits. In all cases tracer simulations were performed with an initial start time of 1sec representative of the addition of receptor to a reaction containing free tracer (L) and unlabelled competitor (I), absolute values are the average of 200 simulations.

Similarly, the effect of tracer concentration was explored following an off-line addition protocol with the data summarized in Figures 4.11 to 14. In the case of a tracer with an off-rate of 0.1 min^{-1}, increasing tracer concentration with the offline method did not improve the goodness of fit when quantifying competitors with off-rates in the region of 10 min^{-1} but tuning this particular experimental variable may still offer some benefit to researchers without access to detection instruments with injectors, reducing the overall error associated with kinetic determinations.

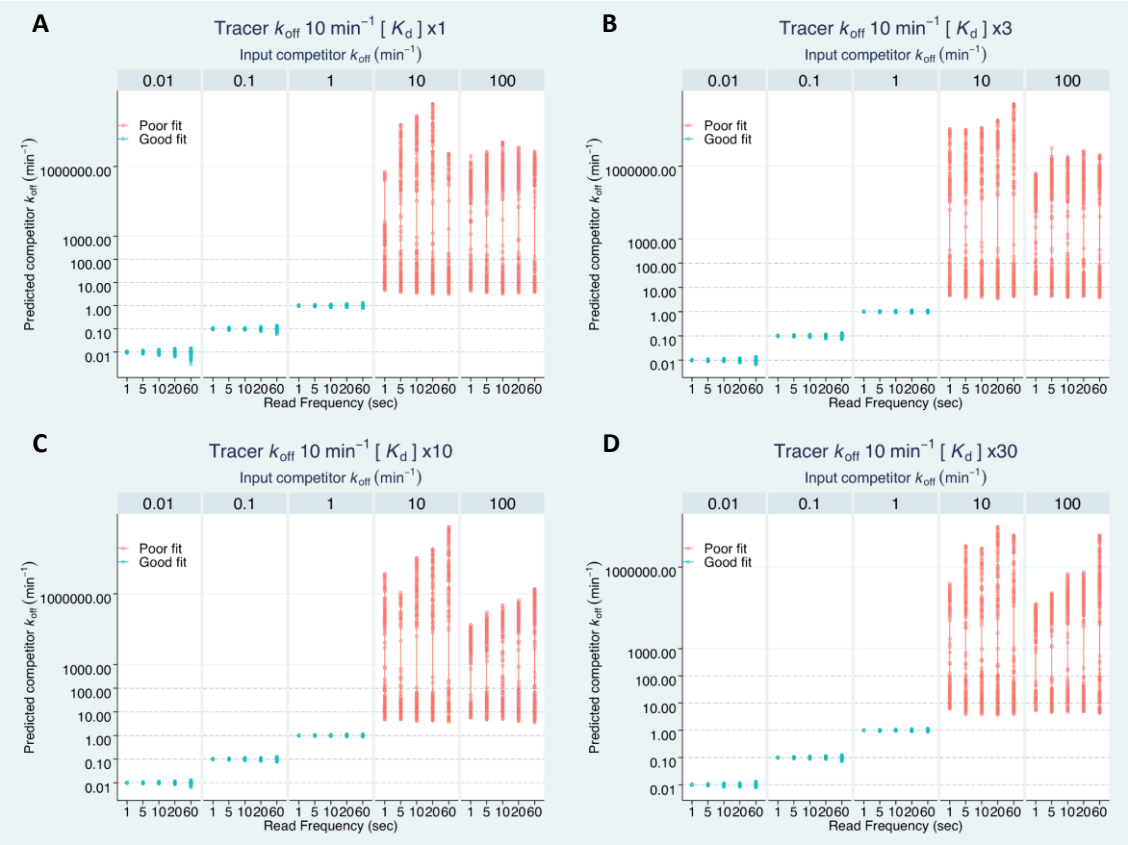


Figure 4.11 Monte-Carlo simulation results exploring the effect of tracer kinetics and assay start and read frequency-time on the accurate determination of competitor kinetic parameters representative of offline addition protocol. Effect of assay read interval time on measured k_{off} of unlabelled competitor compounds with varied kinetics in competition with different concentrations of a very rapidly dissociating tracer with kinetic parameters; k_{off} of 10min^{-1}, k_{on} of 3x10^{7} M^{-1} min^{-1}. Tracer concentrations were **(A)** 1x K_d, **(B)** 3x K_d , **(C)** 10x K_d and **(D)** 30x K_d. Blue open symbols represent conditions which returned >90% reliable fits. Red open symbols represent conditions which returned <90% reliable fits. In all cases tracer simulations were performed with an initial start time of 30sec representative of the addition of receptor to a reaction containing free tracer (L) and unlabelled competitor (I), absolute values are the average of 200 simulations.

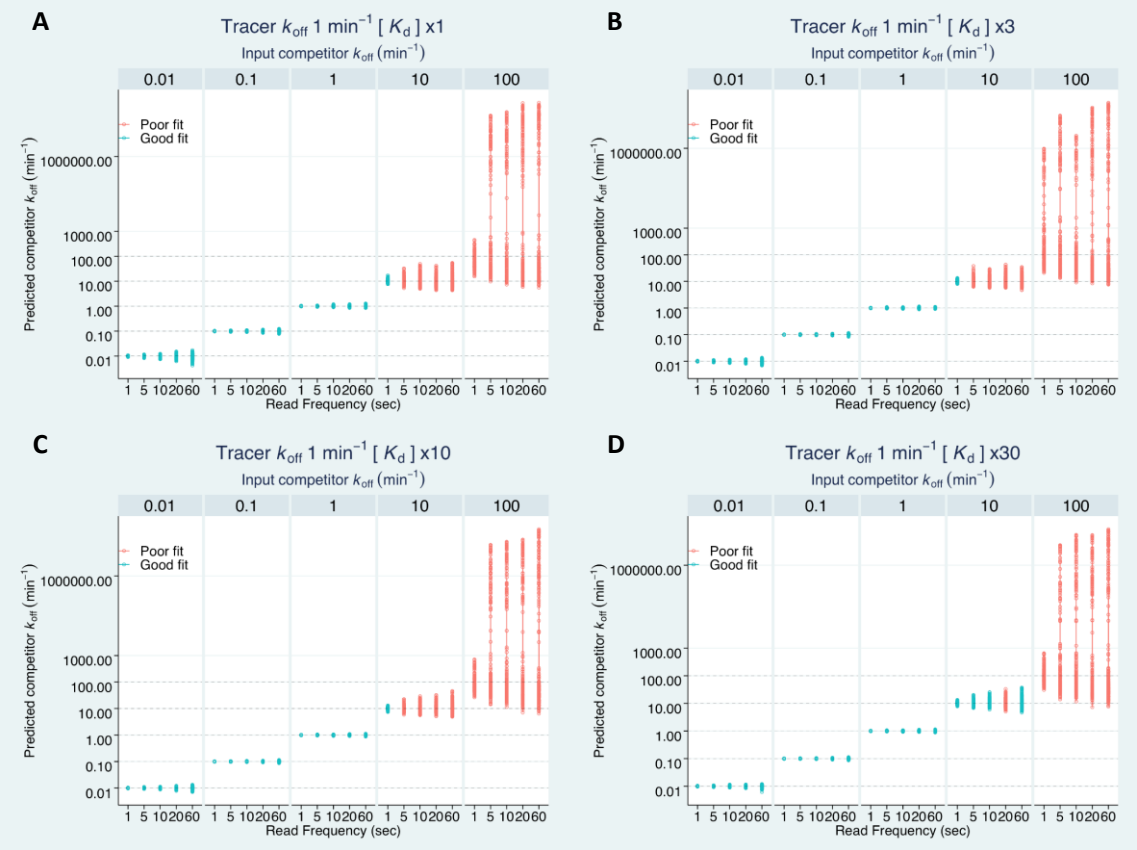


Figure 4.12. Monte-Carlo simulation results exploring the effect of tracer kinetics and assay start and read frequency-time on the accurate determination of competitor kinetic parameters representative of offline addition protocol. Effect of assay read interval time on measured k_{off} of unlabelled competitor compounds with varied kinetics in competition with different concentrations of a rapidly dissociating tracer with kinetic parameters; k_{off} of 1min^{-1}, k_{on} of 1x10^{7} min^{-1}. Tracer concentrations were **(A)** 1x K_d, **(B)** 3x K_d, **(C)** 10x K_d and **(D)** 30x K_d. Blue open symbols represent conditions which returned >90% reliable fits. Red open symbols represent conditions which returned <90% reliable fits. In all cases tracer simulations were performed with an initial start time of 30sec representative of the addition of receptor to a reaction containing free tracer (L) and unlabelled competitor (I), absolute values are the average of 200 simulations.

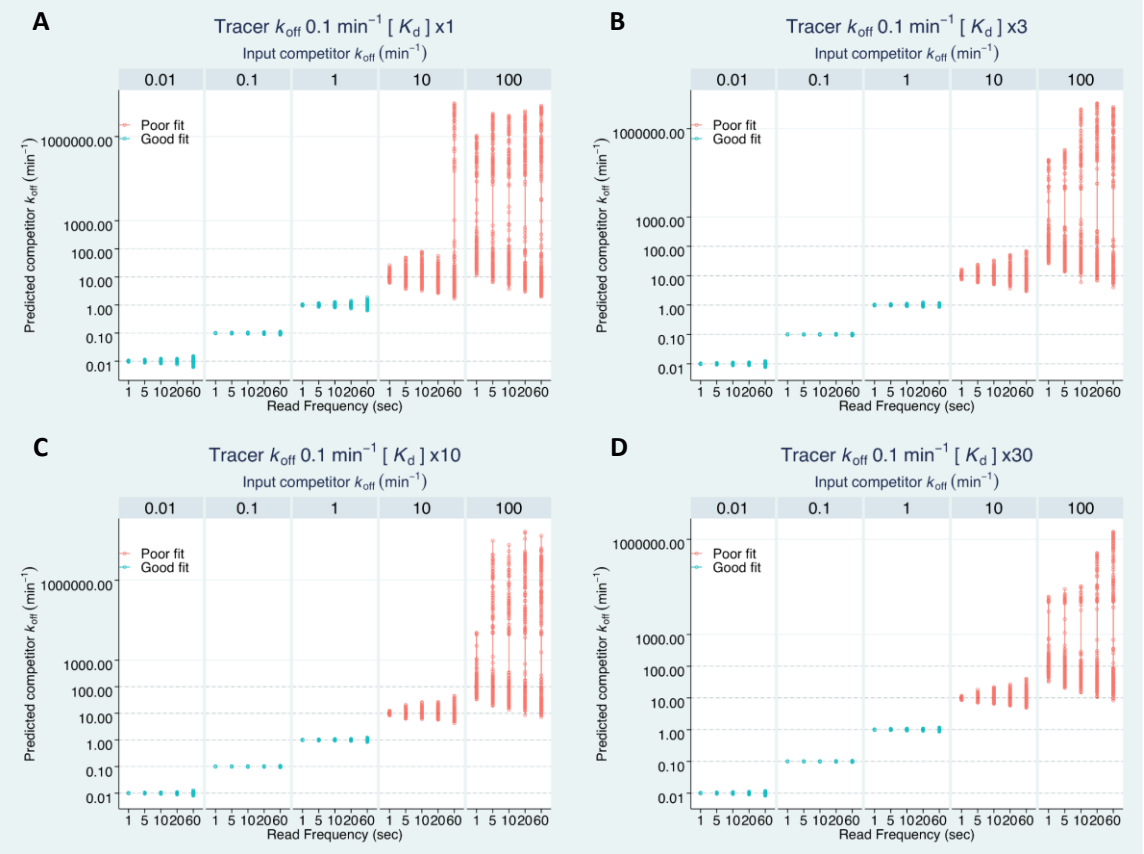


Figure 4.13. Monte-Carlo simulation results exploring the effect of tracer kinetics and assay start and read frequency-time on the accurate determination of competitor kinetic parameters representative of offline addition protocol. Effect of assay read interval time on measured k_{off} of unlabelled competitor compounds with varied kinetics in competition with different concentrations of a slowly dissociating tracer with kinetic parameters; k_{off} of 0.1min^{-1}, k_{on} of 1x10^{8} min^{-1}. Tracer concentrations were **(A)** 1x K_d, **(B)** 3x K_d, **(C)** 10x K_d and **(D)** 30x K_d. Blue open symbols represent conditions which returned >90% reliable fits. Red open symbols represent conditions which returned <90% reliable fits. In all cases tracer simulations were performed with an initial start time of 30sec representative of the addition of receptor to a reaction containing free tracer (L) and unlabelled competitor (I), absolute values are the average of 200 simulations.

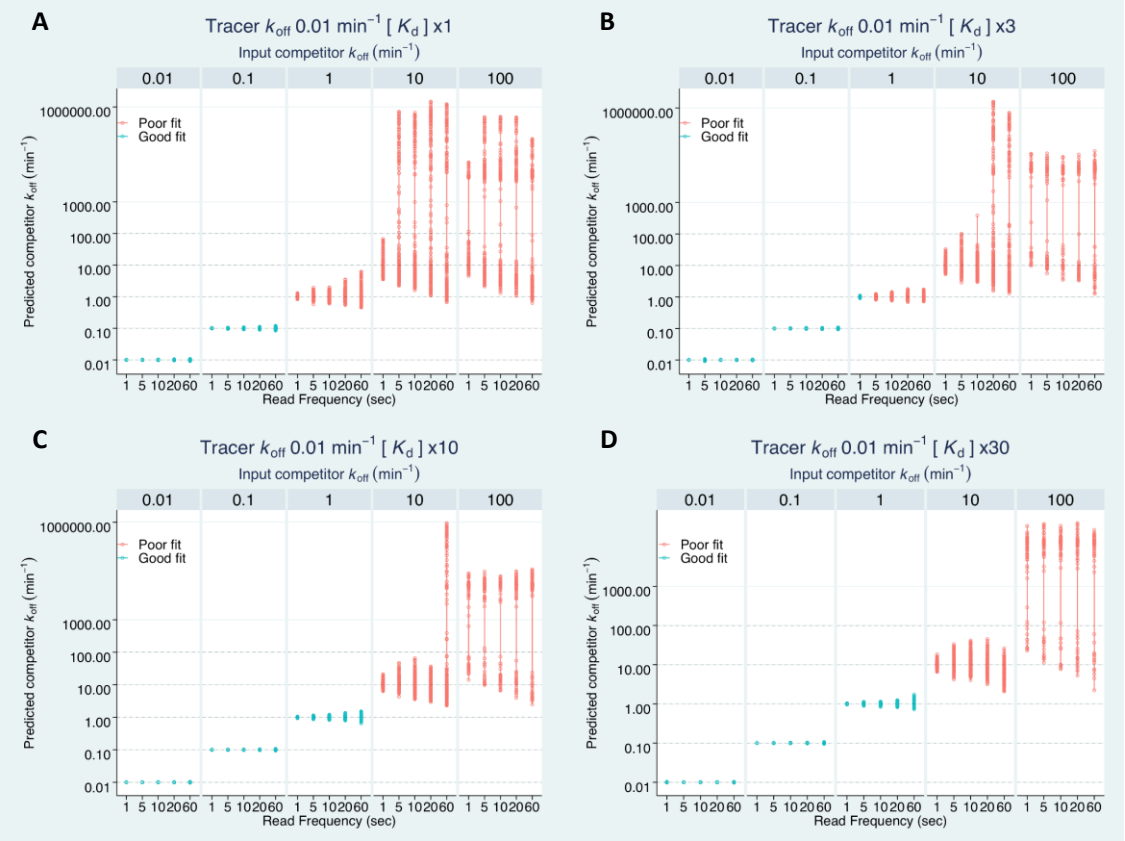


Figure 4.14. Monte-Carlo simulation results exploring the effect of tracer kinetics and assay start and read frequency-time on the accurate determination of competitor kinetic parameters representative of offline addition protocol. Effect of assay read interval time on measured k_{off} of unlabelled competitor compounds with varied kinetics in competition with different concentrations of a slowly dissociating tracer with kinetic parameters; k_{off} of 0.01min^{-1}, k_{on} of 1x10^{9} min^{-1}. Tracer concentrations were **(A)** 1x K_d, **(B)** 3x K_d, **(C)** 10x K_d and **(D)** 30x K_d. Blue open symbols represent conditions which returned >90% reliable fits. Red open symbols represent conditions which returned <90% reliable fits. In all cases tracer simulations were performed with an initial start time of 30sec representative of the addition of receptor to a reaction containing free tracer (L) and unlabelled competitor (I), absolute values are the average of 200 simulations.

Fragment screening using competition-kinetic association binding assays

Monte-Carlo simulations were performed to recreate the competition profile expected with low-affinity fragments (31 in total with K_d values ranging from 1 μM to 1000 μM). These competitor fragments with varied kinetic parameters (k_{off} ranging from 3 to 200 min^{-1} and k_{on} from 3 $x10^6$ to 2 $x10^5$ M^{-1} min^{-1}) were simulated in competition with a fixed concentration (3x K_d) of a rapidly dissociating tracer (k_{off} of 10min^{-1}, k_{on} of 3$x10^7$ M^{-1} min^{-1}). Chapter 8, Supplementary Figure 8.1A shows the expected inhibition of tracer binding caused by a low-affinity competitor, fragment 25 (affinity of 0.25 mM, k_{off} of 87.1 min^{-1}, k_{on} of 5 $x10^5$ M^{-1} min-1) tested at two concentrations, 10 and 100 μM. Using a start time of 1 sec and a read frequency of 5 sec it was possible to estimate the affinity of such fragments with a high degree of accuracy as shown by the correlation of input K_d with output K_d (see Chapter 8, Supplementary Figure 8.1B). In contrast as the k_{off} of the fragment increases then the degree of error associated with the estimation of k_{off} and k_{on} is increased, (as judged by the increase in the overall standard deviation associated with the mean) however the overall correlation of input and output kinetic parameters remains extremely good, see Chapter 8, Supplementary Figure 8.1C and 8.1D. In all cases using this 2-point method the number of ambiguous fits was below 5%. Interestingly this analysis demonstrates that the affinity of the fragments is estimated with a much higher degree of accuracy than the individual kinetic measurements, demonstrating the overriding influence of the final equilibrium position on kinetic parameter estimation. A similar analysis was performed using single concentrations of compound (10 or 100 μM) and demonstrates the benefit of a 2-point approach (Turner and Charlton 2005), with the errors associated with each estimate being larger and the number of ambiguous fits increasing proportionally.

4.3.2 Experimental validation of the Monte Carlo simulation approach

To validate the findings of these Monte Carlo simulations exploring the effect of tracer characteristics on kinetic determinations using the Motulsky-Mahan approach we undertook an experimental study designed to explore the limits of a previously well-characterised system, the dopamine D_{2L} receptor using a TR-FRET-based system. In this study, we chose to focus on a small number of compounds with diverse kinetics and employ the BMG PHERAstar FS (plate reader) injectors to assess tracer binding at the very earliest time points.

Determining the kinetic of D_2R fluorescent tracers

Representative kinetic association curves for PPHT-red and spiperone-d2 using a start time of ~1 sec and a read frequency of 5 sec are shown in Figure 4.15A and C respectively. The kinetic parameters determined from these plots are presented in Table 4.2. PPHT-red dissociated rapidly from the dopamine D_2R with a $t_{1/2}$ of 2.2 min ($0.693/k_{off}$) whereas spiperone-d2 dissociated more slowly ($t_{1/2}$ of 8.7 min). The removal of data points to reflect off-line addition (i.e. the first ~30 sec) or increasing read frequencies (10 to 60 sec) had little influence on the determination of the kinetic parameters of these two fluorescent tracers reflective of the fact that they are not so rapidly dissociating that the early time points are critical for an accurate estimation of their kinetic parameters. Figure 4.15B and D show the expected linear relationship between PPHT-red and spiperone-d2 concentration and the observed rate of association (or k_{obs}) and suggest that the law of mass action is observed.

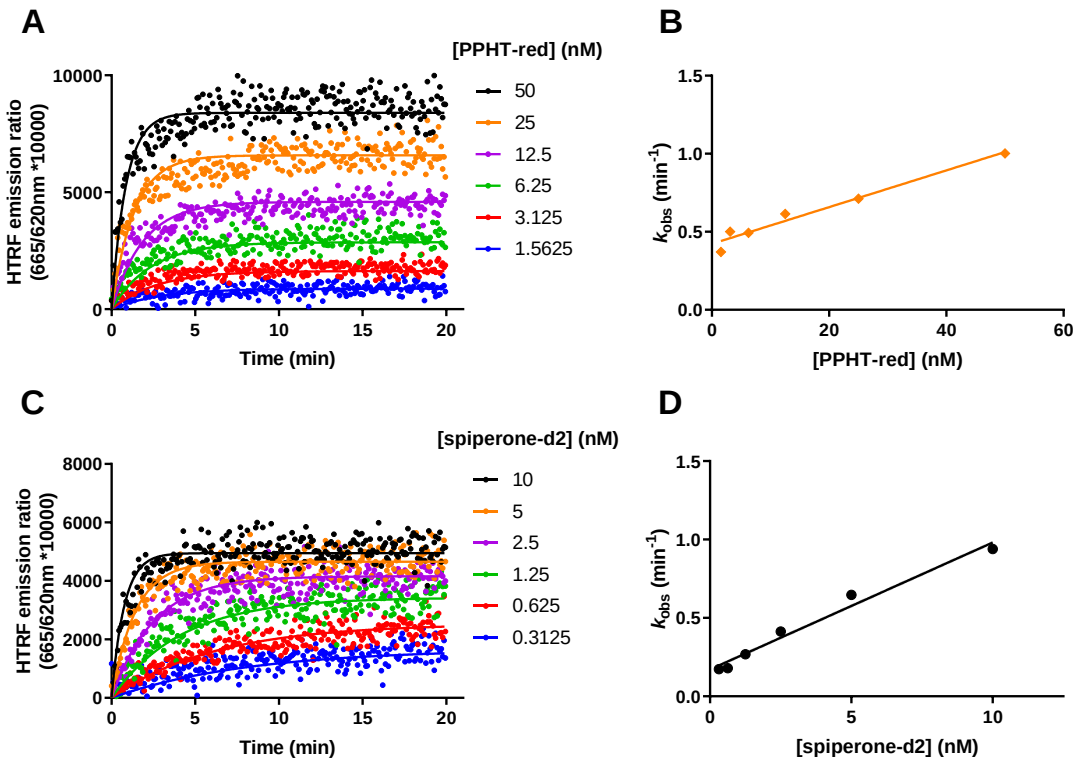


Figure 4.15. Determination of PPHT-red and spiperone-d2 kinetic binding parameters. **(A)** The observed association of PPHT-red binding to the human dopamine $D_{2L}R$. CHO–$D_{2L}R$ cell membranes (2 µg per well) were incubated for 20 min with gentle agitation with increasing concentrations of PPHT-red. Data are presented in singlet form from a representative of 4 experiments. **(B)** A plot of PPHT-red concentration versus k_{obs}. Binding followed a simple law of mass action model, k_{obs} increasing linearly with fluorescent ligand concentration. Data are representative of a total of 4 experiments. **(C)** The observed association of spiperone-d2 binding to the human dopamine D_2R. CHO-D_2R cell membranes (2 µg per well) were incubated for 20 min with gentle agitation with increasing concentrations of spiperone-d2. Data are presented in singlet form from a representative of 4 experiments. **(D)** A plot of spiperone-d2 concentration versus. k_{obs}. Binding followed a simple law of mass action model, k_{obs} increasing linearly with fluorescent ligand concentration. Data are representative of a total of 4 experiments. All binding reactions were performed in the presence of GppNHp (0.1 mM) with non-specific-binding levels determined by the inclusion of haloperidol (10 µM).

Table 4.2. Kinetic binding parameters of the tracers PPHT-red and spiperone-d2 determined from association binding studies using human dopamine D_{2L} CHO cell membranes. Data are mean ± S.E.M. from N separate experiments.

Tracer	**Tracer K_D (nM)**	**Tracer k_{off} (min^{-1})**	**Tracer k_{on} (M^{-1} min^{-1})**	**Nº of observations (n)**
PPHT-red	16.9 ± 1.1	0.32 ± 0.02	1.93 ± 0.21 $x10^7$	4
Spiperone-d2	0.62 ± 0.08	0.08 ± 0.01	1.30 ± 0.17 $x10^8$	4

Effect of tracer kinetics on dopamine D_2R ligand kinetic determinations

To experimentally test the effect of tracer kinetics on k_{off} estimates of unlabeled ligands, competition association experiments were performed for 6 dopamine D_2 ligands; chlorpromazine, ropinirole, pergolide, domperidone, (+)butaclamol and bromocriptine (Figure 4.16). The associated errors and therefore the accuracy of kinetic determinations for rapidly dissociating compounds is highly dependent on the kinetic properties of the tracer employed to measure them. In contrast, the error associated with more slowly dissociating compounds is largely comparable and seemingly independent of the tracers kinetic properties. This is illustrated in Figure 4.16A and Figure 4.16B and shows that the error associated with kinetic determinations made with the more slowly dissociating tracer spiperone-d2 is in general much larger than for the more rapidly dissociating tracer PPHT-red. This is evident from the spread of k_{off} values on the x-axis (spiperone-d2) being wider than the spread of the k_{off} values on the y-axis (PPHT-red). The errors associated with kinetic determinations of rapidly dissociating compounds following off-line addition of PPHT-red (Figure 4.16A) is little changed compared to on-line addition (Figure 4.16B), however there was a tendency for the error to increase for the more slowly dissociating compounds, this situation is replicated for spiperone-d2, (see Figure 4.16A and Figure B) and potentially represents the imprecise fitting of the tracer 'overshoot'.

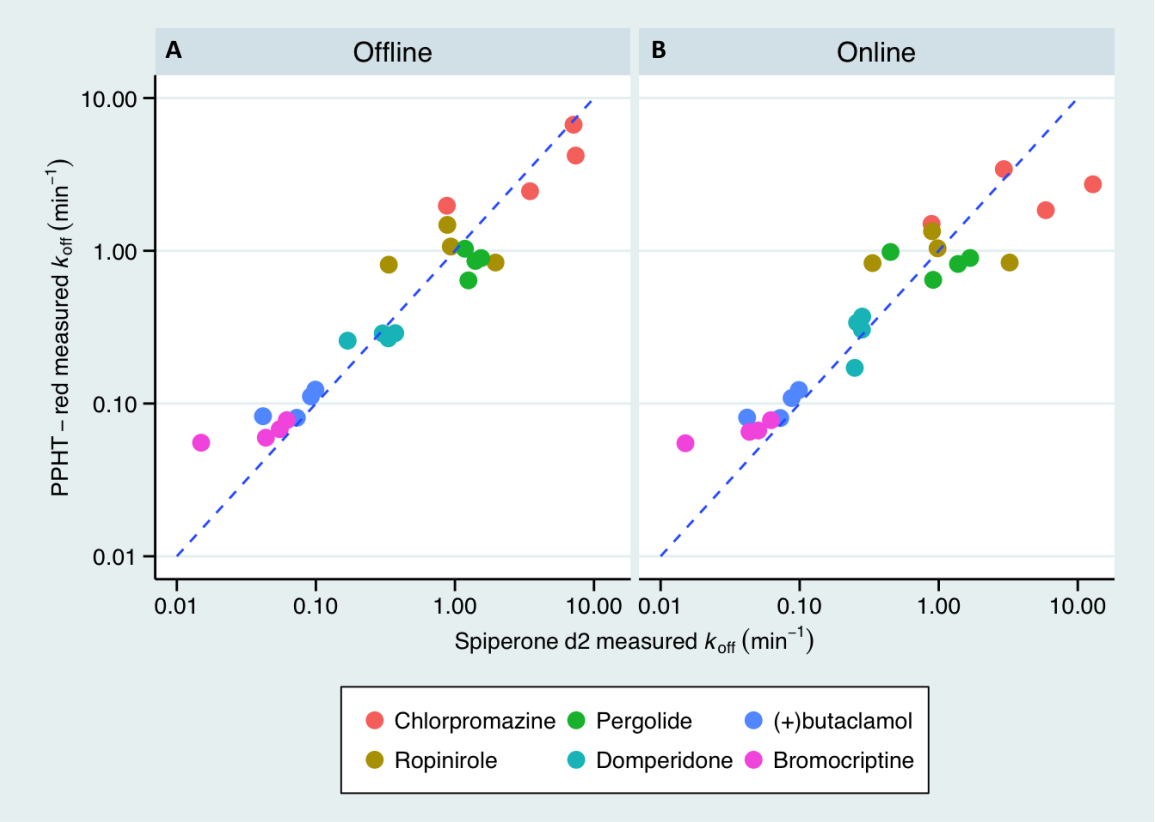


Figure 4.16. Effect of tracer properties and assay configuration on the determination of unlabeled compound kinetic parameters at the human dopamine D_2 receptor. Comparison of unlabelled compound kinetic parameters with associated errors determined using spiperone-d2 and PPHT-red, **(A)** following an off-line injection protocol with a 5sec interval and **(B)** an on-line addition protocol with a 5sec interval. CHO-D_{2L}R cell membranes (2 µg per well) were incubated for 20 min with gentle agitation with a fixed concentration of PPHT-red (12.5 nM) or spiperone-d2 (5 nM) and increasing concentrations of the competitor. Data are presented as individual estimates from 4 experiments.

4.4 Discussion

The growing awareness of the importance of optimising drug-binding kinetics has led to a rapid increase in the development and utilisation of assay systems capable of measuring the kinetics of unlabelled compounds. A popular format for investigating membrane-bound targets is the competition association binding assay, first described by Arányi (1980), then popularized by Motulsky and Mahan (1984) and used extensively to characterise many different receptor systems (Gillard et al., 2002; Dowling and Charlton, 2006; Sullivan et al., 2006; Fleck et al., 2012; Sykes et al., 2014; Riddy et al., 2015; Nederpelt et al., 2016; Guo et al., 2017; Bouzo-Lorenzo et al., 2019). A key observation during this time has been that the accuracy of estimating kinetic parameters of rapidly dissociating molecules is poorer when using a slowly dissociating ligand as the tracer (Sykes et al., 2012; Klein-Herenbrink et al., 2016; Bosma et al., 2019).

The purpose of the current study was to explore the effect of tracer kinetics on our ability to accurately estimate the kinetics of unlabelled compounds using the competition-association binding method. In particular, we were interested to test the limits of this model system in terms of its ability to assess the binding of very rapidly dissociating compounds likely to be representative of compounds identified in a screening campaign. In practical terms, we were also keen to investigate the importance of read frequency to assist with experimental design. To our knowledge, the current study is the first to fully explore these elements and provide clear guidance for the use of this assay format at all stages of the drug discovery process.

As shown in Figure 4.1 and Chapter 8, Supplementary Table 8.1, for simulated data sets it was generally possible to derive accurate estimates (< 2-fold difference) of the tracer kinetic parameters using the global association method, see Equation 2.5, as described in Chapter 2 section 2.2.8 Signal detection and data analysis. For the more rapidly dissociating tracers the key to obtaining more accurate kinetic parameters was to reduce the assay start-time and the read frequency. Our ability to control these parameters is largely instrument (reader)-dependent. For example, assay start-time is dependent upon the ability to inject sample whilst simultaneously reading from the same well. In addition, assay sensitivity determines the required

sample acquisition time, which restricts minimal read frequency. Consequently, the option to vary these parameters can be considered as critical factors in the process of determining unlabeled compound kinetics. This is readily illustrated in a comparison of Figure 4.1B and D. Provided an initial start time of 1 sec was used (representative of on-line injection) it was possible to accurately determine the kinetics of all model tracers with less than 10% variation around the mean. In contrast, employing a start time of 30 sec prevented accurate kinetic determinations for the most rapidly dissociating tracer even when the read frequency was restricted to 1 sec (Figure 4.2C and D), demonstrating the importance of on-line injection.

The situation with the Motulsky-Mahan model (see Equation 2.7 as described in Chapter 2 section 2.2.8 Signal detection and data analysis) for the estimation of unlabeled compound kinetics was a little more complicated. Although it was possible to derive accurate rate constant estimates for the majority of conditions, some combinations failed to return reproducible estimates (see Chapter 8, Supplementary Tables 8.2 to 8.5). In general, employing a tracer concentration at 3x its K_d it was not possible to reliably estimate k_{on} and k_{off} where the dissociation of the tracer was (≥ 10-fold) slower than the unlabeled competitor. For example, the accurate estimation of the rate constants of a rapidly dissociating ligand with k_{off} of 100 min^{-1} requires a tracer that is also rapidly dissociating, i.e. in the range of 10 min^{-1}. The initial read time was also critically important to determine the kinetics of unlabeled compounds. Where the simulations were started from 1 sec, mimicking an on-line injection protocol, the kinetic parameters of unlabeled compounds were generally accurately estimated. In contrast, when measurements were started (sampled) 30 sec after the beginning of the experiment, mimicking off-line addition, the estimates were poorer, particularly for rapidly dissociating ligands. This highlights the importance of early time points measured before equilibrium is established. This problem is exacerbated as read frequency is increased since the definition of the tracer association curves is lost. In contrast, a short read frequency is associated with an increase in the number of data points, which is useful from an accuracy perspective (as illustrated by reduced % CV values see Chapter 8, Supplementary Tables 8.2). However, short read frequency will have a negative impact on throughput, which is an important consideration, especially when profiling 100-1000s of compounds during screening.

To date, SPR has been the main method for measuring the kinetics of fragments at receptors however this technique is traditionally limited to artificially stabilized receptors (Patching 2014; Shepherd et al., 2014). Thus the competitive binding model presented is an attractive alternative to SPR and should theoretically allow the investigator to reveal the kinetics of low-affinity fragments with off-rates in the order of 10 min^{-1} should an appropriate tracer be identified (see Chapter 8, Supplementary Figure 8.1 and 8.2).

In a previous paper exploring dopamine D_2R agonist kinetics, we were able to demonstrate the importance of tracer properties on our ability to determine the kinetics of rapidly dissociating ligands (Klein-Herenbrink et al., 2016). In the current study, we have further explored this observation employing an on-line injection protocol. In the previous study [^{3}H]-spiperone was unable to accurately determine the kinetics of the most rapidly dissociating D_2R agonists. This is likely the result of a number of factors including; its slower measured off-rate from the dopamine D_2R, the relatively lower concentration of spiperone employed in the competition binding experiments i.e. 3x [^{3}H]-spiperone (versus 10x K_d spiperone-d2 in the current study) and the decision to employ an initial start time of 30 sec.

As predicted by the Monte Carlo simulations PPHT-red a tracer with a relatively fast off-rate was more reliable at determining the kinetic off-rates of the most rapidly dissociating antagonists and agonists tested in this study. In contrast spiperone-d2 (10x K_d) although adequate at determining the off-rates of the more slowly dissociating compounds was prone to more variation in its determination of the off-rates of the most rapidly dissociating compounds. Importantly what this study demonstrates is that a failure to demonstrate an accurate fit of the kinetics of a rapidly dissociating compound ($10min^{-1}$) can be overcome using higher concentrations of a slowly dissociating tracer and by shortening the start and read frequency timings (see Figure 4.7). As one might predict the use of higher tracer concentrations could not compensate for an increase in the assay start time, representative of an off-line addition protocol (see Figure 4.10).

What is apparent from this study is that for a competitive binding approach to be utilized throughout the different phases of the drug discovery process then the kinetics of the tracer need to be tailored to the appropriate properties of the

unlabeled compounds. For low-affinity compounds, such as initial hits or fragments, a rapidly equilibrating tracer is required to accurately determine rate constants. This is fortunate as it opens the possibility to fluorescently label an early hit to serve as a tracer to discover and characterize new fragments. In this format, it would be necessary to read relatively small numbers of wells in rapid succession (i.e. a shortened read frequency) using a repeat on-line injection protocol to resolve the kinetics of the most rapidly dissociating fragments. Also apparent is that as we move further along the drug discovery pathway towards lead optimization, it may be beneficial to label a more slowly dissociating compound, allowing the off-line addition of tissue and increased sample throughput through extended read frequency. The decision to employ shorter read times is ultimately a compromise between throughput and the accurate resolution of kinetic parameters.

4.5 Conclusions

In summary, we have improved the current understanding of the Motulsky-Mahan approach providing clear guidelines on the use of tracers to measure the kinetics of unlabeled competitors. Based on the detailed Monte Carlo approach presented we propose the following four factors as being important considerations when formulating competition association binding experiments:

1. Tracer kinetics; fast off tracer in the region of 0.1-1 min^{-1} appear to be critical for the determination of unlabeled compounds with rapid off kinetics in the region of 1-10 min^{-1}.
2. Tracer concentration appears to play a crucial role in our ability to determine the kinetics of binding with greater accuracy and can even increase the range of compounds off rates which we can reliably measure.
3. Online Injection capability proved critical to determine the off-rates of compounds and tracers which dissociate with off-rates in the region of 10 min^{-1}.
4. Rapid read frequency dramatically improves the goodness of fit and reduces experimental variability and like online injection can rescue our ability to resolve the kinetics of the most rapidly dissociating compounds.

Experimental conditions can also be manipulated to enhance our ability to measure the kinetics of a particular tracer or competitor ligand. For example, reducing assay temperature will slow the off-rates of both the tracer and the competitor compound, a ploy that has been successfully used in the past to enable the determination of off-rates of more rapidly dissociating compounds using the off-line addition protocol (Contreras et al., 1986, Guo et al., 2012). It should be noted, however, that kinetic parameters calculated at lower temperatures are unlikely to reflect those in a physiological system, significantly limiting their translational utility.

Overall, the findings in this chapter highlight the importance of considering tracer kinetics and assay read start and read frequency times when developing competition association assays. Notably, these simulations suggest that under the right conditions, the kinetic parameters of very low affinity (mM) competitors can be

measured, providing the opportunity for kinetic fragment-based receptor screens and the development of SKRs at all phases of the drug discovery cascade.

Authorship Contributions

Contributed new analytic tools: Jain

Chapter 5 - Extrapyramidal side effects of antipsychotics are linked to their association kinetics at the dopamine D_2 receptor

5.1 Introduction

5.1.1 Antipsychotic drug action and classification

Imbalances in dopamine signalling are believed to play an integral part in the symptoms of schizophrenia (Carlsson and Lindqvist 1963; Johnstone et al., 1978; Davis et al., 1991) with elevated presynaptic dopamine synthesis levels and increased release (inferred from PET displacement studies) being reported in numerous studies of schizophrenic patients (Howes and Kapur 2009). Currently, all known marketed anti-schizophrenia drugs which modulate the dopamine hyper-function accompanying this condition bind to the dopamine D_2 receptor, acting either as antagonists or low efficacy partial agonists (Howes et al., 2009; Miyamoto et al., 2012).

The current pharmacological treatments of schizophrenia can be divided into two main categories; first-generation antipsychotics (FGAs), also called classic or conventional antipsychotics or neuroleptics; and second-generation antipsychotics (SGAs), also called atypical or nonconventional antipsychotics (Meltzer 2013). The term ‘atypical’ is often used to refer to APDs that have at least equal antipsychotic efficacy compared to conventional drugs, with less EPS and/or prolactin elevation (Leucht et al., 2009).

The EPS which often accompany antipsychotic treatment are characterised by a number of symptoms which include acute dystonic reactions, akathisia, Parkinsonism and tardive dyskinesia. Extrapyramidal symptoms are caused by excessive dopamine blockade in the basal ganglia, the largest component of which is the striatum; with this lack of dopamine often mimicking idiopathic pathologies of the extrapyramidal system (Blair and Dauner 1992). Such side effects can be particularly distressing for the patient often resulting in poor drug compliance and even discontinuation of therapy (Perkins 2002; Cortesi et al., 2013). Understanding the causes of such side effects is, therefore, a critical step to the design of better therapeutics.

5.1.2 Two theories of atypicality the ‘fast off’ hypothesis and the multi-receptor hypothesis

So-called ‘on-target’ adverse side effects are thought to be the consequence of reductions in D_2R signalling in the nigrostriatal dopamine system in the case of

extrapyramidal symptoms (Chiodo and Bunney 1983; Burki 1979) and the tuberohypophyseal pathway in the case of prolactin secretion (Caron et al., 1978). Atypical, or second-generation APDs are used extensively for the treatment of schizophrenia due to their limited tendency to produce EPS and are considered as effective as or in certain cases (eg. amisulpride, clozapine, olanzapine, and risperidone) more effective than typical APDs in treating the 'positive' symptoms (e.g. hallucinations and delusions) of schizophrenia (Leucht et al., 1999; Leucht et al., 2009). This effect is linked to the blockade of dopamine D_2 receptors in the mesolimbic region of the brain where pathological dopamine hyper-function is predominant (Davis et al., 1991; Moore et al., 1999; Abi-Dargham et al., 2000). Perhaps, more importantly, these same drugs in the main are more effective than typical APDs at treating the 'negative' symptoms of schizophrenia (eg. lethargy and apathy) and the depression that often accompanies this complex and poorly understood disease (Leucht et al., 1999; Krause et al., 2018).

There are two main theories to explain 'atypicality'. One of these is the multi-receptor hypothesis which arises since many atypical APDs have high affinity at other neurotransmitter receptors in addition to dopamine D_2 receptors, in particular at serotonin 5-HT2A receptors (Janssen et al., 1988; Meltzer et al., 1989). Blockade of the 5-HT2A receptors is thought to help promote normal dopamine signalling in the nigrostriatal pathway which helps to reduce on-target side effects (reviewed in Kapur and Remington 1996; Schotte et al., 1996). In contrast typical APDs, like haloperidol and chlorpromazine bind more specifically to dopamine D_2 receptors and consequently lack this additional therapeutic effect (Meltzer et al., 1989). However there are important anomalies within this proposed classification such as for the atypical APD amisulpride, which is considerably more dopamine D_2 selective over 5-HT2A (Kusumi et al., 2015) and yet still shows reduced EPS (Kapur and Seeman 2001) and perhaps more surprisingly is just as effective at treating the negative symptoms of schizophrenia (Leucht et al., 2009).

The second theory of 'atypicality' is based on the observation that atypical APDs tend to have lower affinity for the D_2R than typical APDs and consequently bind more 'loosely' to the receptor (Burki 1986; Seeman et al., 1996, 1997a, 1997b). Subsequently, this theory was refined, and it was proposed that it was not the affinity per se of APDs but rather how rapidly they dissociate from the postsynaptic D_2R

that determines their atypical profile (Seeman & Tallerico 1998, 1999; Kapur & Seeman 2000).

5.1.3 The kinetic basis of atypicality and typicality

In their landmark study using radiolabelled compounds, Kapur & Seeman investigated the affinity and the kinetics of nine typical and atypical APDs (Kapur & Seeman 2000). The two atypical APDs studied, clozapine and quetiapine displayed fast dissociation from rat striatal dopamine D_2 receptors with kinetic half-lives of < 30 and 14 sec respectively. In contrast dissociation of the typical APDs, including chlorpromazine the first recognised treatment for schizophrenia, was considerably slower with kinetic half-lives between 18-355 mins. In this study values of kinetic dissociation rate (k_{off}) varied as much as a 1000-fold from (from 0.002 to 3.013 min^{-1}), whereas much less variation was observed in apparent of k_{on} (from $1.1x10^8$ to $1.7x10^7$ M^{-1} min^{-1}, 15 fold) which was derived from the relationship ($K_d = k_{off}/k_{on}$).

This body of work led Seeman and Kapur to propose the 'fast off hypothesis' of 'atypicality' suggesting that rapid dissociation from the D_2R directly contributes to the reduced side effect profile of atypical APDs (Kapur & Seeman 2001). Rapid receptor dissociation is relevant to clinical effect only when it is considered within the context of receptor occupancy since D_2 receptor occupancy is ultimately responsible for the side effect profile of clinically used APDs (Kapur et al., 2000a). Thus, it is estimated from PET studies that typical APDs must occupy 65-70% of dopamine D_2 receptors in the striatum to produce their APD effect (Farde et al., 1992; Nyberg et al., 1999, Tauscher et al., 1999; Tauscher & Kapur 2001; Seeman 1995). The therapeutic margins are relatively tight and >80% occupancy significantly increases the risk of EPS due to excessive blockade of dopamine signalling (Norde & Farde 2011; Farde et al., 1992 and Kapur & Seeman 2001).

It has been shown that the endogenous neurotransmitter dopamine is released at nM levels in the striatum, and previous kinetic studies suggest that it should bind rapidly to free D_2R (Sulzer et al., 2016; Klein-Herenbrink et al., 2016). As a consequence, rapid APD-receptor dissociation helps facilitate normal physiological neurotransmission. Whereas slow receptor dissociation promotes the phenomenon of hemi-equilibrium (Charlton & Vauquelin 2010) characterised functionally as a depressed agonist response. In the synapse dopamine concentrations are likely to

fluctuate on a very short time scale due to efficient synaptic uptake mechanisms which prevent persistent signalling and allow greater temporal control of neurotransmission. Therefore, the potential for persistent receptor blockade precipitated by slowly dissociating antagonists is thought to increase the probability of triggering EPS. Acutely side effects can be improved by administering an anti-muscarinic agent, but the usual course of action to prevent further instances of EPS is to either reduce the dose, and therefore the level of dopamine D_2 occupancy, or to switch to an atypical antipsychotic (D'Souza and Hooten 2019).

Certain anomalies exist in the multi-receptor hypothesis described above the most compelling is the finding that amisulpride a drug which selectively targets $D_{2/3}$ receptors produces a relatively low incidence of side effects and is also effective against negative symptoms (Leucht et al., 2009; Leucht et al., 2013). Due to this anomaly in multi-receptor hypothesis and the attraction of the rapid dissociation from a mechanistic perspective 'atypicality' is now more usually linked to a compounds' short residence time ($1/k_{off}$) at the D_2R than their ability to antagonise 5-HT2A receptors (Seeman 2002).

5.1.4 Challenges to the kinetic hypothesis

The assertion by Kapur and Seeman that APDs exhibit more or less the same k_{on} for dopamine D_2 receptors has led to the belief that affinity differences between atypical and typical APDs are determined purely by differences in the magnitude of k_{off} (Kapur and Seeman 2000; Horacek et al., 2006). Other research has questioned this link between affinity and 'atypicality', highlighting the fact that the atypical APDs olanzapine and risperidone have a relatively high affinity for the D_2R and thus should, in theory, dissociate as slowly from the D_2R as the classical typical APD haloperidol (Meltzer 2013).

Indeed, it has been suggested that absolute D_2R affinity values are unimportant in dictating side effects, with a high D_2R affinity being compensated for by a higher relative affinity for the 5-HT2A receptor (Meltzer et al., 1989; Meltzer 1992). This idea was first postulated in the 1970s when it was suggested that the anti-serotonergic properties of clozapine, in relation to its anti-dopaminergic properties, might account for its lack of EPS (Sulpizio et at., 1978; Lai et at., 1980). The reality, of course, is that APD receptor kinetics could play a role in this scenario too,

determining the relative levels of 5-HT2A: D_2 receptor occupancy. This reasoning reinforces the need to kinetically profile all current and future APDs and in doing so improve our powers to predict the side effect profile of any newly emerging therapies.

The existing kinetic data on dopamine D_2 clinical atypical and typical APDs are from a variety of groups using an assortment of different methods and measured over several decades (Kapur and Seeman 2000; Seeman 2005; Horacek et al., 2006; Langlois et al., 2012; Carboni et al., 2012). The experimental conditions chosen for our kinetic binding studies was an important initial consideration since both ionic strength and temperature have been demonstrated to affect dopamine D_2R binding affinities (Newton et al., 2016; Hall et al., 1988). Thus, the current study aimed to use a higher-throughput method to determine the kinetics of a large number of clinically used APDs under physiological conditions of temperature and sodium ion concentration, and in doing so explore the kinetic basis for the distinction between atypical and typical APDs.

5.2 Materials and methods

5.2.1 Materials

PPHT derivative labelled with a red fluorescent probe (PPHT-red) was obtained from Cisbio Bioassays (Bagnols-sur-Cèze, France). The sources of all other materials used in the experiments described in the following sections are detailed in Chapter 2, section 2.1 Materials.

5.2.2 Cell culture

The host Chinese hamster ovary (CHO) K1 cell line was provided by Prof. J. Baker, University of Nottingham (ATCC #CCL-61) and the CHO-D_{2L} cell line established as described in Chapter 3, section 3.2.2 Cell culture. Cells were maintained as described in Chapter 2, section 2.2.1 Cell culture.

5.2.3 Terbium labelling of SNAP-tagged D_{2L} cells and membrane preparation

Cell culture medium was removed from the t175cm^2 flasks containing confluent adherent CHO-D_{2L} cells. Cells were labelled with SNAP-Lumi4-Tb as detailed in Chapter 2, section 2.2.5 Terbium labelling of SNAP-tagged cells and membrane preparation. Before their use, the frozen membranes were thawed, and the membranes suspended in the assay buffer at a membrane concentration of 0.2mg/ml.

5.2.4 [^{3}H]-Spiperone saturation binding assays.

Increasing concentrations of [^{3}H]-spiperone (0.020 -1.2nM) were incubated with human dopamine D_{2L} CHO cell membranes (10 μg per well) at 37^{o}C in assay binding buffer (20mM Hepes 138mM NaCl. 6mM $MgCl_2$, 1mM EGTA and 1mM EDTA pH 7.4) containing 100 μM GppNHp and 0.1% ascorbic acid in a 1 ml reaction volume. Non-specific binding was determined in the presence of 3 μM (+)-butaclamol. After a 2h incubation period bound and free [^{3}H]-spiperone were separated by fast-flow filtration through GF/B filters using a Filter Mate Harvester (PerkinElmer) followed by 2ml wash with ice-cold PBS (Lonza). After drying, filter bound radioactivity was measured following the addition of 40 μL of Microscint 20 (PerkinElmer) using a

Topcount^{TM} microplate scintillation counter (PerkinElmer). Aliquots of [^{3}H]-spiperone were also quantified accurately to determine how much radioactivity was added to each well using liquid scintillation spectrometry on a Tri-Carb liquid scintillation counter (PerkinElmer).

5.2.5 Fluorescent ligand-binding assays

All fluorescent binding experiments using PPHT-red were conducted in white 384-well Optiplate plates, in assay binding buffer, 20 mM HEPES, 138mM NaCl, 6 mM $MgCl_2$, 1 mM EGTA, 1 mM EDTA, pH7.4 containing 1% DMSO, 0.02% pluronic acid, 0.1% ascorbic acid and 100 µM GppNHp (HEPES-salt buffer). In all cases, non-specific binding was determined in the presence of 10 µM haloperidol.

Determination of PPHT-red binding kinetics

To accurately determine association rate (k_{on}) and dissociation rate (k_{off}) values for PPHT-red the observed rate of association (k_{obs}) was calculated using at least four different concentrations as described in Chapter 2, section 2.2.6 Determination of tracer binding kinetics and equilibrium affinity. The appropriate concentration of PPHT-red was incubated with human dopamine D_{2L} CHO cell membranes (2 µg per well) in assay binding buffer (final assay volume, 40 µL). The degree of PPHT-red bound to the receptor was assessed at multiple time points by HTRF detection to allow construction of association binding curves.

The resulting data were globally fitted to the association kinetic model using GraphPad Prism 6.0 to simultaneously calculate k_{on} and k_{off} (Equation 2.5, Chapter 2) and a one-phase exponential association model (Equation 2.6, Chapter 2) to derive an estimate of k_{on} and k_{off} from plotting tracer concentration versus observed association (k_{obs}) as described in Chapter 2, section 2.2.8 Signal detection and data analysis. PPHT-red tracer binding was carried out essentially as previously described (see Klein-Herenbrink et al., 2016).

Competition Binding Kinetics

To determine the association and dissociation rates of D_2R ligands, we used a competition kinetic binding assay we recently described to profile the kinetics of a series of D_2R agonists (Klein-Herenbrink *et al*., 2016). This approach involves the simultaneous addition of both fluorescent ligand and competitor to the receptor

preparation so that at t = 0 all receptors are unoccupied. 12.5 nM PPHT-red (a concentration which avoids ligand depletion in this assay volume, (see Carter *et al*., 2007) was added simultaneously with the unlabeled compound (at t = 0) to CHO cell membranes containing the human dopamine D_{2L} receptor (2 μg per well) in 40 μL of assay buffer. The degree of PPHT-red bound to the receptor was assessed at multiple time points by HTRF detection as described in section 5.2.6 Signal detection and data analysis.

Non-specific binding was determined as the amount of HTRF signal detected in the presence of haloperidol (10 μM) and was subtracted from each time point, meaning that t = 0 was always equal to zero. Each time point was conducted on the same 384-well plate incubated at 37°C with orbital mixing (1sec of 100 RPM/cycle). An optical plate seal was used to cover the wells and prevent evaporation.

Multiple concentrations of unlabeled competitor were tested, for determination of rate parameters. Data were globally fitted using (Equation 2.7, Chapter 2) to simultaneously calculate k_{on} and k_{off} of unlabelled compounds. Different ligand concentration ranges were chosen, as compounds with a long residence time equilibrate more slowly, so a higher relative concentration is required to ensure the experiments reach equilibrium within a reasonable time frame (120 minutes), while still maintaining a good signal-to-noise.

5.2.6 Signal detection and data analysis.

For the binding experiments, described signal detection was performed on a PHERAstar FS (BMG Labtech, Offenburg, Germany) using standard HTRF filter settings (dual emission), as described in Chapter 2, section 2.2.8 Signal detection and data analysis. HTRF ratios and specific binding were calculated as describes in Chapter 2, section 2.2.8 Signal detection and data analysis.

All experiments were analyzed using GraphPad Prism 6.0. Saturation binding data were analysed by non-linear regression according to a one-site model, Fitting the total and NSB data sets simultaneously to Equation 2.1 described in Chapter 2, provides one best-fit value for both the K_d and the B_{max} of a fluorescent tracer. Specific binding, obtained by subtracting non-specific binding from total binding, was fitted to Equation 2.2 Chapter 2, a one-site binding model that describes a rectangular hyperbola or binding isotherm. Competition displacement binding data

were fitted to sigmoidal (variable slope) curves using a “four-parameter logistic equation”, see Equation 2.3, Chapter 2. IC_{50} values obtained from the inhibition curves were converted to K_i values using the method of Cheng and Prusoff (1973), see Equation 2.4, Chapter 2.

Fluorescent ligand (tracer) association data were fitted to a global fitting model using GraphPad Prism 6.0 to simultaneously calculate k_{on} and k_{off} using Equation 2.5, Chapter 2. Also, tracer association data were analysed using non-linear regression to fit the specific binding data to a one-phase exponential association equation, see Equation 2.6, Chapter 2. Where tracer binding follows a simple law of mass action model, k_{obs} increases linearly as a function of tracer concentration. The slope of the resulting line fitted using linear regression equates to the association rate (k_{on}), and extrapolation of the plot to y = 0 yields the dissociation rate (k_{off}) (Sykes et al., 2010).

Association and dissociation rates for unlabeled antagonists were calculated using the equations described by Motulsky and Mahan (1984), see Equation 2.7, Chapter 2. PPHT-red dissociation data was fitted to a one-phase mono-exponential decay function to estimate the dissociation rate of PPHT-red directly as described in Chapter 2, Equation 2.8. Assuming free diffusion of ligand the estimated time taken for 50% of a ligand to dissociate from D_2R was calculated using the following relationship dissociation $t_{1/2} = 0.693/k_{off}$.

5.2.7 Modelling striatal dopamine D_2R re-binding

Drug receptor rebinding values were calculated as described in Chapter 2, section 2.2.9 Modelling drug-receptor re-binding. All data were analyzed using GraphPad Prism 6.0.

5.2.8 Relationship between binding kinetics and clinical side effect profile

Binding kinetic values determined in this study were correlated with published clinical schizophrenia treatment data taken from a comprehensive meta-analysis of clinically used APDs performed by Leucht et al., (2013) as described in Chapter 2 section 2.2.10 Comparing binding kinetics and clinical side effect profile. Differences were considered significant at $P< 0.05$. All analysis was performed using GraphPad Prism 6.0.

5.3 Results

5.3.1 Characterisation of PPHT-red binding from saturation analysis

Specific PPHT-red binding to human D_{2L} receptor expressed in CHO membranes was saturable and best described by the interaction of the fluorescent ligand with a single population of binding sites (see Figure 5.1A). From these studies, the equilibrium dissociation constant (K_d) of PPHT-red was determined to be 16.2 ± 0.8 nM, n=23. The expression level of the human D_{2L} receptor recombinantly expressed in CHO cells was assessed, using [^{3}H]-spiperone saturation binding and determined to be 1.1 ± 0.1 pmol·mg^{-1} protein (radioligand binding expression data provided by Lisa Stott).

The binding kinetics of PPHT-red was characterised by monitoring the observed association rates at six different ligand concentrations (Figure 5.1B). The observed rate of association was linearly related to PPHT-red concentration (Figure 5.1C). Kinetic rate parameters for PPHT-red were calculated by globally fitting the association time courses, resulting in a k_{on} of 2.3 ± 0.1 x10^7 M^{-1} min^{-1} and a k_{off} of 0.33 ± 0.01 min^{-1}, n=23. The resulting K_d (k_{off} / k_{on}) of 15.4 ± 0.1 nM was comparable to that obtained previously (Klein-Herenbrink et al., 2016). Ligand dissociation was also estimated directly by adding an excess of haloperidol. A k_{off} value of 0.52 ± 0.04 min^{-1}, n=4, was determined which was in good agreement with the value estimated from the global association time course described above (Figure 5.1D).

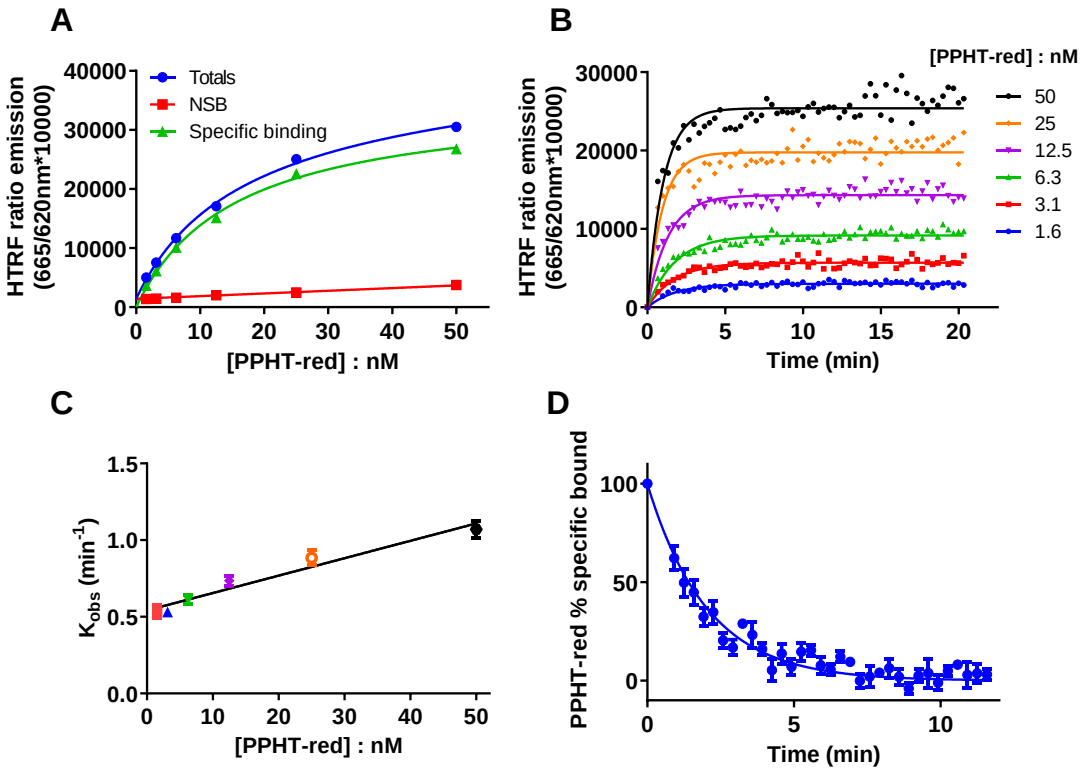


Figure 5.1. Determination of PPHT-red equilibrium and kinetic binding parameters. **(A)** Saturation analysis of the binding of PPHT-red to CHO membranes expressing the human dopamine D_{2L} receptors. Cell membranes (2 μg per well) were incubated for 120 min with gentle agitation with increasing concentrations of PPHT-red. NSB was defined by the inclusion of 10 μM haloperidol. Data are presented as single values representative of 23 experiments. **(B)** Observed association kinetics of the interaction of PPHT-red with CHO membranes expressing the human dopamine D_{2L} receptors. Data are presented in as single values representative of 23 experiments. **(C)** A plot of ligand concentration versus k_{obs}. Binding followed a simple law of mass action model, k_{obs} increasing linearly with radioligand concentration. Data are presented in mean ± S.E.M. from 23 experiments. **(D)** PPHT-red dissociation following addition of haloperidol (10 μM). Data are presented as mean ± S.E.M. from n=4 experiments.

5.3.2 Characterisation of unlabelled D_2R ligands

The binding affinity of the dopamine D_2 ligands for the dopamine D_{2L} receptor was measured at equilibrium in a buffer containing GppNHp (0.1 mM) at 37°C to ensure that antagonist binding only occurred to the uncoupled form of the receptor. Binding affinities (K_i values) for atypical and typical APDs are summarized in Table 5.1 and example competition curves are presented in Figure 5.2A. The separation of these two classes of compound, atypical and typical is based purely on historical nomenclature with appropriate references provided.

Representative competition association curves for selected dopamine D_2 ligands are shown in Figure 5.2, B–F. Progression curves for PPHT-red alone and in the presence of competitor were globally fitted to Equation 2.7, Chapter 2, enabling the calculation of both k_{on} (k3) and k_{off} (k4) for each of the ligands, as reported in Table 5.1.

	k_{off} (min^{-1})	k_{on} ($M^{-1}min^{-1}$)	Dissociation $t_{1/2}$ (min)	Kinetic pK_d	Equilibrium pK_i	n	Receptor occupancy reversal rate or k_r (min^{-1})
SGA/Atypical							
Paliperidone	0.44 ± 0.04	1.80 ± 0.29 x10^8	1.58	8.60 ± 0.07	8.54 ± 0.07	4	0.01035
*(-)Sulpiride	2.23 ± 0.93	1.60 ± 0.67 x10^8	0.31	7.87 ± 0.06	7.58 ± 0.10	4	0.05881
Remoxipride	1.90 ± 0.55	1.16 ± 0.37 x10^7	0.36	6.79 ± 0.04	6.68 ± 0.07	4	0.517
*Melperone	1.48 ± 0.18	1.99 ± 0.41 x10^7	0.47	7.11 ± 0.04	7.05 ± 0.03	4	0.2647
Clozapine	1.67 ± 0.25	8.23 ± 1.42 x10^7	0.41	7.69 ± 0.02	7.60 ± 0.02	4	0.0835
Amisulpride	0.83 ± 0.05	3.44 ± 0.50 x10^8	0.83	8.61 ± 0.06	8.49 ± 0.07	4	0.01033
Ziprasidone	1.07 ± 0.52	1.61 ± 0.50 x10^9	0.65	9.19 ± 0.18	9.16 ± 0.19	4	0.002871
Risperidone	0.43 ± 0.05	4.38 ± 0.52 x10^8	1.61	9.05 ± 0.01	8.95 ± 0.05	4	0.004223
Zotepine	1.41 ± 0.34	9.15 ± 1.63 x10^8	0.49	8.76 ± 0.17	8.69 ± 0.11	5	0.006656
Sertindole	0.59 ± 0.01	4.91 ± 0.82 x10^8	1.17	8.92 ± 0.07	8.89 ± 0.03	4	0.00516
Quetiapine	1.01 ± 0.33	6.57 ± 0.85 x10^6	0.69	6.82 ± 0.02	6.75 ± 0.07	4	0.4013
Olanzapine	1.12 ± 0.12	1.79 ± 0.44 x10^8	0.62	8.17 ± 0.09	8.08 ± 0.11	4	0.02651
Asenapine	0.93 ± 0.06	2.17 ± 0.65 x10^9	0.75	9.29 ± 0.16	9.29± 0.12	4	0.001853
*Loxapine	2.14 ± 0.33	4.04 ± 1.04 x10^8	0.32	8.25 ± 0.05	8.18 ± 0.05	4	0.02269
*Molindone	1.69 ± 0.45	8.69 ± 2.6 x10^7	0.41	7.69 ± 0.10	7.57 ± 0.12	6	0.08016

FGA/Typical							
(+)Butaclamol	0.026 ± 0.004	6.82 ± 2.44 x10^8	26.65	10.37 ± 0.12	10.32 ± 0.13	6	0.000164
Flupenthixol	0.072 ± 0.010	3.50 ± 0.72 x10^8	9.63	9.67 ± 0.07	9.68 ± 0.10	4	0.0008807
Haloperidol	0.65 ± 0.07	2.13 ± 0.52 x10^9	1.07	9.49 ± 0.08	9.48 ± 0.08	4	0.001322
Fluphenazine	0.040 ± 0.004	1.13 ± 0.01 x10^9	17.33	10.46 ± 0.06	10.29 ± 0.04	4	0.0004893
Chlorpromazine	2.20 ± 0.44	3.76 ± 0.70 x10^9	0.32	9.24 ± 0.04	9.01 ± 0.11	6	0.002647
*Thioridazine	1.41 ± 0.25	2.37 ± 0.61 x10^9	0.49	9.21 ± 0.03	8.93 ± 0.05	4	0.002575
Perphenazine	0.23 ± 0.02	1.29 ± 0.17 x10^9	3.01	9.73 ± 0.06	9.53 ± 0.04	4	0.0007705
Trifluroperazine	0.22 ± 0.01	1.10 ± 0.20 x10^9	3.15	9.69 ± 0.10	9.48 ± 0.04	4	0.0009388
Spiperone	0.038 ± 0.006	2.55 ± 0.12 x10^9	18.24	10.84 ± 0.07	10.54 ± 0.04	4	0.00003054
Nemonapride	0.018 ± 0.001	1.44 ± 0.04 x10^9	38.50	10.91 ± 0.03	10.39 ± 0.04	5	0.00005397
Droperidol	0.38 ± 0.04	2.01 ± 0.38 x10^9	1.82	9.71 ± 0.10	9.99 ± 0.10	4	0.0008184
*Raclopride	0.53 ± 0.14	6.69 ± 2.04 x10^8	1.31	9.08 ± 0.04	8.91 ± 0.08	4	0.003416
Peripheral acting							
**Domperidone	0.14 ± 0.02	9.73 ± 1.66 x10^8	4.95	9.83 ± 0.07	9.81 ± 0.09	6	ND

Table 5.1. Kinetic binding parameters of unlabelled dopamine D_2 antagonists for human dopamine D_{2L} receptors. Data are mean ± S.E.M. of n separate experiments, each performed in singlet, where n equals the number of observations. FGA/typical or SGA/atypical classification is based on reference sources (Leucht *et al*., 2013; Seeman 2002). * Some conjecture surrounds the classification of the atypical APDs (-)sulpiride, melperone, loxapine and molindone and the typical APDs thioridazine and raclopride. ** Domperidone is not an APD and is used to block dopamine D_2 receptors in the periphery. Assuming free diffusion

of ligand the estimated time taken for 50% of a ligand to dissociate from D_2R ($t_{1/2}$ values) was calculated using the following relationship $t_{1/2} = 0.693/k_{off}$. ND, Not determined.

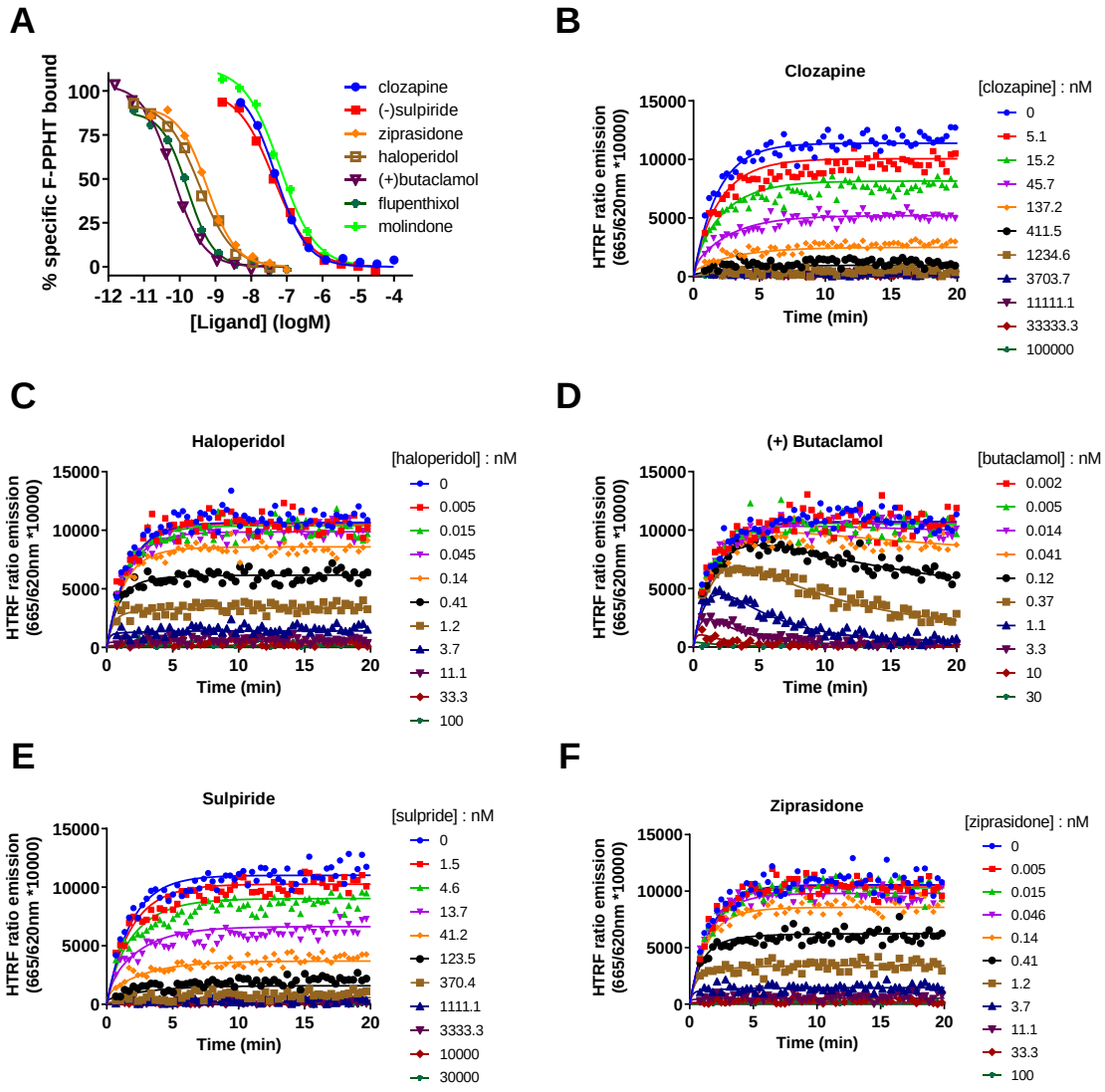


Figure 5.2. Equilibrium competition and kinetic competition binding between PPHT-red and representative atypical and typical APD at the human dopamine D_{2L} receptors in membranes prepared from the CHO cells in the presence of GppNHp (100 μM). Displacement of PPHT-red (12.5 nM) by increasing concentrations of **(A)** clozapine, (-)sulpiride, ziprasidone, haloperidol, (+)butaclamol, fluphenthixol and molindone at equilibrium. PPHT-red competition kinetic curves in the presence of **(B)** clozapine, **(C)** haloperidol, **(D)** (+)butaclamol, **(E)** (-)sulpiride and **(F)** ziprasidone. Plates were incubated at 37°C for the indicated time points and non-specific binding levels were determined in the presence of 10 μM haloperidol. Data are representative of four or more experiments. Kinetic and equilibrium data were fitted to the equations described in Materials and Methods to calculate K_i, K_d and k_{on} and k_{off} values for the unlabeled ligands; these are summarized in Table 5.1.

There was a very wide range in dissociation rates for the different ligands, with dissociation derived $t_{1/2}$ values between 0.32 minutes for chlorpromazine to 38.5 mins for nemonapride. To validate the rate constants, the kinetically derived dissociation constant (K_d) values (k_{off} / k_{on}) were compared with the dissociation constant (K_i) obtained from equilibrium competition binding experiments (see Figure 5.3). There was a very good correlation between these two values for both the atypical and typical APD tested (two-tailed Pearson's correlation $r^2 = 0.99$, $P < 0.0001$ and $r^2 = 0.98$, $P < 0.0001$ respectively) indicating the measured kinetic parameters are consistent with equilibrium affinity data obtained at equilibrium.

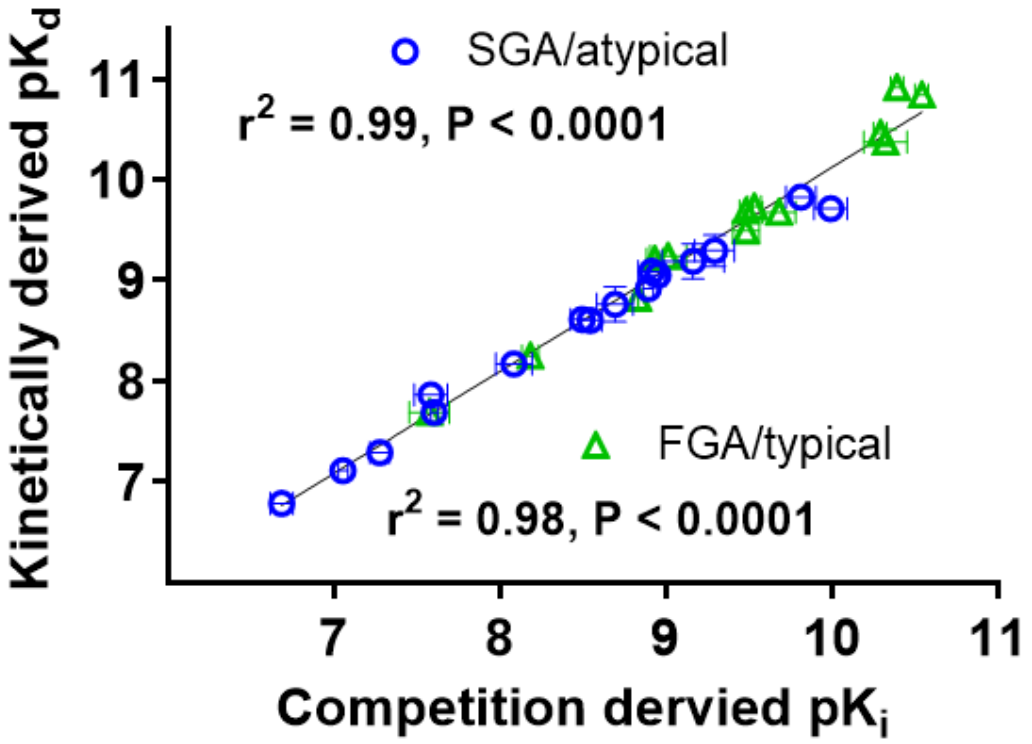


Figure 5.3. Comparing equilibrium and kinetically derived parameters of dopamine D_2 atypical and typical APDs. Correlation between pK_i and kinetically derived pK_d for the 29 test ligands. pK_i values were taken from PPHT-red competition binding experiments at equilibrium shown in Figure 5.2A. The values composing the kinetically derived pK_d (k_{off}/ k_{on}) were taken from the experiments shown in Figure 5.2B-F. All data used in these plots are detailed in Table 5.1. Data are presented as mean ± S.E.M. from four or more experiments.

5.3.3 Relationship between dopamine D_2 antagonist kinetics and atypical and typical classification

Historically the link between dopamine D_2 APD affinity and dissociation rate is based on the assumption that APDs exhibit more or less the same k_{on} for dopamine D_2 receptors (Kapur & Seeman 2001). The correlations presented in Figure 5.4A and B demonstrate that for atypical APDs, kinetic k_{on} (two-tailed Pearson's correlation $P<0.0001$, $r^2=0.94$) has a much stronger influence than k_{off} (two-tailed Pearson's correlation $P<0.05$, $r^2=0.33$) in determining the affinity of this class of compound. This is apparent in the increased range in k_{on} values (>100 fold) for the atypical APDs compared to their relatively small range in k_{off} values (<10 fold). Contrastingly for typical APDs, there was a much narrower variation in the value of k_{on} with differences in affinity seemingly driven by changes in k_{off} (two-tailed Pearson's correlation $P<0.0001$, $r^2= 0.81$). However, some of the typical APDs exhibit k_{off} values very similar to or indeed faster off than that of some of the atypical APDs eg. chlorpromazine

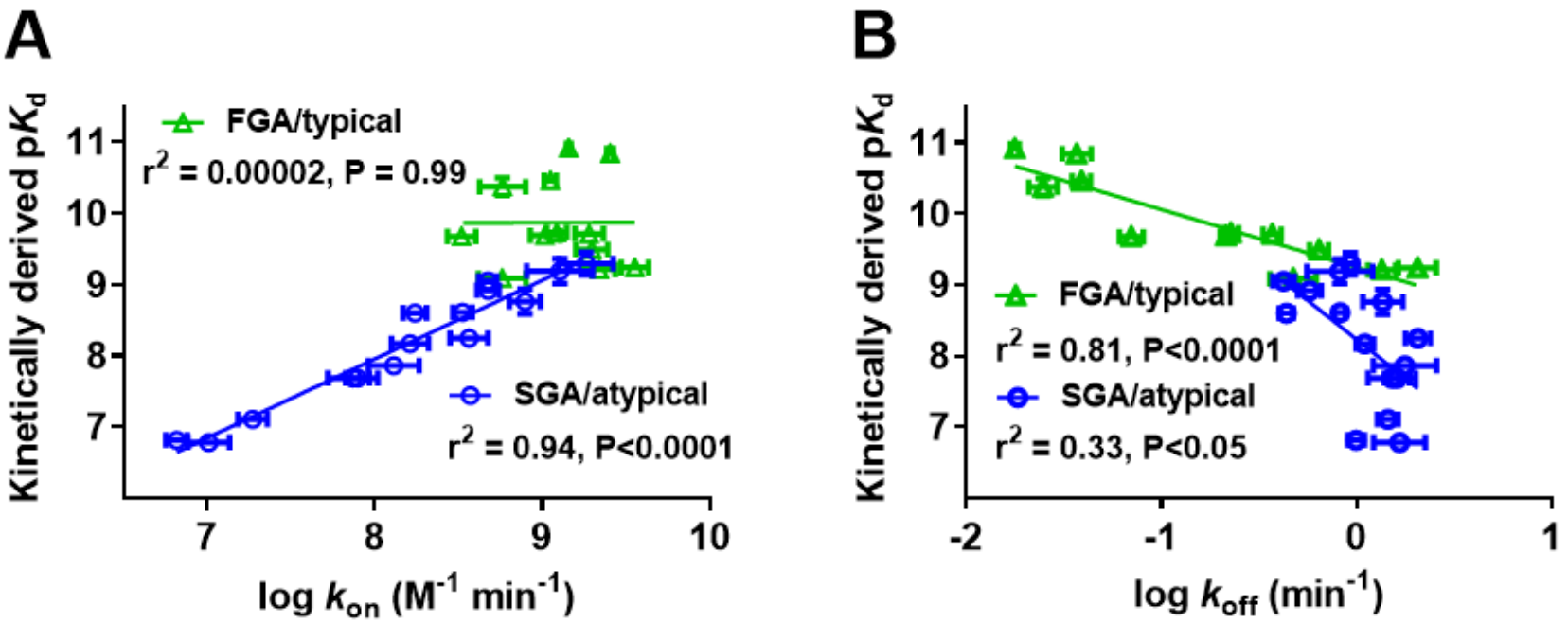


Figure 5.4. Equilibrium and kinetic competition binding between PPHT-red and representative atypical and typical APD at the human dopamine D_{2L} receptor expressed in the CHO cells in the presence of GppNHp (100 μM). Correlation between pK_d and log k_{on} **(A)** and log k_{off} **(B)** determined for the test APDs. pK_d values were taken from competition kinetic binding experiments. All data used in these plots are detailed in Table 5.1. Data are presented as mean ± S.E.M. from four or more experiments. The relationship between two variables was assessed using a two-tailed Pearson's correlation. A *P* value of 0.05 was used as the cutoff for statistical significance and relationships depicted as trend lines.

5.3.4 Relationship between Kinetics and Clinical measures of Dopamine D_2 Antagonist Reversibility

A meta-analysis is a statistical analysis which combines the results of multiple clinical studies. This type of analysis allows drugs, in this case APDs, to be compared using direct and indirect information against a single specific condition such as EPS. We have correlated our kinetic binding data with clinical findings taken from a recent study detailing the relative efficacy and tolerability of a diverse group of clinical APDs using a multiple-treatments meta-analysis (Leucht et al., 2013). In terms of tolerability, prolactin increases and EPS are thought to reflect 'on-target' toxicity and are directly related to D_2R blockade, whilst other adverse effects such as QTc prolongation (corrected QT, see Desai et al., 2015), which can result in sudden death from ventricular fibrillation, sedation and weight gain are generally considered 'off-target' effects.

In accordance with the 'rapid dissociation hypothesis' of Seeman and Kapur (Kapur and Seeman 2000; Kapur and Seeman 2001), prolactin increases were correlated with the kinetic k_{off} but not the k_{on} (see Figure 5.5A and B, Spearman's r_s= -0.82, P< 0.05 and r_s = 0.12, P = 0.78 respectively). In contrast, the kinetic k_{on} but not the k_{off} rate was positively correlated with the incidence of EPS (determined by odds ratio), see Figure 5.5D and C, Spearman's r_s = 0.68, P< 0.05 and r_s = -0.13, P = 0.68, respectively. In accordance and reflective of the fact that k_{on} is driving the affinity of these clinically used APDs, it was demonstrated that the kinetically derived affinity (pK_d = *-log* (k_{off}/ k_{on}) was also closely linked with the incidence of EPS (Spearman's r_s = 0.64, P = 0.05, data not shown). The lack of correlation of EPS with measured kinetic off-rate is surprising, especially in light of current knowledge of EPS which are recognised to result from excessive blockade of dopamine D_2 receptors in the nigrostriatal dopamine system.

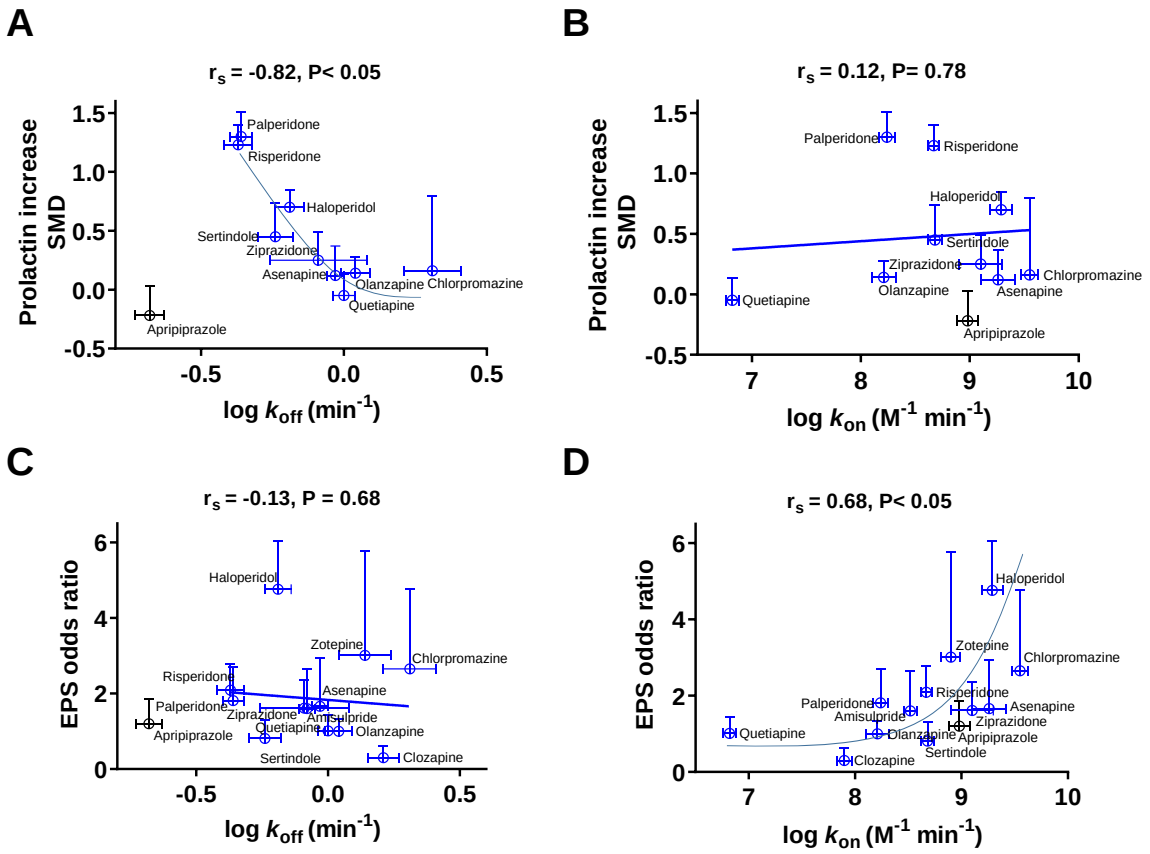


Figure 5.5. Correlating clinical data on APD 'on target' effects with kinetically derived parameters. Correlation plot showing the relationship between **(A)** log k_{off} and prolactin increase and **(B)** log k_{on} and prolactin increase. Correlation plot showing the relationship between **(C)** log k_{off} and EPS odds ratio and **(D)** log k_{on} and EPS odds ratio. All kinetic data used in these plots are detailed in Table 5.1 and clinical data are taken from Leucht et al., 2013. Aripiprazole was not included in the correlation analysis as it is a D_2R partial agonist. Kinetic data are presented as mean ± S.E.M. from four or more experiments and clinical data as standardised mean difference (SMD) for prolactin increase and odds ratio for EPS with associated credible intervals. The relationship between two variables was assessed using a two-tailed Spearman's rank correlation allowing the calculation of the correlation coefficient, r_s. A *P* value of 0.05 was used as the cutoff for statistical significance and relationships depicted as trend lines.

The active odds ratio, a measure of clinical efficacy based on symptoms (negative values being more active), was positively correlated with the kinetic k_{on} but not the k_{off} (see Figure 5.6A and B, Spearman's $r_s = 0.70$, $P < 0.05$, Spearman's $r_s = -0.05$, $P = 0.88$ respectively). The all-cause discontinuation odds ratio, a measure of the incidence of treatment discontinuation was positively correlated with the kinetic k_{on} but not the k_{off} (see Figure 5.6C and D, Spearman's $r_s = 0.70$, $P < 0.05$, $r_s = -0.14$, $P = 0.66$ respectively).

Certain side effects of atypical and typical APDs are considered 'off-target' (e.g. QTc prolongation) and as such their prevalence should be independent of D_2R pharmacology. Reassuringly no correlation was observed between measured k_{on} nor k_{off} in terms of QCTc prolongation (Spearman's $r_s = 0.09$, $P = 0.81$, and $r_s = 0.30$, $P = 0.41$ respectively see Figure 5.6E and F). Neither was there any correlation with D_2R affinity (Spearman's $r_s = -0.14$, $P=0.72$ data not shown).

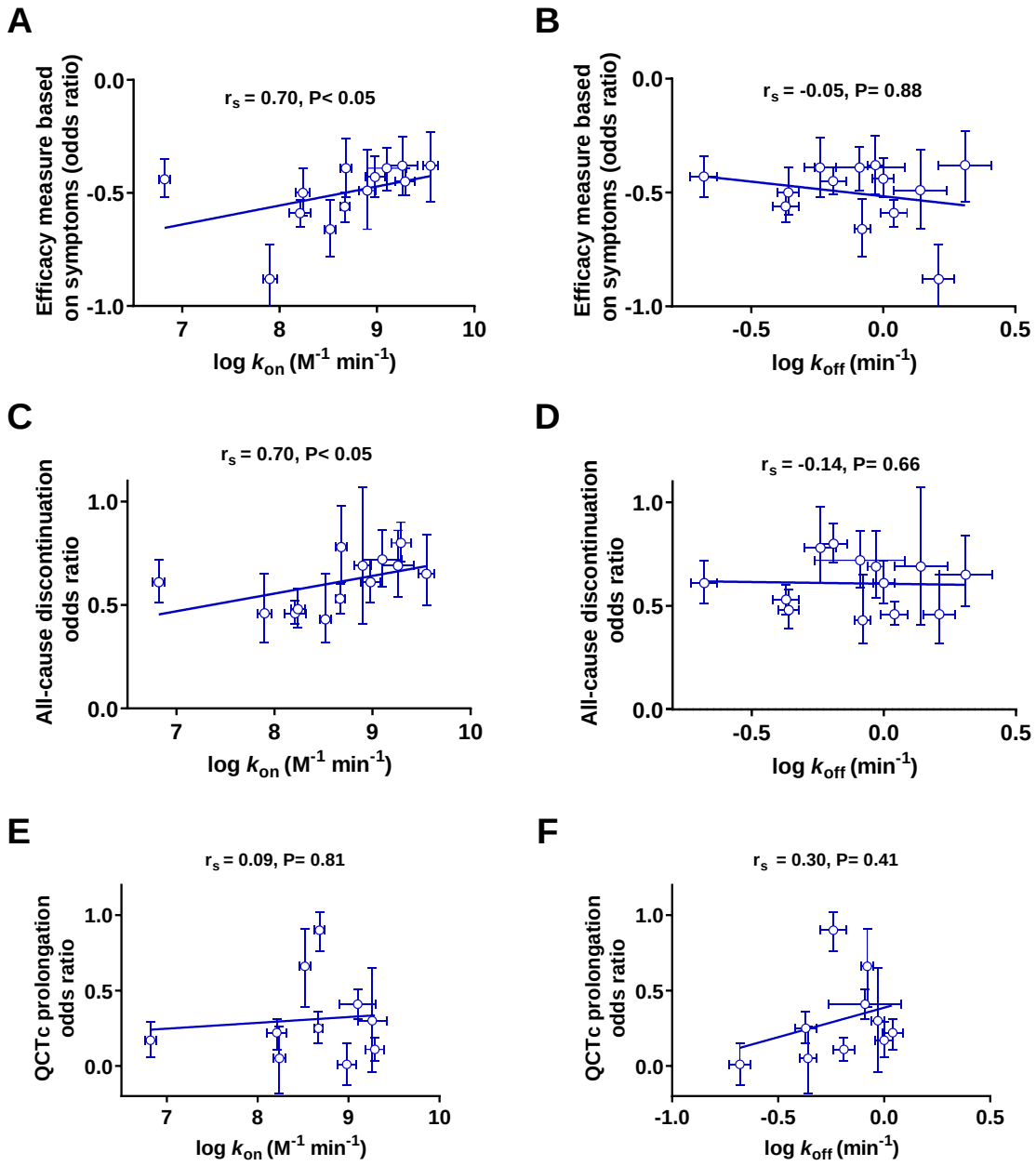


Figure 5.6. Correlating clinical data on APD efficacy, all-cause discontinuation and 'off-target' effects with kinetically derived parameters. Correlation plot showing the relationship between **(A)** log k_{on} and efficacy measure based on symptoms odds ratio and **(B)** log k_{off} and efficacy measure based on symptoms odds ratio. Correlation plot showing the relationship between **(C)** log k_{on} and all-cause discontinuation odds ratio and **(D)** log k_{off} and all-cause discontinuation odds ratio. Correlation plot showing the relationship between **(E)** log k_{on} and QCTc prolongation odds ratio and **(F)** log k_{off} and QCTc prolongation odds ratio. All kinetic data used in these plots are detailed in Table 5.1 and clinical data are taken from Leucht *et al*.,

2013. Kinetic data are presented as mean ± S.E.M. from four or more experiments and clinical data as odds ratios with associated credible intervals. The relationship between two variables was assessed using a two-tailed Spearman's rank correlation allowing the calculation of the correlation coefficient, r_s. A *P* value of 0.05 was used as the cutoff for statistical significance and relationships depicted as trend lines.

5.3.5 Modelling the effects of rebinding on APD dissociation rates

The synapses of the nigrostriatal system are essentially minute gaps across which dopamine impulses pass by diffusion and as such should be considered special receptor micro-compartments. These physical barriers hinder free diffusion out of the compartment, meaning recently dissociated drug molecules are more likely to rebind the same or nearby receptor than diffuse out of the compartment into the bulk aqueous phase. In addition to the nature of the physical barriers, rebinding is favoured by the presence of receptors in high density and a rapid drug association rate constant (Vauquelin and Charlton 2010).

Models of receptor rebinding in situations with limited diffusion allow the effect of k_{on} and k_{off} on the reversal of antagonist receptor occupancy to be considered collectively by deriving an overall reversal rate parameter (k_r) that provides a measure of the local duration of antagonist effect Vauquelin and Charlton 2010. The potential for rebinding of APDs was modelled according to two different scenarios; under conditions of free diffusion (see Figure 5.7A) where the law of mass action is applicable and under conditions of limited diffusion (see Figure 5.7B), such as encountered at the level of the synapse. As predicted based on current knowledge of rebinding processes k_{on} was the dominant factor in terms of extending the length of target-receptor occupancy under conditions of limited diffusion. In direct contrast, k_{on} has no role to play in determining target occupancy when the conditions for free diffusion are in force.

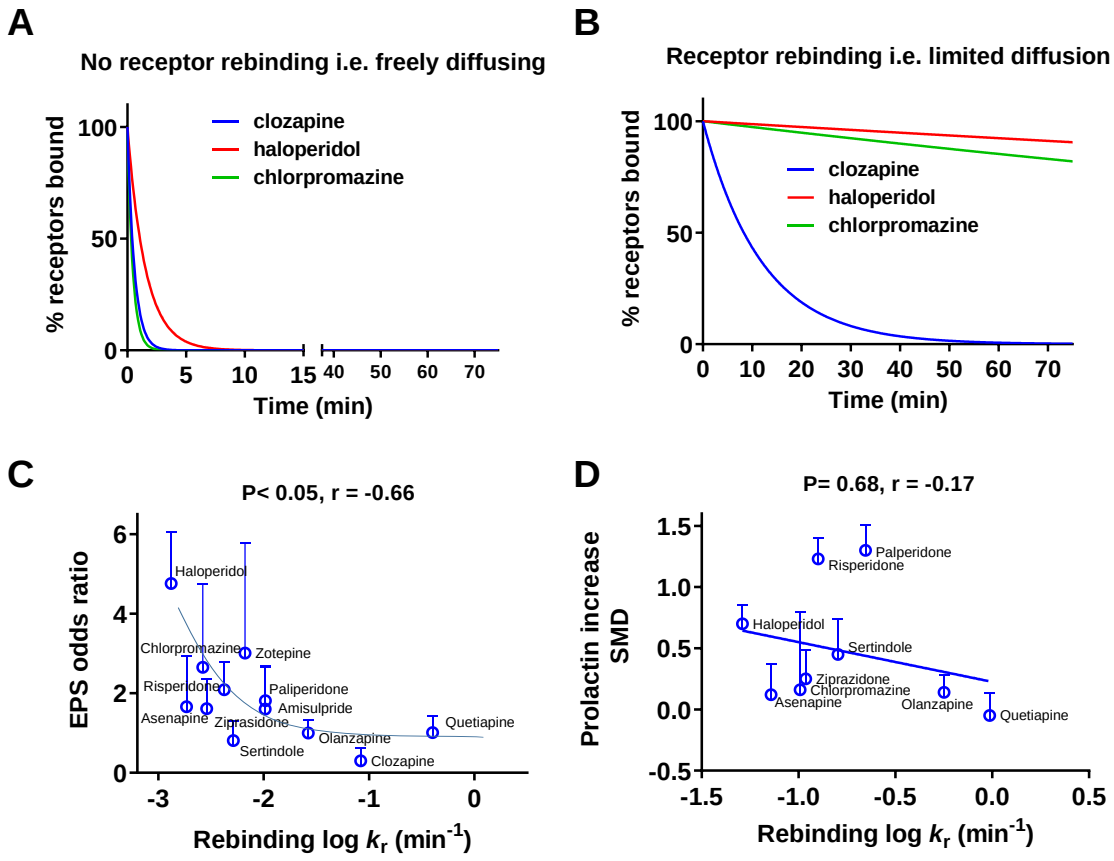


Figure 5.7. Modelling APD dopamine D_2 receptor rebinding and its consequences for clinical 'on target' toxic effects. Simulated dissociation rates of clinically relevant APDs at human D_{2L} receptors **(A)** under conditions of free diffusion based on measured off-rates (k_{off}) determined in competition kinetic binding experiments **(B)** under conditions of limited diffusion based on the association (k_{on}) and dissociation (k_{off}) rates determined in competition kinetic binding experiments. All kinetic parameters used to these plots are detailed in Table 5.1 of the results section, determined from fitting competition association data to Equation 2.7, detailed in Chapter 2. For simulation purposes the receptor occupancy reversal rate, k_r was based on the model of an immunological synapse as described in detail in Chapter 2 section 2.2.9 Modelling drug-receptor re-binding. Correlating clinical 'on target' effects with the kinetically derived rebinding parameter k_r. Correlation plot showing the relationship between **(C)** log k_r and EPS odds ratio and **(D)** log k_r and prolactin increase. All kinetic data used in these plots are detailed in Tables 5.1 and clinical data are taken from Leucht et al., 2013. Kinetic data are presented as mean ± S.E.M. from four or more experiments and clinical data as standardised mean

difference (SMD) for prolactin secretion and odds ratio for EPS with associated credible intervals. The relationship between two variables was assessed using a two-tailed Spearman's rank correlation allowing the calculation of the correlation coefficient, r_s. A *P* value of 0.05 was used as the cutoff for statistical significance and relationships depicted as trend lines.

5.3.6 The relationship between relative drug rebinding and clinical effects

Reassuringly the correlation between APD k_{on} values and the incidence of EPS observed was mirrored by the receptor occupancy reversal rate or k_r, suggesting that k_{on} is important in dictating the reversal of D_2R occupancy at the level of the synapse (Spearman's r_s = -0.66, P< 0.05, see Figure 5.7C). In direct contrast, k_r was not significantly correlated with elevations of prolactin (which is in agreement with the lack of correlation with k_{on}, Spearman's r_s = -0.17, P= 0.68, see Figure 5.7D). The significant correlation observed between receptor occupancy reversal rate (k_r) and the active odds ratio suggests that rebinding is also a factor in determining the effectiveness of APD treatment (see Figure 5.8A, Spearman's r_s = -0.61, P <0.05), with compounds showing a reduced tendency to rebind dopamine D_2 receptors being more effective. This may be due to issues with compliance as a significant correlation was observed between receptor occupancy reversal rate (k_r) and discontinuation odds ratio, likely as the result of the increased propensity for EPS (Spearman's r_s = -0.69, P< 0.01, see Figure 5.8B).

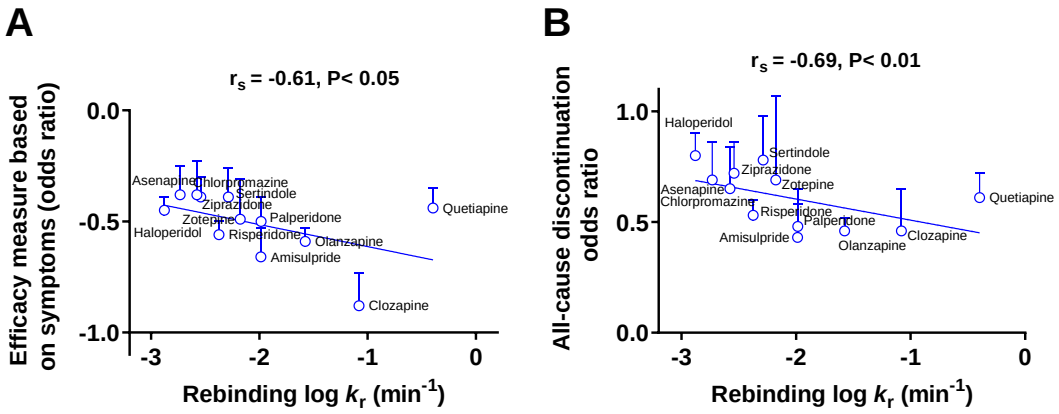


Figure 5.8. Relationship between APD dopamine D_2 receptor rebinding and measures of clinical efficacy and all-cause discontinuation. Correlation plot showing the relationship between **(A)** log k_r and efficacy measures based on symptoms odds ratio. **(B)** log k_r and all-cause discontinuation odds ratio. All kinetic parameters used to produce these plots are detailed in Table 5.1 and their determination is detailed in Chapter 2 section 2.2.9 Modelling drug-receptor re-binding. Clinical data are taken from Leucht *et al*., 2013. For simulation purposes, the rebinding constant k_r was based on the model of an immunological synapse as described in the methods section. Kinetic data are presented as mean ± S.E.M. from four or more experiments and clinical data as odds ratio with associated upper credible interval. The relationship between two variables was assessed using a two-tailed Spearman's rank correlation allowing the calculation of the correlation coefficient, r_s. A *P* value of 0.05 was used as the cutoff for statistical significance and relationships depicted as trend lines.

5.4 Discussion

Traditionally target occupancy has been calculated using a drug's equilibrium dissociation constant or K_d, which relates to the affinity of a drug at equilibrium with its receptor. This simplified view of target occupancy fails to capture the full kinetic and structural determinants of drug-receptor interactions which are temporal in nature. It is interesting to note that while the emphasis of many papers focuses on the design of compounds with slow off-rates (k_{off}) to enhance potency, k_{on} can also play a significant and often unappreciated role (Sykes *et al*., 2014). Indeed, it has widely been reported that APD potency for dopamine D_2 receptors is largely driven by differences in their receptor off-rates (Kapur and Seeman 2000; Kapur and Seeman 2001). Related to this is the idea that higher affinity typical antipsychotics exert on-target side effects due to their slower rate of dissociation (determined by k_{off}) from the D_2R (Kapur and Seeman 2001).

The purpose of the current study was to test the 'fast dissociation hypothesis' of Kapur and Seeman in the context of a single study capturing all commercially available clinically used APDs and relate these results to other published work and clinical studies. To my knowledge, the current study is the first time that kinetic rate constants have been derived for a large number of dopamine D_2 antagonists in a binding assay performed at physiologic temperature and sodium concentrations in the presence of guanine nucleotide.

Previous radioligand binding studies have reported differences in dissociation rates of the order of 100-fold between the typical APD chlorpromazine and the atypical drugs amisulpride, clozapine and quetiapine, (Seeman and Tallerico 1999; Seeman and Kapur 2000; Seeman 2005) however the present study could not corroborate these findings. The most plausible explanation for the differences observed between this and the original studies is the use of different temperatures to study the kinetics of these compounds coupled with the use of a sub-saturating concentration of dopamine (100nM), employed specifically to mimic dopamine signalling at the level of the synapse (Seeman and Tallerico 1999; Seeman 2005).

However, the current kinetic study does appear to support some of the original findings of Kapur and Seeman (2001) in that certain typical and atypical APDs can be readily distinguished based on kinetic k_{off}. Importantly our results suggest that

the currently used system of designating APDs as FGA/typical and SGA/atypical in the context of receptor kinetics may be of limited value. For example, risperidone exhibited the slowest off-rate of all the atypical APD tested, which was not dissimilar to that of haloperidol. And conversely, we have identified typical APDs with k_{off} values not dissimilar to clozapine, such as chlorpromazine, although importantly they exhibit more rapid association rates.

Our kinetic studies also reveal for the first time the important disconnect between increasing APD affinity and k_{off}. For the least potent APDs tested, affinity is largely driven by changes in k_{on} and not by changes in k_{off} (see Figure 5.3A). This is important because APD affinity has been used to estimate the kinetic rate constant k_{off} for a number of clinically relevant APDs assuming k_{on} is a constant for all ligands (Kapur and Seeman 2001; Roth et al., 2003; Horack *et al*., 2006). For example, it has been suggested that higher affinity atypical APDs e.g. olanzapine and risperidone should share kinetic properties similar to haloperidol, rather than the rapid off, lower affinity atypical APDs clozapine and quetiapine (Meltzer 2013). In contrast, the current study demonstrates that olanzapine dissociates from the dopamine D_{2L} receptor more rapidly than haloperidol whilst risperidone dissociates more slowly than haloperidol, reinforcing the importance of measured kinetic off rates over calculated off rates based on equilibrium affinity.

To rationalise the propensity of certain APDs to cause EPS the duration of target occupancy needs to be considered. The original 'fast dissociation hypothesis' suggests that compounds with slower dissociation rates from the D_2R are more likely to cause EPS, with atypical APDs dissociating more rapidly than typical APDs. Recently, however, whole-cell functional data have been presented suggesting other factors may contribute. Using an electrophysiological method, Sahlholm and colleagues measured dopamine D_2 receptor-evoked potassium channel activation and compared the reversibility of dopamine D_2 APD receptor antagonism (Sahlholm et al., 2014). Functional response recovery rates differed between atypical drugs by up to 15-fold, but importantly and in agreement with the kinetic binding values obtained in this study the rates of recovery for the typical APD chlorpromazine and the atypical APDs amisulpride, clozapine and quetiapine are shown to differ by less than two-fold an indication that these compounds should share very similar measured kinetic off-rates from the dopamine D_2 receptor.

I have correlated the kinetic binding data obtained in this study with clinical findings taken from a recent review exploring the relative efficacy, and tolerability of a diverse group of clinical APDs using a multiple-treatments meta-analysis (Leucht et al. 2013). Of significant consequence for drug design and in support of the 'fast dissociation hypothesis' the kinetic k_{off} but not the k_{on} was positively correlated with prolactin increases. Prolactin release from the anterior pituitary gland is regulated via the action of dopamine, which functions as a hypothalamic hormone to inhibit prolactin secretion via its action on dopamine D_2 receptors located on lactotroph cells (MacLeod *et al*., 1970; Kamberi *et al*., 1970; Mansour *et al*., 1990). Variations in the levels of dopamine in the portal blood readily account for changes in prolactin secretion in various physiological conditions and dopaminergic agonists are well documented to be effective at suppressing prolactin secretion in vivo (Ben-Jonathan *et al*., 1977; Ben-Jonathan *et al.*, 1980; Gibbs & Neill 1978; Hilfiker-Kleiner et al., 2012).

Surprisingly, however, I found it was k_{on} and not k_{off} that was positively correlated with the incidence of EPS, challenging the current belief that dissociation rate is the sole determinant of a compound's liability to produce this side effect. To further explore this finding, I employed a more holistic model of receptor binding that integrates both the association and dissociation rates in a system designed specifically to mimic the environment of the striatal synapse. This model assumes that diffusion of the drug out of the synapse is reduced by the physical barriers created by the pre- and post-synaptic membranes, which effectively create a compartment separating striatal dopamine D_2 receptors from the bulk aqueous phase. The consequence of this is that freshly dissociated ligands tend to remain in close proximity with membrane surfaces for longer, increasing the probability of a second binding event to the same or nearby D_2R (Vauquelin and Charlton 2010). By using the measured association and dissociation rates in this model I have estimated the overall relative rate of reversal of D_2R blockade, termed k_r (Vauquelin and Charlton 2010).

The effects of hindered diffusion on D_2R target occupancy are illustrated in Figures 5.7A and B which shows the potential of three kinetically diverse clinical APDs to rebind the D_2R in the synaptic cleft under conditions of free (see Figure 5.7A) and limited diffusion (see Figure 5.7B), demonstrating the potential of compounds with

more rapid on-rates to effectively occupy the D_2R for extended periods of time due to their propensity to rebind receptors rather than diffuse away into the bulk aqueous phase. Thus, compounds of equal affinity and/or kinetic k_{off} rate do not share the same potential to rebind receptors, a process which in the face of limited diffusion and sub-saturating dopamine concentrations is governed not by k_{off} but by k_{on}. In the rodent striatum in vivo the concentration of dopamine has been estimated to be in the range of 100–400 nM following a single stimulation pulse (Sulzer et al., 2016). Concentrations which would be expected, based on dopamine's affinity for the D_2R (6.6 μM, Klein-Herenbrink et al., 2016) to occupy less than 10% of available receptors.

When I calculated the receptor occupancy reversal rate, k_r ($k_r = k_{off}/(1+ k_{on} *[R]/k-$) using the measured kinetic parameters, I found it was significantly correlated with the incidence of EPS, (Spearman's $r_s = -0.66$; $P<0.05$ see Figure 5.7C). This result contradicts current thinking which suggests that compound dissociation rate (k_{off}) directly determines a compounds liability to produce EPS, suggesting a more important role for k_{on}. The active odds ratio, a measure of the effectiveness of treatment, produced a similar correlation with k_{on} and k_r strongly suggesting that the process of rebinding and increased EPS liability may be a limiting factor in determining treatment effectiveness (see Figure 5.6A and 5.8A), ultimately leading to discontinuation of therapy (see Figure 5.6C and 5.8B). Intriguingly, radioligand binding studies have demonstrated that sub-saturating concentrations of dopamine less readily displaces more rapidly associating radioligands such as chlorpromazine compared to more slowly associating radioligands such as clozapine, despite their off-rates being almost identical (Seeman and Tallerico 1999). It is tempting to speculate this observed difference is due to compound rebinding a consequence of a faster on-rate, and potentially the increased lipophilicity of chlorpromazine compared to clozapine ($clogD_{7.4}$ 3.42 vs 2.72). Indeed it has previously been demonstrated for the β_2 adrenoceptor that the kinetic association rate constant is directly related to compound lipophilicity and more specifically their ability to partition into biological membranes, with increasing local drug concentration driving a faster-observed association rate (Sykes et al., 2014; Gherbi et al., 2018). Gaining an understanding of receptor-specific versus non-specific membrane-driven differences in association rates would be an interesting topic for further study.

These factors are likely to be crucial considerations when optimising APDs where the primary goal is to reduce on-target toxicity.

In direct contrast to EPS, prolactin increase was not correlated with k_r reflecting the lack of correlation with k_{on}. This may reflect a lower diffusion limitation in the pituitary gland, perhaps because dopamine acts as a blood-borne hormone rather than a neurotransmitter to inhibit prolactin release (MacLeod et al., 1970). Thus, the rebinding potential is lower, so the reversal of APD-receptor occupancy will occur at a rate dependent on the dissociation rate constant (measured $k_{off,}$ see Figure 5.7A). Therefore 'on-target' toxicity at the level of the pituitary gland may largely result from insurmountable antagonism, hence the strong correlation of prolactin release with measured off-rates.

The view of APD binding presented above may also explain the reported regional brain selectivity of certain APDs which has long been suspected as contributing to atypicality (Natesan et al., 2008). The degree to which a particular APD rebinds the D_2R will be very much dependent on anatomical location and also the free concentration of dopamine at the synapse (Lawley and Keener 2017; Strange 2001).

It is important, however, to acknowledge that the data presented in this study do not rule out the possibility that other mechanisms contribute to the reduced side effect profile of clinically used APDs. Indeed it is noteworthy that certain compounds such as ziprasidone, sertindole and asenapine, which are thought to enhance dopamine signaling through either their agonist effect at the $5\text{-}HT_{1A}$ receptor, or antagonist activity at 5-HT2A receptors (Newman-Tancredi and Kleven 2011; Meltzer *et al*., 1989), and therefore exhibit a lower EPS profile than predicted solely by their forward rebinding constant (k_r).

In summary, I propose to expand the kinetic hypothesis for APD side effects by considering not only the dissociation rate (and therefore propensity to display insurmountable antagonism) but also their association rate and potential for receptor rebinding, leading to increased competition with dopamine at the synapse (see Figure 5.9A). Based on this scheme I propose the following three, broad classes of compound, to explain how these different kinetic characteristics may influence observed on-target side effects in different tissues:

1. Fast on, slow off compounds that display both high receptor-rebinding potential (and therefore high EPS) and insurmountable antagonism (and therefore increased prolactin release), e.g. haloperidol
2. Fast on, fast off compounds that have high rebinding potential (therefore high EPS) but reduced insurmountability (and therefore a reduced propensity for hyperprolactinaemia), e.g. chlorpromazine
3. Slow on, fast off compounds with low propensity for rebinding and insurmountability, and therefore lowest on-target side effect potential, e.g. clozapine

This model, which is summarised in Figure 5.9B, suggests that fast off/slow on compounds may be the optimal profile in terms of kinetics for clinically effective dopamine D_2 APD treatments. Thus, by careful optimization of both these kinetic parameters in parallel, it may be possible to discover ‘clozapine like’ compounds with sufficient affinity, low on-target side effect potential and overall reduced toxicity to be useful in the clinic.

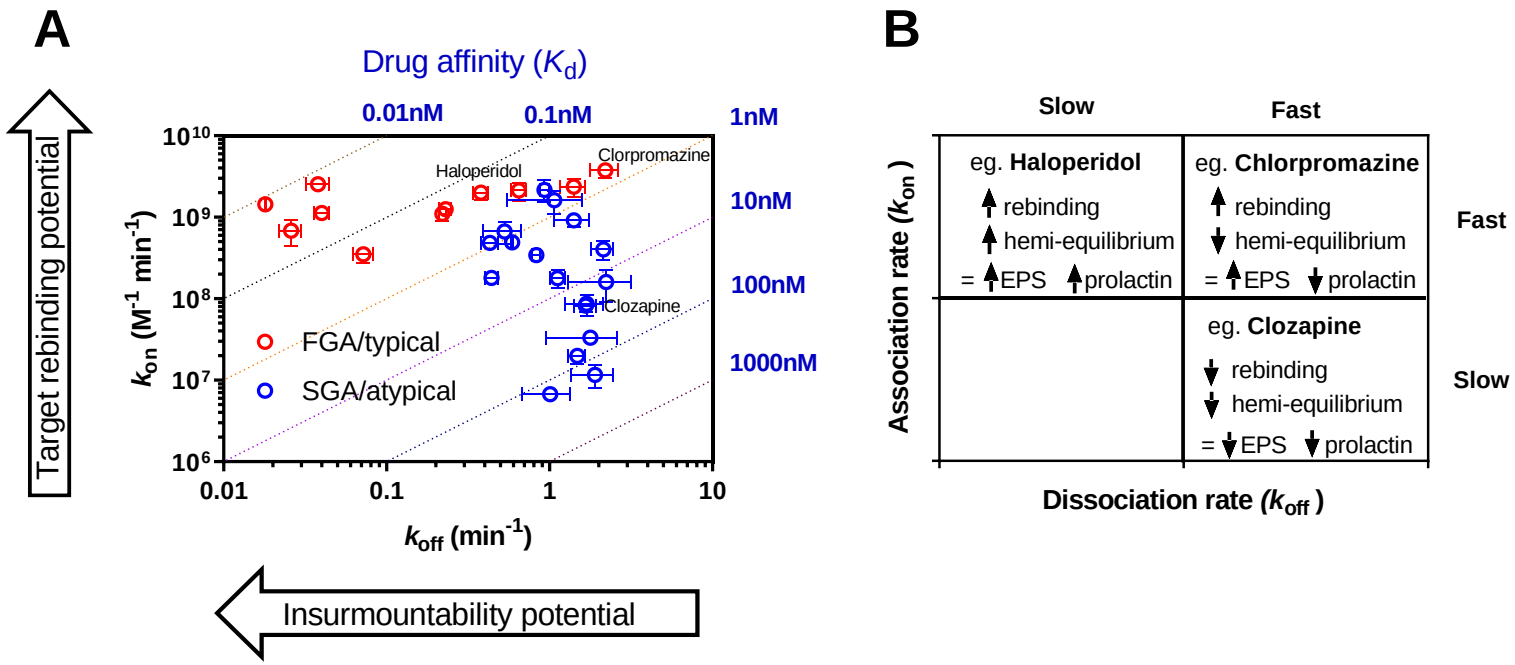


Figure 5.9. Summarizing the role of kinetics and rebinding in dictating the 'on-target' toxicity of SGA/atypical and FGA/typical APDs. **(A)** Dopamine D_2 APD kinetic maps plotted as dissociation rate constants (k_{off}) versus association (k_{on}) rate constants and the combinations of k_{on} and k_{off} that result in identical affinity (K_d) values (diagonal dotted lines). The arrows on the graph indicate the directions of increasing rebinding and insurmountability potential (due to hemi-equilibrium) dictated by k_{on} and k_{off} respectively. **(B)** The 3 main types of APD identified from this kinetic study are represented in the box plot along with their potential for 'on target' toxic effects eg. Increased prolactin and EPS. Kinetic data are presented as mean ± S.E.M. from four or more experiments.

5.5 Conclusion

In conclusion, the overall picture of dopamine D_2 APDs from a pharmacological and kinetic perspective has been somewhat confused mainly due to a paucity of directly comparable kinetic data obtained at physiological temperature and sodium ion concentration. The results of the current study suggest that at the level of the synapse, k_{on} is an important factor in determining the reversibility of APDs due to the tendency of compounds to rebind free receptors when free diffusion is limited, increasing and maintaining local drug concentration. This finding has major implications for drug design and our hope is that the new kinetic information detailed in this thesis can be used in conjunction with other known contributing factors to EPS to develop a new generation of safer drugs for a disease area which is still of great unmet medical need.

Chapter 6 - Investigating a role for serotonin 5-HT2A and 5-HT1A receptors in the reduced incidence of EPS of clinically used antipsychotics; the influence of differential receptor target coverage

6.1 Introduction

6.1.1 Schizophrenia and on-target side effects 'The Dopamine Hypothesis'

The common mechanism of APD action is postsynaptic dopamine antagonism which forms the basis of the original 'dopamine hypothesis' of schizophrenia formulated by Carlsson and Lindqvist (1963), who identified that these drugs increased the metabolism of dopamine when administered to animals. Then during the 1970s, it was shown that the clinical effectiveness of these compounds could be correlated back to their affinity for the D_2R (Seeman and Lee 1975; Creese et al., 1975 and Seeman et al., 1976).

This original hypothesis was updated in the early 1990s in a publication by Davis et al., (1991). In this visionary article they describe a 'modified dopamine hypothesis of schizophrenia' they argue for the regional specificity of dopamine signalling characterised by frontal hypodopaminergia (leading to negative symptoms) and a subcortical striatal hyperdopaminergia (leading to positive symptoms). With lesions in the prefrontal cortex resulting in increased D_2R numbers, and dopamine and its metabolites in the striatum of animal models (Pycock et al., 1980), with similar findings in humans (Davis et al., 1991).

However, signalling pathways other than the dopaminergic pathway have been suggested to play a key role in both the therapeutic and favourable side effect profile of atypical APDs over conventional or typical APD treatments (Meltzer 1999; Karam et al., 2010). Atypical APDs are often described as those that produce a lower incidence of side effects at clinically effective doses (Meltzer 1999). Consequently, there is still great interest in understanding the mechanism of action (MOA) of APDs and the resulting features of typical and atypical behaviour which are usually ascribed to a particular pharmacological property (Meltzer et al., 1989; Kapur and Seeman 2001; Sykes et al., 2017).

In truth, APDs rarely fall neatly into one of these two classes since their side effects comprise multiple, pharmacologically separable events, reflective of their pharmacological heterogeneity (Kusumi et al., 2015; Mackin and Thomas 2011). For example, the commonly occurring side effect of weight gain which occurs with

the use of certain APDs is associated with high affinity for central histamine H_1 receptors (Kroeze et al., 2003; He et al., 2013). Whilst agranulocytosis which is associated with clozapine treatment has been linked to activity at the histamine H_4 receptor (Goto et al., 2016). Consequently, a more rational approach to APD classification and drug design is to consider a continuum (or scale) based on the specific pharmacology of a given side effect, rather than the current dichotomous system. Thus, in order to better understand the pharmacodynamics of APDs, we must fully characterise their pharmacological properties which are unique to a particular drug or subclass of an agent. Atypical APDs can be assigned to three distinct subclasses based on affinity; those considered relatively specific for dopamine receptors, (the so-called dopamine D_2/D_3 APDs eg. amisulpride, sulpiride and remoxipride), serotonin-dopamine antagonists (eg. risperidone, sertindole and iloperidone), and finally multi-acting receptor-targeted antipsychotics or MARTAS (eg. clozapine, olanzapine, asenapine, ziprasidone and quetiapine) which share properties of the second class but in addition may display direct effects at other receptors (eg 5-HT1A agonism). However as has been discussed previously certain APDs classed as typical such as chlorpromazine and zotepine share many of the pharmacological properties of atypical agents, at least in terms of their reported affinity (receptor cross-reactivity/promiscuity see Meltzer 2013), meaning that these distinctions are not absolute and that other factors may account for atypicality (eg. kinetic influences such as reduced receptor rebinding see Chapter 5 and Sykes et al., 2017).

6.1.2 5-HT2A and 5-HT1A receptors anatomical location and physiology

5-HT2A receptors are expressed at a high density in the forebrain regions of the brain including the cerebral cortex and limbic regions (Pazos et al., 1987a; Hall et al., 2000). Whereas high densities of 5-HT1A receptors are found in both the raphe nuclei and limbic regions (Pazos et al., 1987b; Ohno et al., 2013; Hall et al., 1997; Pike et al., 1998; Farde et al., 1998). Serotonin neurones innervate dopamine neurones either directly via postsynaptic 5-HT2A receptors on the dopamine neurone, or indirectly on GABA interneurons (de Almeida and Mengod 2007; Celada et al., 2013). 5-HT has been proposed to act at these 5-HT2A receptors and inhibit the release of dopamine whereas antagonists have been proposed to increase

release (Stahl 2008; Stahl 2013; Horacek et al., 2006; Lucas and Spampinato 2000). The opposite occurs at 5-HT1A autoreceptors present on 5-HT neurones, with activation thought to lead to a reduction in 5-HT release and a subsequent reduction in 5-HT2A postsynaptic receptor activation and as a consequence accelerated (or disinhibited) dopamine release (Stahl 2008; Stahl 2013; Horacek et al., 2006). A role for serotonin receptors in the MOA of certain atypical APDs (such as clozapine, quetiapine, olanzapine, risperidone, and ziprasidone) has long been postulated and is thought to underlie the purported superior efficacy and tolerability of these agents which belong specifically to the MARTA class (for a review see Meltzer 2013).

6.1.3 The 'serotonergic-dopamine' theory of atypicality a historical perspective.

Meltzer and colleagues were first to label simultaneous 5-HT2A and D_2 receptor blockade as a pharmacodynamic (PD) mechanism which differentiates the clinical effect of typical and atypical agents (Meltzer et al., 1989). In their seminal paper they defined atypicality using two criteria; firstly, as drugs with greater affinity for the 5-HT2A receptor over D_2 receptor and secondly as a reduced affinity for D_2 receptors than seen for conventional APDs.

It has been suggested that tissue-selective antagonism of D2/5-HT2A receptors by atypical APDs may play a role in both their improved efficacy against negative symptoms but also their reduced side effect profile (Sulpizio et at., 1978; Meltzer et al., 1989; Meltzer 1992; Schotte et al., 1996; Leucht et al., 2009 and 2013). Tissue selective antagonism at the level of the mesolimbic dopaminergic pathway in the nucleus accumbens permits efficacy against the positive symptoms of schizophrenia whilst sparing dopamine receptors in the mesocortical pathway thought to be involved in the production of negative symptoms through increased release of dopamine via blockade of 5-HT2A receptors (Kuroki et al., 1999; Morrissette and Stahl 2011). This hypothesis is partly supported by reports that clozapine a D2/5-HT2A receptor blocker proposed to improve negative symptoms, induces an increase in the turnover of dopamine in the prefrontal cortex of rodents, an effect not seen with typical antipsychotics (Ichikawa et al., 2001; Kapur and Remington 1996). However, the efficacy of the dopamine D2/3 specific antagonist amisulpride against both positive and negative symptoms when compared to typical

APDs suggests strongly that 5-HT2A blockade may not be a prerequisite for such actions (Leucht et al., 2009). In terms of the on-target side effect profile of clinically used APDs a model has been proposed whereby antagonism of 5-HT2A receptors in the cortex results in increased dopamine release from neurons in the striatum reducing striatal APD occupancy and decreasing the subsequent risk of EPS (reviewed in Kapur and Remington 1996; and Schotte et al., 1996).

5-HT2A/D2 receptor affinity. What is missing from this model is a consideration of the kinetic properties of the APDs at both the serotonergic 5-HT2A and dopamine D_2 receptors and the potential influence this will have on D_2R occupancy over time. The original serotonergic-dopamine hypothesis was based purely on differences in receptor affinity but as has been described previously there is a marked disconnect between APD brain occupancy and drug plasma pharmacokinetic (PK) parameters (Tauscher et al., 2002), most likely as a consequence of restricted drug diffusion in the brain and the predilection for drugs to rebind to receptors concentrated within synaptic appositions (Vauquelin and Charlton 2010; Sykes et al., 2017).

6.1.4 Rapid dissociation hypothesis and the phenomenon of rebinding

Another pharmacological mechanism of atypicality and one we have explored previously (Chapter 5) relates directly to the 'rapid dissociation hypothesis' (Kapur and Seeman 2001) and the proposal that APD dissociation rate (k_{off}) governs the incidence of clinically observed EPS. This hypothesis is built essentially around the concept of slow ligand dissociation in the face of increased striatal dopamine concentrations due to the phenomenon of receptor insurmountability. Receptor insurmountability is characterised by a diminished cellular second messenger response, shaped by the phenomenon of hemiequilibria. Hemi equilibrium describes the failure of an agonist to reach equilibrium with its receptor over the normal time frame of the observed response, due to the slow dissociation of a competitive antagonist (Charlton and Vauquelin 2010).

We recently established an alternative mechanism of atypicality based on a restricted drug diffusion model, which suggests that for the majority of compounds association rate and not dissociation rate better predicts the overall rate of D_2R reversal in the striatum through a process of receptor rebinding (Sykes et al., 2017).

This model is entirely consistent with PET data demonstrating the persistent binding of typical APDs such as haloperidol to D_2 receptors in the CNS which we now believe results from their inherently high association rates (k_{on}) (Seeman et al., 2002; Sykes et al., 2017). Consequently, such agents do not just block the positive symptoms of schizophrenia, but they also are more predisposed to cause EPS and potentially exacerbate secondary negative symptoms. In direct contrast, atypical APDs with lower association rates show a more rapid reversal of D_2R target coverage (Seeman et al., 2002). This is important as it means these agents can block the D_2R to exert an antipsychotic effect but are less prone to cause EPS or add to negative symptoms. In the aforementioned study the correlation of D_2R binding reversal rate (k_r) with clinically derived EPS was not perfect and there were certain compounds whose EPS profile was not so well described by this model leading us to speculate that the 'serotonin-dopamine hypothesis' at least in terms of EPS profile may have some validity for compounds with significant affinity for 5-HT2A receptors.

6.1.5 Role of 5-HT1A in psychosis/EPS

Another potential contribution to reduced APD on-target side effects stems from the ability of certain APDs to act as agonists at 5-HT1A receptors. Such agents are thought to reduce positive symptoms through conventional D_2 receptor blockage but also enhance dopamine release in the striatum which theoretically will simultaneously improve EPS and the negative, cognitive and affective symptoms of schizophrenia (Benloucif and Galloway 1991; Stahl 2008; Shimizu et al., 2010). This hypothesis is supported by research in mice demonstrating that the selective 5-HT1A antagonist (s)-WAY-100135 can completely reverse the anti-EPS action of the selective 5-HT1A agonist (±)-8-OH-DPAT. Thus, it was proposed that 5-HT1A agonists reduce antipsychotic-induced EPS primarily through activation of postsynaptic 5-HT1A receptors in the striatum and motor cortex (Shimizu et al., 2013).

The precise effect of 5-HT2A blockade and 5-HT1A agonism on dopamine release in different regions of the brain remains controversial and it would appear that under certain experimental conditions blockade of the 5-HT2A and activation of the 5-HT1A receptor rather than increasing dopamine release in the striatum may actually

reduce its release (Alex and Pehek 2007). This has led to speculation that blockade of the 5-HT2C receptor may be more important for the reduced incidence of EPS observed with clinically used atypical APDs (Alex and Pehek 2007; Alex et al., 2005; Reavill et al., 1999). However although the atypical drug clozapine shows a similar propensity to block 5-HT2A and 5-HT2C receptors, in contrast the atypical drug risperidone would appear to be more 5-HT2A selective (>100-fold) both in binding, and in functional studies (Kusumi et al., 2015; Canton et al., 1994).

Despite this underlying controversy, as originally described a dual 5-HT2A antagonist/5-HT1A agonist may show additive or even synergistic effects. To understand the role of 5-HT1A efficacy in the MOA of clinically used APDs we have determined the efficacy, potency, equilibrium affinity and binding kinetics of these compounds at the human 5-HT1A receptor in a salt containing buffer. The importance of buffer composition and sodium ions in the formulation of 5-HT1A binding assays has been highlighted previously (Harikumar and Chattopadhyay 2001). In addition, we have measured the human 5-HT2A equilibrium affinity and binding kinetics of the same series of clinically used compounds.

The overall aim of this chapter is to consider the role of 5-HT2A and 5-HT1A receptors and receptor binding kinetics in dictating the side effect profile of clinically used antipsychotic agents and in doing so explore the relevance to the ‘serotonin-dopamine hypothesis’ and possible strategies for the development of novel kinetically optimised antipsychotic agents that modulate both serotonergic and dopamine function in a manner beneficial to the treatment of this chronic and debilitating disease.

6.2 Materials and Methods

6.2.1 Materials

The CellAura fluorescent 5-HT2A/2B receptor antagonist 4F4PP oxalate-red (CA201019), and the 5-HT1A specific tracer NAN190-red was obtained from Hello Bio (Bristol, UK). The sources of all other materials used in the experiments described in the following sections are detailed in Chapter 2, section 2.1 Materials.

6.2.2 Cell culture

The host Chinese hamster ovary (CHO) K1 cell line, was transiently transfected using Fugene (Fugene: DNA ratio 3:1) with the cDNA encoding a SNAP-tagged human serotonin 5-HT2A receptor (Cisbio Bioassays, Bagnols-sur-Cèze, France) and receptors labelled with terbium-cryptate 24h later as detailed below. Full transfection details are provided in Chapter 2 sections 2.2.4 Transient transfections. CHO-5-HT2A cells were maintained as described in Chapter 2, section 2.2.1 Cell culture. CHO-D_{2L} and CHO-5-HT1A cells stably transfected with the cDNA encoding a SNAP-tagged human receptor from Genbank (ref: NM_000795) and CisBio respectively, were were maintained as described in Chapter 2, section 2.2.1 Cell culture. Full transfection and clone selection details are provided in Chapter 2, section 2.2.2 Stable transfections and section 2.2.3 Dilution cloning.

6.2.3 Terbium labelling of SNAP-tagged cells

Cell culture medium was removed from the t175cm^2 flasks containing confluent adherent CHO-D_{2L}, CHO-5-HT2A or CHO-5-HT1A cells and labelled with terbium as described in Chapter 2, section 2.2.5 Terbium labelling of SNAP-tagged cells and membrane preparation. Before their use, the frozen membranes were thawed and the membranes suspended in the assay buffer at a membrane concentration of 0.4mg/ml (CHO-5-HT2A), 0.2mg/ml (CHO-D_{2L}) or 0.04mg/ml (CHO-5-HT1A).

6.2.4 Fluorescent ligand-binding assays

5-HT2A and 5-HT1A fluorescent binding experiments employed 4F4PP oxalate-red and NAN190-red respectively whilst PPHT-red was employed in the case of the human dopamine D_{2L} receptor. Experiments were conducted in white 384-well Optiplate plates, in assay binding buffer, HBSS containing 5 mM HEPES, 0.02% pluronic acid, 1% DMSO pH 7.4 and 100 µM GppNHp. In the case of the human 5-HT2A receptor, non-specific binding was determined in the presence of sertindole (10 µM), whereas 5-HT1A non-specific binding was determined in the presence of spiperone (100 µM) and D_{2L} non-specific PPHT-red ligand binding was determined in the presence of haloperidol (10 µM). In all instances, total binding was determined in the presence of a vehicle control (assay buffer).

Determination of tracer binding kinetics

To accurately determine 4F4PP oxalate-red and NAN190-red association rate (k_{on}) and dissociation rate (k_{off}) values for the CHO-h5-HT2A and CHO-h5-HT1A receptor respectively, the observed rate of association (k_{obs}) was calculated using five or six different concentrations of each fluorescent tracer as described in Chapter 2, section 2.2.6 Determination of tracer binding kinetics and equilibrium affinity. The appropriate concentrations of 4F4PP oxalate-red and NAN190-red was incubated with 5-HT2A CHO cell membranes (4 µg per well) or 5-HT1A CHO cell membranes (0.4 µg per well) respectively, in assay binding buffer (final assay volume, 40 µL). The degree of fluorescent ligand bound to the receptor was assessed at multiple time points by HTRF detection to allow construction of association kinetic curves.

The resulting data were fitted to a global fitting model using GraphPad Prism 6.0 to simultaneously calculate k_{on} and k_{off} (Equation 2.5, Chapter 2) and a one-phase exponential association model (Equation 2.6, Chapter 2) to derive an estimate of k_{on} and k_{off} from plotting tracer concentration versus observed association (k_{obs}) as described in Chapter 2, section 2.2.8 Signal detection and data analysis. PPHT-red tracer binding was carried out essentially as previously described (see Sykes et al., 2017).

Competition binding kinetics

To determine the association and dissociation rates of 5-HT2A specific ligands, we used the competition kinetic binding assay approach described in Chapter 2, section 2.2.7 Competition binding kinetics. Specifically, 50 nM 4F4PP oxalate-red was added simultaneously with unlabeled compound (at t = 0) to CHO cell membranes containing the human 5-HT2A (4 μg per well) in 40 μL of assay buffer. The degree of 4F4PP oxalate-red bound to the receptor was assessed at multiple time points by HTRF detection. Similarly, for 5-HT1A kinetic determinations NAN190-red was employed at a concentration of 10 nM whilst D_2 receptor-specific ligands were profiled essentially as previously described (see Sykes et al., 2017).

Non-specific binding was determined as the amount of HTRF signal detected in the presence of sertindole (10 μM) in the case of the 5-HT2A receptor and spiperone (100 μM) in the case of the 5-HT1A receptor and was subtracted from each time point, meaning that t = 0 was always equal to zero. Each time point was conducted on the same 384 well plate incubated at 37°C with orbital mixing (1sec of 100 RPM/cycle). Multiple concentrations of unlabeled competitor were tested, for determination of rate parameters. Data were globally fitted using (Equation 2.7, Chapter 2) to simultaneously calculate k_{on} and k_{off} of unlabelled compounds. The estimation of lurasidone and iloperidone binding kinetics at the D_2R was carried out as previously described (Sykes et al., 2017).

6.2.5 Signal detection and data analysis.

Signal detection was performed as described in Chapter 2, section 2.2.8 Signal detection and data analysis. All experiments were analyzed by non-linear regression using GraphPad Prism 6.0. Saturation binding data were analysed according to a one-site model, Fitting the total and NSB data sets simultaneously to Equation 2.1 described in Chapter 2, provides one best-fit value for both the K_d and the B_{max} of a fluorescent tracer. Specific binding, obtained by subtracting non-specific binding from total binding, was fitted to Equation 2.2, Chapter 2, a one-site binding model that describes a rectangular hyperbola or binding isotherm. Competition displacement binding data were fitted to sigmoidal (variable slope) curves using a “four-parameter logistic equation”, see Equation 2.3, Chapter 2. IC_{50} values

obtained from the inhibition curves were converted to K_i values using the method of Cheng and Prusoff (1973), see Equation 2.4, Chapter 2.

Fluorescent ligand (tracer) association data were fitted to a global fitting model using GraphPad Prism 6.0 to simultaneously calculate k_{on} and k_{off} using Equation 2.5, Chapter 2. In addition, tracer association data were analysed using non-linear regression fitting the specific binding data to a one-phase exponential association equation, see Equation 2.6, Chapter 2. Where tracer binding follows a simple law of mass action model, k_{obs} increases linearly as a function of tracer concentration. The slope of the resulting line fitted using linear regression equates to the association rate (k_{on}), and extrapolation of the plot to y = 0 yields the dissociation rate (k_{off}) (Sykes et al., 2010).

Association and dissociation rates for unlabeled antagonists were calculated using the equations described by Motulsky and Mahan (1984), see Equation 2.7, Chapter 2. Fluorescent ligand dissociation data were fitted to a one-phase mono-exponential decay function to estimate the dissociation rate of ligands directly as described in Chapter 2, Equation 2.8. Specific binding was determined by subtracting the non-specific HTRF ratio from the total HTRF ratio.

Statistical differences were determined by one-way ANOVA with individual differences between test groups tested by Bonferroni t-test. Differences were considered significant at $P< 0.05$. All analyses were performed using GraphPad Prism 6.0.

6.2.6 5-HT1A [^{35}S]-GTPγS binding

The ability of antipsychotics to effect receptor-linked G-protein activation was measured by [^{35}S]-GTPγS binding. CHO-h5-HT1A membranes (10 μg protein) were incubated at room temperature in duplicate with the endogenous agonist 5-HT and antipsychotics in assay buffer containing HEPES 20mM, NaCl 100mM, GDP 10μM, $MgCl_2$ 10mM. Non-specific binding was defined with 10μM GTPγS. [^{35}S]-GTPγS (1250 Ci/mmol, PerkinElmer) 100pM was added to the reaction after an incubation period of 60 min and incubated for a further 40 min. Assays were terminated by rapid filtration through GF/B filter plates followed by a brief wash with ice-cold PBS.

The amount of [^{35}S]-GTPγS bound to human 5-HT1A receptors was determined by liquid scintillation counting.

6.2.7 Operational modelling and clinical effect

To determine tau (τ) values for each agonist [^{35}S]-GTPγS binding data are fitted to the operational model (Black and Leff 1983). This model describes the relationship between biologic response and agonist concentration [A] as a function of four parameters: E_m, K_A, n, and τ.

$$E = \frac{E_m\, t^n [A]^n}{(K_A + [A])^n + t^n [A]^n} \qquad \text{Equation 6.1}$$

Where, E_m, or the operational maximum, represents the maximum possible effect (the top plateau of the 5-HT dose-response curve), and n represents the transduction slope which describes the relationship between receptor occupancy and effect. K_A is the dissociation constant of the agonist, and τ defines the operational efficacy of an agonist and is sometimes referred to as the 'transducer ratio' (Black et al., 1985). τ is effectively the transducer constant, and a practical measure of drug efficacy. It is the inverse of the fraction of receptors that must be occupied by an agonist to obtain the half-maximal response. If tau equals 10, that means that the occupation of only 10% of the receptors leads to a half-maximal response.

When this equation was applied to GTPγS data, [A] was varied according to experimental design, K_A was fixed to the value obtained in competition binding assays and E_m was globally fitted across all data sets, leaving n and τ as the only terms fitted individually for each agonist.

Low 5-HT1A agonist receptor occupancy in a highly amplified system may have clinical relevance. In order to account for this possibility, we have modelled effect as a function of agonist concentration by applying the operational model of agonism described above with [A] fixed at clinically relevant D_2 occupancy (i.e. 70%) (Farde et al., 1992), K_A fixed to the value obtained in competition binding assays, n and t were fixed individually with E_m shared, leaving E to be calculated for each agonist.

To simulate signal amplification individual τ values derived from [^{35}S]-GTPγS binding experiments were multiplied by a factor of 1 and 100. Our choice to increase the τ factor is based on this apparent lack of signal amplification in GTPγS assays which has been well documented (Strange 2010). GTPγS assays specifically measure agonist stimulation of nucleotide binding to G proteins (^{35}S-GTPγS), allowing an assessment of GPCR activation close to the receptor with little amplification of the signal. As a consequence τ values will likely increase when measurements of agonist cellular effect are taken downstream of G protein activation (Sykes *et al*., 2009).

6.2.8 5-HT2A calcium assay

The ability of the antipsychotics sertindole and clozapine to block 5-HT2A receptor-linked G-protein activation was assessed through 5-HT stimulated Ca^{2+} release. Briefly, CHO-h5-HT2A cells (40,000 per well) were plated into black 96-well plates and grown overnight in F-12: DMEM containing 10% dialysed FBS. Intracellular calcium was detected using a FLIPR calcium 5 no-wash assay kit and read on a FlexStation 3 plate reader (Molecular Devices, Sunnyvale USA).

Cells were incubated in duplicate with the antipsychotics sertindole and clozapine at 10, 30 and 100 xK_d based on their respective binding affinities at the 5-HT2A receptor for 60min. Dye and compounds were made up in assay buffer (HBSS containing 20mM HEPES and 0.1%(w/v) BSA (pH 7.4) and added directly to cells in media.

Activation of CHO-h5-HT2A receptors was initiated through the application of the endogenous agonist 5-HT and calcium responses were monitored for a period of 90 seconds. Maximal calcium responses were determined by calculating maximal response – minimal response (Max-Min).

6.2.9 Rebinding at Dopamine D2 and serotonin 5-HT2A receptors as a cumulative measurement of drug effect

Drug receptor rebinding values were calculated as described in Chapter 2, section 2.2.9 Modelling drug-receptor re-binding. Based on this rebinding model the effectiveness of APDs to reverse D_2R blockade and therefore relieve the symptoms of EPS via their effects at 5-HT2A receptors was estimated. This was achieved by calculating the relative affinities of clinically used APDs for 5-HT2A: D2 receptors, and through determining area under the curve (AUC) estimates of 5-HT2A and D_2R relative receptor occupancy (5-HT2A:D2) at D_2R occupancy levels between 80-65% (i.e. those relevant to antipsychotic and EPS through combined serotonergic and D_2R blockade see Kasper et al., 1999). AUC estimates of 5-HT2A and D_2R relative receptor occupancy (5-HT2A: D2) were assessed utilising previously reported human $D_{2L}R$ specific kinetic values (Sykes et al., 2017) and the 5-HT2A values reported herein.

In all cases initial dopamine D_2R striatal occupancy was assumed to reach 80% with individual 5-HT2AR starting occupancies varied based on the relative affinities of these clinically used antipsychotics for the D_2R and 5-HT2AR, The resulting AUC values are an integrated measurement of receptor occupancy based on a rebinding phenomenon and are used as a cumulative measurement of drug effect. All data were analyzed using GraphPad Prism 6.0.

6.2.10 Comparing binding kinetics and clinical side effect profile.

Binding kinetic values determined in this study were correlated with published clinical schizophrenia treatment data taken from a comprehensive meta-analysis of clinically used APDs performed by Leucht et al., (2013) as described in Chapter 2 section 2.2.10 Comparing binding kinetics and clinical side effect profile.

6.2.11 Structure-property relationships

Chemicalize.org was used for generating structure-property prediction and calculations, chemicalize.org (http://www.chemicalize.org).

6.3 Results

6.3.1 Characterization of 4F4PP oxalate-red binding to the human 5-HT2A receptor

Specific binding of the antagonist 4F4PP oxalate-red to human 5-HT2A receptors expressed in CHO membranes was saturable and best described by the interaction of the fluorescent ligand with a single population of binding sites (Figure. 6.1A). Non-specific binding was linear and represented just over 50% of total binding. This could reflect the relatively high log D of the parent molecule (3.63) at physiological pH 7.4, which suggests it may penetrate biological membranes creating the potential for increased non-specific proximity. From these studies, the equilibrium dissociation constant (K_d) of 4F4PP oxalate-red was determined to be 3.98 ± 0.65 nM, n=23.

The binding kinetics of 4F4PP oxalate-red was characterised by monitoring the observed association rates at six different ligand concentrations (Figure 6.1B). Its observed rate of association was related to 4F4PP oxalate-red concentration in a linear fashion up to a concentration of 50nM (>10x K_d). The highest concentration of fluorescent ligand employed (100nM, >30x K_d), on average showed a variable and inconsistent deviation in k_{obs} creating an apparent non-linear relationship. There are at least two plausible explanations for such behaviour; the simplest of which could arise from inadequate tracer-receptor mixing, a result of the relatively high concentrations of tracer employed (Figure. 6.1C). Descriptions of such a phenomenon in the literature are lacking presumably since these same procedures have in the past been performed with radioligands where the aim is to keep ligand concentrations as low as practically possible due to the problems associated with rising NSB. An alternative explanation is that the receptor-bound fluorescent tracer (i.e. 4F4PP oxalate-red-R) is undergoing isomerisation leading to the formation of a higher affinity state, leading to the curved k_{obs} plot (i.e. 4F4PP oxalate-red-R*). If this is the case, then the Motulsky-Mahan equations used to fit the experimental data would not adequately describe such a mechanism as they only describe the binding of ligands to a single receptor species (Tummino and Copeland 2008).

In view of this apparent non-linearity at the highest 4F4PP oxalate-red concentration tested, kinetic rate parameters for 4F4PP oxalate-red were calculated based on a limited concentration range (3.12-50 nM) from a global fit of association curves to derive a single best-fit estimate for k_{on} and k_{off}, resulting in a k_{on} estimate of 4.21 ± 0.47 x10^7 M^{-1} min^{-1} and a k_{off} of 0.09 ± 0.01 min^{-1}, n= 24, see Figure 6.1B. The resulting K_d (k_{off} / k_{on}) of 2.82 ± 0.47 nM was comparable to that obtained from the equilibrium studies described above.

In addition, the kinetic rate parameters for 4F4PP oxalate-red (3.12-50 nM) were calculated from plots of tracer concentration versus observed rates of association (k_{obs}), resulting in a k_{on} estimate of 2.37 ± 0.27 x10^7 M^{-1} min^{-1} and a k_{off} of 0.25 ± 0.03 min^{-1}, n= 24, see Figure 6.1C. The resulting K_d (k_{off} / k_{on}) of 13.1 ± 1.6 nM was significantly different from that obtained from the equilibrium saturation binding studies described above (Bonferroni's multiple comparisons test, P<0.0001).

Ligand dissociation estimated directly through the addition of an excess of sertindole revealed a k_{off} value of 0.36 ± 0.06 min^{-1} which was significantly faster than the value estimated from the global fit of association curves described above (Bonferroni's multiple comparisons test, P<0.0001), see Figure 6.1D. The reason for this discrepancy in direct off-rate versus the global fit of association curves is unknown but there are at least three plausible explanations. The membranes are incubated at 37^{o}C before addition to the assay plate wells, however it is possible that some cooling occurs during the transfer step to the plate resulting in a slowing in 4F4PP oxalate-red observed association. Another potential explanation arises if we consider the kinetic association step itself. Here the ligand 4F4PP oxalate-red binds to the receptor and in accordance with the law of mass action should dissociate at a rate consistent with the direct dissociation step. However, it is entirely possible that the ligand is now able to rebind the same or a nearby receptor without fully diffusing away into bulk aqueous and it could be this phenomenon that is contributing to an apparent slowing in the tracer dissociation rate.

Another potential explanation is that 4F4PP is demonstrating some degree of negative cooperativity, potentially across a dimer interface, which could imply the presence of 5-HT2A homodimers or heterodimers (May et al., 2011; Gherbi et al., 2015 Brea et al., 2009). The Motulsky-Mahan equations assume that the law of

mass action applies, and that binding of a ligand to one binding site does not alter the affinity or kinetics of another ligand binding to a different site on the same or different receptor. In situations where negative cooperativity has been observed these assumptions do not hold and the presence of negative cooperativity in the current study would, therefore, undermine the current analysis.

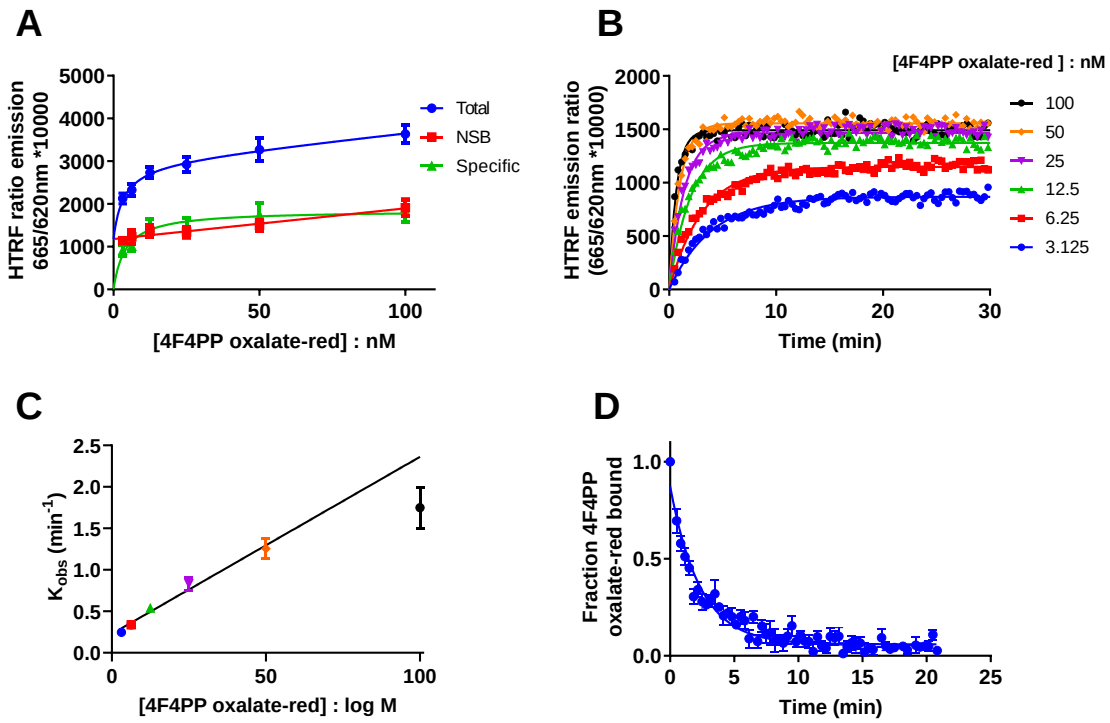


Figure 6.1. Determination of 4F4PP oxalate-red equilibrium and kinetic binding parameters. (**A**) Saturation analysis showing the binding of 4F4PP oxalate-red to the human 5-HT2A receptor. CHO-5-HT2A receptor cell membranes (4 μg per well) were incubated for 60 min with gentle agitation with increasing concentrations of 4F4PP oxalate-red. Data are presented in duplicate form from a representative of 23 separate experiments. (**B**) The observed association of 4F4PP oxalate-red to the human 5-HT2A receptor. Data are presented as the mean from 24 separate experiments. (**C**) A plot of 4F4PP oxalate-red concentration versus k_{obs}. Data are presented as mean ± S.E.M. from a total of 24 separate experiments. k_{obs} data for the highest concentration of fluorescent ligand tested (100nM, >30x K_d), is shown but was excluded from the analysis. (**D**) 4F4PP oxalate-red dissociation following the addition of sertindole (10 μM). Dissociation data are presented in mean ± S.E.M. from 4 experiments performed in singlet. All binding reactions were performed in the presence of GppNHp (0.1mM) with non-specific binding levels determined by the inclusion of sertindole (10 μM).

6.3.2 Characterization of unlabeled APDs binding to the human 5-HT2A receptor

The binding affinity of the various ligands for the human 5-HT2AR was measured at equilibrium at 37°C in a buffer containing GppNHp (0.1 mM) to ensure that antagonist binding only occurred to the G protein-uncoupled form of the receptor. 5-HT2AR binding affinities (K_i values) for the APDs studied are summarized in Table 6.1, and competition curves are presented in Figure. 6.2A and B. In Table 6.1 APDs are separated into those described in the literature as typical or atypical and those described as both. Dopamine D_{2L} receptor-specific kinetics parameters for lurasidone and iloperidone are summarised in Table 6.2.

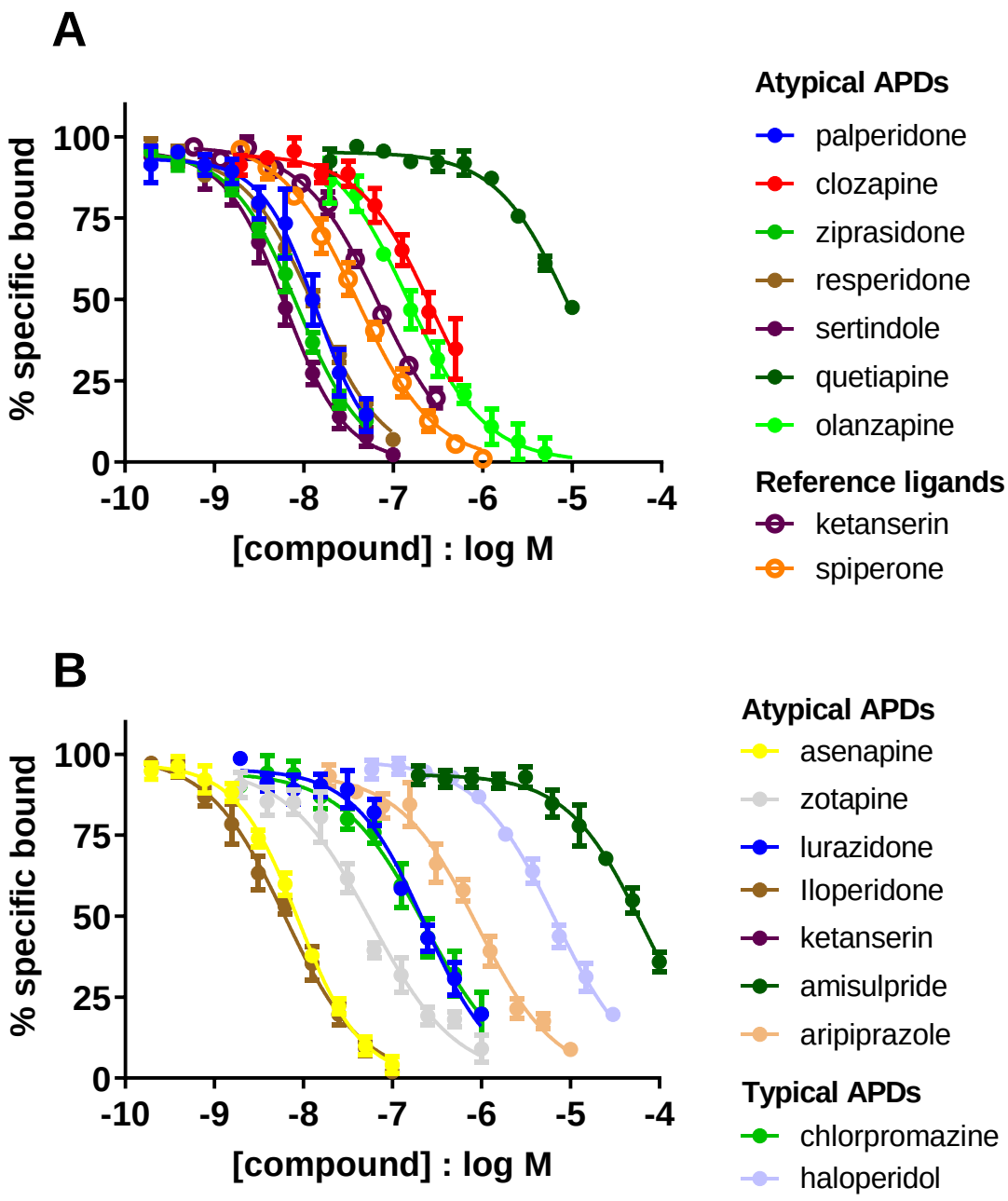


Figure 6.2. Equilibrium competition binding for APDs and reference ligands at the human 5-HT2A receptor. (A) and **(B)** Competition between 4F4PP oxalate-red (50 nM) and increasing concentrations of atypical APDs, typical APDs and 5-HT2A reference ligands for the human 5-HT2A receptor. All binding reactions were performed in the presence of GppNHp (0.1mM) with non-specific-binding levels determined by the inclusion of sertindole (10 μM). Equilibrium data were fitted to the equations described in Chapter 2 (Equation 2.3 and 2.4) to calculate K_i, values for the unlabeled ligands; these are summarized in Table 6.1. Data are presented as

mean ± S.E.M. values from four or five separate experiments performed in duplicate. The number of observations (n) for each ligand is stated in Table 6.1. All data used in these plots are detailed in Table 6.1. *Zotepine was originally introduced as an atypical APD but is sometimes described as a typical APD, based on its side effects profile. Classification is based on reference sources see Sykes et al., 2017.

Table 6.1. Kinetic binding parameters of unlabelled clinically used APDs and reference antagonists for human 5-HT2A receptors and their historical classification as atypical or typical and those characterized as typical/atypical.

	5-HT2A receptor						**D_{2L} receptor**	***D2/5-HT2A affinity ratio based on K_d***
	k_{off} (min^{-1})	***k_{on} ($M^{-1}min^{-1}$)***	***Dissociation $t_{1/2}$ (min)***	***pK_d***	***pK_i***	**n**	***pK_d***	
SGA/Atypical								
Paliperidone	0.23 ± 0.05	5.08 ± 1.69 $x10^8$	3.0	9.31 ± 0.07	8.99 ± 0.08	4	8.60	5.13
Clozapine	2.50 ± 0.42	3.62 ± 1.01 $x10^8$	0.3	8.11 ± 0.14	7.93 ± 0.13	5	7.69	2.63
Ziprasidone	0.60 ± 0.19	2.93 ± 1.34 $x10^9$	1.2	9.60 ± 0.08	9.32 ± 0.06	4	9.19	2.57
Risperidone	0.26 ± 0.03	4.85 ± 0.73 $x10^8$	2.7	9.26 ± 0.04	9.00 ± 0.01	4	9.05	1.62
Sertindole	0.04 ± 0.01	1.86 ± 0.41 $x10^8$	17.3	9.65 ± 0.10	9.34 ± 0.07	4	8.92	5.37
Quetiapine	2.32 ± 0.54	5.34 ± 1.65 $x10^6$	0.3	6.36 ± 0.06	6.16 ± 0.05	4	6.82	0.35
Olanzapine	0.57 ± 0.21	1.00 ± 0.53 $x10^8$	1.2	8.17 ± 0.10	7.79 ± 0.19	4	8.17	1.00
Asenapine	0.70 ± 0.19	2.06 ± 0.66 $x10^9$	1.0	9.45 ± 0.03	9.18 ± 0.03	4	9.29	3.39
Amisulpride	0.17± 0.02	5.48± 0.88 $x10^4$	4.1	5.50 ± 0.05	5.35 ± 0.11	4	8.61	0.00078
[a]Lurasidone	0.84 ± 0.19	9.12 ± 2.62 $x10^7$	0.8	8.01 ± 0.04	7.76 ± 0.13	4	9.41	0.040
[a]Iloperidone	0.28 ± 0.05	1.07 ± 0.27 $x10^9$	2.5	9.54 ± 0.07	9.32 ± 0.07	4	8.96	3.80
FGA/Typical								
Haloperidol	1.20 ± 0.55	3.30 ± 1.64 $x10^6$	0.6	6.43 ± 0.04	6.29 ± 0.06	5	9.49	0.00087

Chlorpromazine	3.04 ± 0.82	2.52 ± 0.87 x10^8	0.2	8.00 ± 0.05	7.74 ± 0.17	4	9.24	0.058
Spiperone	1.25 ± 0.28	6.49 ± 1.11 x10^8	0.6	8.77 ± 0.07	8.58 ± 0.09	5	10.84	0.22
Typical/atypical								
Zotepine	1.25 ± 0.30	6.54 ± 2.93 x10^8	0.6	8.59 ± 0.15	8.36 ± 0.13	4	8.76	0.68
TGA/atypical								
Aripiprazole	0.17± 0.02	4.58 ± 1.07 x10^6	4.1	7.40 ± 0.07	7.22 ± 0.18	4	9.43	0.0093
5-HT2A ref. antag.								
Ketanserin	1.45 ± 0.22	5.23 ± 0.85 x10^8	0.5	8.56 ± 0.03	8.31± 0.02	4	ND	ND

Data are mean ± S.E.M. for the number of observations (n) stated, each performed in duplicate. FGA/typical and SGA/atypical classification is based on reference sources see Sykes et al., 2017. $D_{2L}R$ affinity values taken from Sykes et al., 2017 unless otherwise stated. [a]$D_{2L}R$ affinity values determined in the current study. ND = not determined.

Table 6.2. Kinetic binding parameters of unlabelled clinically used APDs and reference antagonists for human D_{2L} receptors and their historical classification as atypical APDs.

	k_{off} (min^{-1})	k_{on} ($M^{-1}min^{-1}$)	Dissociation $t_{1/2}$ (min)	pK_d	pK_i	N	Receptor occupancy reversal rate *or* k_r (min^{-1})
SGA/Atypical							
Lurasidone	0.11 ± 0.00	2.95 ± 0.40 $x10^8$	6.36	9.41 ± 0.09	9.57 ± 0.14	4	0.005405
Iloperdone	0.99 ± 0.13	1.03 ± 0.30 $x10^9$	0.79	8.96 ± 0.10	8.99 ± 0.10	6	0.03128

Data are mean ± S.E.M. for the number of observations (n) stated, each performed in singlet.

Representative 4F4PP oxalate-red competition association binding curves for selected D_2R ligands are shown in Figure 6.3A-E. Progression curves for 4F4PP oxalate-red alone and in the presence of competitor were fitted to Equation 2.7, Chapter 2 enabling the calculation of both k_{on} (k3) and k_{off} (k4) for each of the ligands, as reported in Table 6.1.

There was a very wide range of dissociation rates for the different ligands, with dissociation half-lives ($t_{½}$) (where, $t_{½}$ = 0.693/ k_{off}) between 0.2 minutes for chlorpromazine to 17.3 mins for sertindole. Confidence intervals on the kinetic fits for sertindole were on average much smaller, compared to the rapidly dissociating chlorpromazine, reflective of both the tracers own kinetic properties and the off-line addition protocol chosen for these studies. To validate the rate constants, the kinetically derived dissociation constant (K_d) values (k_{off} / k_{on}) were compared with the dissociation constant (K_i) obtained from equilibrium competition binding experiments (see Figure 6.4). There was a very good correlation between these two values for all APDs tested (Two-tailed Pearson's correlation r^2 = 0.99, P <0.0001) indicating the kinetic parameters were consistent with the equilibrium derived affinity values. Previous radioligand binding studies have reported dissociation rates for [^{3}H]-ketanserin in the rat of 0.7 min^{-1} ($t_{1/2}$ = 1min) in a salt containing buffer at 37^{o}C which is similar (2-fold slower) to the values we report in our current study (Leysen et al., 1982). Any differences observed between this and the original studies could potentially have arisen from the use of different species (rat cortical tissue), or the use of a more alkaline buffer of lower salt concentration (eg. 50mM Tris-HCl, 120mM NaCl pH7.7) (Leysen et al., 1982; Schotte et al., 1983).

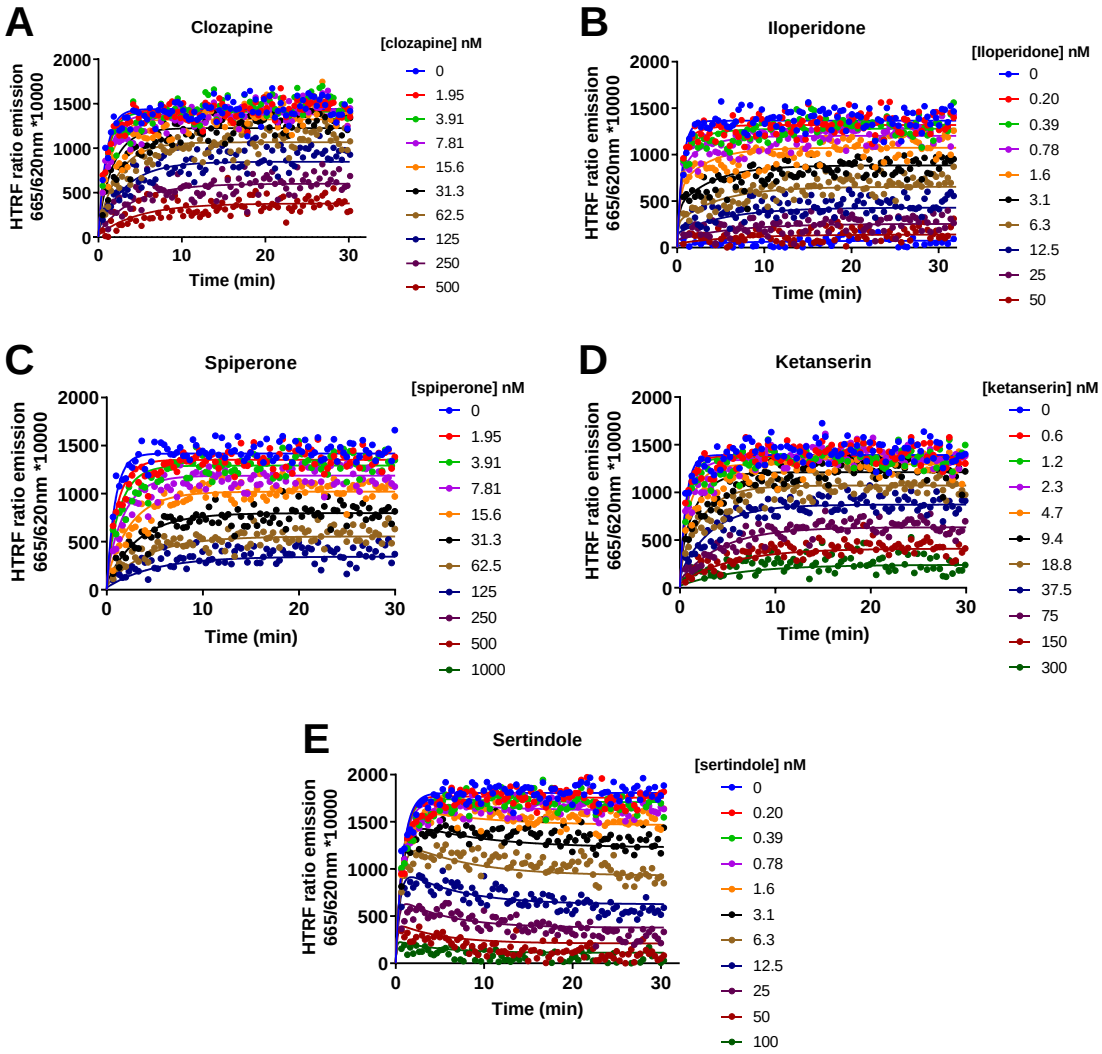


Figure 6.3. Competition association binding at the 5-HT2A receptor. Competition between 4F4PP oxalate-red (50 nM) and increasing concentrations of representative atypical and typical APDs **(A)** clozapine, **(B)** iloperidone, **(C)** spiperone, **(D)** ketanserin and **(E)** sertindole at the human 5-HT2A receptor. All binding reactions were performed in the presence of GppNHp (0.1mM) with non-specific-binding levels determined by the inclusion of sertindole (10 μM). Kinetic and equilibrium data were fitted to the equations described in Chapter 2, section 2.2.8 Signal detection and data analysis to calculate K_i, K_d, and k_{on} and k_{off} values for the unlabeled ligands; these are summarized in Table 6.1. Data are presented as mean ± S.E.M. values from at least 3 or more separate experiments performed in duplicate. The number of observations (n) for each ligand is stated in Table 6.1. All data used in these plots are detailed in Table 6.1.

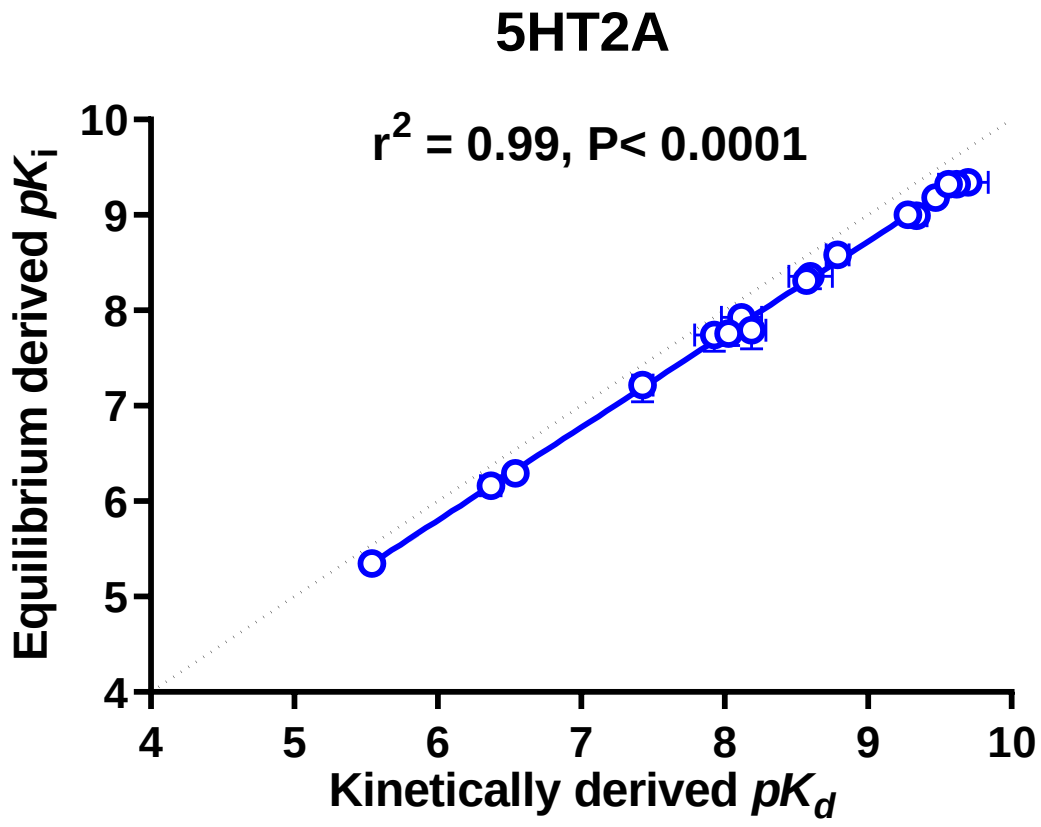


Figure 6.4. Correlating serotonergic receptor equilibrium and kinetically derived parameters of atypical and typical APDs and reference ligands. Correlation between kinetically derived pK_d (-log(k_{off}/k_{on})) and 5-HT2A pK_i values for the test ligands. pK_i values were taken from competition binding experiments at equilibrium. All data used in these plots are detailed in Table 6.1. Data are presented as mean ± S.E.M. from 4-5 experiments. The relationship between pK_i and kinetically derived pK_d was assessed using a two-tailed Pearson's correlation coefficient (r^2). A *P* value of 0.05 was used as the cut off for statistical significance.

6.3.3 Characterization of NAN190-red binding to the human 5-HT1A receptor

Specific binding of the antagonist NAN190-red to human 5-HT1A receptors expressed in CHO membranes was saturable and best described by the interaction of the fluorescent ligand with a single population of binding sites (Figure 6.5A). Non-specific binding is linear and specific binding represents over 70 % of total binding (log D of the parent molecule (2.47) at physiological pH 7.4). From these studies, the equilibrium dissociation constant (K_d) of NAN190-red was determined to be 2.98 ± 0.49 nM, n=11.

The binding kinetics of NAN190-red was characterised by monitoring the observed association rates using at least five different ligand concentrations (Figure 6.5B). Kinetic rate parameters for NAN190-red were calculated from a global fit of association curves to derive a single best-fit estimate for k_{on} and k_{off}, resulting in a k_{on} estimate of 4.6 ± 0.37 x10^7 M^{-1} min^{-1} and a k_{off} of 0.12 ± 0.01 min^{-1}, n=11. The resulting K_d (k_{off} / k_{on}) of 2.91 ± 0.34 nM was comparable to that obtained from the equilibrium studies described above.

The observed rate of association was linearly related to NAN190-red concentration (Figure 6.5C). Kinetic rate parameters for NAN190-red were calculated from plots of tracer concentration versus observed rates of association (k_{obs}), resulting in a k_{on} estimate of 2.01 ± 0.24 x10^7 M^{-1} min^{-1} and a k_{off} of 0.24 ± 0.02 min^{-1}, n=11. The resulting K_d (k_{off} / k_{on}) of 13.5 ± 0.2 nM was significantly different from that obtained from the equilibrium studies. Ligand dissociation estimated directly through the addition of an excess of spiperone revealed a k_{off} value of 0.40 ± 0.01 min^{-1}, n=5 (see Figure 6.5D), which was in reasonably good agreement with the value estimated from the ligand concentration versus k_{obs} plots described above but significantly different from the global fit of association curves. The reasons for these discrepancies in direct off-rate versus the global fit of association curves is unknown but could potentially result from initial fluctuations in assay well temperature on first addition of membranes or perhaps the phenomenon of tracer rebinding or potentially negative cooperativity as described above for the 5-HT2A receptor.

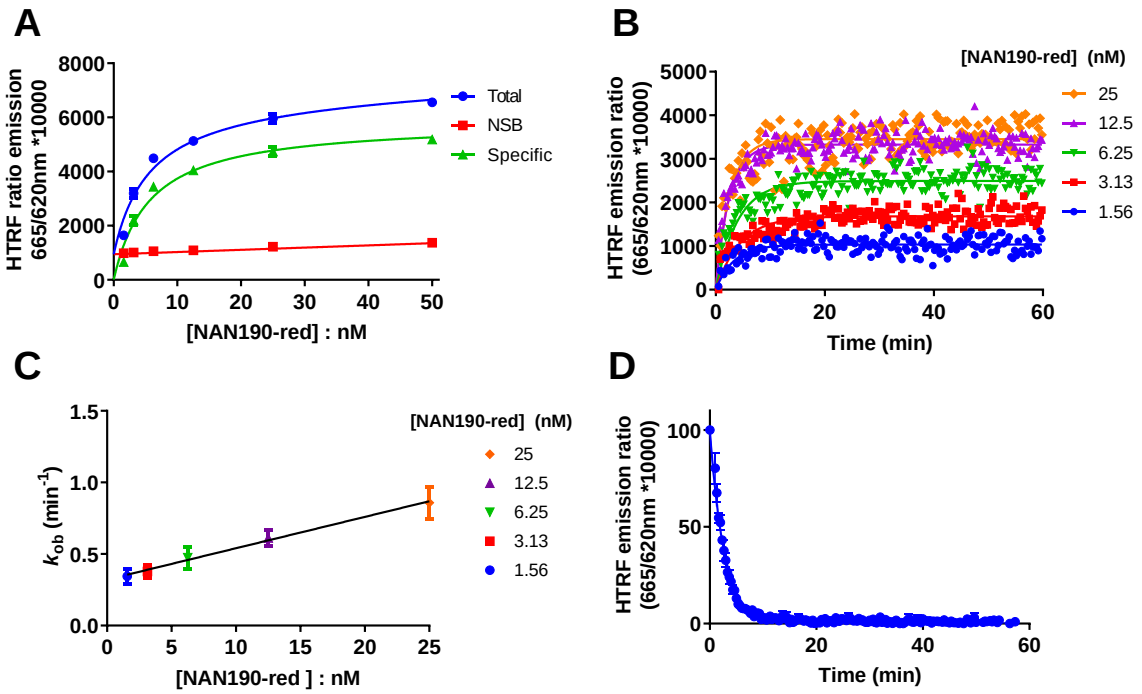


Figure 6.5. Determination of NAN190-red equilibrium and kinetic binding parameters at the human 5-HT1A receptor. **(A)** Saturation analysis showing the binding of NAN190-red to the human 5-HT1A receptor. CHO-5-HT1A receptor cell membranes (0.4 μg per well) were incubated for 60 min with gentle agitation with increasing concentrations of NAN190-red. Data are presented in singlet form from a representative of 11 separate experiments. **(B)** The observed association of NAN190-red to the human 5-HT1A receptor. Data are presented in singlet form from a representative of 11 separate experiments. **(C)** A plot of NAN190-red concentration versus k_{obs}. Binding followed a simple law of mass action model, k_{obs} increasing linearly with fluorescent ligand concentration. Data are presented as mean ± S.E.M. from a total of 11 separate experiments. **(D)** NAN190-red dissociation following the addition of spiperone (100 μM). Dissociation data are presented in mean ± S.E.M. from 5 experiments performed in singlet. All binding reactions were performed in the presence of GppNHp (0.1mM) with non-specific binding levels determined by the inclusion of spiperone (100 μM).

Binding affinities (K_i values) for the APDs studied using NAN190-red at the human 5-HT1AR are summarized in Table 6.3, and equilibrium competition binding curves are presented in Figure. 6.6A. Representative NAN190-red competition association association binding curves for selected D_2R ligands are shown in Figure. 6.6B-D. Progression curves for NAN190-red alone and in the presence of competitor were fitted to Equation 2.7, Chapter 2 enabling the calculation of both k_{on} (k3) and k_{off} (k4) for each of the ligands, as reported in Table 6.3.

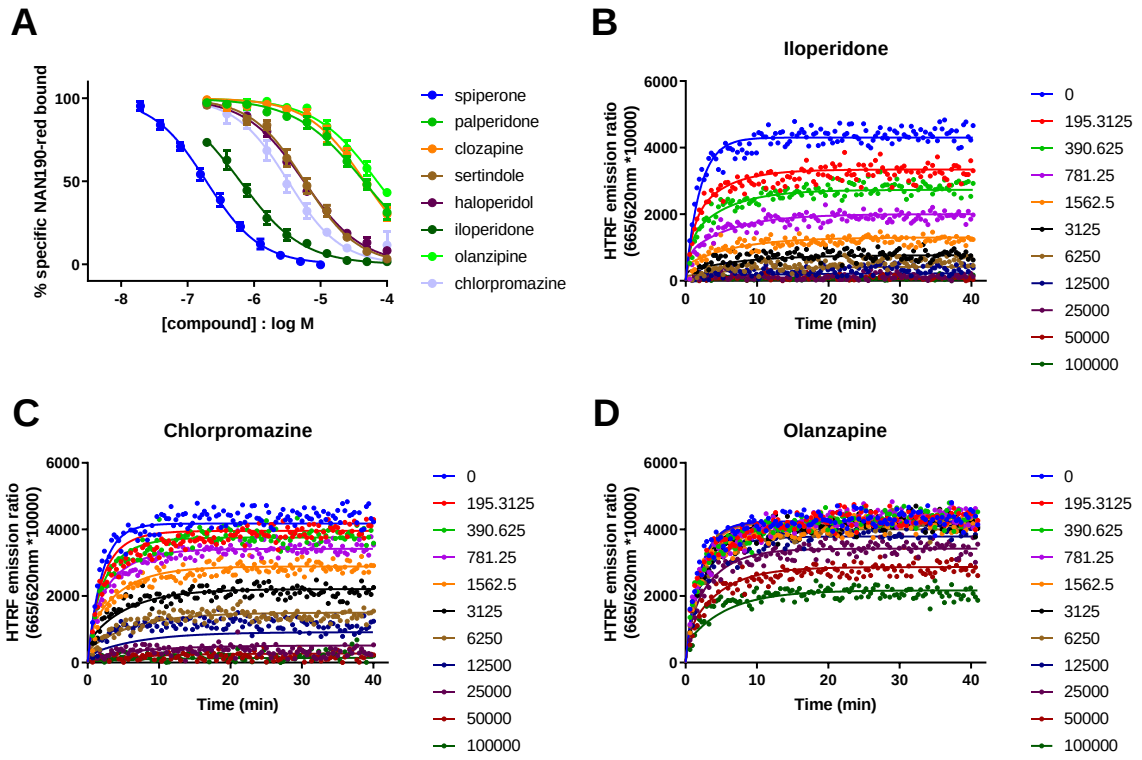


Figure 6.6. Equilibrium and competition association binding at the human 5-HT1A receptor. (A) Competition between NAN190-red (50 nM) and increasing concentrations of reference ligands, atypical and typical APDs spiperone, clozapine, iloperidone, olanzapine, chlorpromazine, sertindole and paliperidone at the human 5-HT1A receptor. Competition association binding between NAN190-red (50 nM) and increasing concentrations of representative atypical and typical APDs **(A),** iloperidone **(B)**, chlorpromazine **(C)** and olanzapine **(D)** at the human 5-HT1A receptor. All binding reactions were performed in the presence of GppNHp (0.1mM) with non-specific-binding levels determined by the inclusion of spiperone (100 µM). Kinetic and equilibrium data were fitted to the equations described in the Methods section to calculate K_i, K_d, and k_{on} and k_{off} values for the unlabeled ligands; these are summarized in Table 6.3. Equilibrium binding data are presented as the mean of at least three separate experiments performed in singlet. Kinetic data are representative of at least three separate experiments performed in singlet. All data used in these plots are detailed in Table 6.3 with individual n numbers stated in the table**.**

There was a relatively narrow range of dissociation rates for the different ligands, with dissociation half-lives ($t_{½}$) between 0.8 minutes for olanzapine to 3.3 mins for aripiprazole. To validate the rate constants, the kinetically derived dissociation constant (K_d) values (k_{off} / k_{on}) were compared with the dissociation constant (K_i) obtained from equilibrium competition binding experiments (see Figure 6.7). There was a very good correlation between these two values for all APDs tested (Two-tailed Pearson's correlation $r^2 = 0.99$, $P < 0.0001$) indicating the kinetic parameters were consistent with the equilibrium affinity estimates.

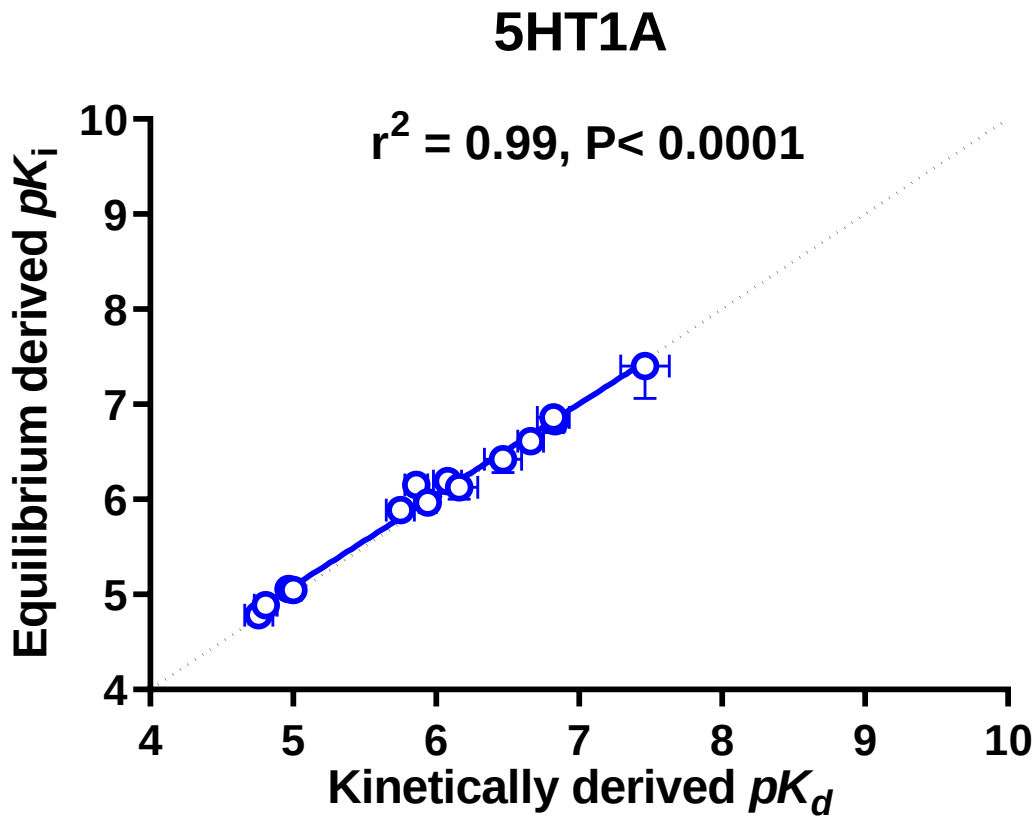


Figure 6.7. Correlating serotonergic 5-HT1A receptor equilibrium and kinetically derived parameters of atypical and typical APDs and reference ligands. Correlation between kinetically derived pK_d (-log(k_{off}/k_{on})) and 5-HT1A pK_i values for the test ligands. pK_i values were taken from competition binding experiments at equilibrium. All data used in these plots are detailed in Table 6.3. Data are presented as mean ± S.E.M. from 3-5 experiments. The relationship between pK_i and kinetically derived pK_d was assessed using a two-tailed Pearson's correlation coefficient (r^2). A *P* value of 0.05 was used as the cut off for statistical significance.

Further validation of the off-rates of these unlabelled compounds was obtained through direct saturation and dissociation experiments performed with fluorescent tracer spiperone-d2 and terbium labelled CHO-5-HT1A membranes. Saturation analysis from a single experiment revealed a K_d for spiperone-d2 of 217 nM (Figure 6.8A). Dissociation of fluorescent spiperone-d2 appeared to follow a simple exponential decay and k_{off} value of 0.29 min^{-1} (see Figure 6.8B). This value compares very favourably with the value obtained using unlabelled spiperone 0.30 ± 0.04 min^{-1} in the competition association assay formulated with NAN190-red.

Table 6.3. Kinetic binding parameters and relative efficacy of unlabelled clinically used APDs and reference antagonists for human 5-HT1A receptors and their historical classification as atypical or typical and those characterized as typical/atypical.

	5-HT1A receptor					***[^{35}S]-GTPγS binding***		***5-HT1A/D2 affinity ratio based on K_d***
	k_{off} (min^{-1})	***k_{on} ($M^{-1}min^{-1}$)***	***pK_d***	***pK_i***	***n***	***EC50 (nM)***	***Relative efficacy (fold over basal)***	
SGA/Atypical								
Paliperidone	0.58 ± 0.11	6.60 ± 2.10 x10^4	5.00 ± 0.06	5.05 ± 0.07	5	ND	~1	0.00025
Clozapine	0.64 ± 0.15	6.01 ± 1.55 x10^4	4.97 ± 0.05	5.06 ± 0.05	5	6.18 ± 0.11	2.77 ± 0.22	0.00191
Ziprasidone	0.56 ± 0.15	2.66 ± 1.63 x10^6	6.47 ± 0.13	6.42 ± 0.14	5	7.11 ± 0.06	3.28 ± 0.25	0.00191
Risperidone	0.82 ± 0.25	7.46 ± 2.72 x10^5	5.94 ± 0.06	5.97 ± 0.10	3	ND	~1	0.00078
Sertindole	0.36 ± 0.06	3.12 ± 1.11 x10^5	5.86 ± 0.08	6.15 ± 0.21	5	5.66 ± 0.05	0.35 ± 0.05	0.00087
Quetiapine	N/A	N/A	N/A	4.76 ± 0.11	3	5.74 ± 0.06	3.52 ± 0.38	0.00871
Olanzapine	0.83 ± 0.23	4.82 ± 1.25 x10^4	4.76± 0.10	4.78± 0.09	3	6.01 ± 0.26	1.52 ± 0.15	0.00039
Asenapine	0.27 ± 0.05	1.79 ± 0.10 x10^6	6.83 ± 0.07	6.82 ± 0.07	3	7.85 ± 0.23	1.42 ± 0.10	0.00813
Amisulpride	0.58 ± 0.16	3.66 ± 0.72 x10^4	4.81± 0.08	4.89 ± 0.11	3	4.62 ± 0.13	0.20 ± 0.06	0.00016
Lurasidone	0.27 ± 0.01	1.26 ± 0.24 x10^6	6.66 ± 0.09	6.61 ± 0.11	3	6.77 ± 0.19	1.86 ± 0.23	0.00178
Iloperidone	0.35 ± 0.02	2.56 ± 0.76 x10^6	6.82 ± 0.11	6.86 ± 0.16	3	6.25 ± 0.07	0.50 ± 0.03	0.00724
FGA/Typical								
Haloperidol	0.33 ± 0.05	2.05 ± 0.69 x10^5	5.75 ± 0.10	5.89 ± 0.02	3	5.36 ± 0.09	0.33 ± 0.04	0.00018

Chlorpromazine	0.39 ± 0.10	5.08 ± 1.22 x10^5	6.08 ± 0.10	6.19 ± 0.08	3	5.82 ± 0.08	0.19 ± 0.02	0.00069
Spiperone	0.30 ± 0.04	7.91 ± 1.18 x10^6	7.41 ± 0.04	7.51 ± 0.04	3	6.84 ± 0.05	0.30 ± 0.01	0.00037
Nemonapride	0.24 ± 0.05	8.86 ± 1.59 x10^5	6.57 ± 0.05	6.54 ± 0.08	3	7.47 ± 0.06	3.89 ± 0.43	0.000058
Cyanopindolol	0.21 ± 0.01	4.42 ± 0.53 x10^5	7.31 ± 0.07	7.41 ± 0.08	3	ND	ND	ND
Typical/atypical								
Zotepine	0.26 ± 0.03	3.95 ± 1.12 x10^5	6.16 ± 0.13	6.13 ± 0.13	3	5.94 ± 0.03	1.09 ± 0.03	0.00251
TGA/atypical								
Aripiprazole	0.21 ± 0.01	6.81 ± 2.52 x10^6	7.46 ± 0.17	7.40 ± 0.34	3	6.83 ± 0.06	2.91 ± 0.26	0.03090

Data are mean ± S.E.M. from three or more experiments performed in singlet. FGA/typical and SGA/atypical classification is based on reference sources see Sykes et al., 2017. ND = no consistent agonism detected. N/A 5-HT1A or 5-HT2A data not available

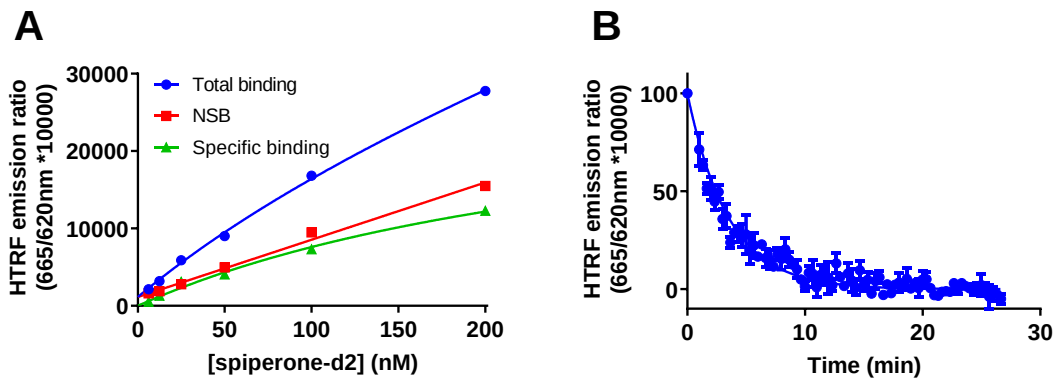


Figure 6.8. Determination of the fluorescent spiperone-d2 equilibrium and dissociation rate (k_{off}) parameters from the human dopamine 5-HT1A receptor. **(A)** Saturation analysis showing the binding of fluorescent spiperone-d2 to the human 5-HT1A receptor. CHO-5-HT1A receptor cell membranes (0.4 μg per well) were incubated for 30 min with gentle agitation with increasing concentrations of fluorescent spiperone-d2 performed in singlet. **(B)** Fluorescent spiperone-d2 dissociation following the addition of spiperone (100 μM). Dissociation data are presented in mean ± S.E.M. from a single experiment performed in triplicate. All binding reactions were performed in the presence of GppNHp (0.1mM) with non-specific binding levels determined by the inclusion of spiperone (100 μM).

A comparison of the equilibrium and kinetic binding properties of APDs at 5-HT2A and 5-HT1A receptors is shown in Figure 6.9. These correlation plots reveal the expected 5-HT2A affinity-based selectivity of the majority of these clinically used APDs (Figure 6.9A), which in some cases amounted to a selectivity ratio >10,000 (D2R affinity/5-HT2A receptor affinity). Surprisingly kinetic off-rates at the 5-HT1A receptor were largely similar to the dissociation rates measured at the 5-HT2A receptor despite affinities for this receptor being by and large significantly lower (Figure 6.9B see Table 6.1 and 6.3). Notably, kinetic on-rates are in general much reduced at the 5-HT1A receptor by up to 3-orders of magnitude. Factors which are thought to affect the association process include diffusion, desolvation and the molecular orientation of the molecule (Copeland 2006; Nunez et al., 2012; Pan et al., 2013).

These findings make sense from a kinetic binding perspective since a 3-order change in 5-HT2A affinity for a 1nM compound with an off rate of $1min^{-1}$ mediated by a change in k_{off} would necessitate an off-rate of 1,000 min^{-1}. This would, in turn, produce a $t_{1/2}$ of dissociation of 0.04sec, far faster than any known $t_{1/2}$ of dissociation value reported in the literature including low molecular weight fragment molecules which are considered to be rapidly dissociating. One very plausible explanation for the reduction in apparent association or on-rates of APDs binding the 5-HT1A receptor stems from the reduced number of aromatic residues in the 5-HT1A receptor binding pocket compared to the dopamine D_2 and 5-HT2A receptors (Yap et al., 2012). A lack of hydrophobic residues in the 5-HT1A binding pocket will potentially affect association in several different ways, reducing the ease with which ligands lose their associated water shells (so-called dewetting) but also affecting their ability to evacuate water from the ligand-binding pocket. In a case such as this water essentially acts as a barrier to successful ligand binding (Dror et al., 2011). Alternatively, steric clashes in the 5-HT1A binding pocket may simply reduce the ease of ligand access and egress.

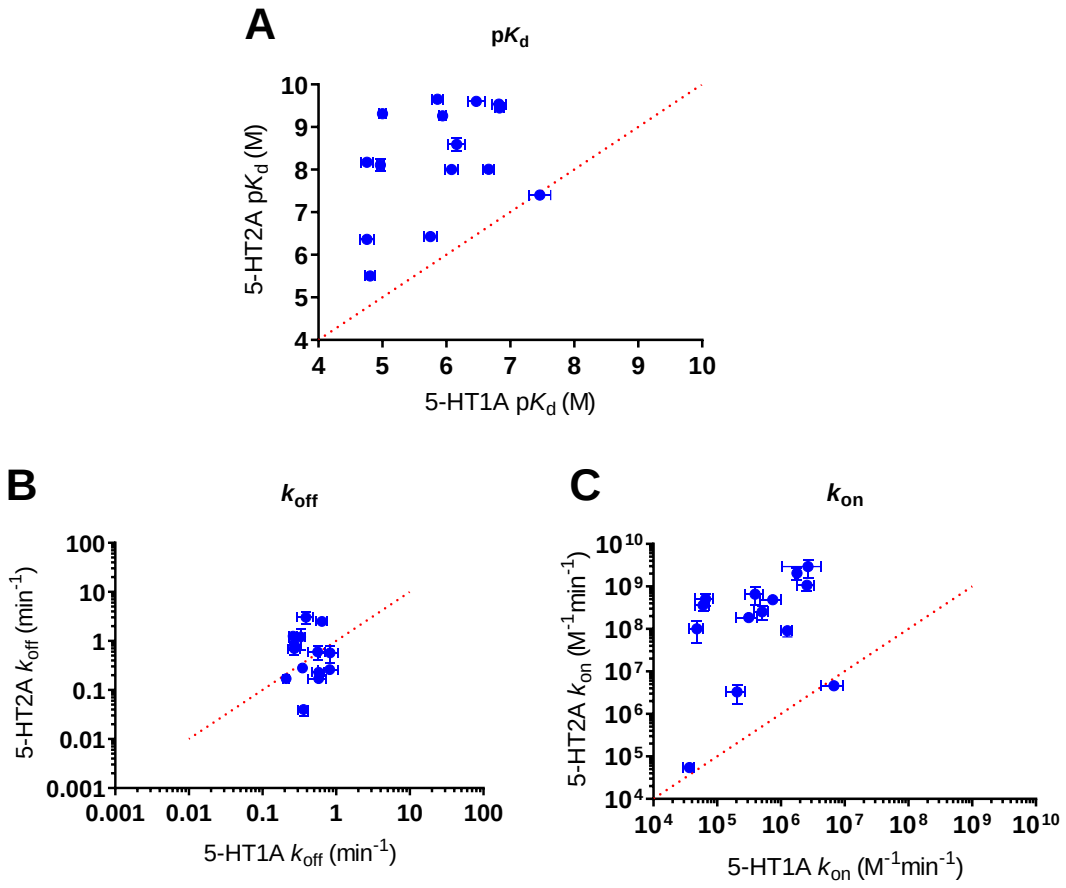


Figure 6.9. Exploring the relationship between 5-HT1A and 5-HT2A kinetically derived parameters of atypical and typical APDs and reference ligands. Correlation between APD 5-HT1A and 5-HT2A receptor **(A)** pK_d values **(B)** k_{off} values and **(C)** k_{on} values. The values composing the kinetically derived pK_d (-log (k_{off}/k_{on})) were taken from competition kinetic association experiments as exemplified in Figure 6.3 and 6.6. All data used in these plots are detailed in Table 6.1 and Table 6.3. Data are presented as mean ± S.E.M. from at least 3 separate experiments. N numbers for individual ligands are stated in Tables 6.1 and 6.3. The dotted red line represents the line of identity.

6.3.4 Assessing antipsychotic 5-HT1A agonism and its potential to reduce EPS in the clinic

The full range of 5-HT1A pharmacological efficacy was observable, with the clinically used APDs chosen for study from highly efficacious agonists eg. nemonapride, to very weak partial agonists eg. paliperidone and risperidone and inverse agonism eg. sertindole (see Figure 6.10A-C). GTPγS binding assays are notorious for producing little evidence of signal amplification (Strange 2010) and so τ values are always low and unlikely to reflect the true sensitivity of a cellular system to 5-HT1A agonists. As such low 5-HT1A agonist receptor occupancy in a highly amplified system may have clinical relevance. In order to account for this possibility, we have modelled effect (E) as a function of agonist concentration at clinically relevant D_2 occupancy (70%) by applying the operational model of agonism first introduced by Black and Leff (1983) to the GTPγS binding data presented in Figure 6.10A-C, see Figure 6.10D.

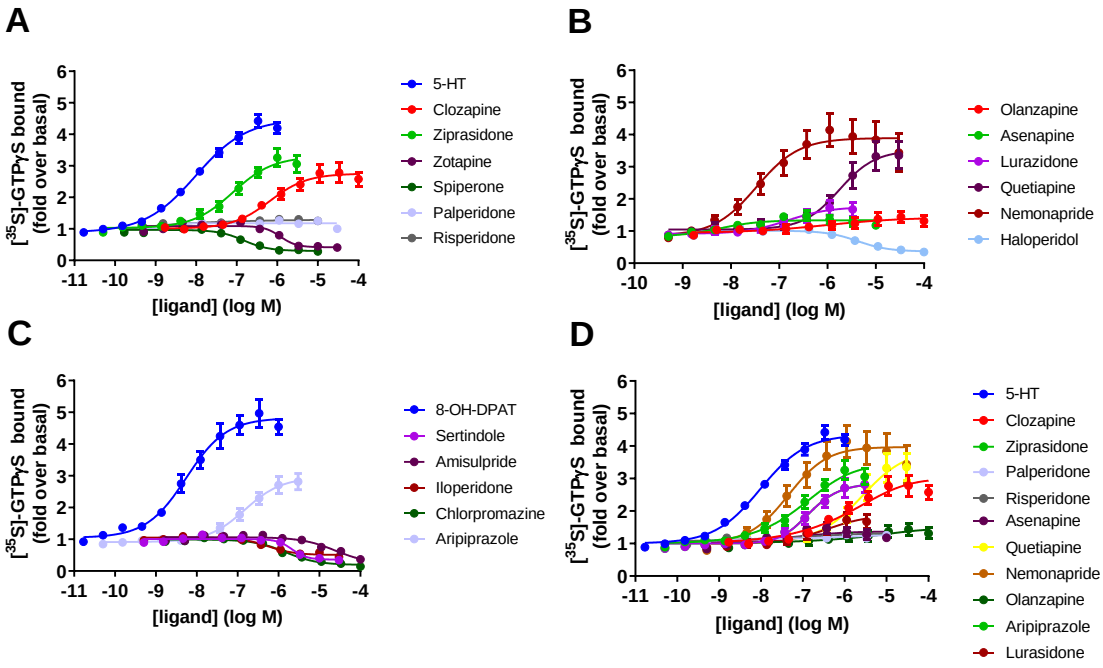


Figure 6.10. Assessing the efficacy of clinically used antipsychotics at the 5-HT1A receptor. Concentration-response curves of 5-HT1A agonists, measuring [^{35}S]-GTPγS binding to CHO-5-HT1A membranes prepared from CHO-5-HT1A cells **(A-C)**, and **(D)** fitted to the operational model to derive τ. GTPγS binding data are mean S.E.M. from four or more separate experiments. EC_{50} and relative efficacy values are detailed in Table 6.2.

In consideration of a role for 5-HT1A receptors, and more specifically 5-HT1A agonism in the reduced incidence of EPS observed with clinically used APDs we compared the relative effect values (see Table 6.3 and Figure 6.11) with clinically observed EPS, findings taken from a recent meta-analysis of multiple-treatments studies comparing EPS side effect profiles across a diverse group of APDs (Leucht et al., 2013). No obvious relationship was observed between clinically observed EPS (Figure 6.11A) and 5-HT1A modelled functional effect (Figure 6.10B) for the 5-HT1A agonists, using either a t value equal to 1 (Figure 6.11B) or 100 (Figure 6.11C), designed to mimic signal amplification. This could reflect the fact that although some clinically used compounds show relatively high levels of 5-HT1A activation and low levels of clinically observed EPS (eg. clozapine), when signal amplification is taken into account, there are contrastingly APDs such as ziprasidone which although equally efficacious at clinically relevant D_2 occupancy levels exhibit an elevated EPS odds ratio compared to clozapine (see Figure 6.11C). 5-HT1A occupancy for all ligands is likely to be relatively insignificant at clinical doses (see Table 6.3). Importantly none of the clinically tested APDs is as efficacious as 5-HT the natural ligand. Thus, a reduced 5-HT1A receptor affinity could be therapeutically important with regards to selectivity and the potentiation of dopamine release. For example, atypical APDs with 5-HT2A blocking potential will likely cause the release of 5-HT which will indirectly activate 5-HT1A receptors in the absence of any significant 5-HT1A receptor blockade.

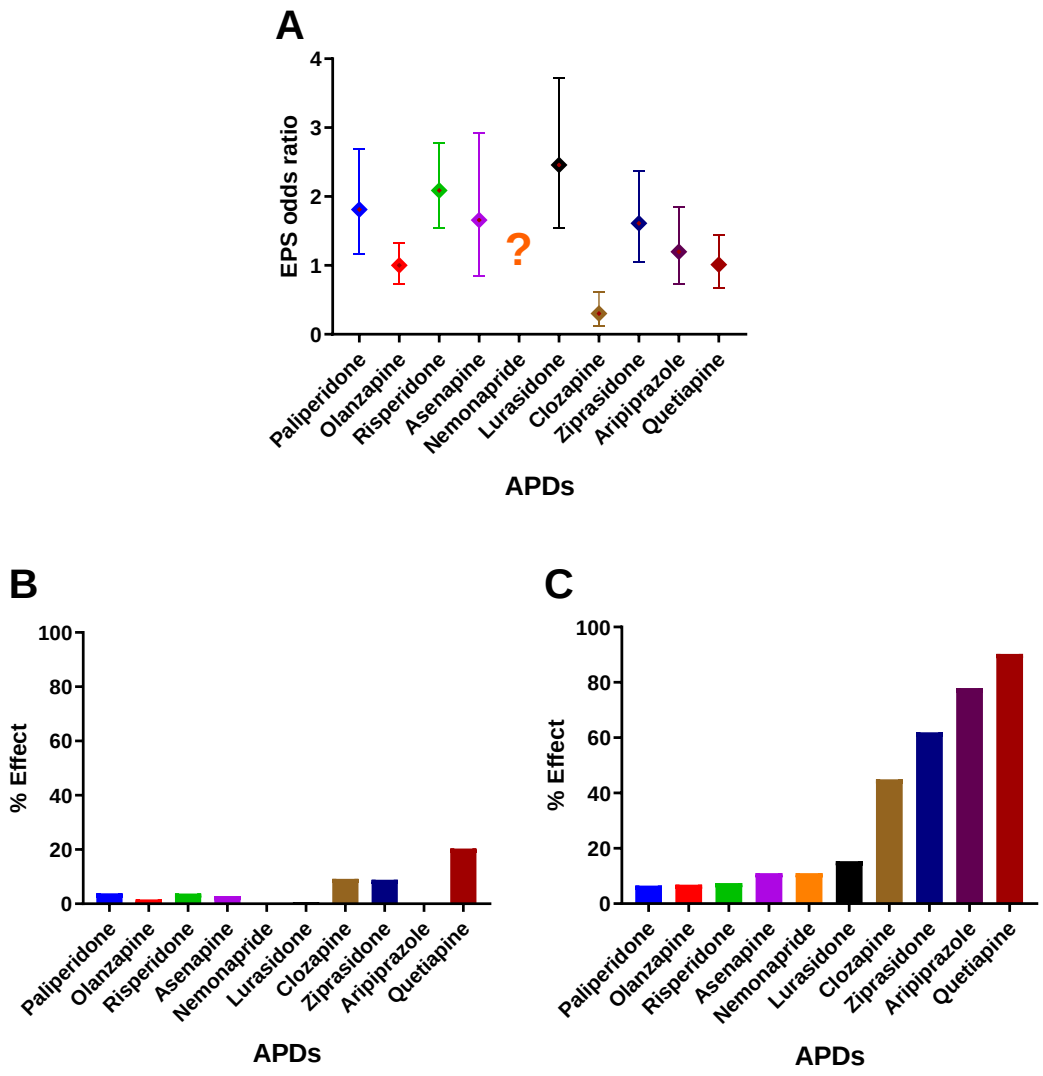


Figure 6.11. Exploring the relationship between 5-HT1A agonism and EPS levels exhibited by clinically used APDs. Bar graph showing **(A)** Clinical APD EPS odds ratio plus associated 95% credible intervals presented in order of increasing 5-HT1A predicted effect maximum (%), derived from [^{35}S]-GTPγS binding experiments using a τ value of 100. 5-HT1A effect maximum (%) estimated using the operational model of agonism and concentrations of APDs producing 70% D2 occupancy using **B)** a τ value of one. (**C)** a τ value of a hundred. All data used in these plots are detailed in Table 6.3 with clinical EPS odds ratio data taken from Leucht et al (2013). Effect data are presented as mean from four experiments and clinical data as the odds ratio for EPS with associated credible intervals where indicated.

6.3.5 Functional consequences of slow dissociation from 5-HT2A receptors

Like our previous study comparing the binding of APDs to the $hD_{2L}R$ we observed a wide range in k_{on} values between the APDs (>10,000-fold) and a relatively wide range in k_{off} values (~70-fold) for ligands binding to the human 5-HT2A receptor. In contrast to the previous dopamine $D_{2L}R$ study described in Chapter 5, the typical APDs examined here exhibited a much wider variation in the value of k_{on}, driving differences in 5-HT2A receptor affinity. More variation in both on and off-rates were observed for atypical APDs, notably, sertindole exhibited a k_{off} value much slower than any other clinically used atypical APDs tested (Table 6.1).

Calcium assays are useful bioassays to assess the kinetics of antagonist binding since slowly dissociating antagonist readily suppress calcium signalling leading to reductions in measurable agonist response. This occurs since calcium assays are by nature non-equilibrium assays with agonist responses occurring over a short time frame (seconds) and usually insufficient for the binding of agonist and antagonist to reach a true equilibrium (Charlton and Vauquelin 2010; Bdioui et al., 2018). The ability of sertindole to display insurmountable antagonism at 5-HT2A receptors in response to increasing concentrations of 5-HT in a calcium release assay at physiological temperature is highlighted in Figure 6.12B. In contrast, clozapine's effects are almost fully reversible reflecting its relatively rapid off-rate from 5-HT2A receptors Figure 6.12A.

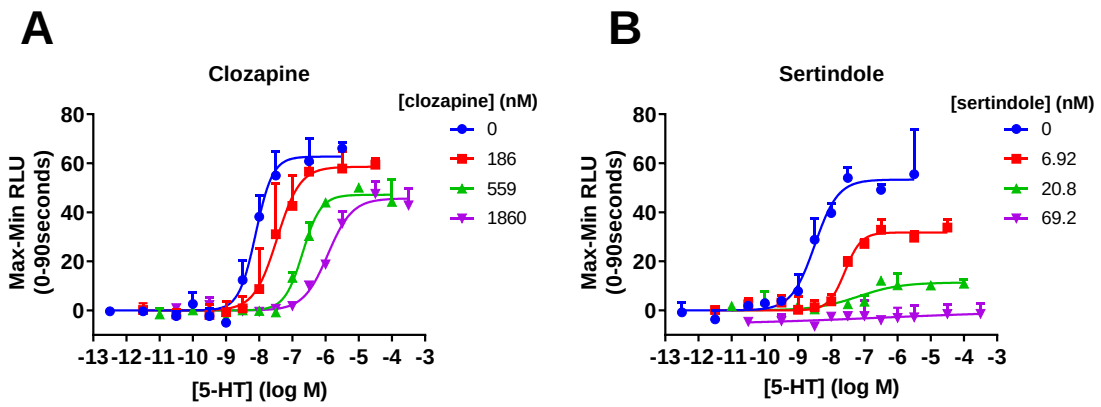


Figure 6.12. 5-HT concentration calcium responses curves obtained in CHO-5-HT2A cells in the absence and presence of the atypical APDs **(A)** clozapine and **(B)** sertindole at 37ºC. Calcium data are presented as mean ± range from a representative of four separate experiments performed in duplicate.

6.3.6 Modelling the relative effects of 5-HT2A and dopamine D_2 receptor rebinding

At least in the brain, it would appear that target rebinding models are useful predictors of the long-term effects of APDs and reflective of PET studies (Vauquelin and Charlton 2010; Sykes et al., 2017; Seeman 2002). I have therefore assessed relative 5-HT2A and D_2 receptor target occupancy expressed as a function of time by estimating individual drug-receptor target reversal (k_r) at an initial D_2R striatal occupancy of 80%, based on the rebinding model we reported previously (Sykes et al., 2017). Relative 5-HT2A and D_2R occupancy (5-HT2A : D2) was determined by calculating AUC at D_2R occupancy levels between 80-65% (i.e. those relevant to antipsychotic and EPS through combined serotonergic and D_2R blockade see Kasper et al., 1999). The relative 5-HT2A and D_2 receptor target occupancies of a selection of test agents expressed as a function of time are shown in Figure 6.13A-G with receptor occupancy markers between 80 and 65% marked by the dotted lines. To achieve a fair comparison, I have considered differences in cortical 5-HT2A receptor density relative to striatal D_2R receptor density. Previous human and animal studies indicate that 5-HT2A receptor numbers are at least 2-3 times greater in the (prefrontal) cortex relative to the striatum (Joyce et al., 1991; Muguruza et al., 2013; Muguruza et al., 2014; Jafari et al., 2013).

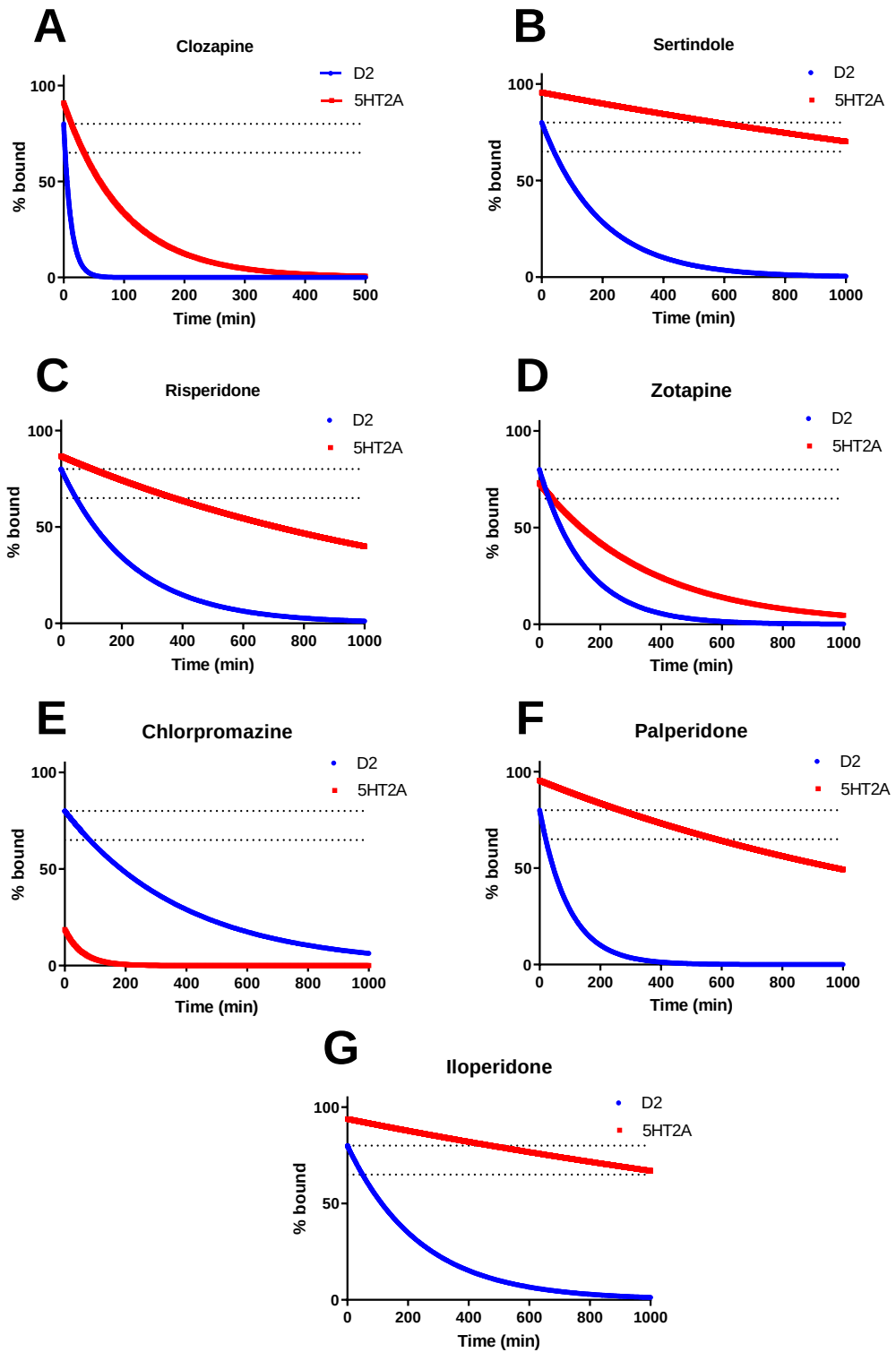


Figure 6.13. Modelling relative APD D_2R and 5-HT2A receptor rebinding. Simulated dissociation rates of clinically relevant APDs from human D_2 and 5-HT2A receptors, **(A)** clozapine **(B)** sertindole **(C)** risperidone **(D)** zotepine **(E)** chlorpromazine **(F)** paliperidone and **(G)** iloperidone under conditions of limited

diffusion based on the association (k_{on}) and dissociation (k_{off}) rates determined in competition kinetic binding experiments. All kinetic parameters used to these plots are taken from Table 6.1 and 6.2 and Sykes et al., 2017 with k_r values calculated using Equation 2.9, Chapter 2. For simulation purposes the reversal rate k_r was based on the model of an immunological synapse as detailed in Chapter 2, section 2.2.9 Modelling drug-receptor re-binding. The dotted lines represent the levels of dopamine D_2R occupancy 80-65% thought to be relevant in the occurrence of EPS with clinically used APDs at therapeutic doses (see Kasper et al., 1999).

The original ‘serotonin-dopamine hypothesis’, uses the 5-HT2A/D_2 equilibrium affinity ratio (based on pK_i) to predict the relative incidence of EPS (Meltzer et al., 1989). A plot of the 5-HT2A : D_2R affinity ratio (based on 1/K_d) versus clinically observed EPS (dopamine D_2R affinity values taken from Sykes et al., 2017) did not wholly predict the incidence of clinically observed EPS (Figure 6.14A). As shown in Figure 6.14B the correlation of 5-HT2A: D2 k_r AUC versus clinically observed EPS odds ratio did not drastically improve our ability to predict EPS.

It can be argued that it is not appropriate to group and correlate compounds with essentially no 5-HT2A affinity with compounds with significant 5-HT2A affinity as essentially, they may have a different mechanism of action (Meltzer et al., 2003). However, in both instances, if we remove compounds with 5-HT2A : D_2R affinity ratios of <1, or 5-HT2A: D_2R k_r AUC ratios <1, the correlations described above are made significantly worse.

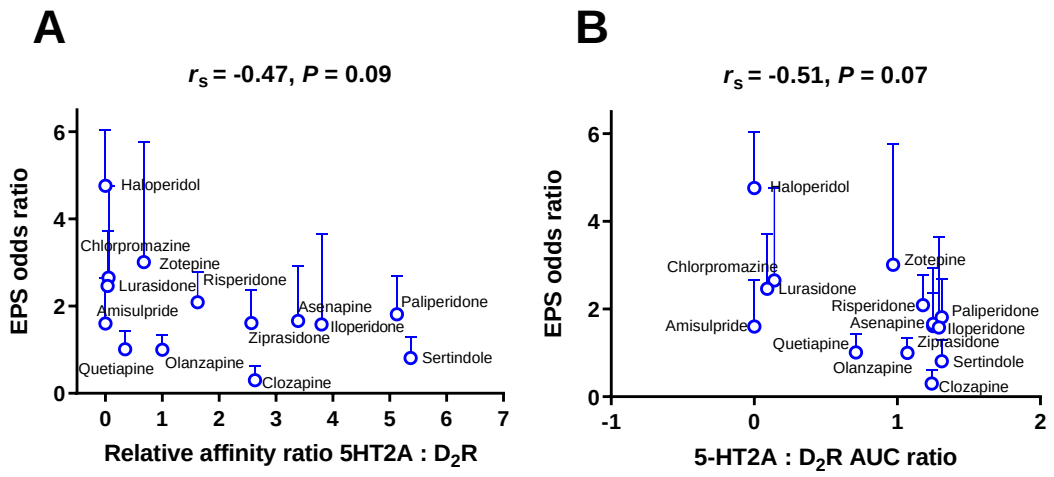


Figure 6.14. Correlating clinical APD EPS with kinetically derived parameters. Correlation plots showing the relationship between **(A)** relative 5-HT2A : D_2R affinity ratio (based on $1/K_d$) and EPS odds ratio and **(B)** 5-HT2A: D2R (80-65%) AUC and EPS odds ratio. Relative affinity derived from the kinetic K_d (k_{off}/ k_{on}) and kinetic data used in these plots are detailed in Table 6.1 and Table 6.2 and Chapter 5, Table 5.1 with clinical data taken from Leucht et al., (2013). Kinetic data are presented as mean ± S.E.M. from at least four experiments and clinical data as the odds ratio for EPS with associated upper credible interval where indicated. The relationship between two variables was assessed using a two-tailed Spearman's rank correlation allowing the calculation of the correlation coefficient, r_s. A P value of 0.05 was used as the cut off for statistical significance.

6.4 Discussion

The novel TR-FRET kinetic binding assays described herein have enabled us to accurately quantify, for the first time, the kinetic rate constants of a large number of unlabelled clinically used APDs at 5-HT2A and 5-HT1A receptors under similar test conditions, allowing us to investigate a role for 5-HT2A/5-HT1A receptor target coverage in the reduced side effect profile of clinically used APDs. Furthermore, we have profiled the functional effects of these compounds at 5-HT1A receptors in a [^{35}S]-GTPγS assay specifically formulated to uncover the full spectrum of compound efficacy from agonism to inverse agonism.

There is good evidence from rodent studies that agonist activity at the 5-HT1A receptor can control the absolute levels of EPS which are associated with blockade of dopamine D_2 receptors in the striatum. For example, 8-OH-DPAT, the prototypical 5-HT1A receptor agonist, prevents catalepsy produced by the typical APD haloperidol (Broekkamp et al., 1988; Invernizzi et al., 1988). Such effects may not require full efficacy since the addition of buspirone and tandospirone, two 5-HT1A partial agonists decrease signs of EPS in schizophrenic patients treated with antipsychotics (Goff et al., 1991; Moss et al., 1993; Yoshida et al., 1998).

In the current study using the inherent 5-HT1A agonism, of certain APDs measured in a [^{35}S]-GTPγS assay and their relative binding affinities, we were able to predict using the operational model of agonism, potential functional effect, based on concentrations producing 70% D_2R occupancy. These functional effect predictions suggests that 5-HT1A agonism does not play a significant role in the reduced overall incidence of EPS observed with clinically used APDs tested in this study. This is perhaps best illustrated by contrasting the higher incidence of EPS observed with ziprasidone compared to clozapine, this despite ziprasidone being marginally more efficacious than clozapine at 5-HT1A receptors at concentrations of these drugs which occupy 70% of D_2 receptors. Also, and perhaps crucially the inverse agonist sertindole has a much-reduced incidence of EPS compared to ziprasidone. The reasons for this apparent lack of effect in clinical studies most likely relates to the dominant role of other serotonergic receptors blocked by the MARTA class. Nonetheless, it is worth bearing in mind that the native agonist 5-HT is a fuller

agonist than any of the APDs tested. Hence blockade of 5-HT2A receptors which has been suggested to release dopamine may be sufficient in the absence of any additional 5-HT1A stimulation (which reduces activation of 5-HT2A receptors) to reduce the overall EPS observed with MARTAs. As such further 5-HT1A receptor occupation by these clinically used APDs might if anything create functional antagonism of 5-HT responses, thereby increasing 5-HT release, with subsequent activation of 5-HT2A receptors (inhibiting dopamine release) leading to an overall increase in EPS. The role of signal amplification in these circumstances is open to question since early studies of 5-HT1A activation in NIH-3T3 cells (mouse embryonic fibroblasts) would suggest that this receptor does not seemingly obey the rules behind the operational model, in that increases in 5-HT1A receptor number do not lead to increases in 5-HT potency (Varrault et al., 1992). Amplification may occur downstream of the G Protein as evidenced by more potent effects for (+)8-OH-DPAT on ERK1/2 phosphorylation in Hela cells (~30-fold) however amplification close to the G protein appears to be minimal (Newman-Tancredi et al., 2009).

In consideration of a role for 5-HT2A receptors in the reduced incidence of EPS it has been widely reported that the 5-HT2A affinity of certain clinically used atypical antipsychotics is much higher than their corresponding affinities at dopamine D_2 receptors (Meltzer et al., 1989; Richelson and Souder 2000; Horacek et al., 2006; Kusumi et al., 2015). For example, estimates for clozapine taken directly from these papers range from 14 to 80-fold higher affinity for the 5-HT2A receptor over the D_2 receptor. A comparison of the equilibrium and kinetic parameters of these compounds for these two receptors is shown in Figure 6.15. The TR-FRET data revealed a surprisingly small difference in affinity for D_2 and 5-HT2A receptors across the clinically used atypical serotonin-dopamine antagonists (eg. risperidone, sertindole and iloperidone) and MARTAs studied. Others have reported similar conclusions to our own (Seeman et al., 1997) although the notion of significantly higher 5-HT2A affinity for atypical APDs persists (Langlios et al., 2012; Meltzer and Massey 2011). The most likely explanation for discrepancies in D_2R affinity estimates stems from the often-overlooked phenomenon of ligand depletion. This results in an underestimation of the affinity of high-affinity radioligands such as [^{3}H]-spiperone and as a direct consequence, unlabelled compound affinities, due to the nature of the Cheng-Prusoff correction (see Seeman 2010). Differences in assay

temperature and buffer salt concentration may also contribute to these discrepancies.

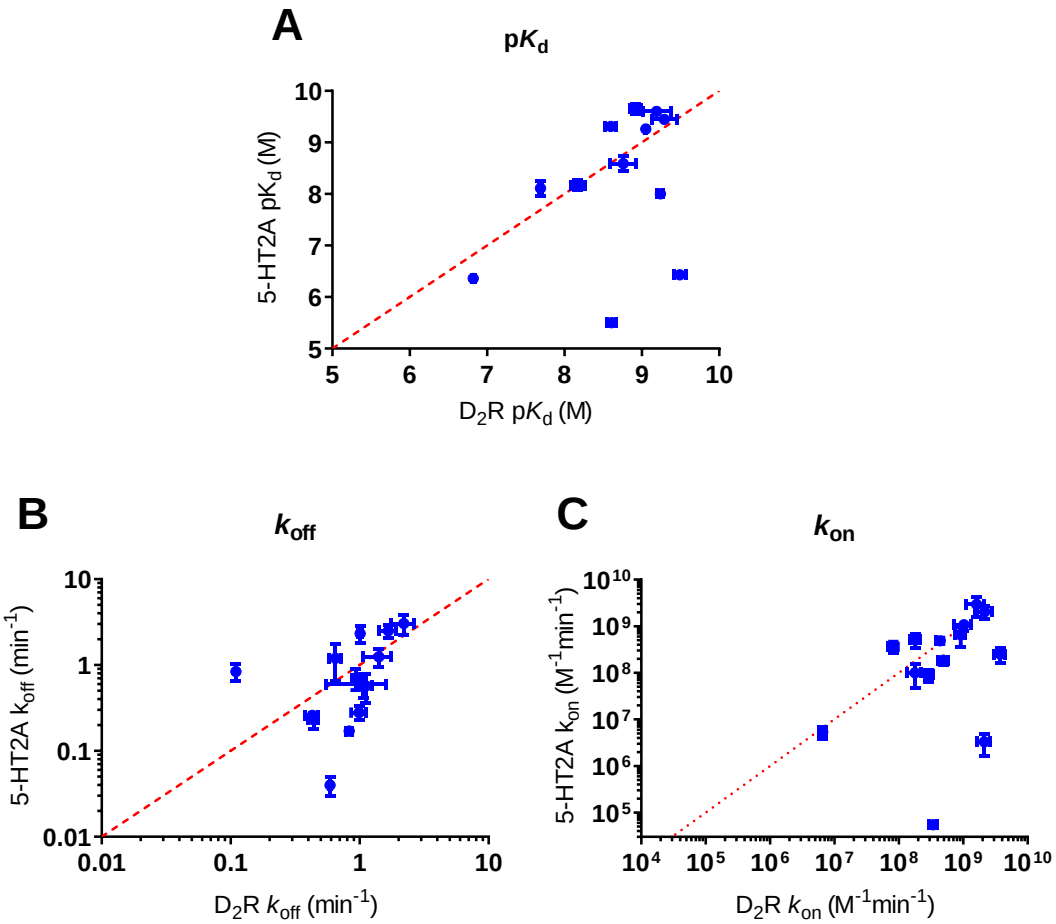


Figure 6.15. Correlating 5-HT2A and dopamine D_2R kinetically derived parameters of atypical and typical APDs and reference ligands. Correlation between dopamine D_2R and 5-HT2AR **(A)** pK_d (-log(k_{off}/k_{on})) values **(B)** k_{off} values and **(C)** k_{on} values. 5-HT2A pK_d values were taken from 4F4PP oxalate-red competition association binding experiments as exemplified in Figure 6.3. All data used in these plots are detailed in Table 6.1 and 6.2 whilst other D_2R kinetic and pK_d values were taken from Chapter 5, Table 5.1. Data are presented as mean ± S.E.M. from at least four experiments.

It is suggested that typical APDs only decrease dopamine stimulated output via their inhibitory action at D_2 receptors throughout the brain. In contrast atypical antipsychotics with 5-HT2A inhibitory effects have more complex net actions on dopamine activity and are able to not only decrease dopamine activity at D_2 receptors but also potentially increase dopamine release via 5-HT2A receptor blockade and thus promote dopamine signalling in certain select regions of the brain (Stahl 2008; Horacek et al., 2006; Lucas and Spampinato 2000). Consequently, it has been suggested that these agents will have therapeutic actions not just on the positive symptoms of schizophrenia but also on negative, cognitive and affective symptoms (Horacek et al., 2006). Also, a significant reduction in the incidence of EPS might be expected through increased dopamine release in the striatum (Horacek et al., 2006) and potentially a reduction in hyperprolactinemia through increased dopamine release at the level of the hypothalamus (Compton and Miller 2002).

Target occupancy in the brain is not well described by traditional models of receptor binding which assume free diffusion. Thus, to compare relative dopamine D_2R and 5-HT2A receptor occupancy we have employed a model which accounts for rebinding of molecules in conditions of limited diffusion (Vauquelin and Charlton 2010; Sykes et al., 2017). The relative 5-HT2A and D_2 receptor target occupancies of selected test agents under the influence of this model and expressed as a function of time is shown in Figure 6.13A-G. What is apparent is the wide variation in relative occupancy of atypical APDs at these two receptors when plotted as a function of time, with certain molecules such zotepine, which historically has been classed as both atypical and typical showing a smaller degree of occupancy at the 5-HT2A receptor whereas other agents such as clozapine appear to be more balanced and relatively short-acting at both receptors. In contrast, there are atypical compounds which show a high level of (long-lasting) occupancy at both receptors such as sertindole, a compound known for its potent and long-lasting effects at 5-HT2A receptors (Sanchez et al., 1991; Hyttel et al., 1992). The ability of this compound to produce insurmountable antagonism is highlighted in Figure 6.12B. In direct contrast to sertindole, clozapine's effects are largely reversible (minimal reduction in E_{max}) under identical conditions (Figure 6.12A). Thus, it would appear that the balance between 5-HT2A and D_2 receptor occupancy is the key to the reduced side

effect profile observed with sertindole. Hypothetically augmented dopamine release due to sustained 5-HT2A residency could partially compensate for high striatal D_2R occupancy as a result of robust 5-HT2A receptor rebinding and a relatively slow dissociation rate (k_{off}).

By correlating the 5-HT2A kinetic binding data with clinical EPS data taken from a recent and relatively comprehensive multiple-treatment meta-analysis of APD efficacies (Leucht et al., 2013) we were able to assess the relative role of the 5-HT2A receptor in the reduced incidence of this important and potentially efficacy limiting on-target side effect. Crucially the suggestion that higher 5-HT2A affinity alone of atypical APDs such clozapine relates to their reduced EPS profile is not supported by our kinetic (or equilibrium) affinity data (See Figure 6.14A). Intriguingly however strong dopamine D_2R re-binders such as chlorpromazine, lurasidone, haloperidol and zotepine with low 5-HT2A : D2 affinity ratios (i.e <1) showed the widest range in EPS odds ratios. Theoretically, this occurs if none of these agents following dosing in patients can positively modulate the endogenous release of dopamine via the 5-HT2A receptor to lower overall D_2R occupancy and reduce the risk of EPS (i.e. no brakes), with acute EPS effects dependent primarily on the level of initial D_2R blockade.

Through the application of a rebinding model, we found 5-HT2A: D2 AUC ratios were no better correlated with the incidence of EPS Figure 6.14B. Seemingly there is a limit to the effectiveness of these compounds in terms of their relative receptor coverage at 5-HT2A and dopamine D_2 receptors. However, this plot reveals drugs such as sertindole which shows lower levels of EPS in the clinic than predicted by its calculated k_r value (or D_2R rate of binding reversal) in the striatum (see Sykes et al., 2017) (Figure 6.14B). On the other hand, compounds such as paliperidone were highlighted, having relatively high 5-HT2A:D2 AUC ratios but giving no clear benefit to patients in terms of relieving the symptoms of EPS (Figure 6.14B). Suggesting that sertindoles actions are unique and stem from its very slow off rate from the 5-HT2AR. A plot of k_r versus the 5-HT2A : D_2R affinity ratio reveals two distinct groups of APDs (Figure 6.16). Those whose initial receptor target coverage is greater for D_2Rs (i.e. 5-HT2A : D_2R affinity ratio <1), and those whose receptor target coverage is specific for both D_2R and 5-HT2A receptors (i.e. 5-HT2A : D_2R affinity ratio >1).

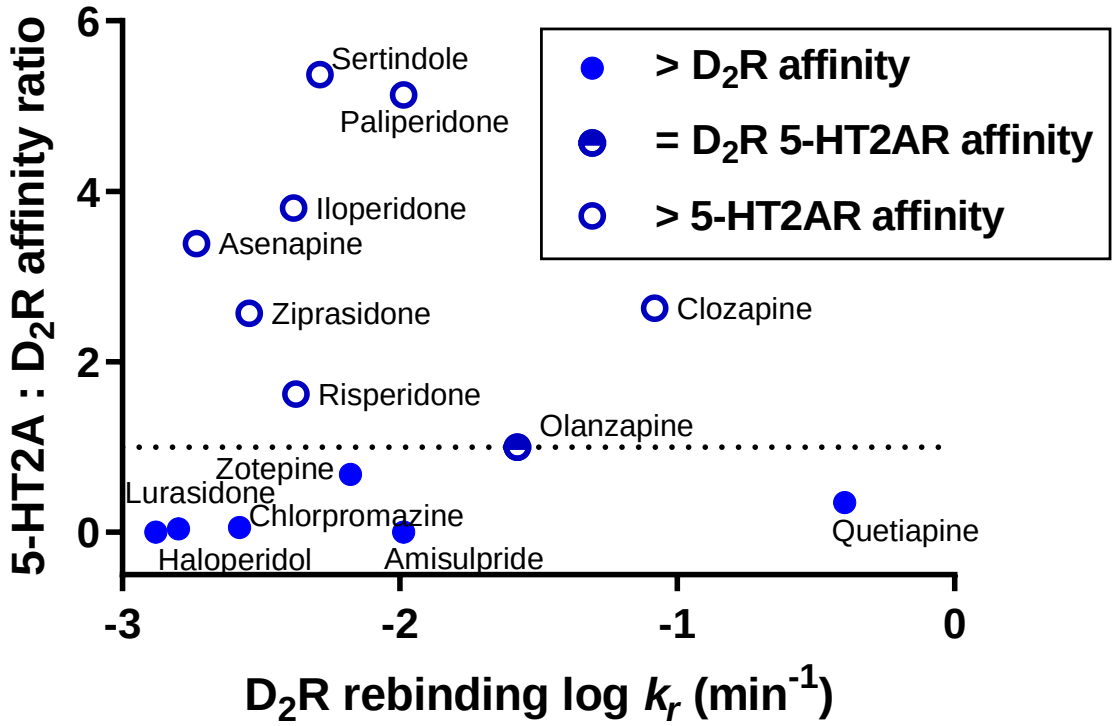


Figure 6.16. Plot showing the relationship between APDs overall D_2R reversal rate (log k_r) and relative 5-HT2A : D_2R affinity. D_2R occupancy specific compounds (those with 5-HT2A : D_2R affinity receptor affinity ratios less than one) are coloured blue. All affinity ratio data used in these plots are detailed in Table 6.1 with k_r values taken from Sykes et al., 2017.

Other factors are likely important in dictating the absolute levels of EPS of these clinically used APDs. One factor could be the slower D_2R reversal rates (i.e. reduced k_{off}) of certain compounds. The implication being that paliperidone's and risperidone's relatively high EPS result in part from their slow dissociation from the D_2R in the face of raised dopamine levels rather than a lack of activity at 5-HT2A receptors per se.

These two distinct groups of APDs identified through this reductionist approach are represented graphically in Figure 6.17 under the influence of D_2R k_r but in the absence of their perceived 5-HT2A effects on dopamine release. To illustrate a potential role for k_{off} from the D_2R I have highlighted the compounds which show significant coverage at 5-HT2A receptors relative to D_2Rs and coloured them according to their relative rates of dissociation from the D_2R. This plot suggests that the relative level of dopamine output dictated by 5-HT2A: D2R occupancy over time could have an impact on observed EPS and may partly explain the imperfect correlation we observed with the binding reversal rate (k_r) in our previous study (Sykes et al., 2017). Increased concentrations of dopamine in the striatal compartment could potentially outcompete APDs in the striatum preventing rebinding and decreasing the subsequent risk of EPS. The degree of competition and subsequent reduction in striatal APD occupancy would be likely dictated by the relative ease of reversibility of these drugs. Conventional APDs being particularly difficult to eliminate from the striatal compartment due to their very rapid on-rates (Sykes et al., 2017). Interestingly sertindole's effects on EPS appear to be underestimated by this model potentially as a result of its own uniquely slow off-rate from the 5-HT2A receptor in the face of increasing serotonin levels. At equal 5-HT2AR occupancy, a drug such as sertindole which dissociates very slowly from the 5-HT2A receptor will always produce a more effective release of dopamine from the striatum due to its propensity for hemi-equilibrium (Sykes et al., 2016).

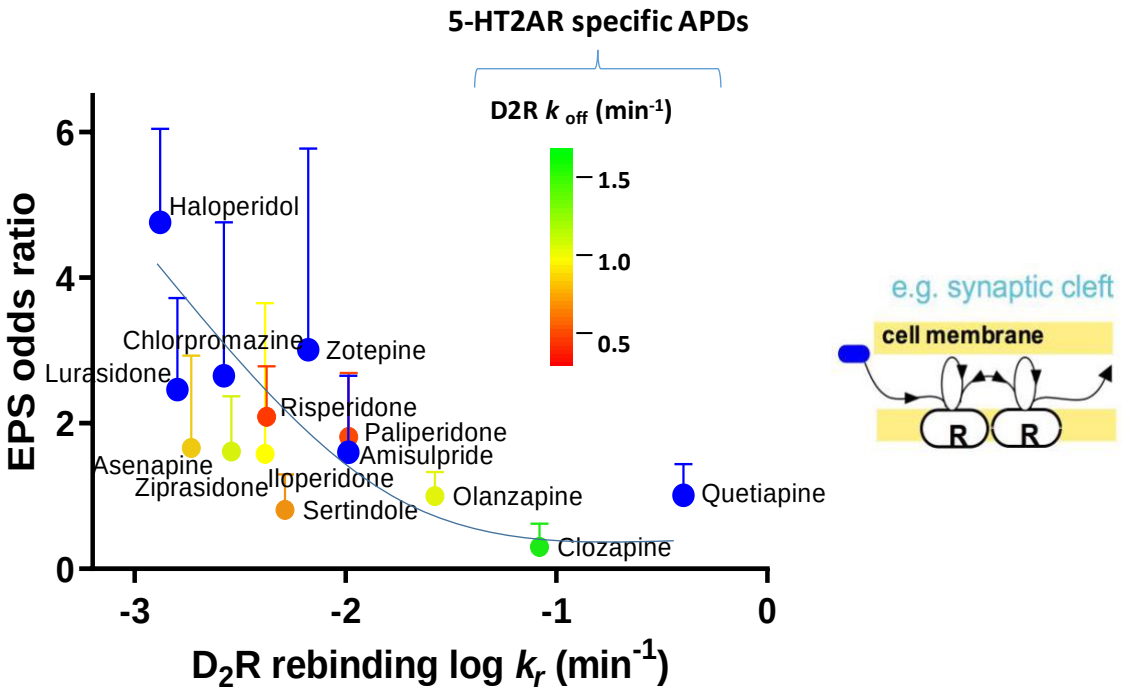


Figure 6.17. Modelling APD D_2R rebinding and the potential for 5-HT2A mediated reductions in rebinding and its consequences for clinical 'on target' toxic effects. Correlation plot showing the relationship between overall D_2R reversal rate (log k_r) and EPS odds ratio for D_2R specific compounds, taken from Leucht et al. (2013). D_2R specific compounds (those with D2:5-HT2A receptor affinity ratios less than one) are coloured blue whilst 5-HT2A specific compounds with significant affinity for the 5-HT2A receptor are highlighted according to their measured dissociations rates (k_{off}) from the D_2R. All kinetic data used in these plots are detailed in Chapter 5 Table 5.1 and Table 6.2. Kinetic data are presented as mean ± S.E.M. from four experiments and odds ratio for EPS with associated credible intervals indicated. The relationship between the two variables is depicted as a trend line. The model of the synaptic cleft used in this figure was copied directly from Vauquelin 2016.

What seems certain is that atypicality in terms of on target EPS can be attributed to at least three independent pharmacological properties of APDs; rapid reversal of D_2 receptor occupancy in the striatum due to reduced APD rebinding potential (as is the case for compounds with low 5-HT2A : D2R coverage such as amisulpride) and slow 5-HT2A receptor coverage reversal, combined with relatively rapid D_2R dissociation, the extreme example being sertindole.

6.5 Conclusions

In conclusion, atypical drugs with a significant affinity for the 5-HT2A receptor such as iloperidone, ziprasidone, risperidone and sertindole have been suggested to represent an advance in reducing the on-target side effect profile of APDs relative to conventional APDs. However, none of these agents shows an improvement on clozapine whose use was restricted in the 1970s due to the increased risk of agranulocytosis a potentially life-threatening (but reversible) off-target side effect and the resulting rising treatment costs associated with regular patient blood monitoring (Leucht et al., 2009; Meltzer 2012). In spite of its underlying problems, clozapine has the widest therapeutic index of all currently available APDs as underlined by its effectiveness in treatment-resistant schizophrenia where higher doses of clozapine are required to reveal a therapeutic effect (Meltzer 2012). Its improved properties in such patients are most likely the result of its 'balanced' 5-HT2A and D_2R blocking profile combined with its potential for rapid D_2R dissociation in both the presence and absence of raised striatal dopamine concentrations. Also, its uniquely high affinity for the muscarinic M_1 receptor may be a crucial factor in its overall low incidence of EPS and is an additional factor worthy of future study. Through its blocking action at the M_1 receptor, clozapine could potentially reduce the effects of increased acetylcholine release, which culminate in an increased incidence of EPS (eg. effects on muscle tone and movement), the direct result of excessive D_2R blockade in the striatum.

Evidently, the ideal AP from a reduced on-target side effect perspective is one which can occupy (over time), a significant proportion of 5-HT2A receptors (i.e. greater than the D_2R threshold for EPS i.e. 70%) in the prefrontal cortex, whilst at the same time transiently occupy striatal D_2 receptors. This study suggests that careful optimisation of both D_2R and 5-HT2A kinetic parameters should lead to the development of APDs with a much improved on target side-effect profile with the potential to create a therapy as effective as clozapine but without its life-threatening side effects. Future work in this area should be perhaps focused around understanding and eliminating other unwanted side-effects of these compounds many of which are off-target, the most debilitating of which is perhaps weight gain.

Such considerations may result in APDs with a much-improved therapeutic profile helping to improve patient compliance and transform APD treatment.

Chapter 7 - Discussion

On-target side effects were common during the very earliest years of clinical practice with conventional APDs, with their prevalence not well understood. Indeed, it was usual practice to administer these agents to the point where side-effects were readily observed, with their occurrence accepted as a marker of clinical efficacy (Weiden 2007; Hippius 1989). Hence the original term neuroleptic rather than anti-psychotic. Clozapine's discovery and its widespread use in the absence of serious on-target side-effects led to the first use of the terms atypical and typical, as a means of distinguishing clozapine unique action from that of conventional APDs. Atypical being now synonymous with agents that do not cause side-effects at clinically effective doses i.e. those effective against the positive symptoms of schizophrenia (Kusumi et al., 2015). Since the discovery of clozapine great efforts have been put into understanding the basis of its atypicality, the hope being that this will lead to the discovery of better agents free from side-effects.

The ‘rapid dissociation hypothesis’ as outlined by Kapur and Seeman is perhaps the most well-known theory put forward to explain the atypicality of certain APDs. This theory strongly suggests a role for binding kinetics in the reduced on-target side effects of APDs, which include EPS and hyperprolactinaemia (Kapur and Seeman 2000; Kapur and Seeman 2001). Side-effects are prevalent because occupancy at the same receptor is required to produce the therapeutic benefits of antipsychotic treatment. This body of work suggests that D_2R dissociation rate plays a key role in separating these compounds into their different classes, atypical and typical, based on their differential kinetic profiles. Atypical agents being those that dissociate faster from the dopamine D_2R.

In this chapter, I will discuss the influence affinity and kinetics has had on our understanding of the actions of APDs, specifically in terms of their on-target side effects. Also, I will discuss the relevance of tracer kinetics for the determination of unlabelled antipsychotic kinetic parameters highlighting the need to first kinetically profile experimental tracers to identify the most suitable ligand for compound profiling of the most rapid and slowly dissociating antipsychotics.

Finally, I will discuss the outcomes from the current profiling study, highlighting the benefits of determining the kinetics of clinically relevant antipsychotics in a single study under physiological conditions. The new kinetic data obtained in conjunction

with findings from a recent meta-analysis comparing clinically used antipsychotics (Leucht et al., 2013) have led to the proposal of a new model based on the concept of drug-receptor rebinding to explain the on-target side effects of these agents. In creating this new theory, I challenge the very essence of the original 'rapid dissociation hypothesis' placing a new emphasis on differences in the association rates of these compounds which were once thought to be practically indistinguishable. Considering this new hypothesis, I will re-interpret the results of in vivo PET studies, which measure relative receptor occupancy in different brain regions and the relationship between APD striatal dopamine D_2R occupancy and side effect profile.

7.1 Drug target occupancy and the role of rebinding

Historically target occupancy is defined by the concentration of free drug available to bind in that system and its K_d, the equilibrium dissociation constant, which relates the rate of association (k1 or k_{on}) and dissociation (k2 or k_{off}) of the drug-receptor pair. However in an open system, such as the human body, a drug may never reach equilibrium with its target and as a consequence it is usually the pharmacokinetics (PK) of the compound which plays the major role in dictating the level of occupancy achieved, and in the absence of slow target dissociation also the duration of receptor occupancy. In a recent simulation study, Vauquelin was able to demonstrate that drug association and dissociation can have similar impacts on the duration of target occupancy if the conditions favouring receptor rebinding predominate (Vauquelin, 2016).

Drug-receptor rebinding occurs in situations where free diffusion is limited and describes the process whereby a reversibly bound compound rebinds to the same or nearby receptor before diffusing away into bulk aqueous. Rebinding is characterised by the establishment of a new dynamic equilibrium between the free target and freshly dissociated drug molecules with k_{on} and k_{off} being replaced by the forward (k_f) and reverse (k_r) rate coefficients of binding. Normally when the conditions of free diffusion operate a molecule dissociates according to its dissociation rate constant (or k_{off}) and it is assumed to simply drift away into bulk aqueous. In contrast when rebinding predominates a drug molecule will undergo

multiple encounters with the initial target or nearby receptors in accordance with the estimated effective reverse rate coefficient (k_r) (Vauquelin and Charlton, 2010). k_r like k_{off} is characteristic of a particular ligand but the calculation of k_r which is situation-dependent takes into account the unique tissue microenvironment of the synapse and integrates both the association and dissociation rate constants to calculate the overall rate of reversal of receptor blockade.

The relevance of rebinding simulations to the in vivo situation have been further expanded recently through the work of de Witte and Vauquelin (de Witte et al., 2016). In the in vivo situation, the PK and tissue distribution will have an important effect on the duration of target occupancy. In particular, it is the rate of elimination from the receptor compartment or the 'micro PK' (Sykes et al., 2014; Vauquelin 2015) that will determine the degree of target occupancy and this, in turn, will determine the overall influence of k_{on} in any rebinding process. Until recently the possibility of target rebinding has been largely ignored and the general paradigm was that if the rate of drug-receptor dissociation is not slower than the rate of unbound drug elimination (overall macro PK) then receptor binding kinetics will play no role in extending target receptor occupancy (Dahl and Akerud 2015). Factors which influence the rebinding process are high target affinities, high receptor density and diffusion restrictions (de Witte et al., 2016, Vauquelin and Charlton 2010). Such restrictions will be dependent on the geometry of the effect compartment with various scenarios already accounted for, the cylinder being representative of the dopamine synapses in the brain (Coombs and Goldstein 2004; Vauquelin and Charlton 2010).

7.2 Formulating competition kinetic binding assays; the unappreciated role of tracer kinetics in successful assay development.

In the context of drug discovery programs receptor binding assays are often formulated using a labelled tracer and a purified or semi-purified receptor preparation. Traditionally they are employed to determine the affinity and to a lesser extent the kinetics of unlabelled competitive ligands. To accurately quantify the kinetics of unlabelled compounds at their target receptors it is necessary to accurately determine the kinetic parameters of the tracer (or L). It has been established that the kinetic characteristics of the tracer employed greatly affects the reliability of measured kinetic parameters, and this potentially represents a barrier to successfully introducing kinetic profiling assays earlier in the drug discovery process (Sykes and Charlton 2012; Klein- Herenbrink et al., 2016).

We initially investigated a series of tracers with different kinetic properties in order to assess their capabilities to determine the kinetic binding properties of compounds which show rapid dissociation from the dopamine D_2R. This preliminary assessment revealed that the most slowly dissociating tracers, eg. spiperone-d2 struggled to consistently assess the kinetics of the most rapidly dissociating compounds using the offline addition protocol. A similar scenario was observed using [^{3}H] spiperone albeit at a lower relative tracer concentration (Klein-Herenbrink et al., 2016).

In order to investigate tracer characteristics further I employed a modelling and Monte Carlo simulation approach to identify the optimal tracer characteristics for determining the kinetics of the range of unlabeled ligands typically encountered during the different stages of a drug discovery program (i.e. rapidly dissociating eg. k_{off} = 10min^{-1} low-affinity “hits” through to slowly dissociating eg. k_{off} = 0.01min^{-1} high-affinity “candidates”).

These modelling studies revealed that for more rapidly dissociating tracers (~k_{off} = 1min^{-1}) the key to obtaining more accurate kinetic parameters is to reduce the assay start-time and the read interval-time. Our ability to quantify these parameters is

largely instrument dependent and reliant on our ability to inject sample whilst simultaneously reading from the same well. In addition, assay sensitivity determines the required sample excitation and emission acquisition times, which subsequently restricts minimal interval-time. Consequently, the option to vary these parameters can be considered as critical factors in the process of determining unlabelled compound kinetics. Thus, not all tracers are equal in terms of their ability to assess the binding kinetics of unlabelled compounds with inaccuracies in tracer characterisation inevitably leading to errors in unlabelled compound kinetic determinations (Bosma et al., 2019).

Determining the kinetics of the unlabelled compounds through the competition association method

Motulsky and Mahan (1984) in their seminal paper described a model for the determination of not only the kinetic K_d of the unlabelled compound but also the kinetic rate parameters (k_{on} and k_{off}) of an unlabelled competitor from non-equilibrium competitive binding studies. The interactions of the tracer and unlabelled competitor with the receptors are described by two differential equations which when solved yield a single equation describing the binding of the tracer as a function of time.

Apart from allowing the determination of the association and dissociation rate constants of the competing ligand, it has allowed us to simulate competitive binding reactions under defined conditions allowing us to answer two very specific and so far unanswered questions regarding the kinetics of competitive tracer binding:

1. What are the optimal tracer kinetic parameters best suited for the accurate screening of low-affinity fragments and late-stage development compounds?
2. What are the minimum interval times required to produce accurate estimates of tracer and unlabelled compound kinetics?

In particular, we were interested to test the limits of this model system in terms of its ability to resolve the binding kinetics of very rapidly dissociating compounds, exemplified by atypical APDs such as clozapine. To my knowledge, the current

study is the first to fully explore these elements and provide clear guidance for the use of this technique at all stages of the drug discovery process.

The assessment of unlabelled compound kinetics proved more complex, for although it was possible to derive accurate rate constant estimates for the majority of conditions, certain tracer-unlabelled ligand combinations failed to return reproducible estimates. As a rule, it was not possible to accurately estimate k_{on} and k_{off} values where the dissociation of the tracer was ≥ 10-fold slower than that of the unlabelled competitor unless the tracer concentration was increased significantly from its customary level (eg. 3x K_d). For example, the accurate estimation of the rate constants of a rapidly dissociating ligand with k_{off} of 1 min^{-1} requires a tracer that is also relatively rapidly dissociating, i.e. in the range of 0.1 min^{-1}. These simulations uncover the limitations of using a more slowly dissociating tracer such as fluorescent spiperone-d2 (k_{off} = < 0.1 min^{-1}) as opposed to the more rapidly dissociating fluorescent PPHT-red (k_{off} = 0.4 min^{-1}) for estimating the kinetics of the more the rapidly dissociation APDs. The initial read time was also critically important to determine the kinetics of unlabelled compounds. Where the simulations were started from 1 sec, mimicking an online injection protocol, the kinetic parameters of unlabelled compounds were generally accurately estimated. In contrast, when measurements were started (sampled) 30 sec after the beginning of the experiment, mimicking offline addition, the estimates were poorer, particularly for rapidly dissociating ligands (eg. 100 and 10min^{-1}) likely to be characteristic of low-affinity fragments. This highlights the importance of collecting data at early time points acquired before equilibrium is established. However, it must be acknowledged that short read interval times will have a negative impact on throughput, which is an important consideration especially when profiling 100-1000s of compounds or fragments where off rates are expected to be very rapid. The decision to employ shorter read times is ultimately a compromise between throughput and the degree of precision required for the accurate resolution of kinetic parameters.

Alternatively employing a higher relative concentration of a tracer (eg. >3x K_d) and testing multiple concentration of unlabelled compound also proved to be a useful approach to improving our ability to accurately quantify the kinetics of more rapidly dissociating compounds. These factors were likely crucial in our attempt to

accurately determine the kinetics of the 5-HT2A antagonists where I employed the tracer at a concentration >10x its own K_d and reduced the dilution of competitor compound from 3 to 2-fold to increase the number of points on the displacement curve leading to improved spatial precision.

These simulation studies demonstrate that for the competitive binding approach to be utilized throughout the different phases of the drug discovery process then the kinetics of the tracer needs to be tailored to the appropriate properties of the unlabelled compounds. Overall, these findings highlight the importance of considering tracer kinetics and assay read start and interval-times when developing competition association assays. Notably, the simulations suggested that under the right conditions, the kinetic parameters of very low affinity (mM) competitors can be measured, providing the opportunity for kinetic fragment-based receptor screens. However, the nature of low-affinity fragments which necessitates high test concentrations and solubility considerations means that increasing the concentration of tracer may not be a viable option. Since any such increase will result in a reduction in the number of low-affinity hits, due to rightward shift of the IC_{50} curves, therefore limiting the available chemical space.

7.3 Comparing equilibrium and kinetic binding data with historical data on APDs

In the field of APD research, the majority of clinically used atypical agents are considered to exhibit much higher affinities for the 5-HT2A receptors over the D_2R (Meltzer et al., 1989; Horacek et al., 2006; Kusumi *et al*., 2015). In contrast typical agents are considered to possess lower relative affinities for the 5-HT2A receptor and so an accurate assessment of this basic pharmacological parameter at these two receptors is essential to their classification within this largely dichotomous paradigm.

Previous dopamine D_2R research has relied primarily upon high affinity radioligands to determine the affinities of compounds for the D_2R (Schotte et al., 1995). The use of such high-affinity tracers has its benefits guaranteeing the lowest possible NSB/specific binding ratios but unfortunately, it comes at a price being confounded by the problems associated with ligand depletion, where the concentration of free ligand in the assay system is significantly lower than that originally added. When ligand depletion occurs in this manner, usually due to a correspondingly high receptor concentration, it is likely to lead to potential inaccuracies in the quantification of labelled and unlabelled compound affinities. For example, the tracer K_d values derived from radioligand saturation experiments will be significantly underestimated. Inaccurate tracer affinity characterisation will lead to subsequent inaccuracies in the determination of unlabelled compound affinities due to the nature of the Cheng-Prusoff correction factor which relies on an accurate assessment of not only tracer concentration but also its affinity (eg. see Equation 2.4 Chapter 2).

To illustrate the potential of ligand depletion to affect APD characterisation I have plotted the K_i values obtained in the current study using low affinity PPHT-red (K_d = 15.4nM) against the K_i values obtained using a low-affinity ([^{3}H]-raclopride, K_d = 1.9nM) versus a high-affinity radioligand ([^{3}H]-nemonapride, K_d = 0.068nM) with data taken from Seeman (2010) see Figure 7.1A and B. It becomes apparent that by using a high affinity radioligand we consistently underestimate the affinities of the unlabelled APDs. Support for this conclusion comes when we consider our characterisation of unlabelled nemonapride, which suggest a much lower K_d of

0.012nM than reported by Seeman (2010). Crucially if we were able to correct for this apparent tracer depletion, we would draw the literature values back towards the line of identity and quash any notion of tracer-dependent affinity predictions (Seeman et al., 1997a).

Most 5-HT2A radioligand binding studies have utilised the 5-HT2A ligand [^{3}H]-ketanserin (K_d = 0.6nM) which has a relatively low affinity for the receptor compared to [^{3}H]-nemonapride binding the dopamine D_2R, so it is perhaps not surprising that in general, our data are more comparable to that that observed in the literature see Figure 7.1C. Contrary to the prevailing view in the literature the equilibrium affinity values I have generated for the D_2 and 5-HT2A receptor suggest, at least for clinically used dopamine-serotonergic APDs, that 5-HT2A affinities for this distinct class of agent are at most 5.4-fold higher eg. sertindole see Table 6.1 Chapter 6.

In summary the use of high affinity radioligands has led to the assumption in the field of neuropharmacology that 5-HT2A affinity values for clinically used atypical APDs are in general much higher than D_2R affinity values (Meltzer et al., 1989; Horacek et al., 2006; Kusumi *et al*., 2015). It is important to note that this finding in no-way invalidates the serotonin-dopamine hypothesis of EPS, which suggests that a higher affinity for the 5-HT2A receptor is protective against both EPS and negative symptoms, but it emphasises the importance of a careful approach to the standardisation of binding assay protocols/procedures through a rigorous characterisation of the tracer. Perhaps, more importantly, it strengthens the original hypothesis of schizophrenia emphasising that blocking the D_2R is at the forefront of the clinical action of these compounds.

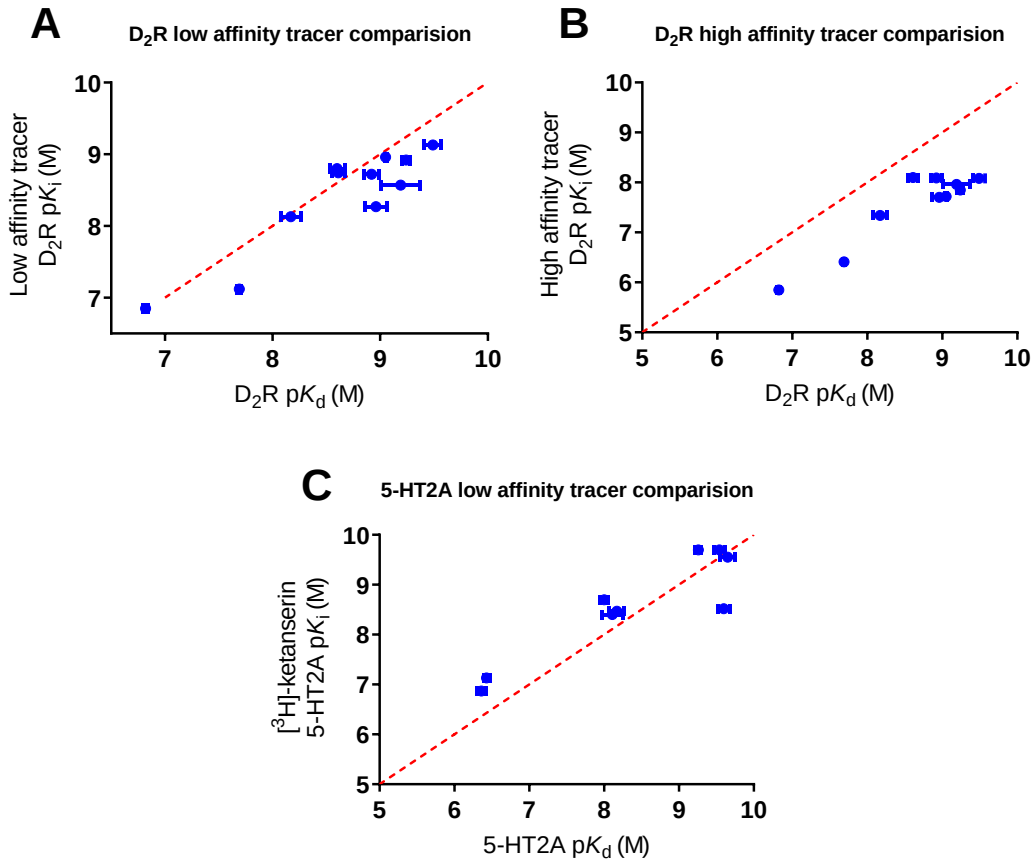


Figure 7.1. **Correlating literature affinity parameters of atypical and typical APDs with dopamine D_2 receptor and 5-HT2A kinetically derived parameters obtained in the current study. (A)** Correlation between APD D_2 receptor kinetically derived affinity values and literature pK_i values obtained with a low affinity tracer ([^{3}H]-raclopride, see Seeman 2010). **(B)** Correlation between APD D_2 receptor kinetically derived affinity values and literature pK_i values obtained with a high affinity tracer ([^{3}H]-nemonapride, see Seeman 2010). **(C)** Correlation between APD 5-HT2A receptor kinetic affinity and pK_i values obtained with a medium affinity tracer ([^{3}H]-ketanserin, see Seeman 2010). The values composing the kinetically derived pK_d (-log(k_{off}/k_{on})) were taken from competition kinetic association experiments as exemplified in Chapter 5 Table 5.1 and Chapter 6 Table 6.1. Data are presented as mean ± S.E.M. from at least 3 separate experiments. N numbers for individual ligands are stated in Chapter 5 Table 5.1 and Chapter 6 Table 6.1. The dotted red line represents the line of identity.

7.4 Historical kinetic data and the relevance of measured dissociation (k_{off}) rates

One of the primary aims of this thesis was to test the 'fast dissociation hypothesis' in the context of a single study capturing all commercially available clinically used APDs, measure their kinetics, and relate these results to other published work and clinical studies.

The kinetic values stated in the literature are dominated by the work of Kapur and Seeman (Kapur and Seeman 2000; Kapur and Seeman 2001 and Seeman 2010) and so I thought it useful for the reader to see a correlation between their reported values and my own measurements. Surprisingly no correlation was observed between the k_{off} values I have generated and Seeman's reported values (Seeman 2010, see Figure 7.2A). Seeman's values were determined by two different methods; using human cloned dopamine D_{2L} receptors and [^{3}H]-APDs, through the addition of an excess of raclopride (100μM) and using a dilution method (the precise dilution factor is not stated) and unlabelled APDs, involving the timed association of [^{3}H]-raclopride, following filtration of the original diluted samples. However, interestingly a good correlation was observed between our measured k_r values and their k_{off} values suggesting that what Seeman may have been measuring is a surrogate for re-binding (see Figure 7.2B). This view is supported by Seeman's earliest attempts to measure the kinetics of APDs in which he describes dissociation experiments with sub-saturating concentrations of dopamine (100nM). As one would predict these rates of dissociation were increased by raising this competing dopamine concentration to μM levels (Seeman and Tallerico 1999).

One major difference between the current study and those of Seeman and colleagues is our use of FRET technology to measure the kinetic parameters of antipsychotic drugs. It must be considered that the large SNAP-tag on the N-terminal of the receptor could have in some way altered the native kinetics of the drugs binding to the human D_{2L} receptor under study. To examine this possibility in more detail I have looked at other literature studies to see if there is any correlations between the current study and those which do not utilise a modified D_{2L} receptor. A study by Langlios utilising four clinically relevant tritiated ligands; risperidone,

palperidone, haloperidol and clozapine, and two different temperatures, conducted in a buffer of similar ionic strength but a higher pH (7.7) to our own, shows a similar rank order of k_{off} measurements to those obtained in the current study Figure 7.2 C. These values being obtained by the addition of a high concentration of raclopride. It is worth noting that the values obtained in the current study appear to match more closely with those obtained at room temperature rather than 37^{o}C. Futher support for the relevance of our kinetic values comes from a competition kinetic study conducted using rat striatal tissue (Carboni et al., 2012). Reassuringly we observe a similar rank order of APD kinetically derived parameters, k_{off}, k_{on}, and kinetic K_d (k_{off}/k_{on}), in line with the values obtained in the current study, see Figure 7.2 D to F. Both of these independent studies conducted using two different methods further strengthen the current findings.

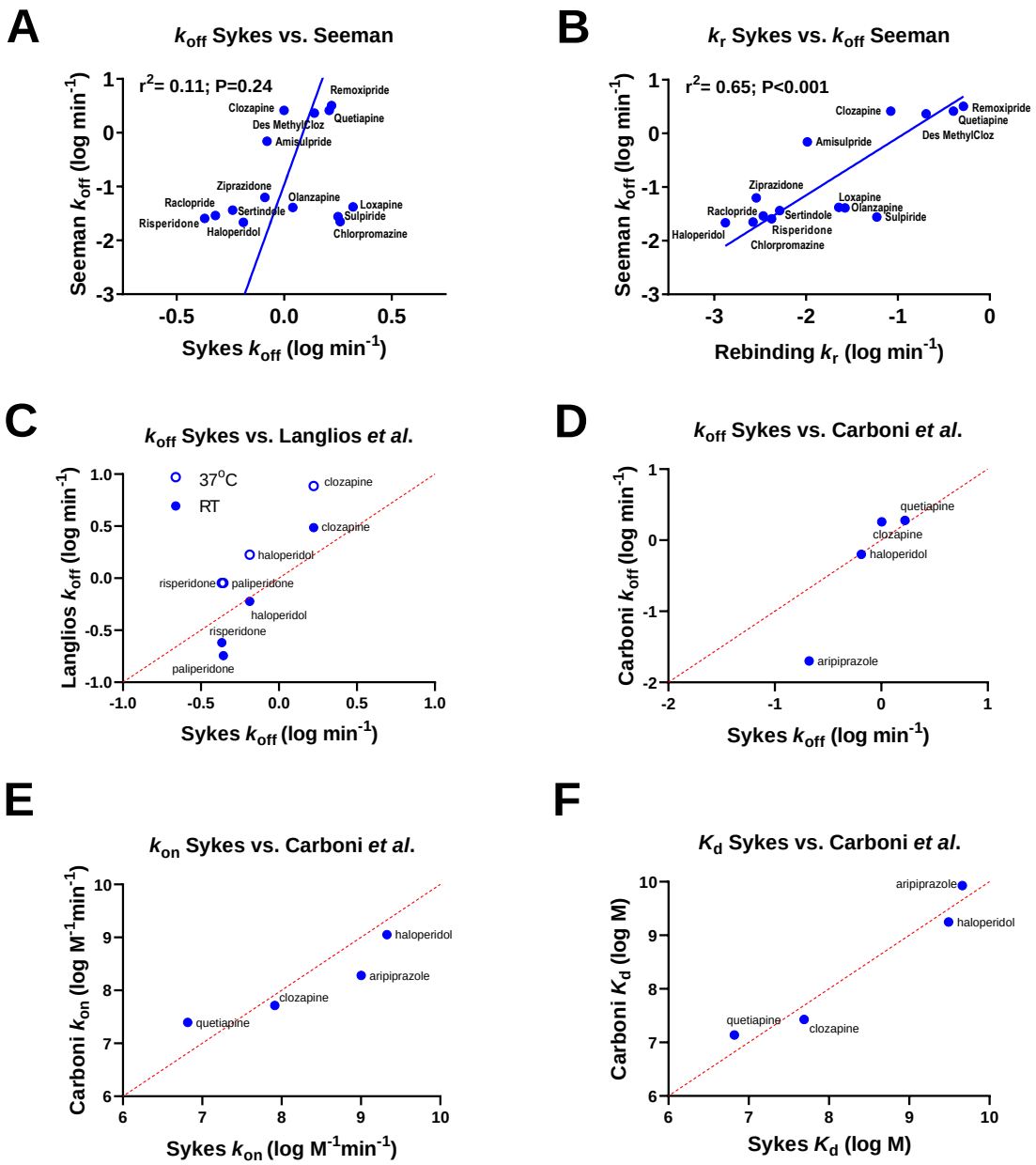


Figure 7.2. Correlating APD dopamine D_2 receptor kinetic parameters with literature kinetic parameters. (A) Correlation between current APD D_2 receptor k_{off} values and literature k_{off} values taken from Seeman 2010. **(B)** Correlation between the current APD D_2 receptor calculated reversal rate (k_r) and k_{off} values taken from Seeman 2010. **(C)** Correlation between current APD D_2 receptor k_{off} values and k_{off} values taken from Langlios et al., 2012. **(D)** Correlation between current APD D_2 receptor k_{off} values and k_{off} values taken from Carboni et al., 2012. **(E)** Correlation between current APD D_2 receptor k_{on} values and k_{on} values taken from Carboni et al., 2012. **(F)** Correlation between current APD D_2 receptor K_d values and K_d values

taken from Carboni et al., 2012. The current log k_{off} and k_{on} and K_d values were taken from competition kinetic association experiments as exemplified in Chapters 3 and 5. All data used in these plots are detailed in Chapter 3 Tables 3.9 and 3.10 plus Chapter 5 Table 5.1. Data are presented as mean from at least 3 separate experiments. n numbers for individual ligands are stated in Chapter 5, Tables 5.1.

7.5 Affinity and the contention that association rates (k_{on}) are constant

Historically, it is the dissociation rate, or k_{off} that is considered the key driver of the drug-receptor complex lifetime *in-vivo* and therefore a key determinant of both therapeutic and on target side effects (Tummino and Copeland 2008; Kapur and Seeman 2001). Atypical APDs have been hypothesized to show reduced EPS due to their rapid dissociation from the dopamine D_2 receptor. However, support for this hypothesis was limited to a relatively small number of observations made across several decades and under different experimental conditions.

Our kinetic studies employing a novel time-resolved fluorescence resonance energy transfer (TR-FRET) assay reveal for the first time the important disconnect between increasing APD affinity and k_{off}. For the least potent APDs tested, affinity is being driven by changes in k_{on} and not by changes in k_{off} as originally asserted by Kapur and Seeman (2000). The significance of this finding is born out of the fact that APD affinity has been used directly to estimate the kinetic rate constant k_{off}, assuming that k_{on} remains constant (Meltzer et al., 2003; Horacek et al., 2006). However, this practice has led to confusion with experimental and theoretical values being directly compared but in the absence of an adequate explanation of their different origins (Horacek et al., 2006). Others have used this original assertion to imply that higher affinity atypical APDs such as olanzapine and risperidone should share kinetic properties similar to haloperidol, rather than the rapid off, lower affinity atypical APDs clozapine and quetiapine (Meltzer 2013). An important finding of the current study is that association rates are not as were previously considered similar for all antipsychotics binding to the D_2R. The current study demonstrates that olanzapine dissociates more rapidly than haloperidol whilst risperidone dissociates more slowly than haloperidol albeit with a slower association rate, reinforcing the importance of using measured kinetic values under physiological conditions over calculated k_{off} rates based on equilibrium affinity.

In trying to understand the propensity of certain APDs to cause EPS, duration of target occupancy needs to be carefully understood. The original ‘fast dissociation hypothesis’ implies that compounds will be more prone to cause EPS as their rates

of dissociation (k_{off}) from the D_2R are reduced promoting the idea that *in vivo* target occupancy for APDs is determined almost exclusively by the rate of drug dissociation (k_{off}) from the D_2 receptor. This misconception has major implications concerning ligand design from a kinetic perspective placing less emphasis on optimising physicochemical parameters which are known to modify k_{on} (Sykes et al., 2019). Indeed, it was the realisation that APD k_{off} rates were by and large a constant factor amongst the clinically used APDs whilst k_{on} was in fact highly variable which led me to explore and eventually formulate the current rebinding hypothesis. The rebinding model employed considers the unique tissue microenvironment of the synapse and integrates both the association and dissociation rates to calculate the overall rate of reversal of receptor blockade (Vauquelin 2010; Vauquelin and Charlton 2010). Figure 7.3 captures all the key features of a model situation designed to recreate a striatal compartment where dopamine D_2 receptor-APD rebinding can occur.

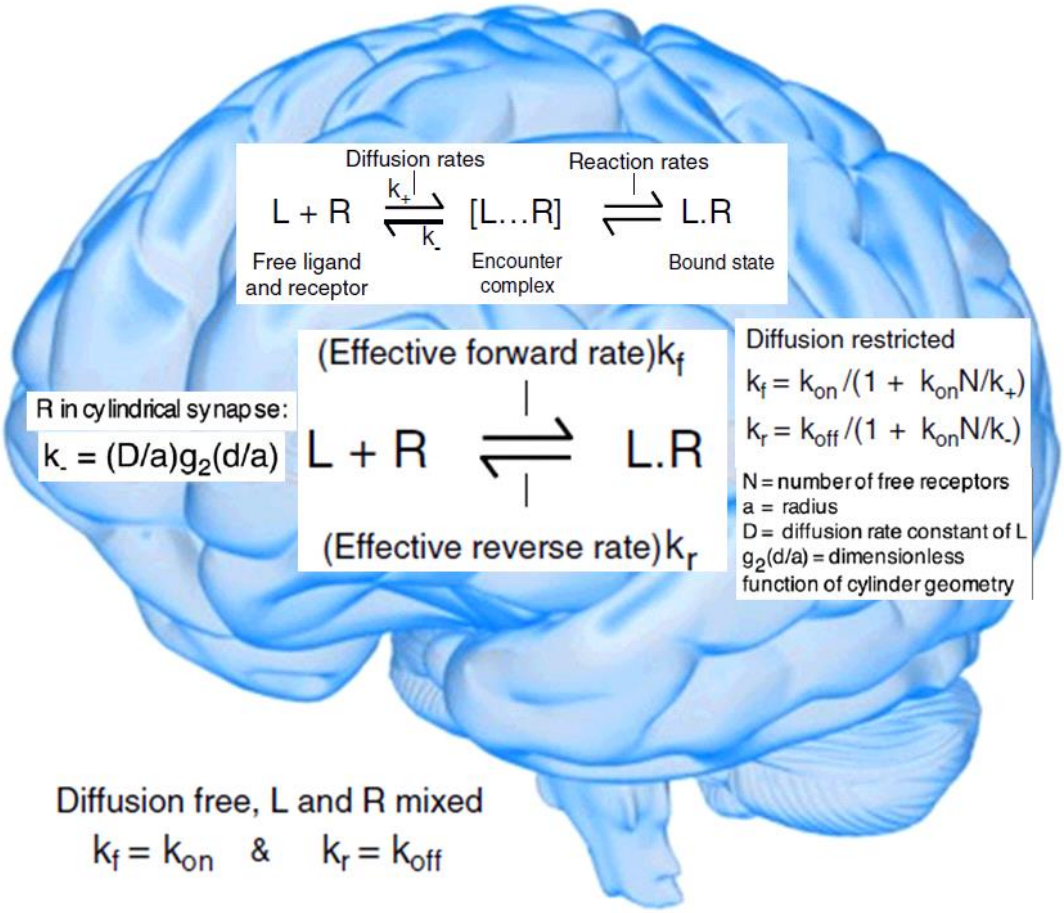


Figure 7.3. Ligand-receptor interactions in a brain micro-compartment. The micro-compartment, in this case, the neuronal synapses of the nigrostriatal dopamine system contains a diffusion boundary with ligand-receptor (LR) binding events characterised by the formation of an intermediate ligand-receptor encounter complex (L...R). A single-step process is sufficient to represent this process with receptor occupation and its reversal governed by the 'effective' forward rate coefficient k_f and the 'effective' reverse rate coefficient k_r. When L and R are homogenously distributed and free to diffuse, a situation closer to events described in the periphery, then these coefficients are equivalent to the 'fundamental' association and dissociation rate constants k_{on} and k_{off}, respectively. k_f and k_r depend on the number of free receptors available or more specifically the receptor density (N) and k+/-, which are not the traditional rate constants for free 3D diffusion of the ligand in solution but rather complex functions thereof being dependent on three factors the radius of the cylinder (a) which mimics the dopamine synapse, the diffusion rate constant of L (D) and a dimensionless function of cylinder geometry ($g_2(d/a)$). For more details see Coombs and Goldstein 2004, Vauquelin 2010, Vauquelin and Charlton 2010, and Vauquelin 2016.

The potential role of k_{on} in dictating ligand dissociation and clinical effect under conditions of limited or hindered diffusion has been previously reviewed (Vauquelin and Charlton 2010; Vauquelin 2016). Hindrance to free diffusion following a pulse of dopamine released from the presynaptic vesicles is created by non-permeable wall-like structures such as the cell membrane and these limitations are exacerbated when the ligand is released into a small membrane surrounding cavity such as that found in the neuronal synapses of the nigrostriatal dopamine system.

One important aspect which this simple rebinding model does not consider is the binding of the endogenous competing agonist dopamine to the D_2R receptor within the synapse. We can surmise that dopamine released from striatal nerves will engage the receptor at relatively low occupancies, with only 30-35% of striatal receptors available, in APD treated patients, based on PET studies (Farde et al., 1992; Kasper et al., 1999). Dopamine itself is a low-affinity ligand, and consequently, it possesses relatively fast-off and on-kinetics (Klein-Herenbrink et al., 2016). Signalling is achieved at sub-saturating occupancy (nM levels of dopamine recorded) potentially as a result of high signal amplification in the striatum (Sulzer et al., 2016). High receptor expression levels in the striatum compared to the limbic system (Hall et al., 1996), will allow dopamine to operate at even lower occupancies (%) and as a consequence dopamine will be relatively immune to slowly dissociating ligands. If such a scenario is true, D_2R antagonism will look competitive and surmountable in the striatum even if an antagonist fails to appreciably dissociate from the receptor. Peak receptor occupancy will be largely dictated by dose, but once free drug concentrations start to fall the phenomenon of rebinding will dictate long term receptor occupancy and the striatal-dopamine response.

EPS was robustly predicted by the rebinding model that considers the unique microenvironment of postsynaptic D_2 receptors and integrates association and dissociation rates to calculate the net rate of reversal of receptor blockade. In direct contrast, prolactin elevation was seemingly controlled by the dissociation rate as outlined in the original fast dissociation hypothesis. This result goes against current dogma which suggests that compound dissociation rate (k_{off}) determines a compounds liability to produce both EPS and prolactin increases, but reassuringly it falls in line with the theoretical rebinding model presented above. To illustrate this

disconnect in side effect profile I have plotted the prolactin increase standardised mean difference (SMD) against the EPS odds ratio. This disconnect occurs since EPS is mediated in the striatum (a central effect) where rebinding is prevalent whereas prolactin secretion is controlled at the level of the pituitary (peripheral effect) by freely circulating dopamine (Figure 7.4). Thus, optimizing the binding kinetics of future APDs for both peripheral and central side-effects mediated through the D_2 receptor may result in compounds with a vastly improved therapeutic profile.

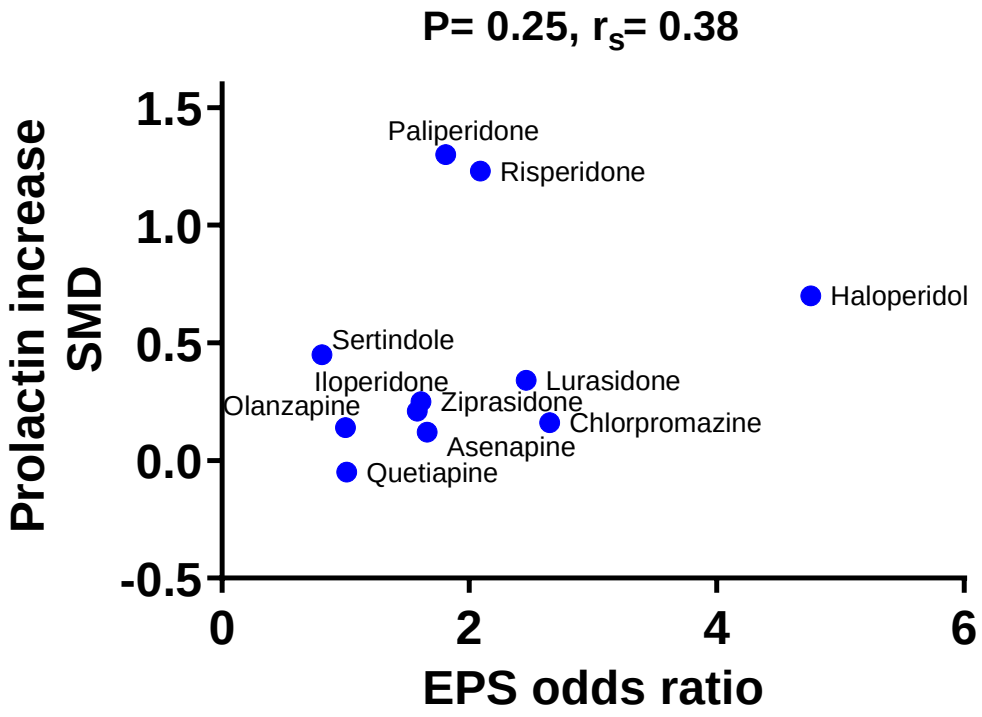


Figure 7.4. Relationship between the incidence of APD clinical EPS and prolactin secretion. EPS is shown as the odds ratio value and prolactin increase as standard mean difference (SMD). Data are taken from Leucht et al., 2013**.**

Interestingly the partial agonist aripiprazole would appear to be effective at inhibiting prolactin release (see Leucht et al., 2013) this in spite of its relatively slow dissociation from the D_2 receptor (Klein-Herenbrink et al., 2016) suggesting that this compound does not behave as a functional antagonist, in the periphery, but instead mimics the action of endogenously released dopamine.

Aripiprazole has been shown in PET studies to achieve higher D_2R occupancies in the striatum but not to cause EPS like symptoms (Yokoi et al., 2002), with direct comparisons made in rats with haloperidol and risperidone (Natesan et al., 2006). This suggests that aripiprazole's partial agonist effect prevents this particular side-effect (as it does prolactin release) (Natesan et al., 2011). These same PET studies suggest that aripiprazole cannot be acting through 5-HT2A receptors to achieve this effect as it affinity and corresponding PET occupancy is much lower at 5-HT2A receptors (Mamo et al., 2007). In this respect its mechanism of action can be readily distinguished from that of sertindole which also occupies a relatively high proportion of D_2R (~68%) in the striatum based PET studies but also a significant proportion of 5-HT2A receptors (Bigliani et al., 2000; Tauscher et al., 2002; Travis et al., 1997).

Aripriprazole, although a D_2R agonist, does not worsen schizophrenia where it appears to act mainly as a functional antagonist, blocking the actions of the higher efficacy endogenous agonist dopamine. This differential action in different tissues is likely related to the lower density of D_2R in the temporal cortex (limbic region), which has been estimated to be 1.5% of that in the putamen (striatum), so here it is more likely to behave as a functional antagonist (Kegeles et al., 2008; Hall et al., 1996). Also, dopamine concentrations in the temporal cortex (compared to the striatum) have been suggested to be much lower (nM cf to μM) which potentially favours its functional antagonist effect (Seamans and Yang 2004; Seeman et al., 1997a).

In terms of drug safety profile, these findings have major implications for the understanding of on-target toxicity which occurs when side-effects result from either extended blockade or over-stimulation of the therapeutic target. Specifically, these results suggest that on-target toxicity, at least in the brain where diffusion is limiting must be reconsidered in terms of the propensity of a drug to rebind receptors in

different regions of the brain. Each area of the brain is likely to differ significantly in terms of the degree to which rebinding plays a role in dictating a drugs receptor occupancy since the main controllers of drug rebinding, receptor numbers (density) and compartment dimensions (geometry) are likely to vary considerably. The effect of receptor density on the effective reverse rate coefficient (k_r) for a series of clinically used APDs is shown in Figure 7.5. In this model, based on an immunological synapse, each drug is uniquely sensitive to receptor number for example clozapine's k_r value is relatively insensitive to changes in dopamine receptor density at the lower end ($1x10^9$ - 10^{10} cm^{-2}), whereas, the typical antipsychotic haloperidol is more or less equally sensitive at all receptor densities studied ($1x10^9$ - 10^{12} cm^{-2}).

This work strongly suggests that it may be possible to target specific areas of the brain containing higher relative receptor concentrations (Hall et al., 1996) or make use of the differing levels of competing neurotransmitters in the different brain regions (Seamans and Yang 2004; Kegeles et al., 2007) and in so doing achieve a degree of tissue selectivity.

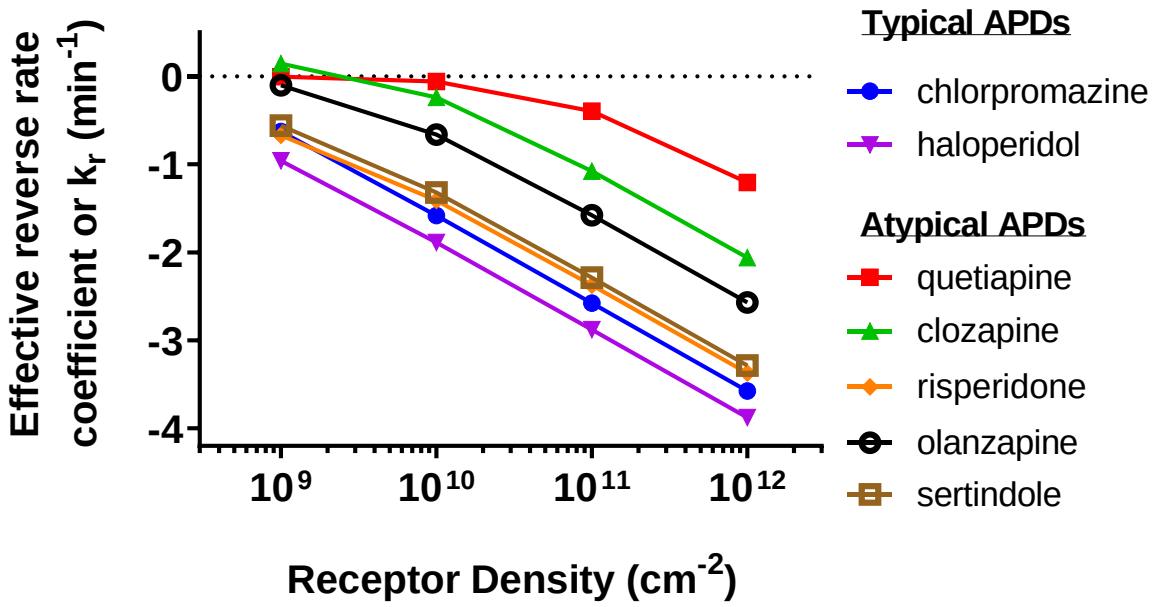


Figure 7.5. The effect of dopamine D_2R density on the rate of APD receptor reversal (k_r). k_r values were modelled based on an immunological synapse, with a compartment volume of 0.176 μm^3, which is within the range described for the dopamine synapse (Coombs and Goldstein 2004). In this model, the overall macroscopic reversal rate (k_r) is described by the following equation; $k_r = k_{off}/(1+ k_{on}$ *R/k-), where: k_{off} = dissociation rate from the receptor (sec), k_{on} = association rate onto the receptor cm^3/sec, [R] = surface receptor density, varied from 1x10^9 to 1x10^{12} cm^{-2}, and k- = the diffusion rate out of the synaptic compartment into bulk aqueous, fixed at 1.2x10^{-5} cm/sec. k-, the diffusion rate out of the synaptic compartment into bulk aqueous is written in the form k- = (D/a)g2(d/a). The value of k- chosen is based on the immunological synapse (Coombs and Goldstein 2004). k- = 1.2 x 10^{-5} cm/sec and is calculated based on a diffusion coefficient of 1 x10^{-6} cm^2/sec (Nicholson and Rice, 1991) where g2(d/a) is a dimensionless function of the immunological synapse with a radius (a) = 2 μm and the distance between synaptic surfaces (d) = 14 nm, such that g2 = 2.6 x 10^{-3}, values taken from Coombs and Goldstein (2004).

7.6 Role of the 5-HT2A receptor in the reduced incidence of side effects

To expand upon on this unique discovery that the process of rebinding might play a key role in the development of EPS, I have attempted to quantify the kinetics of clinically used APDs at other key serotonin receptors originally postulated to be involved in the modulation of EPS, namely serotonin 5-HT2A and 5-HT1A receptors.

Certain atypical APDs have been hypothesized to show reduced EPS due to their ability to promote nigrostriatal dopamine release, through 5-HT2A receptor blockade (Meltzer et al., 1989; Schotte et al., 1996). The strength of this hypothesis was limited to a consideration of the relative receptor affinities of clinically used APDs for the 5-HT2A and dopamine D_2R.

In Chapter 6 I described how we measured the 5-HT2A and 5-HT1A kinetic binding properties of a series of typical and atypical APDs in two novel time-resolved fluorescence resonance energy transfer assays and correlated these properties with their observed EPS at therapeutic doses. For compounds with negligible affinity for 5-HT2A receptors, EPS was robustly predicted by a D_2R specific rebinding model that integrates D_2R association and dissociation rates to calculate the net rate of reversal of receptor blockade (k_r). However, for certain compounds, a combination of high relative 5-HT2A occupancy controlled through a rebinding process, and rapid dopamine D_2R dissociation, in the face of raised levels of dopamine equates to a reduced propensity to cause EPS.

There was positive correlation (r_s = 0.99) between the measured 5-HT2A : D_2R affinity ratio and the projected 5-HT2A : D_2R area under the curve ratio between a striatal D_2R occupancy level of 80-65% (i.e. those thought relevant to the prevalence of EPS). However, as observed in Figure 7.6 there is seemingly a limit to which differential affinity and its dynamic counterpart receptor rebinding can modulate overall APD D_2 and 5-HT2A receptor target coverage. Sertindole and paliperidone have very similar profiles and yet paliperidone treated patients suffer from more EPS, despite its lower rebinding potential. Sertindole therefore stands out as the one compound where slow dissociation from the 5-HT2A receptor could be

significantly contributing to its low incidence of EPS despite its relatively strong D_2R rebinding potential.

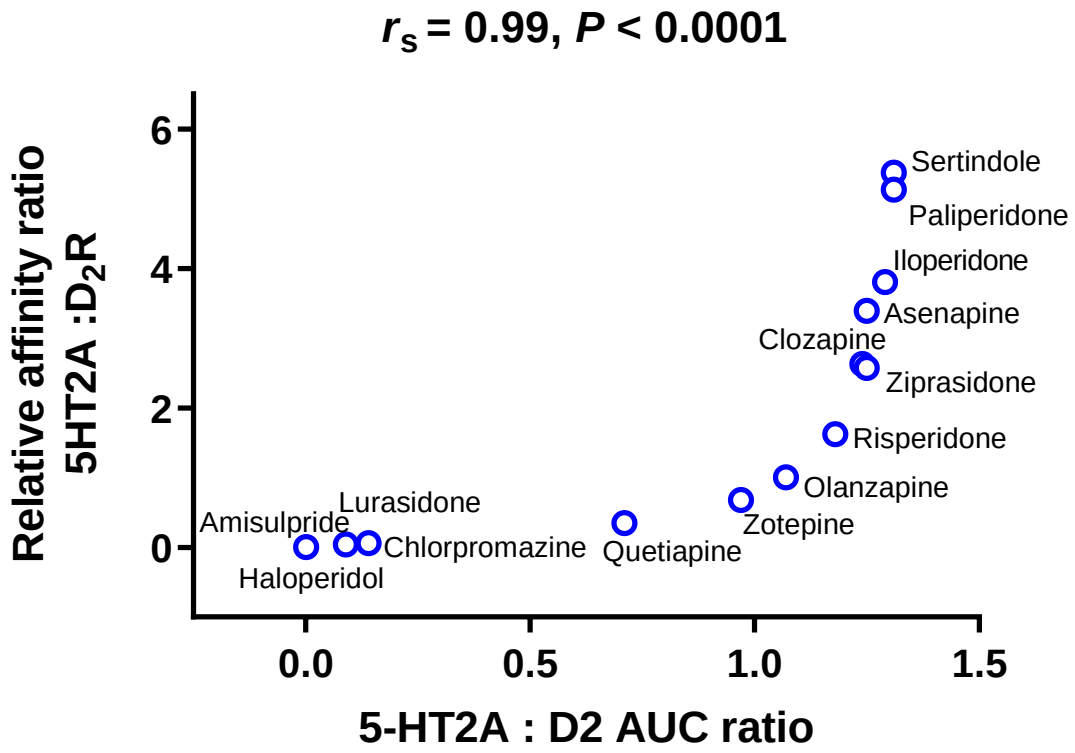


Figure 7.6. The relationship between the 5-HT2A : D_2R affinity ratio and 5-HT2A: D2R AUC ratio between a striatal occupancy of 80-65%. Correlation exists between the measured 5-HT2R : D_2 affinity ratio and the projected 5-HT2A: D_2R AUC ratio estimates between a striatal occupancy D_2R occupancy level of 80-65% (i.e. those thought relevant to EPS). However as observed in the figure there is seemingly a limit to which affinity and differential receptor rebinding itself over this limited, but, crucial occupancy range, can modulate overall D_2 and 5-HT2A receptor target coverage. All data used in these plots are detailed in Chapter 5 Table 5.1 and Chapter 6, Table 6.1 and 6.2. Data are presented as mean from at least 3 separate experiments. N numbers for individual ligands are stated in Chapter 5 Table 5.1 and Chapter 6, Table 6.1 and 6.2.

7.7 Functional data supporting the dopamine D_2R kinetic measurements

The 'fast dissociation hypothesis' explaining the reduced incidence of EPS for atypical APDs can in principle be verified experimentally through functional experiments involving D_2R activity measurements. Compared with binding experiments functional assays yield less direct information about the molecular characteristics of the antagonist-receptor pair but potentially provide more relevant information about their likely effects *in-vivo*. Whole-cell functional data questioning the notion that the rate of reversibility of D_2 receptor antagonism is the key to distinguishing atypical from typical antipsychotics has recently been presented by Sahlholm and colleagues (Sahlholm et al., 2014; Sahlholm et al., 2016). Sahlholm and colleagues employed an indirect functional readout using recombinant oocytes expressing the human D_2R to assess the binding kinetics of a series of clinically used APDs. Using an electrophysiological approach, they measured the activation of inwardly rectifying potassium channels (GIRK) as a surrogate of agonist binding to the D_2R. Performing these experiments in the presence of APDs and employing a washout step they were able to estimate the on and off-rates of these ligands. By reapplying agonist and assuming a competitive binding process, they surmised that the rate of response recovery should reflect the rate of antagonist dissociation since the (k_{off}) of the antagonist would be limiting the rate of agonist access to the receptor.

Figure 7.7 shows the correlation between competition association assay derived k_{off} and k_{on} values and indirectly measured values taken from Sahlholm et al., 2016. Reassuringly a good correlation was observed between these two independently generated data sets, the one outlier being remoxipride. A full explanation for this discrepancy is provided in Sykes et al., 2018. Overall these findings replicate the competition association derived binding data generated through a more conventional approach and add substance to the view that the very early attempts to estimate the kinetics of APDs by Seeman and colleagues may have generated largely erroneous values.

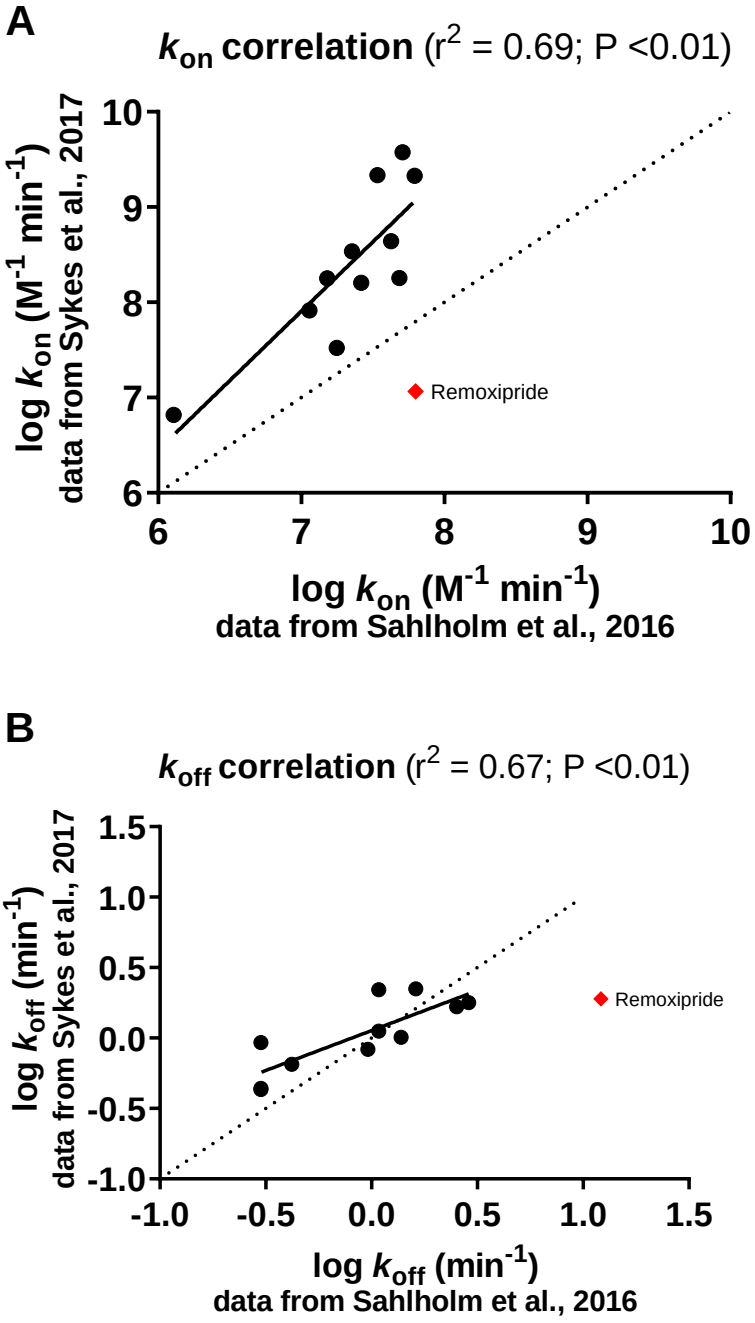


Figure 7.7. Correlating APD dopamine D_2 receptor kinetic parameters with literature kinetic parameters derived from functional studies. Correlation between **(A)** literature functional derived APD D_2 receptor log k_{on} and log k_{on} values measured using the competition association binding method. Correlation between **(B)** literature functional derived log k_{off} values and log k_{off} values measured using the competition association binding method (literature data taken from Sahlholm et al., 2016). The log k_{on} and k_{off} values were taken from competition kinetic association experiments as exemplified in Chapter 5. All data used in these plots are detailed in

Chapter 5, Table 5.1. Data are presented as mean from at least 3 separate experiments. N numbers for individual ligands are stated in Chapter 5, Tables 5.1.

7.8 Cinical data supporting the rebinding hypothesis

The above treatment of APD kinetics in conditions of limited diffusion is theoretical, but to be valid there should be clinical evidence to support such a shift in kinetic emphasis which would effectively re-define the 'fast dissociation hypothesis'. And indeed if the suppositions I have made are in any way true then ligands with more rapid k_{on} rates should, in theory, be more prone to rebind to the D_2 receptors both *in vivo* and *in vitro.* Human PET studies have demonstrated significant differences in the rates of decay of D_2R target coverage which based on the known receptor dissociation (k_{off}) and PK halve lives of these compounds can only be accounted for by differences in the rates of re-binding of these compounds (Seeman 2002; Tauscher et al., 2002).

Further evidence for a differential rebinding process for APDs at D_2R and 5-HT2A receptors is supported by PET data which shows the sustained 5-HT2A receptor occupancy of the archetypal atypical APD risperidone and olanzapine, relative to dopamine D_2R occupancy, this despite their very similar affinities for both receptors (see Figure 7.8, data taken from Tauscher et al. 2002). All things being equal and assuming that plasma concentrations reflect the free concentration of drug in the brain, the difference between the plasma and dopamine D_2R and 5-HT2A levels of receptor occupancy could be taken as a relative indicator of the receptor rebinding potentials of these drugs. The influence of k_{on} in this rebinding process is evident when we compare the rates of change in D_2R and 5-HT2A occupancy for the atypical APDs risperidone and olanzapine with risperidone having the greatest D_2 and 5-HT2A receptor rebinding potential as judged by both the PET data (Figure 7.8) and the in-vitro D_2R and 5-HT2A kinetic binding data. Similar findings with other atypical agents have been reported supported with detailed studies in animal models (Kusumi et al., 2015).

This phenomenon of rebinding has been readily demonstrated in rat striatal slices using the [^{3}H]-SCH23390 a high-affinity dopamine D_1 radiotracer (Gifford et al., 1998). With very slow apparent dissociation from receptors being observed, following infinite dilution in the absence of a competing ligand, very much

reminiscent of the PET data obtained when studying high-affinity D_2 APDs such as haloperidol in the human brain (Seeman 2002).

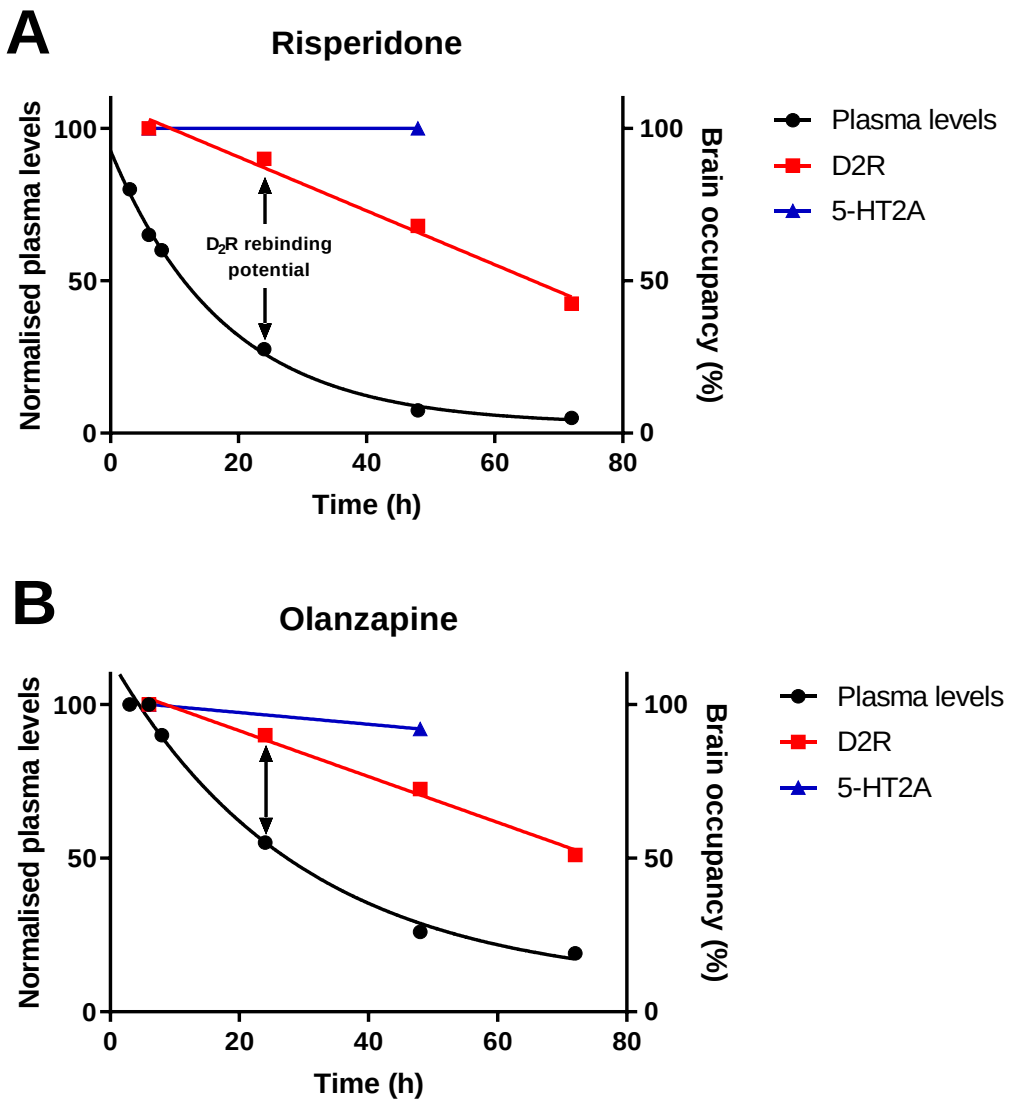


Figure 7.8. PET studies of human 5-HT2A and D_2R occupancy. Positron emission tomography (PET) imaging and blood sampling in healthy controls for **(A)** risperidone and **(B)** olanzapine. Plasma levels of both drugs gradually reduce over the 72hours. Human striatal occupancy of dopamine D_2 receptors by risperidone and olanzapine (determined using [^{11}C]raclopride) drops off more gradually over the measurement period (~ 72 hours). In contrast, despite risperidone's and olanzapine's similar receptor affinity for the 5-HT2A receptor they maintain cortical 5-HT2A occupancy (determined using [^{11}C]setoperone) over the first 48 hrs. Arrows indicate the magnitude of the dopamine D_2R rebinding potential. All results are normalized to 100% of their peak value and redrawn from Tauscher et al. 2002.

7.9 Limbic selectivity is rebinding the driver

Current effective APD treatment is designed to block dopamine receptor signalling in the limbic region of the brain producing a reduction in the positive symptoms eg. altered perception and hallucinations, which characterise this relatively common (1% of the population) and socially debilitating disease. It has been suggested on numerous occasions that for the majority of clinically used APDs at least 65% occupancy of striatal D_2 receptors is required to achieve a therapeutic effect (Ginovart and Kapur 2012; Kapur et al., 2006). D_2 receptor occupancy studies also suggest that striatal receptor occupancy above a certain threshold (~70%) leads to an increased incidence of EPS (Farde and Nyberg 1998; Kasper et al., 1999). Thus, it is often proposed that there is a very narrow range of clinically effective doses, which is largely responsible for treatment complications, at least in terms of on-target side-effects (Tandon and Jibson 2002; Ginovart and Kapur 2012). In contrast clozapine and quetiapine, two atypical antipsychotics with a reported lower incidence of EPS are clinically effective at lower levels of D_2R occupancy in the 40% range (Kapur and Seeman 2001; Kapur et al., 2000b). This picture may not be so simple since the time at which striatal occupancy is assessed seems to be crucial, with measurements taken for clozapine at 2h showing >70% occupancy (Kapur and Seeman 2001). Thus, clozapine would appear to produce a robust antipsychotic effect despite only briefly blocking D_2R neurotransmission in the striatum.

Indeed, clozapine's unique mode of action has been suggested to stem from what has been termed limbic selectivity first identified in animal studies (Zivkovic et al., 1975; Stawarz et al., 1975) and confirmed in PET studies (Pilowsky et al., 1997; Erlandsson et al., 2003). Essentially this is the idea that the efficacy of APDs stems from their ability to block D_2R in the limbic region of the brain, with limbic selectivity resulting in a lower incidence of side-effects due to lower APD binding in the striatum. This idea of limbic selectivity builds upon the work of Bartholini (1976) who identified that clozapine and sulpiride preferentially affect limbic dopaminergic transmission when compared to haloperidol and chlorpromazine. Others have shown in rats that the effects of the atypical APDs clozapine and sulpiride, on exogenously applied dopamine, appear to fade faster in the striatum (putamen), compared to the limbic regions (nucleus accumbens and tuberculum olfactorium)

(Costall and Naylor 1976). This relationship between striatal and limbic regions has been studied in more detail in subsequent PET studies in which multiple APD comparisons were presented (Xiberas et al., 2001; Bigliani et al., 2000; Bressan et al., 2003 and 2004; Stone et al., 2005).

The temporal cortex is often used as a surrogate for the limbic system and was targeted for APD binding measurements in the above studies. Regional binding indices (% bound) were calculated to estimate the relative levels of radioactivity in the temporal cortex and striatum of the treatment groups. Figure 7.9A shows data from published clinical PET studies and demonstrates how a selection of clinically relevant APDs are all effective at blocking D_2R in this region of the brain (binding >75%). However atypical drugs such as clozapine display a characteristic reduction in striatal blockade indicative of this so-called limbic selectivity as described above Figure 7.9A. Figure 7.9A and B demonstrates that limbic selectivity is not necessarily exclusive to atypical APDs. Typical APDs such as haloperidol can display the same phenomenon of limbic selectivity when their dose is reduced Figure 7.9B. Albeit not to the same degree as the more rapidly reversible (higher k_r value) atypical agents. This apparent effect of dose on regional D_2R occupancy has direct repercussions for the treatment of patients since such an intervention has the potential to lower the incidence of side-effects eg. EPS and perhaps improve treatment compliance. The notion of limbic selectivity is not without its critics with others suggesting that occupancy by atypical ligands is only lower in the ventral midbrain/substantia nigra region (Kessler et al., 2005). These areas being involved in motor function and movement.

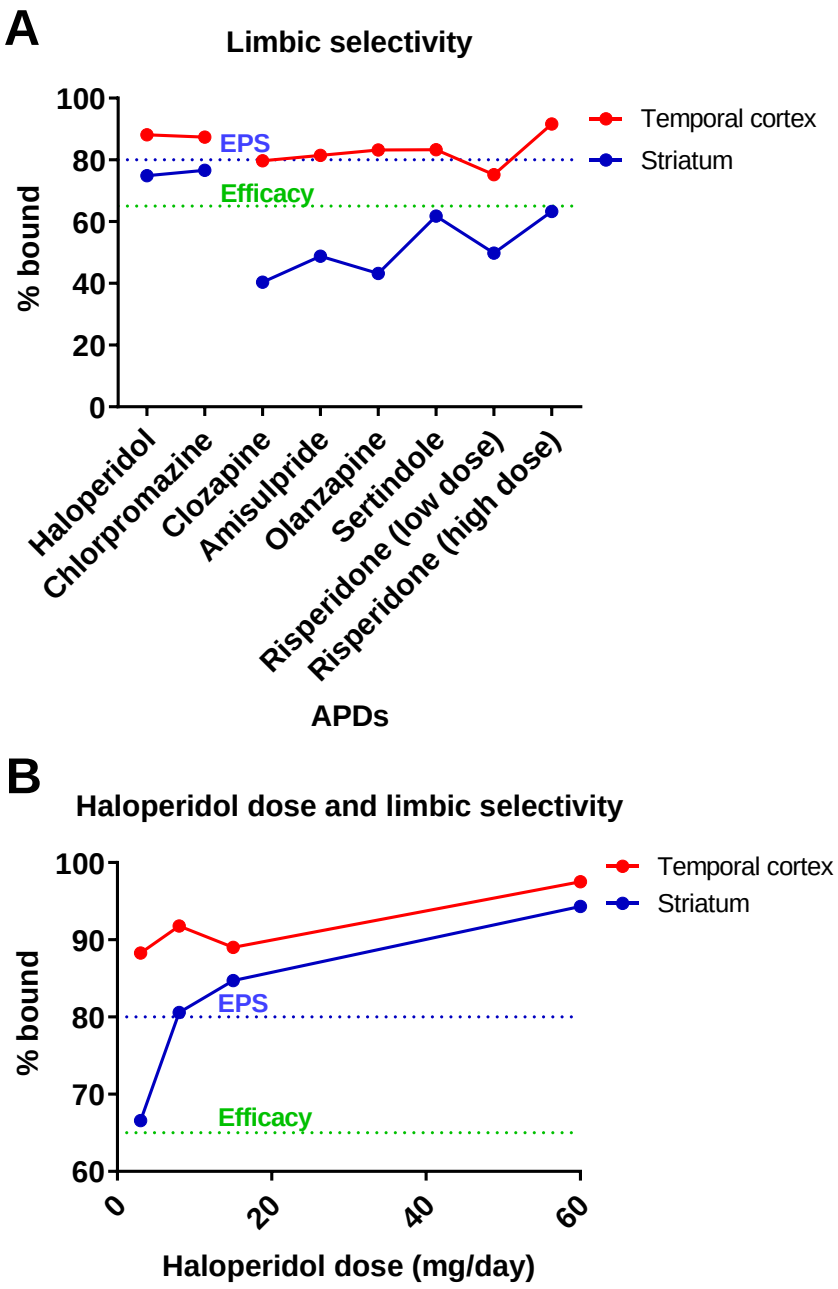


Figure 7.9. The phenomenon of limbic selectivity and its apparent relationship with APD dose. (A) Temporal cortex (limbic) and striatal binding values (%) for different clinically relevant APDs. **(B)** Relationship between haloperidol dose and temporal cortex and striatal binding values. APD temporal cortex (limbic) and striatal binding values (%) were obtained from 4 separate studies Xiberas et al., 2001; Bigliani et al., 2000 and Bressan et al., 2003 and 2004. The blue dotted line at 80% occupancy represents the level of D_2R APD binding thought to be indicative of EPS. The green dotted line at 65% occupancy represents the levels of APD D_2R occupancy in the striatum required to produce clinical efficacy.

In consideration of a role for 5-HT2A receptors in the reduced incidence of side-effects it is important to understand their proposed role in dopamine transmission in the relevant parts of the brain. Presynaptic serotonin (5-HT2A) receptors on dopaminergic neurons could, in theory, inhibit dopamine release in the prefrontal cortex and striatum, but not in the limbic system (Longhurst 1997). If such a scenario is correct then 5-HT2A receptor antagonists should release dopaminergic neurons from this inhibition, which will result in increased dopamine concentrations in the striatum and prefrontal cortex (Longhurst 1997; Stahl 2013). Such an effect will have direct therapeutic implications in terms of reducing APD negative side effects and EPS.

The idea of limbic selectivity under the control of dopamine release mediated by the 5-HT2A receptor blockade might suggest that the beneficial role of the 5-HT2A receptor is to facilitate dopamine release in the striatum. This, in turn, would potentially affect the clearance of atypical APDs such clozapine from the striatum culminating in a reduction in the observed incidence of EPS (Pilowsky et al., 1997; Erlandsson et al., 2003). However, there is good evidence against this being the sole contributing factor. For example it has been shown that the property of limbic selectivity is not unique to serotonin-dopamine antagonists and occurs with the D2/3 selective antagonist amisulpride and to a certain extent haloperidol at lower doses see (Figure 7.9A and Schoemaker et al., 1997), an indication perhaps that D_2 receptor-specific rebinding is the overriding factor in promoting the phenomenon of limbic selectivity. Also and perhaps more importantly dopamine concentrations in the striatum are unlikely to reach sufficient concentrations to drastically affect the process of rebinding. It has been estimated using a carbon-fibre microelectrode that the maximal amplitude of the dopamine overflow in the rodent striatum in vivo is only in the range of 100–400 nM (Sulzer et al., 2016). Whereas full saturation of the dopamine receptor is thought to occur in the mM range, the implication being that theses ‘spare’ receptors prevent a significant reduction in APD concentrations in the synapse. These rodent striatal values of dopamine concentration are consistent with functional D_2R responses which are known to occur in the nM range (Klein-Herenbrink et al., 2016). Interestingly dopamine concentrations in the limbic system have been estimated to be even lower in the nM range (Kegeles et al., 2008), a finding which could partly explain limbic tissue specific APD selectivity.

7.10 A role for the 5-HT2C receptor in reduced EPS

The 5-HT2A-D2 receptor theory of APD atypicality is not without its detractors with animal research suggesting that antagonism at the 5-HT2C receptor may be responsible for the reduced incidence of EPS observed with clinically used APDs (Reavill et al., 1999; Alex et al., 2005; Alex and Pehek 2007). Supporting evidence for a role of 5-HT2C antagonism is provided by 5-HT2C/D2 affinity correlations (Richtand et al., 2007). Proof for such a mechanism can be found in rodent in-vivo studies in which 5-HT2C receptor-specific antagonists have been shown to increase dopamine output in the striatal area an effect which is thought to be linked to their reduced EPS profile (reviewed in Alex and Pehek 2007). Also, in a mouse model of cataplexy (a surrogate for EPS), 5-HT2A receptor knock-out did not affect the sensitivity of these animals to increasing doses of risperidone or a fixed dose of clozapine, suggestive that 5-HT2A receptor blockade is not necessarily protective against EPS (Reavill et al., 1999). However, until more selective serotonergic receptor tools become available then the original D2-5-HT2A theory of Meltzer et al. (1989) is likely to remain largely unchallenged. Interestingly a more recent discussion on the topic of APD induced EPS refers globally to 5-HT2A/C receptor blockade an indication perhaps of a lack of consensus on the precise receptor subtype involved (Ohno et al., 2013). And based on the apparent similarities in 5-HT2A and 5-HT2C binding affinities in the literature I cannot rule out a potential role for 5-HT2C receptor blockade in the control of dopamine release in the striatum (Herrick-Davis et al., 2000; Guiard and Giovanni 2018). In terms of in vivo effects, in rats the clinically effective APDs, sertindole, olanzapine and risperidone inhibited quipazine-induced effects (a model of 5-HT2A activation) more potently than the MK 212 discriminative stimulus (a model of 5HT2C activation) suggesting that for certain atypical APDs 5-HT2A effects will predominate at clinically effective doses of APDs (Sánchez and Arnt 2000).

Besides, the fact that aripiprazole, a partial D_2R agonist and 5-HT2A antagonist, with low EPS potential, is also a 5-HT2C agonist would suggest that 5-HT2C blockade is not an essential pharmacological property for such an effect (Felsing et al., 2019). Furthermore pimavanserin, a 5-HT2A selective antagonist has been shown to reduce the levels of EPS produced by the typical antipsychotic haloperidol

(Meltzer et al., 2012). Similarly, pimavanserin reverses the psychotic-like behavioural deficits in a model of Parkinson's disease psychosis, without disrupting motor behaviours, suggesting that 5-HT2A selective blockade does not further reduce dopamine signalling in the striatum (McFarland et al., 2011). And finally, 5-HT2C agonists have been shown to have positive effects in schizophrenia models suggesting that 5-HT2C blockade could be a disadvantageous treatment factor with non-selective atypical agents (Huang et al., 2011).

7.11 Does k_{off} or k_r play a role in limbic selectivity?

Kapur and Seeman (2002) in direct response to the paper by Xiberas et al., 2001 which supports limbic selectivity, suggested that the more rapid k_{off} of these drugs may account for this apparent regional selectivity. We now know that rebinding is more likely to control the efflux of drugs out of the striatum so, in theory, we should be able to test this using the data provided by Xiberas and colleagues and other studies where regional measurements of D_2R occupancy has been recorded. Figure 7.10A shows a plot of rebinding (k_r) versus the relative ratio of the binding index (eg % bound temporal cortex/% bound striatum). % bound in the temporal cortex is an indicator of limbic brain binding and the ratio an indicator of regional brain selectivity. In this situation, this ratio is likely to be more appropriate as it will account for different levels of tracer loading in the brain (i.e. unequal dose equivalents). As shown the relationship of APD D_2 receptor the dopamine D_2R rebinding reversal parameter (k_r) and APD binding ratios (% bound temporal cortex/striatum) is largely linear suggesting that rebinding may be a factor in the observed limbic selectivity. In contrast, there was no apparent relationship with measured dissociation rate (k_{off}) see Figure 7.10B.

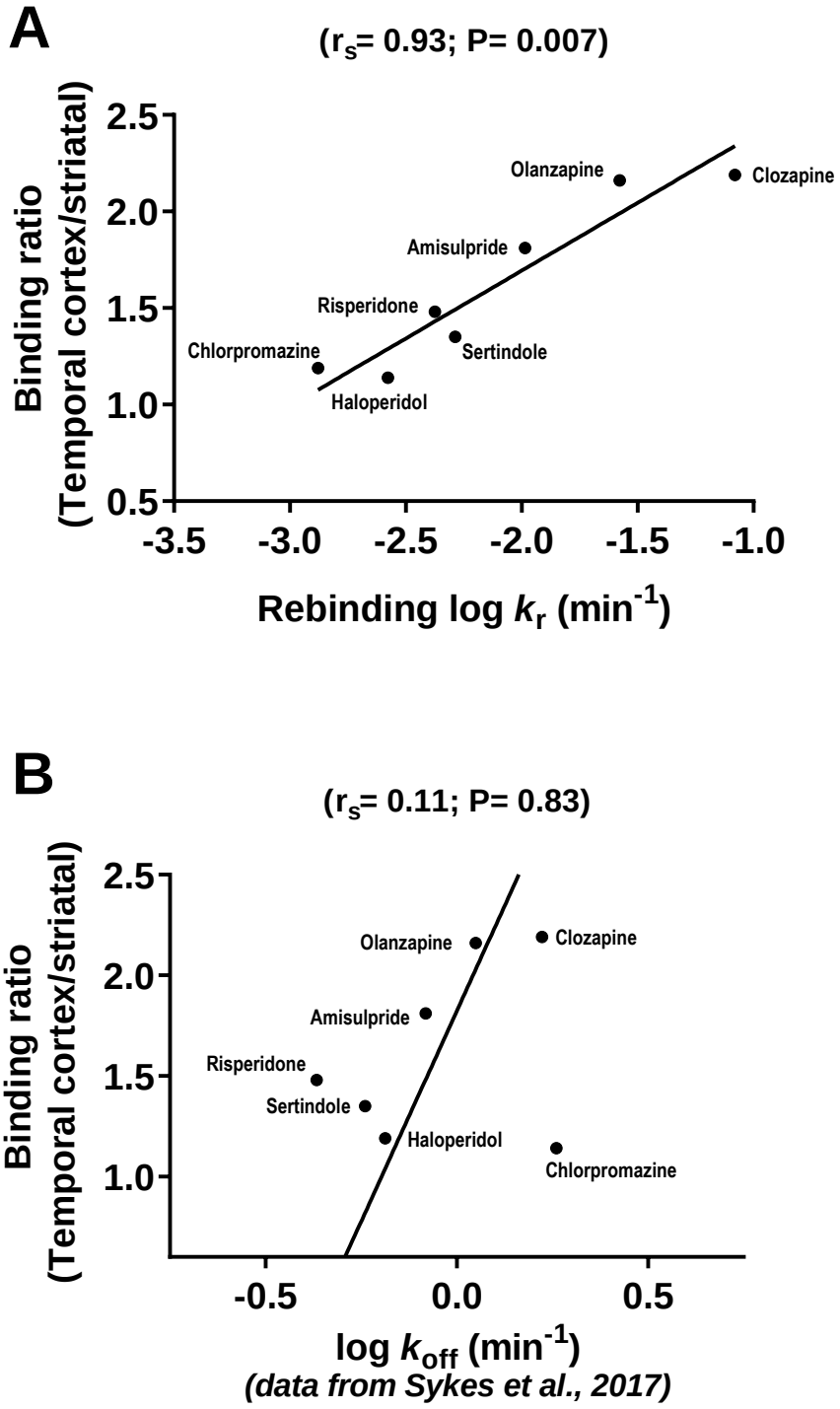


Figure 7.10. Correlating literature APD binding ratios (% bound temporal cortex/striatum) with the dopamine D_2R rebinding reversal parameter (k_r), derived from competition association kinetic experiments. Correlation between **(A)** APD D_2 receptor the dopamine D_2R rebinding reversal parameter (k_r) and APD binding ratios (% bound temporal cortex/striatum). Correlation between **(B)**

measured APD binding log k_{off} values and APD binding ratios (% bound temporal cortex/striatum). APD binding ratios (% bound temporal cortex/striatum) values were obtained from 4 separate studies Xiberas et al., 2001; Bigliani et al., 2000 and Bressan et al., 2003 and 2004. The log k_{off} values were taken from dopamine D_2R competition kinetic association experiments as exemplified in Chapter 5. All data used in these plots are detailed in Chapter 5, Table 5.1 or taken Sykes et al., 2017. Kinetic data are presented as mean values from at least 4-6 separate experiments. The relationship between two variables was assessed using a two-tailed Spearman's rank correlation allowing the calculation of the correlation coefficient, r_s. A P value of 0.05 was used as the cutoff for statistical significance and relationships depicted as trend lines.

7.12 PET/SPECT studies exploring clinical D_2R occupancy and EPS

To further explore this relationship between the APD dopamine D_2R rebinding reversal parameter (k_r) I decided to go a step further and research PET studies in which striatal occupancy was measured and reported along with clinical readouts indicating the prevalence of EPS.

For the resulting correlations to have clinical relevance the EPS measurements in these PET/SPECT studies should reflect the original findings of Leucht at least in terms of the prevalence of EPS observed with individual APDs (Leucht et al., 2013). Reassuringly we see a good correlation between the percentage (%) EPS for APDs explored in the clinical PET studies and the EPS odds ratio (OR) estimated for these same ligands taken from the Leucht study see Figure 7.11A. Interestingly there was no correlation between the APD dopamine D_2R rebinding reversal parameter (k_r) and the % striatal occupancy from these clinical PET studies (Figure 7.11B). Correspondingly there was no correlation between % EPS estimated from clinical PET studies and % striatal receptor occupancy estimated in the same studies (Figure 7.11C). However, we observe an excellent correlation between APD dopamine D_2R rebinding reversal parameter (k_r) and % EPS estimated from these clinical PET studies (Figure 7.11D).

Intriguingly, despite displaying similar levels of striatal occupancy to the other APDs, sertindole displays virtually negligible levels of EPS see Figure 7.11C and D. Taken as a whole, these findings strongly suggest that striatal receptor occupancy and the propensity to cause EPS can be readily separated. This perhaps further highlights the crucial role played by rebinding but also the potential modulatory role of augmented 5-HT2A receptor antagonism and the phenomenon of hemi-equilibrium.

Furthermore, this analysis seems to support the view that the ‘rules’ around striatal occupancy and EPS (Kasper et al., 1999) are not so rigid that they can describe the actions of all APDs. This is particularly true for the atypical APDs where the largest variations in striatal occupancy and EPS were observed (Figure 7.11C). As an extreme example, equivalent striatal occupancy was achieved by the atypical APDs sertindole and risperidone which did not produce equivalent levels of EPS. This

suggests that despite their seemingly similar pharmacological profiles, based on pure affinity these two APDs diverge considerably in terms of their respective toxicological profiles, at least in terms of EPS.

In effect, each non-selective atypical drug or ‘magic shotgun’, as coined by Roth et al (2004) is unique and will produce a distinctive pattern of effects when administered to patients. The role of the clinical pharmacologist involved in the treatment of such patients is akin to that of the ballistics expert, to understand which patterns of pharmacological effect are preferable eg. weight loss or gain and match the correct gun to the right patient.

Looking to the future the technique of PET may be crucial to helping pharmacologists and medicinal chemists understand the specific modes of action of the various atypical agents in terms of their clinical efficacy and side effect profiles since these effects may be regional and receptor specific. However, to tease out this useful information very specific receptor-selective radiotracers or advanced non-radioactive visualisation techniques will be required.

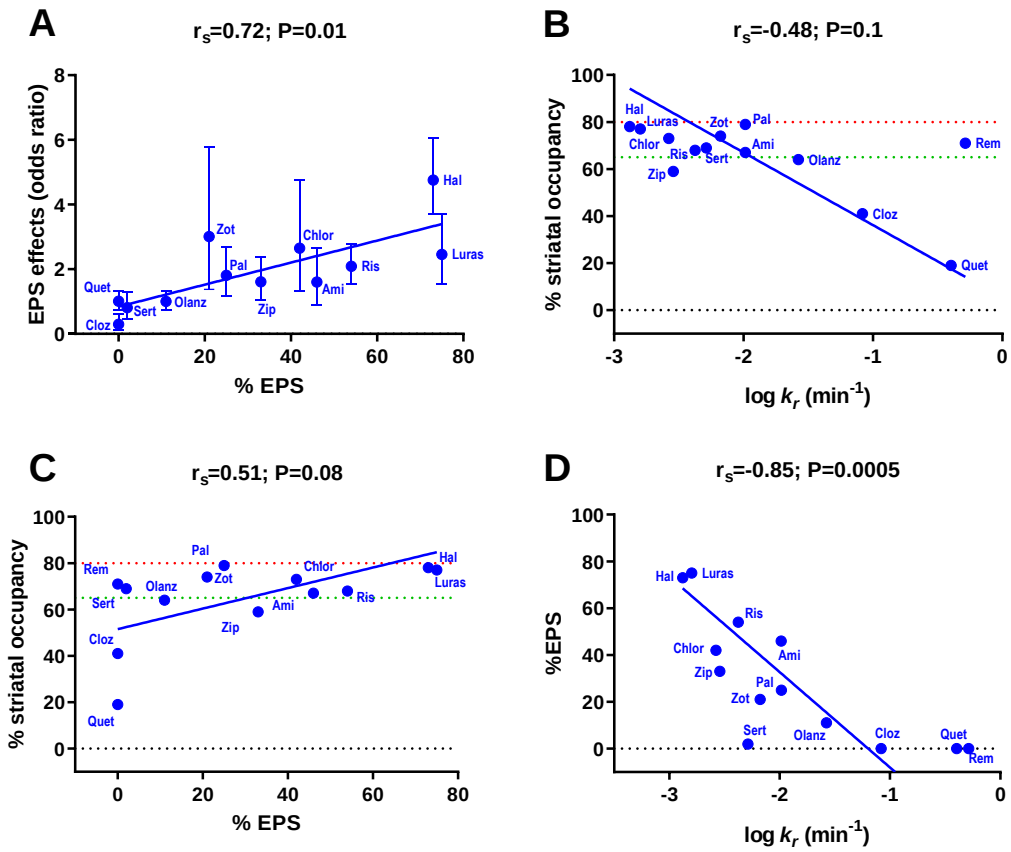


Figure 7.11. Correlating literature EPS and striatal occupancy with the dopamine D_2R rebinding reversal parameter (k_r), derived from competition association kinetic experiments. Correlation between **(A)** the prevalence of APD EPS (% EPS) and APD EPS odds ratios from clinical studies reviewed in Leucht et al., 2013. Correlation between **(B)** APD dopamine D_2R rebinding reverse rate (k_r) and % striatal occupancy from clinical PET studies. Correlation between **(C)** % EPS estimated from clinical PET studies and % striatal receptor occupancy estimated in the same studies. Correlation between **(D)** APD dopamine D_2R rebinding reversal parameter (k_r) and % EPS estimated from clinical PET studies. APD binding index (% striatal occupancy) values were obtained from 20 separate studies (Tauscher et al., 2002a; Tauscher et al., 2002b; Corripio et al., 2002; Kufferle et al., 1996; Bigliani et al., 2000; Farde et al., 1992, Meisenzahl et al., 2008; Barnas et al., 2001; Corripio et al., 2005; Kasper et al., 1998; Arakawa et al., 2007; Wong et al., 2013; Bigliani et al., 1999; Vernaleken et al., 2004; Bressan et al., 2004; Bernardo et al., 2001; Mamo et al., 2008; Tauscher-Wisniewski et al., 2002; Knable et al., 1997; Gefvert et al., 2001). The red dotted line at 80% occupancy represents the level of D_2R APD

binding thought to be indicative of EPS. The green dotted line at 65% occupancy represents the levels of APD D_2R occupancy in the striatum required to produce clinical efficacy. The mean log k_r values were taken from dopamine D_2R competition kinetic association experiments as exemplified in Chapter 5 and from Sykes et al., 2018. The relationship between two variables was assessed using a two-tailed Spearman's rank correlation allowing the calculation of the correlation coefficient, r_S. A P value of 0.05 was used as the cutoff for statistical significance and relationships depicted as trend lines. Figure key: Hal = haloperidol, Ris = risperidone, Cloz = clozapine, Ami = amisulpride, Olanz = olanzapine, Sert = sertindole, Zot = zotepine, Zip = ziprasidone, Quet = quetiapine, Rem = remoxipride, Pal = paliperidone, Luras = lurasidone, Chlor = chlorpromazine.

7.13 Role of the 5-HT1A receptor in the reduced incidence of side effects

We were successfully able to measure the efficacy of all clinically relevant APDs and accurately determine the kinetics of the vast majority of these agents at the 5-HT1A receptor. However, we were not able to demonstrate any relationship between their projected 5-HT1A functional response in a clinical setting (as estimated by an operational modelling approach) and their propensity to reduce EPS.

It is important to note that this in no way rules out 5-HT1A agonism as playing a role in the reduced side effect profile of certain atypical APDs but it would suggest that 5-HT1A agonism is not an essential requirement for reduced EPS of clinically used APDs in just the same way as D_2R antagonism is not an absolute prerequisite for APD activity. Indeed, recent research suggests that a combination of 5-HT1A agonism coupled to weak dopamine D_2R antagonism/partial agonism may produce a new generation of APDs (eg aripiprazole) with atypical features but without the same degree of associated side effects eg. prolactin release and EPS (Leucht et al., 2013, Ye et al., 2014).

Interestingly APDs binding the 5-HT1A receptor, in general, show a much-reduced rate of association compared to the 5-HT2A receptor and it appears to be this factor which controls serotonin receptor 5-HT2A/1A selectivity as opposed to off-rate. The diffusion limit is equal to $1x10^9$ M^{-1} sec^{-1} ($6 x10^{10}$ M^{-1} min^{-1}) and represents the maximum rate at which two molecules can move through an aqueous environment and eventually collide (Alberty and Hammes, 1958; Copeland et al., 2006). Measured k_{on} values at the 5-HT1A receptor were several orders of magnitude lower than the diffusion limit for certain ligands, suggesting that at least for these compounds very few encounters result in a successful binding event. Thus, demonstrating not only the inherent specificity of binding interactions but also explaining why APDs with lower on-rates are likely to diffuse out of a synaptic or cellular compartment rather than rebind to unoccupied receptors. With regards to selectivity, it is very likely that structural differences in the outer regions of the binding pocket of the 5-HT1A and 5-HT2A receptors affects the measured

association rate of the clinically used APDs and determines this differential affinity (Yap et al., 2012).

7.14 Relevance to the classification of antipsychotics

In the context of on-target side effects, the association rate can extend the ability of certain compounds to block receptors in the brain where diffusion rates are much reduced and produce EPS due to the phenomenon of rebinding eg. chlorpromazine. Whilst the dissociation rate appears to influence the ability of these same compounds to causes increased prolactin secretion in the periphery due to the phenomenon of insurmountability which leaves D_2 receptors in the pituitary unresponsive to high local concentrations of dopamine released in a pulsatile manner. Given the clear reduction in EPS observed with sertindole (and higher rates of EPS with paliperidone), we cannot rule out 5-HT2A receptor occupancy and D_2R dissociation rates as factors affecting (modulating) the overall levels of clinical observed EPS.

It is of interesting to this discussion that the dopamine D_2R occupancy profile of the atypical antipsychotic risperidone appears relatively flat in comparison to haloperidol, which is dopamine D_2R selective (Natesan et al., 2006; Kusumi et al., 2015). This could be an indication that the high 5-HT2A receptor occupancy of risperidone can modulate D_2R occupancy, potentially as a result of increased dopamine release in the striatum. Indirect evidence for this scenario comes from a PK-PD model produced through studying the effects of atypical and typical APDs in patients during a 6-week clinical trial (Pilla Reddy et al., 2012). This study by Pilla Reddy and colleagues, confirms that the probability of experiencing EPS, as D_2R receptor occupancy increases, is higher for the D_2R selective typical APDs such as haloperidol compared to atypical antipsychotics with significant 5-HT2A receptor affinity such as ziprasidone. This model and these findings are consistent with a previous study of antipsychotic-induced extrapyramidal symptoms which utilised a D_2R receptor occupancy model incorporating endogenous dopamine release, the result of 5-HT2A inhibition (Matsui-Sakata et al., 2005).

One alternative theory suggests that 5-HT2A receptor blockade could reduce the release of dopamine in the limbic system and therefore the level of dopamine

receptor blockade required in this area of the brain is likely to also be reduced (Howell and Cunningham 2015). This would fit with a reduction in the incidence of positive symptoms and could also partly explain why clozapine is so effective in uncontrolled schizophrenia. As a knock-on effect, a reduction in the absolute level (%) of receptor blockade observed in the striatum, due in part to limbic selectivity might be expected. The outcome, if such a mechanism is correct, should be a reduction in the likelihood of patients experiencing EPS, effectively reinforcing the key role of the 5-HT2A receptor in APD atypicality.

Overall these results suggest that the currently used system of designating APDs as first-generation/typical and second-generation/atypical may be of limited value since it exaggerates differences between groups and overstates similarities between members of each group. It has even been suggested that the current classification system should be abandoned (see Tyrer and Kendall 2009; Leucht et al., 2009) and indeed NICE guidelines (2009) on schizophrenia treatment no longer distinguish between first-generation and second-generation antipsychotics with the exception of clozapine and recommends choosing an antipsychotic on the basis of all its known pharmacological effects.

These ideas on the classification of antipsychotics fall very much in line with the current Neuroscience-based Nomenclature (NbN), which aims at improving the current clinical and scientific terminology in research and clinical psychopharmacology (Brühl and Sahakian, 2017). NbN is very much a science-based approach to describing the neuropsychopharmacology of drugs, with drugs being described specifically by their pharmacological mode of action eg. Dual 5-HT2A/ D_2R blockers. The idea is that this initiative will not only improve scientific communication in research but also the communication between clinicians and patients. The hope is that patients will no longer feel the stigma of being prescribed an ‘antipsychotic’ for the treatment of conditions such as depression where for example quetiapine a dual 5-HT2A/ D_2R blocker has found a use.

7.15 SKR of dopamine D_2 specific ligands

Previous structure kinetic relationships (SKR) derived for dopamine D_2R specific ligands suggest that there is a clear relationship between fast off molecules, and reduced lipophilicity, with smaller more polar compounds exhibiting shorter residence times (Tresadern et al., 2011). In chapter 3 I presented various correlations showing the relationships between pharmacological class (agonist or antagonist) and general physicochemical properties. And it is fair to say that smaller compounds do tend to possess reduced residence times (or a fast k_{off}), although this is not an exclusive feature. And at least for the agonists tested in the current study, the smaller compounds tended to show reduced association rates and receptor affinities, see Chapter 3 Figures 3.21A and C and 3.22 A and C. To understand these relationships in more detail I have re-classified the molecules according to common structural features to explore the SKR in more detail.

In terms of SKR the kinetic data, I collected for D_2R specific ligands would suggest that lipophilicity (as assessed by computed logP) and reducing polar surface area (PSA) drives the association rate of certain key drug classes involved in the treatment of schizophrenia including the tricyclic APDs which include clozapine, see Figures 7.12E & 7.13E. The association rate of the benzamide class would appear also to be influenced by increasing lipophilicity (with the clear exception of remoxipride), see Figures 7.12W. Other classes where I tested five or more ligands show no such relationship with increasing lipophilicity, including the ergot dopamine agonists, see Figures 7.12Z. The reason for this is unclear but it might relate to the wider range in molecular weight (heavy atom count (HAC), this being a surrogate for increasing molecular weight) and polarity of certain ligands within this particular class which may impose a limitation on the measured association rate, see Figures 7.13Z and 7.14Z (Sykes et al., 2019). Other ligand groups with two or three associated ligands show a similar positive relationship with lipophilicity and increasing k_{on}, and undoubtedly this must contribute to the positive relationship between dopamine D_2R antagonist and agonist lipophilicity and association rate, documented in Chapter 3 Figure 3.20B.

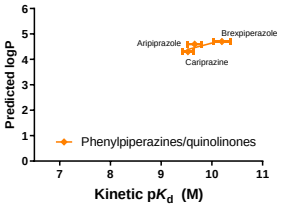
Interestingly there were no significant relationships between lipophilicity and dissociation rate (k_{off}) for any class of ligand containing five or more examples. The only significant correlation with dissociation rate occurred with the phenothiazines, with HAC increasing with increasing residence time (or a reduced k_{off} see Figure 7.14I) and the ergot dopamine agonists, with k_{off} correlating with increasing PSA (see Figures 7.13A.2, P=0.02). Increasing HAC and decreasing k_{off} may also be implicated for this class of compound, but this relationship did not reach statistical significance (see Figure 7.14A.2, P=0.08). This suggests as one might predict that more specific compound features are driving dopamine D_2R residence time (Sykes et al., 2014; Sykes et al., 2019).

kinetic pK_d vs. clogP

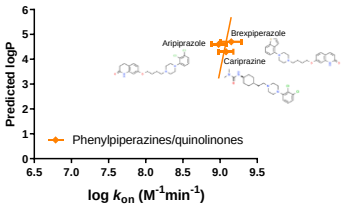
kinetic logk_{on} vs. clogP

kinetic logk_{off} vs clogP

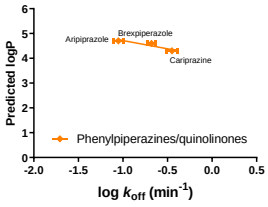
A



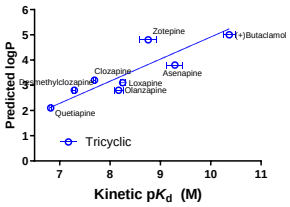
B



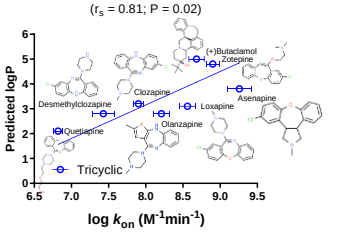
C



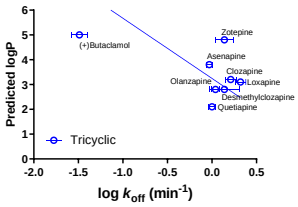
D



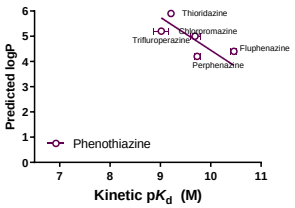
E



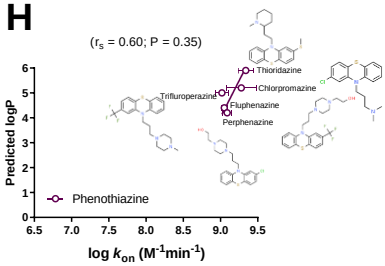
F



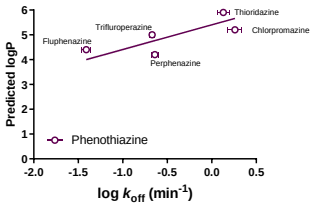
G



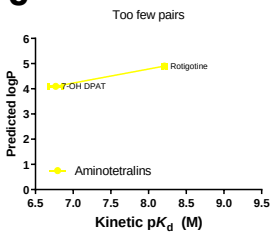
H



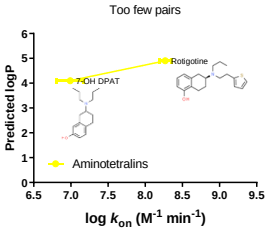
I



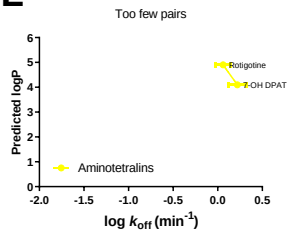
J



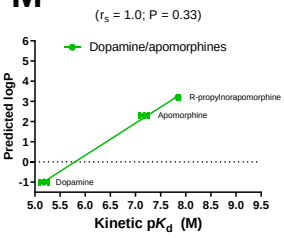
K



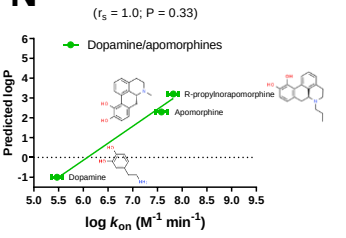
L



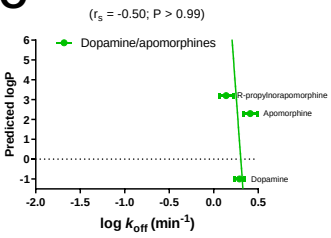
M



N



O



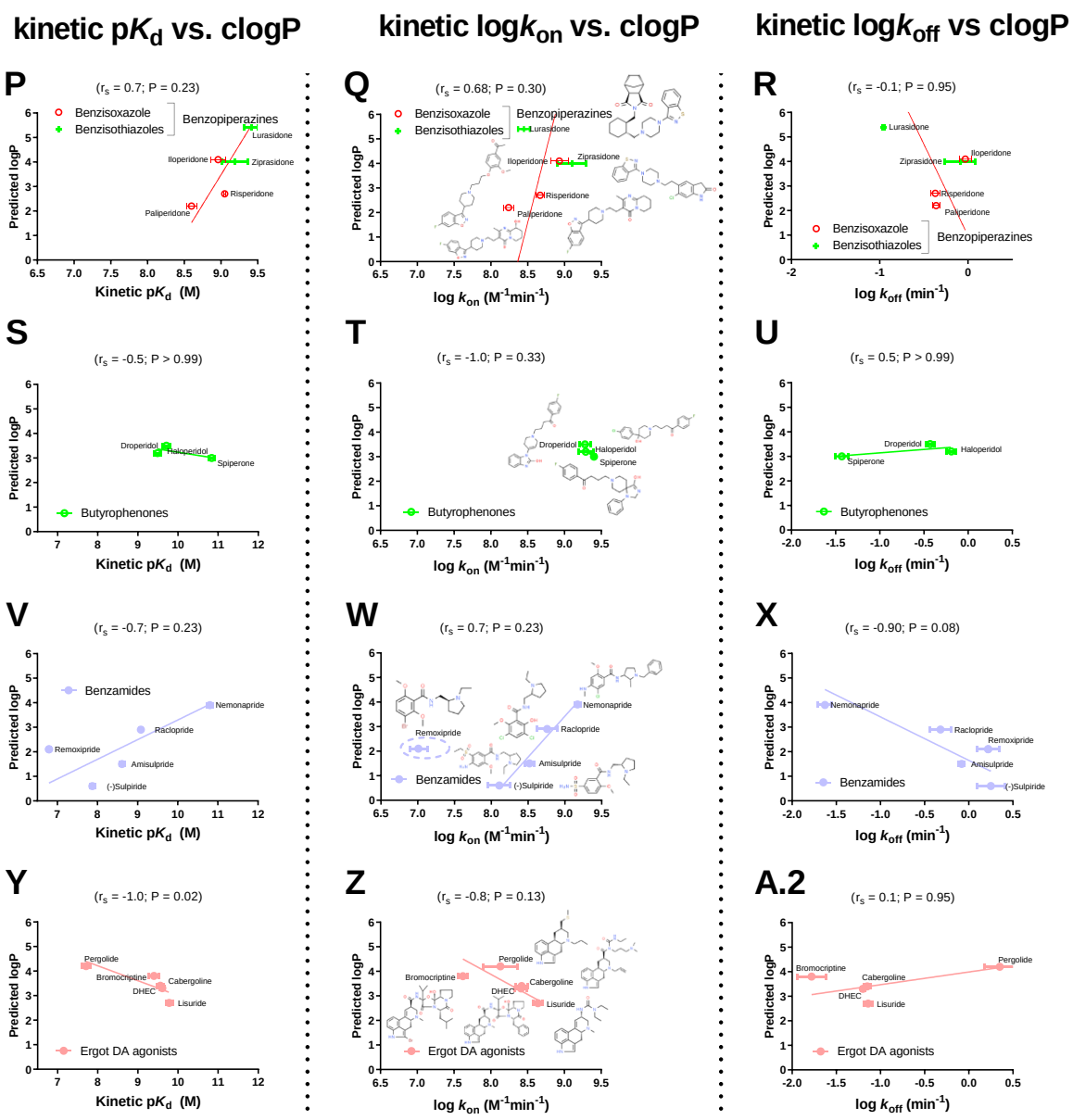


Figure 7.12. Exploring SKR for dopamine D_2R ligands of different chemical classes. Showing the effect of calculated logP (clogP) on kinetic K_d for **(A)** Phenylpiperazines/quinolinones, **(D)** Tricyclic, **(G)** Phenothiazine, **(J)** Aminotetralins, **(M)** Dopamine/apomorphines, **(P)** Benzisoxazole/benzisothiazoles (benzopiperazines), **(S)** Butyrophenones, **(V)** Benzamides and **(Y)** Ergot dopamine agonists. Showing the effect of clogP on k_{on} for **(B)** Phenylpiperazines/quinolinones, **(E)** Tricyclic, **(H)** Phenothiazine, **(K)** Aminotetralins, **(N)** Dopamine/apomorphines, **(Q)** Benzisoxazole/benzisothiazoles (benzopiperazines), **(T)** Butyrophenones, **(W)** Benzamides and **(Z)** Ergot dopamine agonists. Showing the effect of clogP on k_{off} for **(C)** Phenylpiperazines/quinolinones, **(F)** Tricyclic, **(I)** Phenothiazine, **(L)**

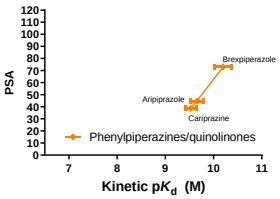
Aminotetralins, **(O)** Dopamine/apomorphines, **(R)** Benzisoxazole/benzisothiazoles (benzopiperazines), **(U)** Butyrophenones, **(X)** Benzamides and **(A.2)** Ergot dopamine agonists. Correlation was determined through a Rank Spearman test. It must be recognised that statistical significance cannot be achieved in cases where there are less than 5 compounds available for comparison. And r^2 values are considered unreliable when the number of observations is below 10. A linear trend line depicts an apparent relationship.

kinetic pK_d vs. PSA

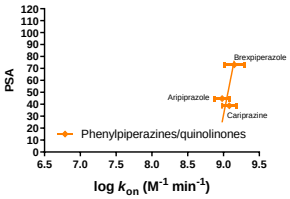
kinetic logk_{on} vs. PSA

kinetic logk_{off} vs PSA

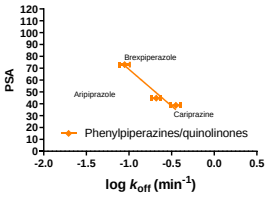
A



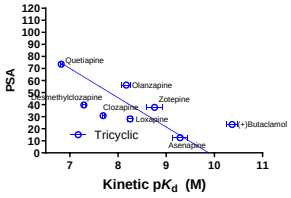
B



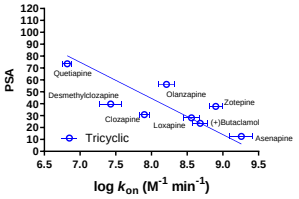
C



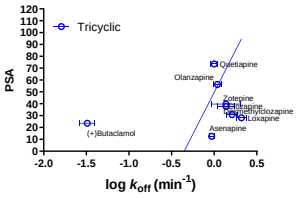
D



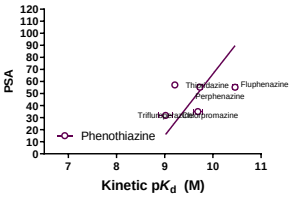
E



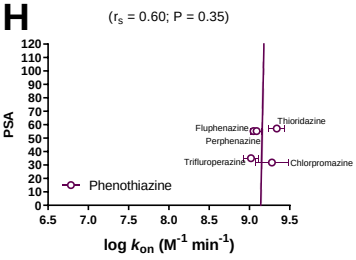
F



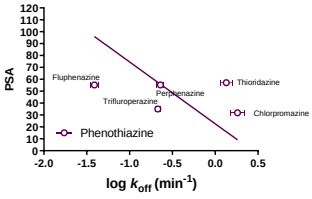
G



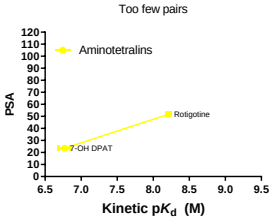
H



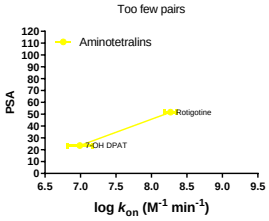
I



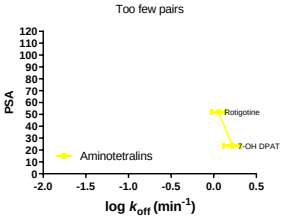
J



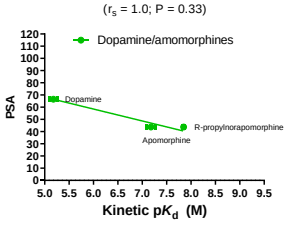
K



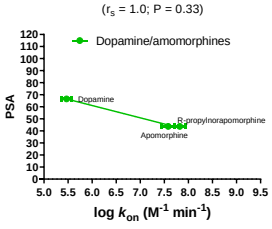
L



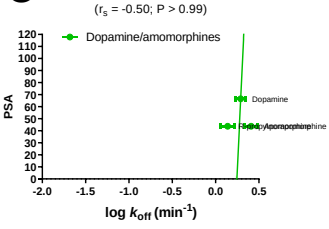
M



N



O



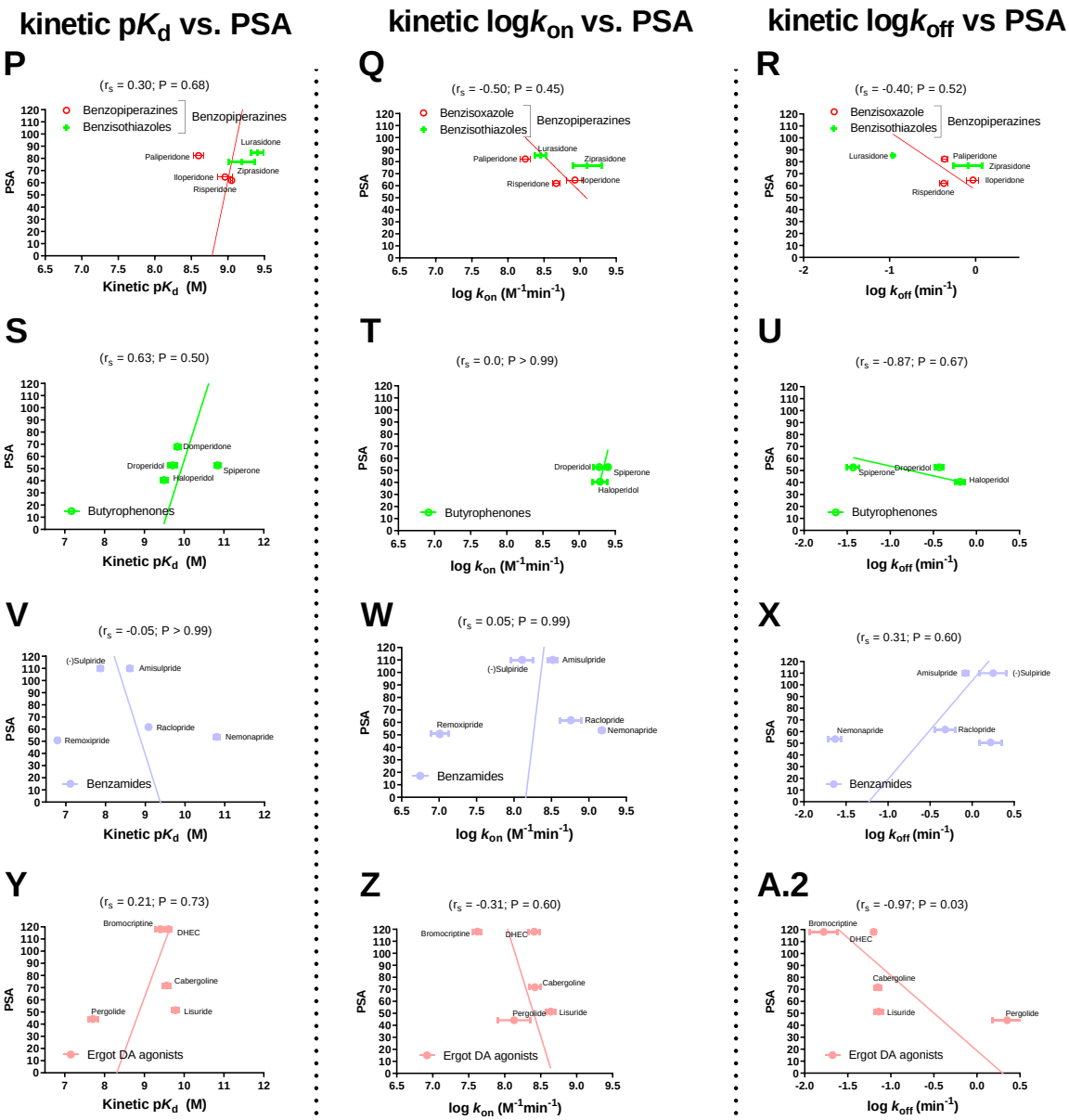


Figure 7.13. Exploring SKR for dopamine D_2R ligands of different chemical classes. Showing the effect of polar surface area (PSA) on kinetic K_d for **(A)** Phenylpiperazines/quinolinones, **(D)** Tricyclic, **(G)** Phenothiazine, **(J)** Aminotetralins, **(M)** Dopamine/apomorphines, **(P)** Benzisoxazole/benzisothiazoles (benzopiperazines), **(S)** Butyrophenones, **(V)** Benzamides and **(Y)** Ergot dopamine agonists. Showing the effect of PSA on k_{on} for **(B)** Phenylpiperazines/quinolinones, **(E)** Tricyclic, **(H)** Phenothiazine, **(K)** Aminotetralins, **(N)** Dopamine/apomorphines, **(Q)** Benzisoxazole/benzisothiazoles (benzopiperazines), **(T)** Butyrophenones, **(W)** Benzamides and **(Z)** Ergot dopamine agonists. Showing the effect of PSA on k_{off} for **(C)** Phenylpiperazines/quinolinones, **(F)** Tricyclic, **(I)** Phenothiazine, **(L)**

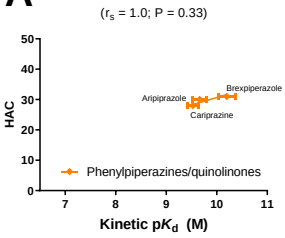
Aminotetralins, **(O)** Dopamine/apomorphines, **(R)** Benzisoxazole/benzisothiazoles (benzopiperazines), **(U)** Butyrophenones, **(X)** Benzamides and **(A.2)** Ergot dopamine agonists. Correlation was determined through a Rank Spearman test. It must be recognised that statistical significance cannot be achieved in cases where there are less than 5 compounds available for comparison. And r^2 values are considered unreliable when the number of observations is below 10. A linear trend line depicts an apparent relationship.

kinetic pK_d vs. HAC

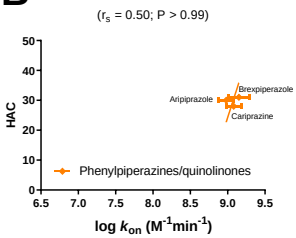
kinetic logk_{on} vs. HAC

kinetic logk_{off} vs HAC

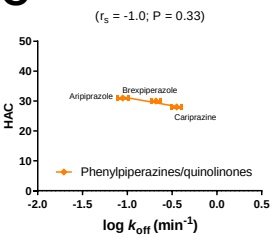
A



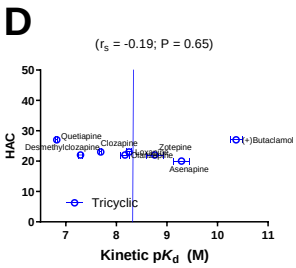
B



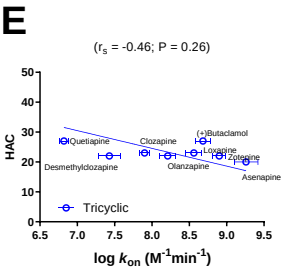
C



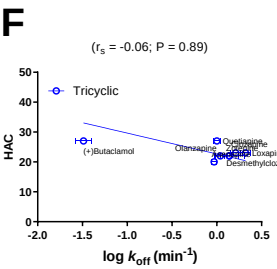
D



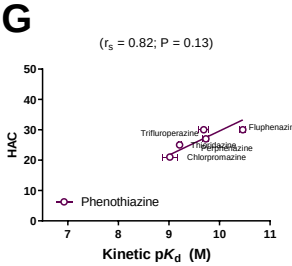
E



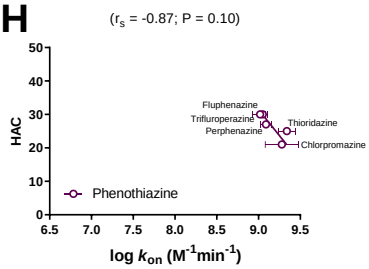
F



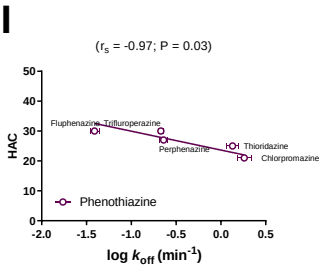
G



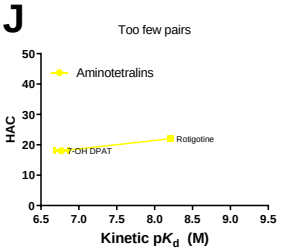
H



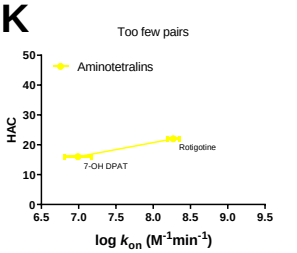
I



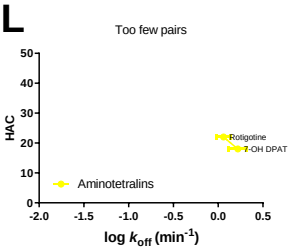
J



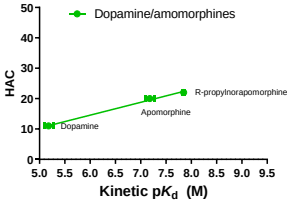
K



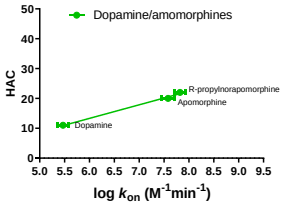
L



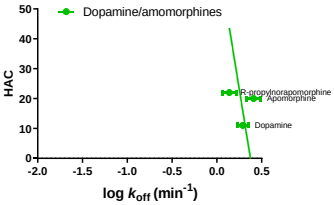
M



N



O



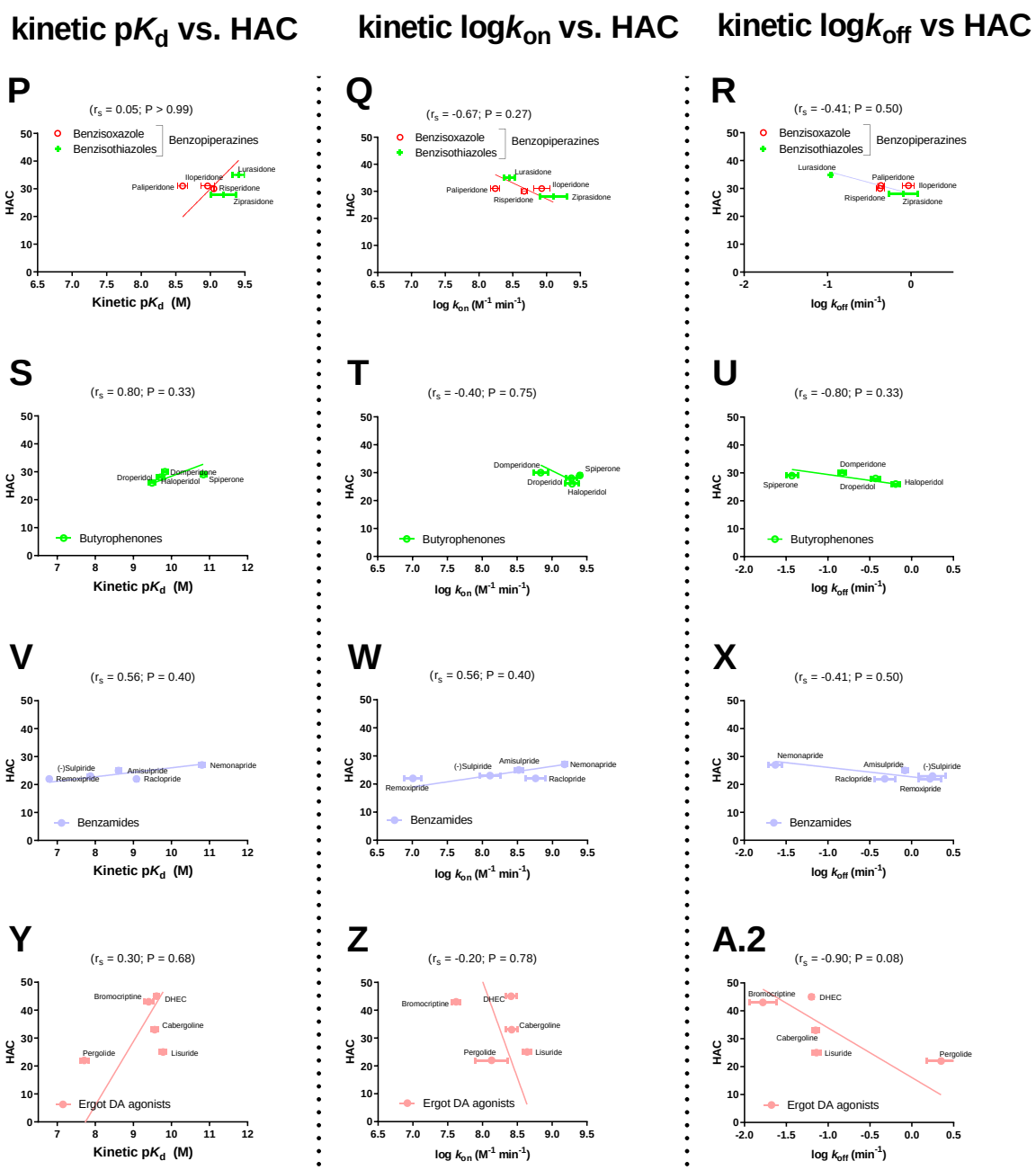


Figure 7.14. Exploring SKR for dopamine D_2R ligands of different chemical classes. Showing the effect of heavy atom count (HAC) on kinetic K_d for **(A)** Phenylpiperazines/quinolinones, **(D)** Tricyclic, **(G)** Phenothiazine, **(J)** Aminotetralins, **(M)** Dopamine/apomorphines, **(P)** Benzisoxazole/benzisothiazoles (benzopiperazines), **(S)** Butyrophenones, **(V)** Benzamides and **(Y)** Ergot dopamine agonists. Showing the effect of HAC on k_{on} for **(B)** Phenylpiperazines/quinolinones, **(E)** Tricyclic, **(H)** Phenothiazine, **(K)** Aminotetralins, **(N)** Dopamine/apomorphines, **(Q)** Benzisoxazole/benzisothiazoles (benzopiperazines), **(T)** Butyrophenones, **(W)**

Benzamides and **(Z)** Ergot dopamine agonists. Showing the effect of HAC on k_{off} for **(C)** Phenylpiperazines/quinolinones, **(F)** Tricyclic, **(I)** Phenothiazine, **(L)** Aminotetralins, **(O)** Dopamine/apomorphines, **(R)** Benzisoxazole/benzisothiazoles (benzopiperazines), **(U)** Butyrophenones, **(X)** Benzamides and **(A.2)** Ergot dopamine agonists. Correlation was determined through a Rank Spearman test. It must be recognised that statistical significance cannot be achieved in cases where there are less than 5 compounds available for comparison. And r^2 values are considered unreliable when the number of observations is below 10. A linear trend line depicts an apparent relationship.

7.16 Conclusions

As discussed, the overall picture of APDs from a pharmacological and kinetic perspective has been somewhat confused due to the lack of kinetic data obtained at the human D_2 receptor under physiological conditions of temperature and sodium ion concentration. The results of the current study achieved through the development of novel TR-FRET-based assays using a rapidly dissociating tracer suggest that the basis for atypically and typicality based solely on the 'fast dissociation hypothesis' is questionable and that the EPS observed in the clinic are linked mainly with increasing rates of drug association (k_{on}) and not dissociation rate (k_{off}) as originally reported. The binding and functional studies outlined in this thesis further emphasis the complexity of the overall pharmacology of clinically used APDs. And this complexity appears not just at the level of affinity as was first recognised by early MOA pioneers such as Meltzer and Roth (Meltzer et al., 1989, Kroeze et al., 2003, Roth et al., 2004) but also at a kinetic level as first proposed by Kapur and Seeman (2001). And whilst it is true that affinity is a key part of the APD clinical story it would appear that in terms of understanding a drug's on-target side effects, kinetics and rebinding is the 'sin qua non' or the essential.

The most effective treatments for schizophrenia have very complex pharmacology and even now after more than 60 years of research, a consensus regarding the ideal kinetic characteristics of an APD from a treatment perspective has not been reached. The finding that lurasidone has a relatively slow off-rate from the D_2R suggests that this could still be a useful property of an 'ideal' APD. Indeed,

aripiprazole a partial agonist which produces functional antagonism of the endogenous dopamine response has a similar measured rate of dissociation and is effective against positive symptoms but with the added advantage that it does not increase prolactin secretion due to its inherent D_2R partial agonism (Natesan et al., 2011). An alternative model of clinical APD action suggests that rapidly dissociating compounds may be more effective when dosing is optimised for the burst state of dopamine release since it necessitates a higher occupancy in the resting state. For example, clozapine may tolerate higher doses (and therefore achieve higher resting occupancy) since the occupancy of rapidly reversing compounds will be reversed more readily in the presence of these higher burst state dopamine concentrations. This could partly explain why high dose clozapine is so effective in treatment-resistant schizophrenia and this is perhaps an interesting area for future preclinical/clinical research (Park and Kang 2013).

The current study adds to the growing appreciation that under certain conditions, binding kinetics or the rates of binding and unbinding (k_{on} and k_{off} respectively) may be a better predictor of pharmacological response than the equilibrium constant (Swinney 2004; Copeland et al., 2006) and that k_{on} can in certain circumstances where diffusion is limited play a dominant role. Thus, no longer can it be assumed that by designing compounds with fast k_{off} rates a reduction in EPS in the clinic is guaranteed due to the dominance of the rebinding process in the synaptic clefts of the striatum and the part played by k_{on}. Factors which may influence k_{on} include the physicochemical properties of the APDs themselves (eg. size and lipophilicity) and the ability of a molecule to lose associated water, but also displace existing molecules within the D_2R binding pocket (Sykes et al., 2014; Sykes et al., 2019 and IJzerman and Guo 2019). These results would suggest that increased 5-HT2A receptor affinity has some advantages in terms of reduced side-effect profile, for high-affinity APDs (eg. sertindole). However, the advantage of affinity for the 5-HT2A receptor for compounds with low D_2 receptor rebinding capability such as clozapine, the most effective antipsychotic known to date remains unproven (Leucht et al., 2013).

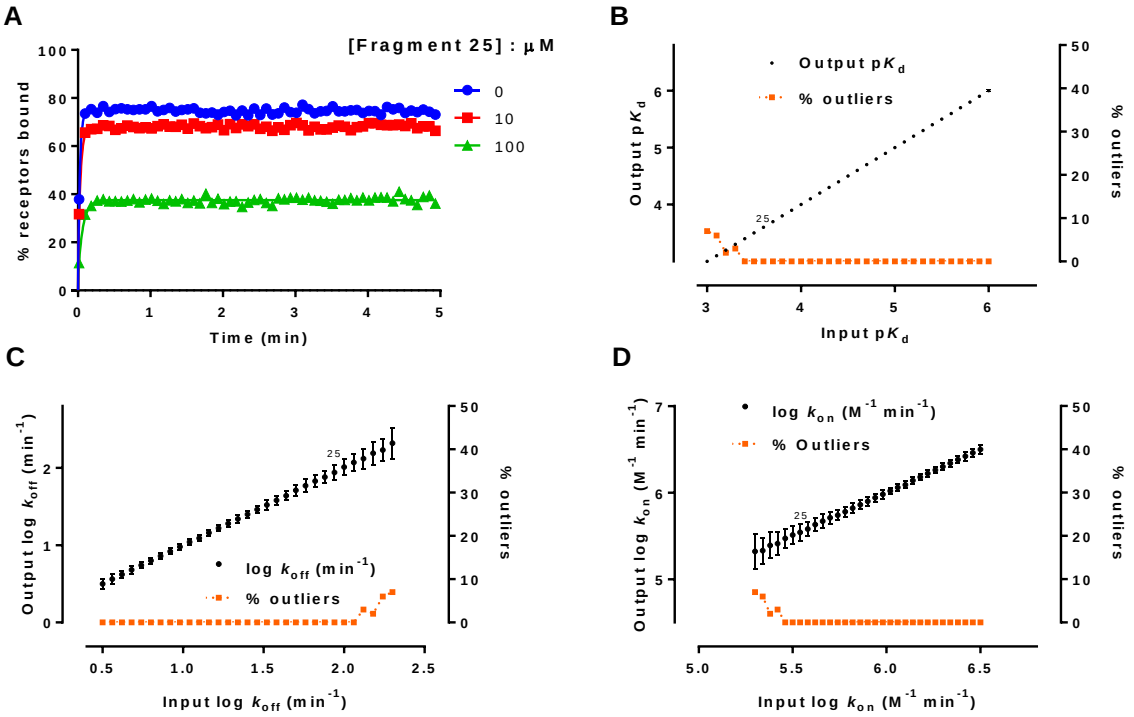
Issues surrounding side effects continue to complicate APD therapy which leaves room for the development of new therapies with fewer side effects. The results

presented here have major implications for kinetic assay development and APD design and I hope that the new kinetic information detailed here in conjunction with the novel mechanistic insight presented reignites research in schizophrenia and other disease areas where kinetics and the association rate, in particular, could play a significant role.

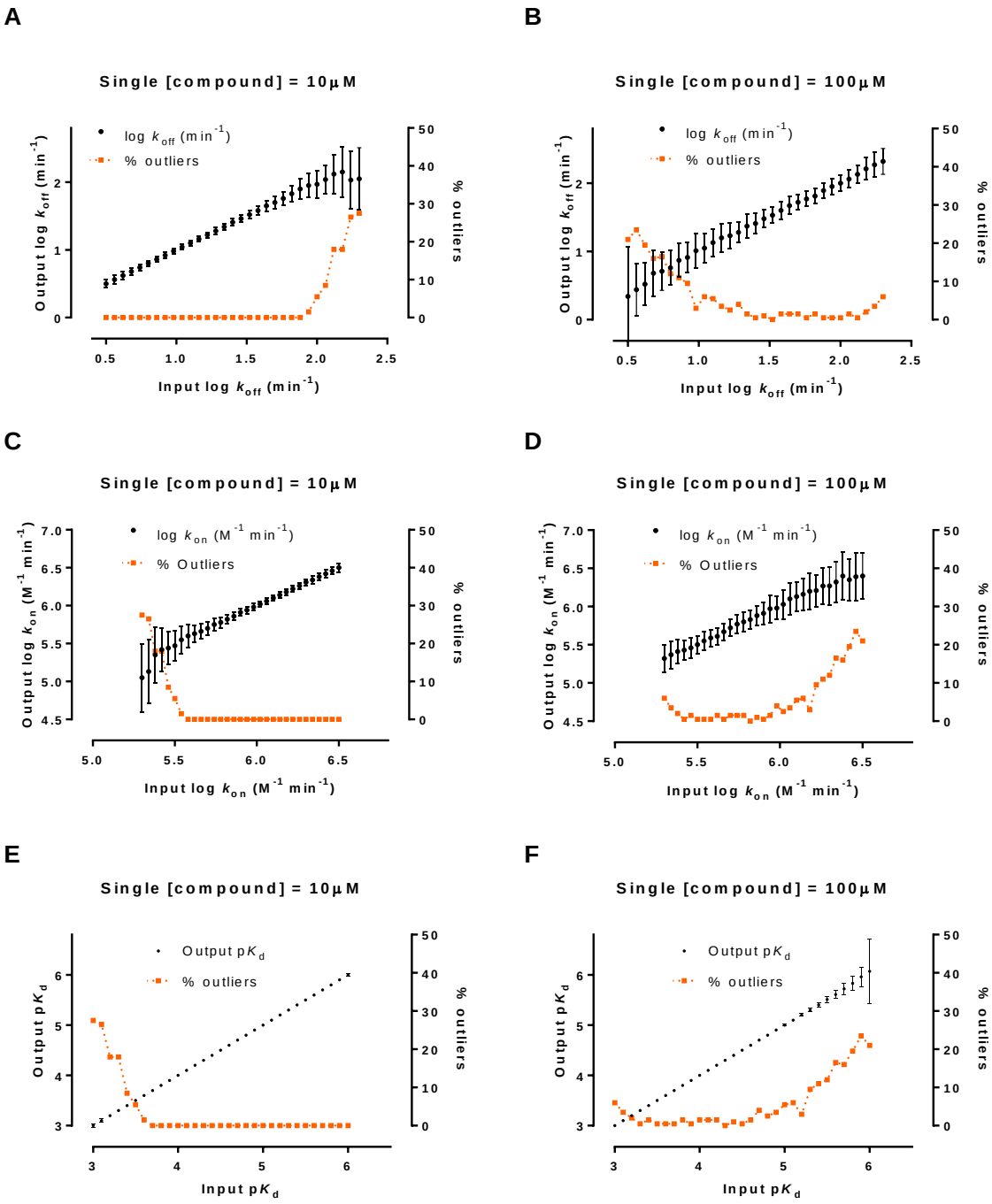
By devotion to science, seek the truth.

Chapter 8 - Appendices and References

8.1 Appendix I – Supplementary data



Supplementary Figure 8.1. Monte-Carlo simulation results representative of the competition profile observed between low affinity fragments 1 to 31 (affinities ranging from 1-1000 µM) tested at 10 and 100 µM in competition with a fixed concentration of a rapidly dissociating tracer. **(A)** Competition between a fixed concentration (3x K_d) of a rapidly dissociating tracer with the following kinetic parameters; k_{off} of 10min^{-1}, k_{on} of 3x10^7 M^{-1} min^{-1}, and competitor fragment 25 with the following kinetic parameters; k_{off} of 87.1 min^{-1}, k_{on} of 5 x10^5 M^{-1} min^{-1}, data shown are representative of 200 simulations. **(B)** Correlation between input K_d and output K_d, **(C)** between input k_{off} and output k_{off}, **(D)** between input k_{on} and output k_{on}. In each case tracer and competitor binding simulations were performed with an initial start time of 1sec (representative of injection of receptor to a reaction containing tracer) and an interval time of 5sec, the data shown points shown in the correlation plots are the average of 200 simulations**.**



Supplementary Figure 8.2. Monte-Carlo simulation results representative of the competition profile observed between low affinity fragments (1-1000µM) tested at 10 and 100µM in competition with a fixed concentration (3x K_d) of a rapidly dissociating tracer with the following kinetic parameters; k_{off} of 10min^{-1}, k_{on} of 3x10^7 M^{-1} min^{-1}. Correlation between A) input k_{off} and output k_{off} at 10µM B) input k_{off} and output k_{off} at 100µM. C) input k_{on} and output k_{off} at 10µM. D) input k_{on} and output k_{off} at 100µM. E) input K_d and output K_d, at 10µM. F) input K_d and output K_d, at 100µM. In each case tracer and competitor binding

simulations were performed with an initial start time of 1sec (representative of injection of receptor to a reaction containing tracer) and an interval time of 5sec, the data shown points shown in the correlation plots are the average of 200 simulations.

Supplementary data files

Supplementary Table 8.1. Summary of the kinetic input parameters and their estimates for the tracer described in Table 4.1, under conditions which mimic online and offline addition, determined from 200 simulated data sets using the global association model equation (see Figure 4.1).

Online injection first read time 1sec							
Number of : (Ambiguous fits; Outliers)	Read frequency (sec)	Input K_d (Output K_d) nM	K_d %CV	Input k_{on} (Output k_{on}) $M^{-1}min^{-1}$	k_{on} %CV	Input k_{off} (Output k_{off}) min^{-1}	k_{off} %CV
(0; 0)	1	333 (333)	0.21	3E7 (3E7)	1.29	10 (10.01)	1.32
(0; 0)	5	333 (333)	0.47	3E7 (3E7)	2.31	10 (10.01)	2.27
(0; 0)	10	333 (333)	0.72	3E7 (3E7)	2.49	10 (10.01)	2.50
(0; 0)	20	333 (334)	0.96	3E7 (3.01E7)	2.34	10 (10.05)	2.40
(0; 0)	60	333 (333)	1.67	3E7 (3E7)	2.72	10 (9.99)	3.07
(0; 0)	1	100 (100)	0.26	1E7 (1E7)	0.44	1 (1.00)	0.53
(0; 0)	5	100 (100)	0.55	1E7 (1E7)	0.93	1 (1.00)	1.18
(0; 0)	10	100 (100)	0.81	1E7 (1E7)	1.34	1 (1.00)	1.71
(0; 0)	20	100 (100)	1.10	1E7 (1E7)	1.62	1 (1.00)	2.10
(0; 0)	60	100 (100)	2.14	1E7 (1E7)	2.74	1 (1.00)	3.52
(0; 0)	1	1 (1)	0.14	1E8 (1E8)	0.14	0.1 (0.1)	0.22

(0; 0)	5	1 (1)	0.32	1E8 (1E8)	0.32	0.1 (0.1)	0.51
(0; 0)	10	1 (1)	0.49	1E8 (1E8)	0.40	0.1 (0.1)	0.70
(0; 0)	20	1 (1)	0.61	1E8 (1E8)	0.64	0.1 (0.1)	1.02
(0; 0)	60	1 (1)	1.03	1E8 (1E8)	1.14	0.1 (0.1)	1.75
(0; 0)	1	0.01 (0.01)	0.29	1E9 (1E9)	0.06	0.01 (0.01)	0.32
(0; 0)	5	0.01 (0.01)	0.68	1E9 (1E9)	0.15	0.01 (0.01)	0.76
(0; 0)	10	0.01 (0.01)	0.91	1E9 (1E9)	0.20	0.01 (0.01)	1.02
(0; 0)	20	0.01 (0.01)	1.51	1E9 (1E9)	0.29	0.01 (0.01)	1.38
(0; 0)	60	0.01 (0.01)	2.50	1E9 (1E9)	0.55	0.01 (0.01)	2.19

Offline addition first read time 30 sec							
Number of : (Ambiguous fits; Outliers)	Read frequency (sec)	Input K_d (Output K_d) nM	K_d %CV	Input k_{on} (Output k_{on}) $M^{-1}min^{-1}$	k_{on} %CV	Input k_{off} (Output k_{off}) min^{-1}	k_{off} %CV
(197; 0)	1	333 (333)	0.21	3E7 (1.12E7)	41.38	10 (37.17)	41.36
(199; 8)	5	333 (333)	0.44	3E7 (1.71E8)	4.92	10 (56.90)	4.86
(200; 2)	10	333 (333)	0.72	3E7 (2.30E8)	9.54	10 (76.78)	9.54
(192; 0)	20	333 (333)	0.95	3E7 (1.67E8)	31.98	10 (55.54)	32.02
(139; 2)	60	333 (333)	1.68	3E7 (1.13E8)	92.76	10 (37.69)	92.28

(0; 0)	1	100 (100)	0.27	1E7 (9.66E6)	0.67	1 (1.00)	0.80
(0; 0)	5	100 (100)	0.55	1E7 (1E7)	1.47	1 (1.00)	1.74
(0; 0)	10	100 (100)	0.83	1E7 (1E7)	2.08	1 (1.00)	2.50
(0; 0)	20	100 (100)	1.16	1E7 (1E7)	2.65	1 (1.00)	3.09
(0; 0)	60	100 (100)	1.94	1E7 (1E7)	3.39	1 (1.00)	4.27
(0; 0)	1	1 (1)	0.14	1E8 (1E8)	0.13	0.1 (0.1)	0.22
(0; 0)	5	1 (1)	0.33	1E8 (1E8)	0.33	0.1 (0.1)	0.52
(0; 0)	10	1 (1)	0.44	1E8 (1E8)	0.47	0.1 (0.1)	0.72
(0; 0)	20	1 (1)	0.63	1E8 (1E8)	0.63	0.1 (0.1)	0.97
(0; 0)	60	1 (1)	1.03	1E8 (1E8)	1.17	0.1 (0.1)	1.77
(0; 0)	1	0.01 (0.01)	0.30	1E9 (1E9)	0.06	0.01 (0.01)	0.33
(0; 0)	5	0.01 (0.01)	0.68	1E9 (1E9)	0.15	0.01 (0.01)	0.77
(0; 0)	10	0.01 (0.099)	0.94	1E9 (1E9)	0.20	0.01 (0.01)	1.05
(0; 0)	20	0.01 (0.01)	1.25	1E9 (1E9)	0.31	0.01 (0.01)	1.41
(0; 0)	60	0.01 (0.01)	2.30	1E9 (9.99E8)	0.53	0.01 (0.01)	2.61

Supplementary Table 8.2. Summary of the kinetic input parameters and their estimates for unlabelled compounds under conditions which mimic online injection and offline addition of membranes, values are determined from 200 simulated data sets using the Motulsky-Mahan model equation and the very low affinity tracer (k_{on} = 3x10^{7} M^{-1}min^{-1}; k_{off} = 10min^{-1} K_d= 3μM).

Online injection first read time 1sec							
Number of : (Ambiguous fits; Outliers)	Read frequency (sec)	Input K_d (Output K_d)	K_d %CV	Input k_{on} (Output k_{on}) M^{-1}min^{-1}	k_{on} %CV	Input k_{off} (Output k_{off}) min^{-1}	k_{off} %CV
(0; 0)	1	10pM (10pM)	1.62	1E9 (1E9)	0.18	0.01 (0.01)	1.77
(0; 0)	5	10pM (10pM)	3.44	1E9 (1E9)	0.41	0.01 (0.01)	3.78
(0; 0)	10	10pM (10pM)	5.29	1E9 (1E9)	0.57	0.01 (0.01)	5.74
(0; 0)	20	10pM (10pM)	6.82	1E9 (1E9)	0.78	0.01 (0.01)	7.42
(0; 0)	60	10pM (10pM)	12.75	1E9 (0.999E8)	1.32	0.01 (0.01)	13.70
(0; 0)	1	1nM (1nM)	1.12	1E8 (1E8)	0.34	0.1 (0.1)	1.38
(0; 0)	5	1nM (0.99nM)	2.73	1E8 (1E8)	0.78	0.1 (0.1)	3.29
(0; 0)	10	1nM (1nM)	3.98	1E8 (1E8)	1.29	0.1 (0.1)	4.99
(0; 0)	20	1nM (0.996nM)	5.37	1E8 (1E8)	1.51	0.1 (0.1)	6.49
(0; 0)	60	1nM (0.991nM)	12.13	1E8 (1E8)	3.31	0.1 (0.1)	14.79
(0; 0)	1	100nM (100nM)	0.30	1E7 (9.99E6)	0.68	1 (1)	0.77
(0; 0)	5	100nM (99.9nM)	0.62	1E7 (1E7)	1.47	1 (1)	1.64

(0; 0)	10	100nM (100nM)	0.90	1E7 (1E7)	2.06	1 (1)	2.38
(0; 0)	20	100nM (99.9nM)	1.42	1E7 (1E7)	2.94	1 (1)	3.42
(0; 0)	60	100nM (99.8nM)	2.47	1E7 (1.01E7)	6.86	1 (1.01)	7.42
(0; 0)	1	10μM (10μM)	0.25	1E6 (1E6)	2.06	10 (10)	2.08
(0; 0)	5	10μM (10μM)	0.62	1E6 (1E6)	5.68	10 (10.02)	5.74
(0; 0)	10	10μM (10μM)	0.92	1E6 (1.01E6)	7.27	10 (10.05)	7.33
(0; 0)	20	10μM (9.99μM)	1.30	1E6 (1.01E6)	6.94	10 (10.05)	7.03
(0; 0)	60	10μM (9.98μM)	2.54	1E6 (1.01E6)	7.93	10 (10.06)	7.73
(0; 0)	1	1mM (1mM)	0.26	1E5 (9.98E4)	14.41	100 (99.81)	14.42
(0; 0)	5	1mM (1mM)	0.58	1E5 (1.04E5)	20.54	100 (103.86)	20.57
(0; 0)	10	1mM (1mM)	0.86	1E5 (1.03E5)	18.60	100 (103.48)	18.71
(0; 0)	20	1mM (1mM)	1.14	1E5 (1.02E5)	16.86	100 (101.83)	17.11
(0; 1)	60	1mM (1mM)	2.36	1E5 (1.02E5)	17.26	100 (102.38)	17.57

Offline addition first read time 30 sec							
Number of : (Ambiguous fits; Outliers)	Read frequency (sec)	Input K_d (Output K_d)	K_d %CV	Input k_{on} (Output k_{on}) $M^{-1}min^{-1}$	k_{on} %CV	Input k_{off} (Output k_{off}) min^{-1}	k_{off} %CV

(0; 0)	1	10pM (10pM)	1.55	1E9 (1E9)	0.17	0.01 (0.01)	1.67
(0; 0)	5	10pM (9.98pM)	3.74	1E9 (1E9)	0.43	0.01 (0.01)	4.09
(0; 0)	10	10pM (10pM)	4.95	1E9 (1E9)	0.56	0.01 (0.01)	5.43
(0; 0)	20	10pM (10pM)	6.79	1E9 (1E9)	0.86	0.01 (0.01)	7.47
(0; 0)	60	10pM (9.94pM)	12.31	1E9 (1E9)	1.42	0.01 (0.01)	13.39
(0; 0)	1	1nM (0.999nM)	1.24	1E8 (1E8)	0.37	0.1 (0.1)	1.52
(0; 0)	5	1nM (1nM)	2.68	1E8 (1E8)	0.90	0.1 (0.1)	3.39
(0; 0)	10	1nM (1nM)	3.79	1E8 (1E8)	1.24	0.1 (0.1)	4.77
(0; 0)	20	1nM (1nM)	5.42	1E8 (1E8)	1.70	0.1 (0.1)	6.73
(0; 0)	60	1nM (0.998nM)	9.62	1E8 (1E8)	2.78	0.1 (0.1)	11.83
(0; 0)	1	100nM (100nM)	0.33	1E7 (1E7)	1.04	1 (1)	1.18
(0; 0)	5	100nM (100nM)	0.70	1E7 (1E7)	2.18	1 (1)	2.38
(0; 0)	10	100nM (100nM)	0.92	1E7 (1E7)	3.05	1 (1)	3.30
(0; 0)	20	100nM (100nM)	1.41	1E7 (9.99E6)	4.28	1 (1)	4.79
(0; 0)	60	100nM (100nM)	1.30	1E7 (1E7)	3.85	1 (1)	4.26
(193; 6)	1	10μM (10μM)	0.28	1E6 (2.42E11)	277.73	10 (2.42E6)	277.65
(192; 19)	5	10μM (10μM)	0.58	1E6 (2.43E11)	261.24	10 (2.44E6)	261.33

(187; 27)	10	10μM (10μM)	0.93	1E6 (3.21E11)	241.99	10 (3.20E6)	241.45
(174; 30)	20	10μM (9.98μM)	1.18	1E6 (5.96E11)	258.44	10 (5.96E6)	258.67
(177; 31)	60	10μM (10μM)	2.19	1E6 (2.70E12)	275.64	10 (2.70E7)	275.21
(197; 0)	1	1mM (1mM)	0.26	1E5 (7.89E7)	143.79	100 (78893.74)	143.79
(191; 5)	5	1mM (1mM)	0.62	1E5 (3.01E8)	209.63	100 (3.01E5)	209.59
(188; 9)	10	1mM (1mM)	0.87	1E5 (2.50E8)	205.46	100 (2.51E5)	205.66
(192; 22)	20	1mM (9.99E-4)	1.14	1E5 (3.84E8)	209.43	100 (3.84E5)	209.53
(191; 36)	60	1mM (1mM)	1.51	1E5 (3.29E8)	170.69	100 (3.30E5)	171.09

Supplementary Table 8.3. Summary of the kinetic input parameters and their estimates for unlabelled compounds under conditions which mimic online injection and offline addition of membranes, values are determined from 200 simulated data sets using the Motulsky-Mahan model equation and the low affinity tracer (k_{on} = 1x10^{7}M^{-1}min^{-1}; k_{off} = 1min^{-1} K_d= 0.1μM).

Online injection first read time 1sec							
Number of : (Ambiguous fits; Outliers)	Read frequency (sec)	Input K_d (Output K_d)	K_d %CV	Input k_{on} (Output k_{on}) M^{-1}min^{-1}	k_{on} %CV	Input k_{off} (Output k_{off}) min^{-1}	k_{off} %CV
(0; 0)	1	10pM (10.03pM)	1.72	1E9 (1E9)	0.21	0.01 (0.01)	1.90
(0; 0)	5	10pM (10.01pM)	3.49	1E9 (1E9)	0.38	0.01 (0.01)	3.78
(0; 0)	10	10pM (10.03pM)	5.17	1E9 (1E9)	0.61	0.01 (0.01)	5.68
(0; 0)	20	10pM (9.96pM)	8.02	1E9 (1E9)	0.90	0.01 (0.01)	8.75
(0; 0)	60	10pM (9.97pM)	12.56	1E9 (0.999E8)	1.49	0.01 (0.01)	13.80
(0; 0)	1	1nM (1nM)	0.48	1E8 (1E8)	0.32	0.1 (0.1)	0.74
(0; 0)	5	1nM (0.9993nM)	1.05	1E8 (1E8)	0.66	0.1 (0.1)	1.53
(0; 0)	10	1nM (1nM)	1.54	1E8 (1E8)	0.98	0.1 (0.1)	2.32
(0; 0)	20	1nM (0.996nM)	2.25	1E8 (9.99E7)	1.35	0.1 (0.1)	3.22
(0; 0)	60	1nM (1.002nM	4.06	1E8 (1E8)	2.67	0.1 (0.1)	6.12
(0; 0)	1	100nM (100nM)	0.20	1E7 (1E7)	0.81	1 (1)	0.88
(0; 0)	5	100nM (100nM)	0.47	1E7 (9.99E6)	1.41	1 (1)	1.53

(0; 0)	10	100nM (100nM)	0.62	1E7 (1E7)	2.20	1 (1)	2.29
(0; 0)	20	100nM (100nM)	0.90	1E7 (1E7)	3.24	1 (1)	3.48
(0; 0)	60	100nM (100nM)	1.67	1E7 (1E7)	7.85	1 (1)	8.46
(0; 0)	1	10μM (10μM)	0.18	1E6 (1.01E6)	4.04	10 (10.07)	4.07
(0; 0)	5	10μM (10μM)	0.43	1E6 (1.01E6)	9.08	10 (10.06)	9.13
(0; 0)	10	10μM (10μM)	0.64	1E6 (1.01E6)	13.24	10 (10.14)	13.32
(0; 0)	20	10μM (10μM)	0.85	1E6 (1.06E6)	27.32	10 (10.57)	27.51
(0; 4)	60	10μM (10μM)	1.52	1E6 (1.03E6)	48.92	10 (10.29)	49.03
(200; 4)	1	1mM (1mM)	0.19	1E5 (1.07E5)	35.44	100 (107.40)	35.47
(194; 23)	5	1mM (1mM)	0.47	1E5 (1.45E5)	96.89	100 (145.64)	97.11
(188; 30)	10	1mM (1mM)	0.56	1E5 (1.25E5)	82.92	100 (124.57)	82.98
(161; 34)	20	1mM (1mM)	0.89	1E5 (1.10E5)	84.50	100 (109.54)	84.29
(110; 54)	60	1mM (1mM)	1.51	1E5 (1.08E5)	79.17	100 (108.44)	79.07

Offline addition first read time 30 sec							
Number of : (Ambiguous fits; Outliers)	Read frequency (sec)	Input K_d (Output K_d)	K_d %CV	Input k_{on} (Output k_{on}) $M^{-1}min^{-1}$	k_{on} %CV	Input k_{off} (Output k_{off}) min^{-1}	k_{off} %CV

(0; 0)	1	10pM (10.02pM)	1.59	1E9 (1E9)	0.19	0.01 (0.01)	1.74
(0; 0)	5	10pM (10.02pM)	3.85	1E9 (1E9)	0.43	0.01 (0.01)	4.20
(0; 0)	10	10pM (10.02pM)	5.34	1E9 (1E9)	0.63	0.01 (0.01)	5.85
(0; 0)	20	10pM (10.05pM)	7.15	1E9 (1E9)	0.81	0.01 (0.01)	7.77
(0; 0)	60	10pM (9.73pM)	13.56	1E9 (9.97E8)	1.53	0.01 (0.01)	14.84
(0; 0)	1	1nM (1nM)	0.53	1E8 (1E8)	0.33	0.1 (0.1)	0.77
(0; 0)	5	1nM (1nM)	1.10	1E8 (9.99E7)	0.79	0.1 (0.1)	1.70
(0; 0)	10	1nM (1nM)	1.52	1E8 (1E8)	1.01	0.1 (0.1)	2.30
(0; 0)	20	1nM (1.002nM)	2.36	1E8 (1E8)	1.44	0.1 (0.1)	3.37
(0; 0)	60	1nM (1.002nM)	3.59	1E8 (1E8)	2.45	0.1 (0.1)	5.39
(0; 0)	1	100nM (100nM)	0.22	1E7 (1E7)	0.87	1 (1)	0.96
(0; 0)	5	100nM (100nM)	0.44	1E7 (1E7)	2.07	1 (1)	2.15
(0; 0)	10	100nM (100nM)	0.67	1E7 (1E7)	2.67	1 (1)	2.85
(0; 0)	20	100nM (99.99nM)	0.91	1E7 (1E7)	3.92	1 (1)	4.14
(0; 0)	60	100nM (100nM)	0.97	1E7 (1E7)	3.75	1 (1)	3.96
(10; 0)	1	10μM (9.998μM)	0.21	1E6 (1.02E6)	11.41	10 (10.22)	11.46
(25; 0)	5	10μM (9.998μM)	0.41	1E6 (1.06E6)	35.34	10 (10.60)	35.44

(24; 9)	10	10μM (9.998μM)	0.64	1E6 (1.01E6)	36.20	10 (11.02)	36.30
(33; 5)	20	10μM (10μM)	0.95	1E6 (1.21E6)	53.14	10 (12.14)	53.50
(15; 11)	60	10μM (10μM)	1.50	1E6 (1.13E6)	48.06	10 (11.35)	48.33
(200; 23)	1	1mM (0.994mM)	0.19	1E5 (6.05E7)	312.35	100 (6.06E4)	312.28
(200; 12)	5	1mM (1mM)	0.44	1E5 (1.47E9)	249.83	100 (1.47E6)	249.81
(192; 33)	10	1mM (1mM)	0.65	1E5 (2.15E8)	273.44	100 (2.16E5)	273.47
(173; 13)	20	1mM (9.99E-4)	0.91	1E5 (2.83E9)	236.28	100 (2.83E6)	235.84
(138; 11)	60	1mM (9.98E-4)	1.42	1E5 (4.33E9)	252.26	100 (4.34E6)	252.33

Supplementary Table 8.4. Summary of the kinetic input parameters and their estimates for unlabelled compounds under conditions which mimic online injection and offline addition of membranes, values are determined from 200 simulated data sets using the Motulsky-Mahan model equation and the low affinity tracer (k_{on} = 1x10^{8}M^{-1} min^{-1}; k_{off} = 0.1min^{-1} K_d= 1nM).

Online injection first read time 1sec							
Number of : (Ambiguous fits; Outliers)	Read frequency (sec)	Input K_d (Output K_d)	K_d %CV	Input k_{on} (Output k_{on}) M^{-1}min^{-1}	k_{on} %CV	Input k_{off} (Output k_{off}) min^{-1}	k_{off} %CV
(0; 0)	1	10pM (10pM)	1.07	1E9 (1E9)	0.18	0.01 (0.01)	1.22
(0; 0)	5	10pM (9.99pM)	2.41	1E9 (1E9)	0.42	0.01 (0.01)	2.74
(0; 0)	10	10pM (10pM)	3.52	1E9 (1E9)	0.62	0.01 (0.01)	4.06
(0; 0)	20	10pM (10pM)	5.05	1E9 (1E9)	0.88	0.01 (0.01)	5.05
(0; 0)	60	10pM (10pM)	8.33	1E9 (1E9)	1.54	0.01 (0.01)	9.55
(0; 0)	1	1nM (1nM)	0.17	1E8 (1E8)	0.29	0.1 (0.1)	0.38
(0; 0)	5	1nM (0.9993nM)	0.38	1E8 (1E8)	0.57	0.1 (0.1)	0.75
(0; 0)	10	1nM (1nM)	0.56	1E8 (1E8)	0.92	0.1 (0.1)	1.24
(0; 0)	20	1nM (0.999nM)	0.81	1E8 (9.98E7)	1.27	0.1 (0.1)	1.73
(0; 0)	60	1nM (0.999nM)	1.34	1E8 (9.99E7)	2.04	0.1 (0.1)	2.78
(0; 0)	1	100nM (100nM)	0.12	1E7 (1E7)	1.23	1 (1)	1.27
(0; 0)	5	100nM (100nM)	0.25	1E7 (1.01E7)	3.10	1 (1)	3.20

(0; 0)	10	100nM (100nM)	0.38	1.01E7 (1E7)	4.0	1 (1.01)	4.15
(0; 0)	20	100nM (100nM)	0.59	1E7 (9.99E6)	6.0	1 (1)	6.17
(0; 0)	60	100nM (99.9nM)	0.99	1E7 (1.02E7)	10.71	1 (1.02)	10.87
(198; 0)	1	10μM (10μM)	0.12	1E6 (1.01E6)	11.55	10 (10.07)	11.57
(167; 1)	5	10μM (10μM)	0.27	1E6 (1.08E6)	30.83	10 (10.84)	30.90
(165; 6)	10	10μM (10μM)	0.35	1E6 (1.17E6)	46.26	10 (11.74)	46.37
(145; 12)	20	10μM (10μM)	0.51	1E6 (1.14E6)	52.10	10 (11.45)	52.30
(138; 38)	60	10μM (9.99μM)	0.98	1E6 (1.31E6)	104.83	10 (13.12)	104.98
(200; 29)	1	1mM (1mM)	0.12	1E5 (3.79E6)	283.24	100 (3789.78)	283.25
(200; 6)	5	1mM (1mM)	0.27	1E5 (1.72E8)	251.19	100 (1.72E5)	251.26
(200; 35)	10	1mM (0.994mM)	7.82	1E5 (2.89E7)	261.12	100 (2.56E4)	245.84
(197; 24)	20	1mM (1mM)	0.54	1E5 (2.52E8)	277.58	100 (2.52E5)	277.30
(175; 13)	60	1mM (1mM)	0.86	1E5 (1.18E9)	240.35	100 (1.18E6)	240.04

Offline addition first read time 30 sec							
Number of : (Ambiguous fits; Outliers)	Read frequency (sec)	Input K_d (Output K_d)	K_d %CV	Input k_{on} (Output k_{on}) $M^{-1}min^{-1}$	k_{on} %CV	Input k_{off} (Output k_{off}) min^{-1}	k_{off} %CV

(0; 0)	1	10pM (10.02pM)	1.21	1E9 (1E9)	0.20	0.01 (0.01)	1.38
(0; 0)	5	10pM (9.99pM)	2.37	1E9 (1E9)	0.43	0.01 (0.01)	2.73
(0; 0)	10	10pM (10.02pM)	3.72	1E9 (1E9)	0.59	0.01 (0.01)	4.21
(0; 0)	20	10pM (10.1pM)	4.55	1E9 (1E9)	0.86	0.01 (0.01)	5.23
(0; 0)	60	10pM (10pM)	8.39	1E9 (9.97E8)	1.51	0.01 (0.01)	9.60
(0; 0)	1	1nM (1nM)	0.17	1E8 (1E8)	0.27	0.1 (0.1)	0.38
(0; 0)	5	1nM (1nM)	0.37	1E8 (1E8)	0.66	0.1 (0.1)	0.88
(0; 0)	10	1nM (1nM)	0.50	1E8 (1E8)	0.88	0.1 (0.1)	1.14
(0; 0)	20	1nM (1nM)	0.74	1E8 (1E8)	1.35	0.1 (0.1)	1.78
(0; 0)	60	1nM (1nM)	1.27	1E8 (1E8)	2.34	0.1 (0.1)	3.13
(0; 0)	1	100nM (100nM)	0.28	1E7 (1E7)	1.57	1 (1)	1.71
(0; 0)	5	100nM (100nM)	0.44	1E7 (1E7)	2.07	1 (1)	2.15
(0; 0)	10	100nM (100nM)	0.35	1E7 (9.96E6)	3.76	1 (1)	3.80
(0; 0)	20	100nM (100nM)	0.51	1E7 (1E7)	5.80	1 (1)	5.91
(0; 0)	60	100nM (100nM)	0.55	1E7 (1E7)	5.52	1 (1)	5.64
(200; 0)	1	10μM (10μM)	0.11	1E6 (1.05E6)	13.71	10 (10.47)	13.74
(189; 5)	5	10μM (10μM)	0.26	1E6 (1.10E6)	30.09	10 (10.96)	30.17

(160; 3)	10	10μM (10μM)	0.35	1E6 (1.11E6)	44.94	10 (11.10)	45.04
(146; 9)	20	10μM (10μM)	0.51	1E6 (1.21E6)	67.30	10 (12.15)	67.49
(127; 32)	60	10μM (9.98μM)	0.96	1E6 (1.33E6)	90.67	10 (13.30)	91.04
(200; 16)	1	1mM (0.994mM)	7.39	1E5 (5.92E6)	326.01	100 (5.30E3)	328.85
(200; 36)	5	1mM (1mM)	0.25	1E5 (1.51E7)	248.87	100 (1.51E4)	249.0
(199; 8)	10	1mM (1mM)	0.33	1E5 (3.17E8)	283.26	100 (3.17E5)	283.26
(173; 23)	20	1mM (9.99E-4)	0.96	1E5 (6.49E8)	235.89	100 (2.83E6)	235.57
(180; 13)	60	1mM (1mM)	0.99	1E5 (5.02E8)	217.62	100 (5.02E5)	217.31

Supplementary Table 8.5. Summary of the kinetic input parameters and their estimates for unlabelled compounds under conditions which mimic online injection and offline addition of membranes, values are determined from 200 simulated data sets using the Motulsky-Mahan model equation and the low affinity tracer (k_{on} = 1x10^{9}M^{-1}min^{-1}; k_{off} = 0.01min^{-1} K_d= 10pM).

Online injection first read time 1sec							
Number of : (Ambiguous fits; Outliers)	Read frequency (sec)	Input K_d (Output K_d)	K_d %CV	Input k_{on} (Output k_{on}) M^{-1}min^{-1}	k_{on} %CV	Input k_{off} (Output k_{off}) min^{-1}	k_{off} %CV
(0; 0)	1	10pM (10pM)	0.10	1E9 (1E9)	0.11	0.01 (0.01)	0.18
(0; 0)	5	10pM (10pM)	0.22	1E9 (1E9)	0.25	0.01 (0.01)	0.41
(0; 0)	10	10pM (10pM)	0.33	1E9 (1E9)	0.34	0.01 (0.01)	0.61
(0; 0)	20	10pM (10pM)	0.45	1E9 (1E9)	0.54	0.01 (0.01)	0.89
(0; 0)	60	10pM (10pM)	0.86	1E9 (9.99E8)	0.84	0.01 (0.01)	1.51
(0; 0)	1	1nM (1nM)	0.05	1E8 (1E8)	0.44	0.1 (0.1)	0.46
(0; 0)	5	1nM (1nM)	0.12	1E8 (1E8)	0.88	0.1 (0.1)	0.93
(0; 0)	10	1nM (1nM)	0.17	1E8 (1E8)	1.47	0.1 (0.1)	1.51
(0; 0)	20	1nM (1nM)	0.24	1E8 (1E8)	1.92	0.1 (0.1)	2.01
(0; 0)	60	1nM (1nM)	0.47	1E8 (1E8)	3.53	0.1 (0.1)	3.75
(7; 0)	1	100nM (100nM)	0.05	1E7 (9.97E6)	3.58	1 (1)	3.59
(43; 0)	5	100nM (100nM)	0.11	1E7 (1.01E7)	8.31	1 (1.01)	8.36

(50; 0)	10	100nM (100nM)	0.15	1E7 (1.01E7)	11.68	1 (1.01)	11.74
(66; 0)	20	100nM (100nM)	0.22	1E7 (1.03E7)	15.59	1 (1.03)	15.65
(80; 2)	60	100nM (99.9nM)	0.37	1E7 (1.07E7)	35.12	1 (1.07)	35.29
1							
(200; 1)	1	10μM (10μM)	0.05	1E6 (1.15E6)	43.79	10 (11.52)	43.81
(200; 29)	5	10μM (10μM)	0.12	1E6 (1.12E6)	66.90	10 (11.25)	66.95
(200; 14)	10	10μM (10μM)	0.16	1E6 (1.75E9)	294.79	10 (17548.04)	294.76
(200; 8)	20	10μM (10μM)	0.24	1E6 (5.64E9)	250.94	10 (56466.86)	251.01
(200; 6)	60	10μM (10μM)	0.39	1E6 (8.72E9)	230.45	10 (87216.14)	230.35
(200; 11)	1	1mM (1mM)	0.05	1E5 (9.55E6)	48.48	100 (9553.29)	48.47
(200; 21)	5	1mM (1mM)	0.12	1E5 (9.79E6)	54.05	100 (9787.06)	54.05
(200; 16)	10	1mM (1mM)	0.15	1E5 (9.77E6)	59.74	100 (9770.79)	59.74
(200; 22)	20	1mM (1mM)	0.21	1E5 (1.17 E7)	98.96	100 (11729.2)	99.01
(200; 16)	60	1mM (1mM)	0.36	1E5 (1.27E7)	92.39	100 (12507.79)	92.30

Online injection first read time 1sec

Number of : (Ambiguous fits; Outliers)	Read frequency (sec)	Input K_d (Output K_d)	K_d %CV	Input k_{on} (Output k_{on}) $M^{-1}min^{-1}$	k_{on} %CV	Input k_{off} (Output k_{off}) min^{-1}	k_{off} %CV
(0; 0)	1	10pM (10pM)	0.10	1E9 (1E9)	0.12	0.01 (0.01)	0.20
(0; 0)	5	10pM (9.99pM)	2.43	1E9 (1E9)	0.46	0.01 (0.01)	2.81
(0; 0)	10	10pM (10pM)	0.33	1E9 (1E9)	0.37	0.01 (0.01)	0.62
(0; 0)	20	10pM (10pM)	0.43	1E9 (1E9)	0.53	0.01 (0.01)	0.86
(0; 0)	60	10pM (10pM)	0.78	1E9	0.87	0.01 (0.01)	1.46
(0; 0)	1	1nM (1nM)	0.05	1E8 (1E8)	0.46	0.1 (0.1)	0.48
(0; 0)	5	1nM (1nM)	0.12	1E8 (9.99E7)	0.89	0.1 (0.1)	0.93
(0; 0)	10	1nM (1nM)	0.16	1E8 (1E8)	1.36	0.1 (0.1)	1.43
(0; 0)	20	1nM (1nM)	0.25	1E8 (1E8)	1.76	0.1 (0.1)	1.88
(0; 0)	60	1nM (1nM)	0.40	1E8 (9.99E7)	2.91	0.1 (0.1)	3.07
(9; 0)	1	100nM (100nM)	0.05	1E7 (1E7)	3.33	1 (1)	3.35
(58; 0)	5	100nM (100nM)	0.12	1E7 (1.01E7)	8.81	1 (1.01)	8.85
(51; 0)	10	100nM (100nM)	0.17	1E7 (1.01E7)	11.53	1 (1.01)	11.59
(68; 0)	20	100nM (100nM)	0.22	1E7 (1.02E7)	18.16	1 (1.02)	18.24
(77; 0)	60	100nM (100nM)	0.23	1E7 (1.05E7)	17.87	1 (1.05)	17.95

(200; 8)	1	10μM (10μM)	0.05	1E6 (1.16E6)	44.00	10 (11.61)	44.02
(200; 17)	5	10μM (10μM)	0.11	1E6 (1.54E6)	115.22	10 (15.39)	115.24
(200; 52)	10	10μM (10μM)	0.14	1E6 (1.28E6)	247.86	10 (12.84)	248.29
(200; 6)	20	10μM (10μM)	0.22	1E6 (1.08E10)	285.87	10 (1.08E5)	285.94
(200; 16)	60	10μM (10μM)	0.39	1E6 (5.38E9)	252.64	10 (53811.80)	252.71
(200; 13)	1	1mM (1mM)	0.05	1E5 (1.02E7)	55.30	100 (10237.89)	55.30
(200; 14)	5	1mM (1mM)	0.11	1E5 (9.95E6)	55.06	100 (9950.64)	55.05
(200; 16)	10	1mM (1mM)	0.15	1E5 (9.68E6))	49.20	100 (9683.19)	49.20
(200; 8)	20	1mM (1mM)	0.20	1E5 (9.63E6)	55.35	100 (9632.49)	55.33
(200; 16)	60	1mM (1mM)	0.40	1E5 (9.98E6)	60.23	100 (9977.35)	60.20

8.2 References

Abi-Dargham A, Rodenhiser J, Printz D, Zea-Ponce Y, Gil R, Kegeles LS, Weiss R, Cooper TB, Mann JJ, Van Heertum RL, Gorman JM, Laruelle M (2000). Increased baseline occupancy of D2 receptors by dopamine in schizophrenia. *Proc Natl Acad Sci U S A.* **97**(14):8104-9.

Alberty RA, Hammes GG (1958). Application of the Theory of Diffusion-controlled Reactions to Enzyme Kinetics. *J. Phys. Chem.* **62**(2):154-159.

Albizu L, Cottet M, Kralikova M, Stoev S, Seyer R, Brabet I, Roux T, Bazin H, Bourrier E, Lamarque L, Breton C, Rives ML, Newman A, Javitch J, Trinquet E, Manning M, Pin JP, Mouillac B, Durroux T (2010). Time-resolved FRET between GPCR ligands reveals oligomers in native tissues. *Nat Chem Biol*. **6**(8):587-94.

Alex KD, Yavanian GJ, McFarlane HG, Pluto CP, Pehek EA (2005). Modulation of dopamine release by striatal 5-HT2C receptors. *Synapse.* **55**(4):242-51.

Alex KD, Pehek EA (2007). Pharmacologic mechanisms of serotonergic regulation of dopamine neurotransmission. *Pharmacol Ther.* **113**(2):296-320.

Arakawa R, Ito H, Takano A, Takahashi H, Morimoto T, Sassa T, Ohta K, Kato M, Okubo Y, Suhara T (2008). Dose-finding study of paliperidone ER based on striatal and extrastriatal dopamine D2 receptor occupancy in patients with schizophrenia. *Psychopharmacology (Berl).* **197**(2):229-35.

Arányi P (1980). Kinetics of the hormone-receptor interaction. Competition experiments with slowly equilibrating ligands. *Biochim Biophys Acta.* **628**(2):220-7.

Auberson YP, Briard E, Sykes D, Reilly J, Healy M (2016) Ligand Specific Efficiency (LSE) Index for PET Tracer Optimization. *ChemMedChem.* **11**(13):1415-27.

Baker JG, Middleton R, Adams L, May LT, Briddon SJ, Kellam B, Hill SJ (2010). Influence of fluorophore and linker composition on the pharmacology of fluorescent adenosine A1 receptor ligands. *Br J Pharmacol*. **159**(4): 772–786.

Bakthavachalam V, Baindur N, Madras BK, Neumeyer JL (1991). Fluorescent probes for dopamine receptors: synthesis and characterization of fluorescein and 7-nitrobenz-2-oxa-1,3-diazol-4-yl conjugates of D-1 and D-2 receptor ligands. *J Med Chem.* **34**(11):3235-41.

Ban TA (2007). Fifty years chlorpromazine: a historical perspective. *Neuropsychiatr Dis Treat*. **3**(4):495-500.

Barnas C, Quiner S, Tauscher J, Hilger E, Willeit M, Küfferle B, Asenbaum S, Brücke T, Rao ML, Kasper S (2001). In vivo (123)I IBZM SPECT imaging of striatal dopamine 2 receptor occupancy in schizophrenic patients. *Psychopharmacology (Berl).* **157**(3):236-42.

Bartholini G (1976). Differential effect of neuroleptic drugs on dopamine turnover in the extrapyramidal and limbic system. *J Pharm Pharmacol.* **28**(5):429-33.

Bdioui S, Verdi J, Pierre N, Trinquet E, Roux T, Kenakin T (2018). Equilibrium Assays Are Required to Accurately Characterize the Activity Profiles of Drugs Modulating Gq-Protein-Coupled Receptors. *Mol Pharmacol.* **94**(3):992-1006.

Ben-Jonathan N, Oliver C, Weiner HJ, Mical RS, Porter JC (1977). Dopamine in hypophysial portal plasma of the rat during the estrous cycle and throughout pregnancy. *Endocrinology.* **100**(2):452-8.

Ben-Jonathan N, Neill MA, Arbogast LA, Peters LL, Hoefer MT (1980). Dopamine in hypophysial portal blood: relationship to circulating prolactin in pregnant and lactating rats. *Endocrinology.* **106**(3):690-6.

Benloucif S, Galloway MP (1991). Facilitation of dopamine release in vivo by serotonin agonists: studies with microdialysis. *Eur J Pharmacol.* **23**;200(1):1-8.

Bernardo M, Parellada E, Lomeña F, Catafau AM, Font M, Gómez JC, López-Carrero C, Gutiérrez F, Pavía J, Salamero M (2001). Double-blind olanzapine vs. haloperidol D2 dopamine receptor blockade in schizophrenic patients: a baseline-endpoint. *Psychiatry Res.* **107**(2):87-97.

Bigliani V, Mulligan RS, Acton PD, Visvikis D, Ell PJ, Stephenson C, Kerwin RW, Pilowsky LS (1999). In vivo occupancy of striatal and temporal cortical D2/D3 dopamine receptors by typical antipsychotic drugs. [123I]epidepride single photon emission tomography (SPET) study. *Br J Psychiatry.* **175**:231-8.

Bigliani V, Mulligan RS, Acton PD, Ohlsen RI, Pike VW, Ell PJ, Gacinovic S, Kerwin RW, Pilowsky LS (2000). Striatal and temporal cortical D2/D3 receptor occupancy by olanzapine and sertindole in vivo: a [123I]epidepride single photon emission tomography (SPET) study. *Psychopharmacology (Berl).* **150**(2):132-40.

Black JW, Leff P (1983). Operational models of pharmacological agonism. *Proc R Soc Lond B Biol Sci.*;**220**(1219):141-62.

Black JW, Leff P, Shankley NP, Wood J (1985). An operational model of pharmacological agonism: the effect of E/[A] curve shape on agonist dissociation constant estimation. *Br J Pharmacol.* **84**(2):561-71.

Blair DT, Dauner A (1992). Extrapyramidal symptoms are serious side-effects of antipsychotic and other drugs*. Nurse Pract.* **17**(11):56, 62-4, 67. Review.

Bosma R, van den Bor J, Vischer HF, Labeaga L, Leurs R (2018). The long duration of action of the second generation antihistamine bilastine coincides with its long residence time at the histamine H1 receptor. *Eur J Pharmacol.* **838**:107-111.

Bosma R, Stoddart LA, Georgi V, Bouzo-Lorenzo M, Bushby N, Inkoom L, Waring MJ, Briddon SJ, Vischer HF, Sheppard RJ, Fernández-Montalván A, Hill SJ, Leurs

R (2019). Probe dependency in the determination of ligand binding kinetics at a prototypical G protein-coupled receptor. Sci Rep. **9**(1):7906.

Bouzo-Lorenzo M, Stoddart LA, Xia L, IJzerman AP, Heitman LH, Briddon SJ, Hill SJ (2019). A live cell NanoBRET binding assay allows the study of ligand-binding kinetics to the adenosine A3 receptor. *Purinergic Signal.* **15**(2):139-153.

Brea J, Castro M, Giraldo J, López-Giménez JF, Padín JF, Quintián F, Cadavid MI, Vilaró MT, Mengod G, Berg KA, Clarke WP, Vilardaga JP, Milligan G, Loza MI (2009) Evidence for distinct antagonist-revealed functional states of 5-hydroxytryptamine(2A) receptor homodimers. *Mol Pharmacol.* **75**(6):1380-91.

Bressan RA, Erlandsson K, Jones HM, Mulligan R, Flanagan RJ, Ell PJ, Pilowsky LS (2003). Is regionally selective D2/D3 dopamine occupancy sufficient for atypical antipsychotic effect? an in vivo quantitative [123I]epidepride SPET study of amisulpride-treated patients. *Am J Psychiatry.* **160**(8):1413-20.

Bressan RA, Erlandsson K, Spencer EP, Ell PJ, Pilowsky LS (2004). Prolactinemia is uncoupled from central D2/D3 dopamine receptor occupancy in amisulpride treated patients. *Psychopharmacology (Berl).* **175**(3):367-73.

Briddon SJ, Kellam B, Hill SJ (2011). Design and use of fluorescent ligands to study ligand-receptor interactions in single living cells. *Methods Mol Biol.* **746**:211-36.

Broekkamp CL, Oosterloo SK, Berendsen HH, van Delft AM (1988). Effect of metergoline, fenfluramine, and 8-OHDPAT on catalepsy induced by haloperidol or morphine. Naunyn Schmiedebergs Arch Pharmacol. **338**(2):191-5.

Brühl AB, Sahakian BJ (2017). Neuroscience-based Nomenclature: improving clinical and scientific terminology in research and clinical psychopharmacology. *Psychol Med.* **47**(8):1339-1341.

Bürki HR (1979). Extrapyramidal side-effects. *Pharmacol Ther B.* **5**(1-3):525-34.

Bürki HR (1986). Effects of fluperlapine on dopaminergic systems in rat brain. *Psychopharmacology (Berl).* **89**(1):77-84.

Canton H, Verrièle L, Millan MJ (1994). Competitive antagonism of serotonin (5-HT)2C and 5-HT2A receptor-mediated phosphoinositide (PI) turnover by clozapine in the rat: a comparison to other antipsychotics. *Neurosci Lett.* **181**(1-2):65-8.

Carboni L, Negri M, Michielin F, Bertani S, Fratte SD, Oliosi B, Cavanni P (2012). Slow dissociation of partial agonists from the D_2 receptor is linked to reduced prolactin release. *Int J Neuropsychopharmacol.* **15**(5):645-56.

Carlsson A, Lindqvist M (1963). Effect of chlorpromazine or haloperidol on the formation of 3-methoxytyramine and normetanephrine in mouse brain. *Acta Pharmacol Toxicol (Copenh)* **20**,140–144.

Caron MG, Beaulieu M, Raymond V, Gagné B, Drouin J, Lefkowitz RJ, Labrie F (1978). Dopaminergic receptors in the anterior pituitary gland. Correlation of [3H]dihydroergocryptine binding with the dopaminergic control of prolactin release. *J Biol Chem.* **253**(7):2244-53.

Carpenter JW, Laethem C, Hubbard FR, Eckols TK, Baez M, McClure D, Nelson DL, Johnston PA (2002). Configuring radioligand receptor binding assays for HTS using scintillation proximity assay technology. *Methods Mol Biol.* **190**:31-49.

Carter, C. M., Leighton-Davies, J. R. & Charlton, S. J (2007). Miniaturized receptor binding assays: complications arising from ligand depletion. *J Biomol Screen* **12,** 255-266.

Castro SW, Strange PG (1993). Differences in the ligand binding properties of the short and long versions of the D2 dopamine receptor. *J Neurochem.* **60**(1):372-5.

Celada P, Puig MV, Artigas F (2013). Serotonin modulation of cortical neurons and networks. *Front Integr Neurosci.* **19**;7:25.

Charlton, S. J. & Vauquelin, G (2010). Elusive equilibrium: the challenge of interpreting receptor pharmacology using calcium assays. *Br J Pharmacol* **161,** 1250-1265.

Cheng, Y. & Prusoff, W. H (1973). Relationship between the inhibition constant (K1) and the concentration of inhibitor which causes 50 per cent inhibition (I50) of an enzymatic reaction. *Biochem Pharmacol* **22,** 3099-3108.

Chiodo LA, Bunney BS (1983). Typical and atypical neuroleptics: differential effects of chronic administration on the activity of A9 and A10 midbrain dopaminergic neurons. *J Neurosci.* **3**(8):1607-19.

Christopoulos A (2001). From 'captive' agonism to insurmountable antagonism: demonstrating the power of analytical pharmacology. *Clin Exp Pharmacol Physiol.* **28**(3):223-9.

Claveria-Gimeno R, Vega S, Abian O, Velazquez-Campoy A (2017). A look at ligand binding thermodynamics in drug discovery. *Expert Opin Drug Discov.* **12**(4):363-377.

Compton MT, Miller AH (2002). Antipsychotic-induced hyperprolactinemia and sexual dysfunction. *Psychopharmacol Bull.* **36**(1):143-64.

Contreras ML, Wolfe BB, Molinoff PB (1986). Kinetic analysis of the interactions of agonists and antagonists with beta adrenergic receptors. *J Pharmacol Exp Ther.* 239(1):136-43.

Coombs, D. & Goldstein, B (2004). Effects of the geometry of the immunological synapse on the delivery of effector molecules. *Biophys J*. **87,** 2215-2220.

Copeland RA, Pompliano DL, Meek TD (2006). Drug-target residence time and its implications for lead optimization. *Nat Rev Drug Discov.* **5**(9):730-9.

Copeland RA (2010). The dynamics of drug-target interactions: drug-target residence time and its impact on efficacy and safety. *Expert Opin Drug Discov.* **5**(4):305-10.

Copeland, R. A. (2011). Conformational adaptation in drug–target interactions and residence time. *Future Medicinal Chem* **3**(12):1491–1501.

Copeland RA (2016). The drug-target residence time model: a 10-year retrospective. *Nat Rev Drug Discov.* **15**(2):87-95.

Corripio I, Catafau AM, Perez V, Puigdemont D, Mena E, Aguilar Y, Carrió I, Alvarez E (2005). Striatal dopaminergic D2 receptor occupancy and clinical efficacy in psychosis exacerbation: a 123I-IBZM study with ziprasidone and haloperidol. *Prog Neuropsychopharmacol Biol Psychiatry*. **29**(1):91-6.

Corripio I, Ferreira A, Portella MJ, Pérez V, Escartí MJ, Del Valle Camacho M, Sauras RB, Alonso A, Grasa EM, Carrió I, Catafau AM, Alvarez E (2012). The role of striatal dopamine D2 receptors in the occurrence of extrapyramidal side effects: iodine-123-iodobenzamide single photon emission computed tomography study. *Psychiatry Res.* **201**(1):73-7.

Cortesi PA, Mencacci C, Luigi F, Pirfo E, Berto P, Sturkenboom MC, Lopes FL, Giustra MG, Mantovani LG, Scalone L (2013). Compliance, persistence, costs and quality of life in young patients treated with antipsychotic drugs: results from the COMETA study. *BMC Psychiatry.* **13**:98.

Costall B, Naylor RJ (1976). A comparison of the abilities of typical neuroleptic agents and of thioridazine, clozapine, sulpiride and metoclopramide to antagonise the hyperactivity induced by dopamine applied intracerebrally to areas of the extrapyramidal and mesolimbic systems. *Eur J Pharmacol.* **40**(1):9-19.

Cottet M, Faklaris O, Maurel D, Scholler P, Doumazane E, Trinquet E, Pin JP, Durroux T (2012). BRET and Time-resolved FRET strategy to study GPCR oligomerization: from cell lines toward native tissues. *Front Endocrinol (Lausanne*). **3**:92.

Creese I, Burt DR, Snyder SH (1975). Dopamine receptor binding: differentiation of agonist and antagonist states with 3H-dopamine and 3H-haloperidol. *Life Sci.* **17**(6):933-1001.

Cunningham C, Peters K (2014). Aetiology of schizophrenia and implications for nursing practice: a literature review. *Issues Ment Health Nurs.* **35**(10):732-8.

Dahl G, Akerud T (2013). Pharmacokinetics and the drug-target residence time concept. *Drug Discov Today.* **18**(15-16):697-707.

Dal Toso R, Sommer B, Ewert M, Herb A, Pritchett DB, Bach A, Shivers BD, Seeburg PH (1989). The dopamine D2 receptor: two molecular forms generated by alternative splicing. *EMBO J.* **8**(13):4025-34.

Davis KL, Kahn RS, Ko G, Davidson M (1991). Dopamine in schizophrenia: a review and reconceptualization. *Am J Psychiatry.* **148**(11):1474-86. Review.

de Almeida J, Mengod G (2007). Quantitative analysis of glutamatergic and GABAergic neurons expressing 5-HT(2A) receptors in human and monkey prefrontal cortex. *J Neurochem.* **103**(2):475-86.

DeBlasi A, O'Reilly K, Motulsky HJ (1989). Calculating receptor number from binding experiments using same compound as radioligand and competitor. *Trends Pharmacol Sci.* **10**(6):227-9.

de Kloe GE, Retra K, Geitmann M, Källblad P, Nahar T, van Elk R, Smit AB, van Muijlwijk-Koezen JE, Leurs R, Irth H, Danielson UH, de Esch IJ (2010). Surface plasmon resonance biosensor based fragment screening using acetylcholine binding protein identifies ligand efficiency hot spots (LE hot spots) by deconstruction of nicotinic acetylcholine receptor α7 ligands. *J Med Chem.* **53**(19):7192-201.

Deganutti G, Zhukov A, Deflorian F, Federico S, Spalluto G, Cooke RM, Moro S, Mason JS, Bortolato A (2017). Impact of protein-ligand solvation and desolvation on transition state thermodynamic properties of adenosine A2A ligand binding kinetics. *In Silico Pharmacol.* **5**(1):16.

Desai N, Venkatesh CR, Kumar SS (2015). QT prolongation and torsades de pointes with psychotropic agents. *Indian J Psychiatry.* **57**(3):305-8.

de Witte WEA, Danhof M, van der Graaf PH, de Lange ECM (2016). In vivo Target Residence Time and Kinetic Selectivity: The Association Rate Constant as Determinant. *Trends Pharmacol Sci.* **37**(10):831-842.

de Witte WEA, Danhof M, van der Graaf PH, de Lange ECM (2018). The implications of target saturation for the use of drug-target residence time. *Nat Rev Drug Discov.* **18**(1):82-84.

Dowling MR, Charlton SJ (2006). Quantifying the association and dissociation-rates of unlabelled antagonists at the muscarinic M3 receptor. *Br J Pharmacol.* **148**(7):927-37.

Dror RO, Pan AC, Arlow DH, Borhani DW, Maragakis P, Shan Y, Xu H, Shaw DE (2011). Pathway and mechanism of drug binding to G-protein-coupled receptors. *Proc Natl Acad Sci U S A.* **108**(32):13118-23.

Dyhring T, Nielsen EØ, Sonesson C, Pettersson F, Karlsson J, Svensson P, Christophersen P, Waters N (2010). The dopaminergic stabilizers pridopidine (ACR16) and (-)-OSU6162 display dopamine D(2) receptor antagonism and fast receptor dissociation properties. *Eur J Pharmacol.* **628**(1-3):19-26.

Emami-Nemini A, Roux T, Leblay M, Bourrier E, Lamarque L, Trinquet E, Lohse MJ (2013). Time-resolved fluorescence ligand binding for G protein-coupled receptors. *Nat Protoc*. **8**(7):1307-20.

Erlandsson K, Bressan RA, Mulligan RS, Ell PJ, Cunningham VJ, Pilowsky LS (2003). Analysis of D2 dopamine receptor occupancy with quantitative SPET using the high-affinity ligand [123I]epidepride: resolving conflicting findings. *Neuroimage.* **19**(3):1205-14.

Farde L, Nordström AL, Wiesel FA, Pauli S, Halldin C, Sedvall G (1992). Positron emission tomographic analysis of central D1 and D2 dopamine receptor occupancy in patients treated with classical neuroleptics and clozapine. Relation to extrapyramidal side effects. *Arch Gen Psychiatry.* **49**(7):538-44.

Farde L, Ito H, Swahn CG, Pike VW, Halldin C (1998). Quantitative analyses of carbonyl-carbon-11-WAY-100635 binding to central 5-hydroxytryptamine-1A receptors in man. *J Nucl Med.* 39(11):1965-71.

Farde L, Nyberg S (1998) Dosing determination for novel antipsychotics – a PET-based approach. *Int J Psychiatr Clin Pract* **2**(1):39-42.

Felsing DE, Canal CE, Booth RG (2019). Ligand-directed serotonin 5-HT2C receptor desensitization and sensitization. *Eur J Pharmacol.* **848**:131-139.

Fleck BA, Hoare SR, Pick RR, Bradbury MJ, Grigoriadis DE (2012). Binding kinetics redefine the antagonist pharmacology of the corticotropin-releasing factor type 1 receptor. *J Pharmacol Exp Ther*. **341**(2):518-31.

Folmer RHA (2018). Drug target residence time: a misleading concept. *Drug Discov Today.* 23(1):12-16.

Gardner B, Strange PG (1998). Agonist action at D2(long) dopamine receptors: ligand binding and functional assays. *Br J Pharmacol.* **124**(5):978-84.

Gautier A, Juillerat A, Heinis C, Corrêa IR Jr, Kindermann M, Beaufils F, Johnsson K (2008). An engineered protein tag for multiprotein labeling in living cells. *Chem Biol.* **15**(2):128-36.

Gefvert O, Lundberg T, Wieselgren IM, Bergström M, Långström B, Wiesel F, Lindström L (2001). D(2) and 5HT(2A) receptor occupancy of different doses of quetiapine in schizophrenia: a PET study. *Eur Neuropsychopharmacol.* **11**(2):105-10.

Georgi V, Schiele F, Berger BT, Steffen A, Marin Zapata PA, Briem H, Menz S, Preusse C, Vasta JD, Robers MB, Brands M, Knapp S Fernández-Montalván A (2018). Binding Kinetics Survey of the Drugged Kinome. *J Am Chem Soc.* **140**(46):15774-15782.

Gherbi K, Briddon SJ and Charlton SJ (2018). Micro-pharmacokinetics: Quantifying local drug concentration at live cell membranes. *Sci Rep*. **8**(1):3479.

Gibbs DM, Neill JD (1978). Dopamine levels in hypophysial stalk blood in the rat are sufficient to inhibit prolactin secretion in vivo. *Endocrinology.* **102**(6):1895-900.

Gifford AN, Gatley SJ, Volkow ND (1998). Evaluation of the importance of rebinding to receptors in slowing the approach to equilibrium of high-affinity PET and SPECT radiotracers. *Synapse.* **28**(2):167-75.

Gillard M, Van Der Perren C, Moguilevsky N, Massingham R, Chatelain P (2002). Binding characteristics of cetirizine and levocetirizine to human H(1) histamine receptors: contribution of Lys(191) and Thr(194). *Mol Pharmacol.* **61**(2):391-9.

Gillard M, Chatelain P (2006). Changes in pH differently affect the binding properties of histamine H1 receptor antagonists. *Eur J Pharmacol.* **530**(3):205-14.

Ginovart N, Kapur S (2012). Role of dopamine D(2) receptors for antipsychotic activity. *Handb Exp Pharmacol.* (**212**):27-52.

Goff DC, Midha KK, Brotman AW, McCormick S, Waites M, Amico ET (1991). An open trial of buspirone added to neuroleptics in schizophrenic patients. *J Clin Psychopharmacol*. **11**(3):193-7.

Goto A, Mouri A, Nagai T, Yoshimi A, Ukigai M, Tsubai T, Hida H, Ozaki N, Noda Y (2016). Involvement of the histamine H 4 receptor in clozapine-induced hematopoietic toxicity: vulnerability under granulocytic differentiation of HL-60 cells. *Toxicol Appl Pharmacol* **306**:8–16.

Grace AA, Bunney BS, Moore H, Todd CL (1997). Dopamine-cell depolarization block as a model for the therapeutic actions of antipsychotic drugs. *Trends Neurosci.* **20**(1):31-7.

Guiard BP and Giovanni GD (2018). 5-HT2A Receptors in the Central Nervous System. Volume 32 of The Receptors, Springer.

Guiramand J, Montmayeur JP, Ceraline J, Bhatia M, Borrelli E (1995). Alternative splicing of the dopamine D2 receptor directs specificity of coupling to G-proteins. *J Biol Chem.* **270**(13):7354-8.

Guldberg CM, Waage P (1864). Studies concerning affinity. C. M. Forhandlinger: *Videnskabs-Selskabet i Christiana* 35.

Guo D, Mulder-Krieger T, IJzerman AP, Heitman LH (2012). Functional efficacy of adenosine A_2A receptor agonists is positively correlated to their receptor residence time. *Br J Pharmacol.* **166**(6):1846-59.

Guo D, Hillger JM, IJzerman AP, Heitman LH (2014). Drug-target residence time--a case for G protein-coupled receptors. *Med Res Rev*. **34**(4):856-92.

Guo D, Heitman LH, IJzerman AP (2017). Kinetic Aspects of the Interaction between Ligand and G Protein-Coupled Receptor: The Case of the Adenosine Receptors. *Chem Rev.* **117**(1):38-66.

Hall H, Wedel I, Sallemark M (1988). Effects of temperature on the in vitro binding of 3H-raclopride to rat striatal dopamine-D2 receptors. *Pharmacol Toxicol.* **63**(2):118-21.

Hall H, Farde L, Halldin C, Hurd YL, Pauli S, Sedvall G (1996). Autoradiographic localization of extrastriatal D2-dopamine receptors in the human brain using [125I]epidepride. *Synapse.* **23**(2):115-23.

Hall H, Lundkvist C, Halldin C, Farde L, Pike VW, McCarron JA, Fletcher A, Cliffe IA, Barf T, Wikström H, Sedvall G (1997). Autoradiographic localization of 5-HT1A receptors in the post-mortem human brain using [3H]WAY-100635 and [11C]way-100635. *Brain Res.* **745**(1-2):96-108.

Harikumar KG, Chattopadhyay A (2001). Modulation of antagonist binding to serotonin1A receptors from bovine hippocampus by metal ions. *Cell Mol Neurobiol.* **21**(5):453-64.

He M, Deng C, Huang XF (2013). The role of hypothalamic H1 receptor antagonism in antipsychotic-induced weight gain. *CNS Drugs*. **27**(6):423-34.

Hein P, Michel MC, Leineweber K, Wieland T, Wettschureck N, Offermanns S (2005). Receptor and binding studies, in: *Practical Methods in Cardiovascular Research*, S. Dhein, F. Mohr, M. Delmar (Eds.), Springer, Berlin Heidelberg. pp723-783.

Heise CE, Sullivan SK, Crowe PD (2007). Scintillation proximity assay as a high-throughput method to identify slowly dissociating nonpeptide ligand binding to the GnRH receptor. *J Biomol Screen.* **12**(2):235-9.

Herrick-Davis K, Grinde E, Teitler M (2000). Inverse agonist activity of atypical antipsychotic drugs at human 5-hydroxytryptamine2C receptors. *J Pharmacol Exp Ther*. **295**(1):226-32.

Hilfiker-Kleiner D, Struman I, Hoch M, Podewski E, Sliwa K (2012). 16-kDa prolactin and bromocriptine in postpartum cardiomyopathy. *Curr Heart Fail Rep.* **9**(3):174-82.

Hippius H (1989). The history of clozapine. *Psychopharmacology (Berl)* **99**: S3–S5.

Holdgate GA, Ward WH (2005). Measurements of binding thermodynamics in drug discovery. *Drug Discov Today.* **10**(22):1543-50.

Horacek J, Bubenikova-Valesova V, Kopecek M, Palenicek T, Dockery C, Mohr P, Höschl C (2006). Mechanism of action of atypical antipsychotic drugs and the neurobiology of schizophrenia. *CNS Drugs* **20,** 389-409.

Howell LL, Cunningham KA (2015). Serotonin 5-HT2 receptor interactions with dopamine function: implications for therapeutics in cocaine use disorder. Pharmacol Rev. **67**(1):176-97.

Howes OD, Egerton A, Allan V, McGuire P, Stokes P, Kapur S (2009). Mechanisms underlying psychosis and antipsychotic treatment response in schizophrenia: insights from PET and SPECT imaging. *Curr Pharm Des.* **15**(22):2550-9.

Howes OD, Kapur S (2009). The dopamine hypothesis of schizophrenia: version III--the final common pathway. *Schizophr Bull.* **35**(3):549-62.

Huang M, Dai J, Meltzer HY (2011). 5-HT(2A) and 5-HT(2C) receptor stimulation are differentially involved in the cortical dopamine efflux-Studied in 5-HT(2A) and 5-HT(2C) genetic mutant mice. *Eur J Pharmacol.* **652**(1-3):40-5.

Hulme EC, Birdsall NJM (1992) Strategy and tactics in receptor-binding studies. In Hulme EC (ed): Receptor-Ligand Interactions: A Practical Approach. Oxford, UK: IRL Press, pp63-176.

Hulme EC, Trevethick MA (2010). Ligand binding assays at equilibrium: validation and interpretation. *Br J Pharmacol.* **161**(6):1219-37.

Hyttel J, Nielsen JB, Nowak G (1992). The acute effect of sertindole on brain 5-HT2, D2 and alpha 1 receptors (ex vivo radioreceptor binding studies). *J Neural Transm Gen Sect.* **89**(1-2):61-9.

Ichikawa J, Ishii H, Bonaccorso S, Fowler WL, O'Laughlin IA, Meltzer HY (2001). 5-HT(2A) and D(2) receptor blockade increases cortical DA release via 5-HT(1A) receptor activation: a possible mechanism of atypical antipsychotic-induced cortical dopamine release. *J Neurochem.* **76**(5):1521-31.

Iliopoulos-Tsoutsouvas C, Kulkarni RN, Makriyannis A, Nikas SP (2018). Fluorescent probes for G-protein-coupled receptor drug discovery. *Expert Opin Drug Discov.* **13**(10):933-947.

IJzerman AP, Guo D (2019). Drug-Target Association Kinetics in Drug Discovery. *Trends Biochem Sci.* **44(**10):861-871.

Invernizzi RW, Cervo L, Samanin R (1988). 8-Hydroxy-2-(di-n-propylamino) tetralin, a selective serotonin1A receptor agonist, blocks haloperidol-induced catalepsy by an action on raphe nuclei medianus and dorsalis. *Neuropharmacology.* **27**(5):515-8.

Jafari S, Huang XF, Andrews JL, Fernandez-Enright F (2013). In vivo pharmacological evaluations of novel olanzapine analogues in rats: a potential new avenue for the treatment of schizophrenia. *PLoS One.* **8**(12):e80979.

Janoff AS, Pringle MJ, Miller KW (1981). Correlation of general anesthetic potency with solubility in membranes. *Biochim Biophys Acta.* **649(**1):125-8.

Janssen PA, Niemegeers CJ, Awouters F, Schellekens KH, Megens AA, Meert TF (1988). Pharmacology of risperidone (R 64 766), a new antipsychotic with serotonin-S2 and dopamine-D2 antagonistic properties. *J Pharmacol Exp Ther*. **244**(2):685-93.

Johnstone EC, Crow TJ, Frith CD, Carney MW, Price JS (1978). Mechanism of the antipsychotic effect in the treatment of acute schizophrenia. *Lancet.* **1**(8069):848-51.

Joyce JN, Janowsky A, Neve KA (1991). Characterization and distribution of [125I]epidepride binding to dopamine D2 receptors in basal ganglia and cortex of human brain. *J Pharmacol Exp Ther.* **257**(3):1253-63.

Kamberi IA, Mical RS, Porter JC (1970). Prolactin-inhibiting activity in hypophysial stalk blood and elevation by dopamine. *Experientia.* **26**(10):1150-1.

Kane JM (2011). Addressing side effects from antipsychotic treatment in schizophrenia. *J Clin Psychiatry.* **72**(2):e07.

Kapur S, Remington G (1996). Serotonin-dopamine interaction and its relevance to schizophrenia. *Am J Psychiatry.* **153**(4):466-76. Review.

Kapur, S. & Seeman, P (2000). Antipsychotic agents differ in how fast they come off the dopamine D2 receptors. Implications for atypical antipsychotic action. *J Psychiatry Neurosci* **25,** 161-166.

Kapur S, Zipursky R, Jones C, Remington G, Houle S (2000a). Relationship Between Dopamine D2 Occupancy, Clinical Response, and Side Effects: A Double-Blind PET Study of First-Episode Schizophrenia. *Am J Psychiatry.* **157**(4):514-20.

Kapur S, Zipursky R, Jones C, Shammi CS, Remington G, Seeman P (2000b). A positron emission tomography study of quetiapine in schizophrenia: a preliminary finding of an antipsychotic effect with only transiently high dopamine D2 receptor occupancy. *Arch Gen Psychiatry.* **57**(6):553-9.

Kapur, S. & Seeman, P (2001). Does fast dissociation from the dopamine d(2) receptor explain the action of atypical antipsychotics?: A new hypothesis. *Am J Psychiatry* **158,** 360-369.

Kapur S, Seeman P (2002). Atypical antipsychotics, cortical D(2) receptors and sensitivity to endogenous dopamine. *Br J Psychiatry.* **180**:465-6.

Kapur S, Agid O, Mizrahi R, Li M (2006). How antipsychotics work-from receptors to reality. *NeuroRx.* **3**(1):10-21.

Karam CS, Ballon JS, Bivens NM, Freyberg Z, Girgis RR, Lizardi-Ortiz JE, Markx S, Lieberman JA, Javitch JA (2010). Signaling pathways in schizophrenia: emerging targets and therapeutic strategies. *Trends Pharmacol Sci.* **31**(8):381-90.

Kasper S, Tauscher J, Küfferle B, Barnas C, Hesselmann B, Asenbaum S, Podreka I, Brücke T (1998). Sertindole and dopamine D2 receptor occupancy in comparison to risperidone, clozapine and haloperidol - a 123I-IBZM SPECT study. *Psychopharmacology (Berl).* 136(4):367-73.

Kasper S, Tauscher J, Küfferle B, Barnas C, Pezawas L, Quiner S (1999). Dopamine- and serotonin-receptors in schizophrenia: results of imaging-studies and implications for pharmacotherapy in schizophrenia. *Eur Arch Psychiatry Clin Neurosci.* **249** Suppl 4:83-9. Review.

Kegeles LS, Slifstein M, Frankle WG, Xu X, Hackett E, Bae SA, Gonzales R, Kim JH, Alvarez B, Gil R, Laruelle M, Abi-Dargham A (2008). Dose-occupancy study of striatal and extrastriatal dopamine D2 receptors by aripiprazole in schizophrenia with PET and [18F]fallypride. *Neuropsychopharmacology*. **33**(13):3111-25.

Kegeles LS, Abi-Dargham A, Frankle WG, Gil R, Cooper TB, Slifstein M, Hwang DR, Huang Y, Haber SN, Laruelle M (2010). Increased synaptic dopamine function in associative regions of the striatum in schizophrenia. *Arch Gen Psychiatry.* **67**(3):231-9.

Kenakin T (2016). The mass action equation in pharmacology. *Br J Clin Pharmacol.* **81**(1):41-51.

Kessler RM, Ansari MS, Riccardi P, Li R, Jayathilake K, Dawant B, Meltzer HY (2005). Occupancy of striatal and extrastriatal dopamine D2/D3 receptors by olanzapine and haloperidol. *Neuropsychopharmacology.* **30**(12):2283-9.

Khan ZU, Mrzljak L, Gutierrez A, de la Calle A, Goldman-Rakic PS (1998). Prominence of the dopamine D2 short isoform in dopaminergic pathways. Proc Natl Acad Sci U S A. 95(13): 7731–7736.

Kim SJ, Kim MY, Lee EJ, Ahn YS, Baik JH (2004). Distinct regulation of internalization and mitogen-activated protein kinase activation by two isoforms of the dopamine D2 receptor. *Mol Endocrinol.* **18**(3):640-52.

Klein Herenbrink C, Sykes DA, Donthamsetti P, Canals M, Coudrat T, Shonberg J, Scammells PJ, Capuano B, Sexton PM, Charlton SJ, Javitch JA, Christopoulos A, Lane JR (2016). The role of kinetic context in apparent biased agonism at GPCRs. *Nat Commun*. **7**: 10842.

Knable MB, Heinz A, Raedler T, Weinberger DR (1997). Extrapyramidal side effects with risperidone and haloperidol at comparable D2 receptor occupancy levels. *Psychiatry Res.* **75**(2):91-101.

Krause M, Zhu Y, Huhn M, Schneider-Thoma J, Bighelli I, Nikolakopoulou A, Leucht S (2018). Antipsychotic drugs for patients with schizophrenia and predominant or prominent negative symptoms: a systematic review and meta-analysis. *Eur Arch Psychiatry Clin Neurosci.* **268(**7):625-639.

Kroeze WK, Hufeisen SJ, Popadak BA, Renock SM, Steinberg S, Ernsberger P, Jayathilake K, Meltzer HY, Roth BL (2003). H1-histamine receptor affinity predicts short-term weight gain for typical and atypical antipsychotic drugs. *Neuropsychopharmacology.* **28**(3):519-26.

Kubale V, Blagotinšek K, Nøhr J, Eidne KA, Vrecl M (2016). The Conserved Arginine Cluster in the Insert of the Third Cytoplasmic Loop of the Long Form of the D2 Dopamine Receptor (D2L-R) Acts as an Intracellular Retention Signal. Int J Mol Sci. 17(7): 1152.

Küfferle B, Brücke T, Topitz-Schratzberger A, Tauscher J, Gössler R, Vesely C, Asenbaum S, Podreka I, Kasper S (1996). Striatal dopamine-2 receptor occupancy in psychotic patients treated with risperidone. *Psychiatry Res.* **68**(1):23-30.

Kusumi I, Boku S, Takahashi Y (2015). Psychopharmacology of atypical antipsychotic drugs: From the receptor binding profile to neuroprotection and neurogenesis. *Psychiatry Clin Neurosci.* **69**(5):243-58.

Kuroki T, Meltzer HY, Ichikawa J (1999). Effects of antipsychotic drugs on extracellular dopamine levels in rat medial prefrontal cortex and nucleus accumbens. *J Pharmacol Exp Ther.* **288**(2):774-781.

Lai H, Carino MA, Houta H (1980) Antiserotonin properties of neuroleptic drugs. In: Yamamura HY, Olsen RW (eds) Psychopharmacology and biochemistry of neurotransmitter receptors. Elsevier, New York, pp 347-353.

Langlois X, Megens A, Lavreysen H, Atack J, Cik M, te Riele P, Peeters L, Wouters R, Vermeire J, Hendrickx H, Macdonald G, De Bruyn M (2012). Pharmacology of JNJ-37822681, a specific and fast-dissociating D2 antagonist for the treatment of schizophrenia. *J Pharmacol Exp Ther.* **342**(1):91-105.

Lawley SD, Keener JP (2017). Rebinding in biochemical reactions on membranes. *Phys Biol.* **14**(5):056002.

Lefkowitz RJ, Mullikin D, Caron MG (1976). Regulation of beta-adrenergic receptors by guanyl-5'-yl imidodiphosphate and other purine nucleotides. *J Biol Chem.* **251**(15):4686-92.

Lepiku M, Järv J, Rinken A, Fuxe K (1997a). Mechanism of modulation of [3H]raclopride binding to dopaminergic receptors in rat striatal membranes by sodium ions. *Neurochem Int.* **30**(6):575-81.

Lepiku M, Rinken A, Järv J, Fuxe K (1997b). Modulation of [3H]quinpirole binding to dopaminergic receptors by adenosine A2A receptors. *Neurosci Lett.* **239**(2-3):61-4.

Leucht S, Pitschel-Walz G, Abraham D, Kissling W (1999). Efficacy and extrapyramidal side-effects of the new antipsychotics olanzapine, quetiapine, risperidone, and sertindole compared to conventional antipsychotics and placebo. A meta-analysis of randomized controlled trials. *Schizophr Res.* **35**(1):51-68.

Leucht, S., Corves, C., Arbter, D., Engel, R. R., Li, C. & Davis, J. M (2009). Second-generation versus first-generation antipsychotic drugs for schizophrenia: a meta-analysis. *Lancet* **373,** 31-41.

Leucht, S. *et al* (2013). Comparative efficacy and tolerability of 15 antipsychotic drugs in schizophrenia: a multiple-treatments meta-analysis. *Lancet* **382,** 951-962.

Leysen JE, Niemegeers CJ, Van Nueten JM, Laduron PM (1982). [3H]Ketanserin (R 41 468), a selective 3H-ligand for serotonin2 receptor binding sites. Binding properties, brain distribution, and functional role. *Mol Pharmacol.* **21**(2):301-14.

Leysen JE, Gommeren W (1984). The dissociation rate of unlabelled dopamine antagonists and agonists from the dopamine-D2 receptor, application of an original filter method. *J Recept Res.* **4**(7):817-45.

Leysen JE, Gommeren W, Van Gompel P (1988). The dissociation rate of unlabelled drugs from receptor sites: a poorly investigated, yet important aspect in receptor research. Studies on the serotonin-S2 receptor. *J Recept Res.* **8**(1-4):547-59.

Lin DY, Wei LJ, Ying Z (2002). Model-checking techniques based on cumulative residuals. *Biometrics.* **58**(1):1-12.

Liu LX, Monsma FJ Jr, Sibley DR, Chiodo LA (1996). D2L, D2S, and D3 dopamine receptors stably transfected into NG108-15 cells couple to a voltage-dependent potassium current via distinct G protein mechanisms. *Synapse*. 24(2):156-64.

Longhurst J (1997). Limbic selectivity of clozapine. *Lancet.* **350**(9088):1399-400.

López-Muñoz F, Alamo C, Cuenca E, Shen WW, Clervoy P, Rubio G (2005). History of the discovery and clinical introduction of chlorpromazine. *Ann Clin Psychiatry*. **17**(3):113-35.

Lucas G, Spampinato U (2000). Role of striatal serotonin2A and serotonin2C receptor subtypes in the control of in vivo dopamine outflow in the rat striatum. *J Neurochem.* **74**(2):693-701.

Mackin P, Thomas SH (2011). Atypical antipsychotic drugs. *BMJ.* 342:d1126.

MacLeod RM, Fontham EH, Lehmeyer JE (1970). Prolactin and growth hormone production as influenced by catecholamines and agents that affect brain catecholamines. *Neuroendocrinology.* **6**(5):283-94.

Malmberg A, Jackson DM, Eriksson A, Mohell N (1993). Unique binding characteristics of antipsychotic agents interacting with human dopamine D2A, D2B, and D3 receptors. *Mol Pharmacol.* **43**(5):749-54.

Mamo D, Graff A, Mizrahi R, Shammi CM, Romeyer F, Kapur S (2007). Differential effects of aripiprazole on D(2), 5-HT(2), and 5-HT(1A) receptor occupancy in patients with schizophrenia: a triple tracer PET study. *Am J Psychiatry.* **164**(9):1411-7.

Mamo DC, Uchida H, Vitcu I, Barsoum P, Gendron A, Goldstein J, Kapur S (2008). Quetiapine extended-release versus immediate-release formulation: a positron emission tomography study. *J Clin Psychiatry.* **69**(1):81-6.

Mansour A, Meador-Woodruff JH, Bunzow JR, Civelli O, Akil H, Watson SJ (1990). Localization of dopamine D2 receptor mRNA and D1 and D2 receptor binding in the rat brain and pituitary: an in situ hybridization-receptor autoradiographic analysis. *J Neurosci.* **10**(8):2587-600.

Markowitz JS, Brown CS, Moore TR (1999). Atypical antipsychotics. Part I: Pharmacology, pharmacokinetics, and efficacy. *Ann Pharmacother.* **33**(1):73-85. Review.

Martella A, Sijben H, Rufer AC, Grether U, Fingerle J, Ullmer C, Hartung T, IJzerman AP, van der Stelt M, Heitman LH (2017). A Novel Selective Inverse Agonist of the CB2 Receptor as a Radiolabeled Tool Compound for Kinetic Binding Studies. *Mol Pharmacol*. **92**(4):389-400.

Matsui-Sakata A, Ohtani H, Sawada Y (2005). Pharmacokinetic-pharmacodynamic analysis of antipsychotics-induced extrapyramidal symptoms based on receptor occupancy theory incorporating endogenous dopamine release. Drug Metab Pharmacokinet. 20(3):187-99.

May LT, Bridge LJ, Stoddart LA, Briddon SJ, Hill SJ. (2011). Allosteric interactions across native adenosine-A3 receptor homodimers: quantification using single-cell ligand-binding kinetics. FASEB J. **25**(10):3465-76.

McCutcheon RA, Abi-Dargham A, Howes OD (2019). Schizophrenia, Dopamine and the Striatum: From Biology to Symptoms. *Trends Neurosci.* **42**(3):205-220.

McFarland K, Price DL, Bonhaus DW (2011). Pimavanserin, a 5-HT2A inverse agonist, reverses psychosis-like behaviors in a rodent model of Parkinson's disease. *Behav Pharmacol.* **22**(7):681-92.

Meisenzahl EM, Schmitt G, Gründer G, Dresel S, Frodl T, la Fougère C, Scheuerecker J, Schwarz M, Boerner R, Stauss J, Hahn K, Möller HJ (2008). Striatal D2/D3 receptor occupancy, clinical response and side effects with amisulpride: an iodine-123-iodobenzamide SPET study. *Pharmacopsychiatry.* **41**(5):169-75.

Meltzer, H. Y., Matsubara, S. & Lee, J. C (1989). Classification of typical and atypical antipsychotic drugs on the basis of dopamine D-1, D-2 and serotonin2 pKi values. *J Pharmacol Exp Ther* **251,** 238-246.

Meltzer HY (1992). The importance of serotonin-dopamine interactions in the action of clozapine. *Br J Psychiatry Suppl.* (**17**):22-9.

Meltzer HY (1999). The role of serotonin in antipsychotic drug action. *Neuropsychopharmacology.* **21**(2 Suppl):106S-115S. Review.

Meltzer HY, Li Z, Kaneda Y, Ichikawa J (2003). Serotonin receptors: their key role in drugs to treat schizophrenia. *Prog Neuropsychopharmacol Biol Psychiatry*. **27**(7):1159-72.

Meltzer HY, Massey BW (2011). The role of serotonin receptors in the action of atypical antipsychotic drugs. *Curr Opin Pharmacol.* **11**(1):59-67.

Meltzer HY (2012). Clozapine: balancing safety with superior antipsychotic efficacy. *Clin Schizophr Relat Psychoses*. **6**(3):134-44. Review.

Meltzer HY, Elkis H, Vanover K, Weiner DM, van Kammen DP, Peters P, Hacksell U (2012). Pimavanserin, a selective serotonin (5-HT)2A-inverse agonist, enhances the efficacy and safety of risperidone, 2mg/day, but does not enhance efficacy of haloperidol, 2mg/day: comparison with reference dose risperidone, 6mg/day. *Schizophr Res.* **141**(2-3):144-52.

Meltzer H. Y. Update on typical and atypical antipsychotic drugs (2013). *Annu Rev Med* **64,** 393-406.

Middleton RJ, Kellam B (2005). Fluorophore-tagged GPCR ligands. *Curr Opin Chem Biol.* **9**(5):517-25. Review.

Miyamoto S, Miyake N, Jarskog LF, Fleischhacker WW, Lieberman JA (2012). Pharmacological treatment of schizophrenia: a critical review of the pharmacology and clinical effects of current and future therapeutic agents. *Mol Psychiatry.* **17**(12):1206-27.

Montmayeur JP, Guiramand J, Borrelli E (1993). Preferential coupling between dopamine D2 receptors and G-proteins. *Mol Endocrinol.* **7**(2):161-70.

Moore H, West AR, Grace AA (1999). The regulation of forebrain dopamine transmission: relevance to the pathophysiology and psychopathology of schizophrenia. *Biol Psychiatry.* **46**(1):40-55. Review.

Morrissette DA and Stahl SM (2011). Affective symptoms in schizophrenia. *Drug Discovery Today: Therapeutic Strategies.* **8**(1-2): 3-9.

Moss LE, Neppe VM, Drevets WC (1993). Buspirone in the treatment of tardive dyskinesia. *J Clin Psychopharmacol.* **13**(3):204-9.

Motulsky, H. J. & Mahan, L. C (1984). The kinetics of competitive radioligand binding predicted by the law of mass action. *Mol Pharmacol* **25,** 1-9.

Motulsky HJ, Mahan LC, Ansel PA (1985). Radioligand, agonists and membrane receptors on intact cells: data analysis in a bind. *Trends in Pharmacological Sciences* **6**:317-319.

Motulsky H, Neubig R (2002). Analyzing radioligand binding data. *Curr Protoc Neurosci.* Chapter 7:Unit 7.5.

Motulsky HJ, Neubig RR (2010). Analyzing binding data. *Curr Protoc Neurosci.* Chapter 7:Unit 7.5.

Muguruza C, Moreno JL, Umali A, Callado LF, Meana JJ, González-Maeso J (2013). Dysregulated 5-HT(2A) receptor binding in postmortem frontal cortex of schizophrenic subjects. *Eur Neuropsychopharmacol*. **23**(8):852-64.

Muguruza C, Miranda-Azpiazu P, Díez-Alarcia R, Morentin B, González-Maeso J, Callado LF, Meana JJ (2014). Evaluation of 5-HT2A and mGlu2/3 receptors in postmortem prefrontal cortex of subjects with major depressive disorder: effect of antidepressant treatment. *Neuropharmacology*. **86**:311-8.

Natesan S, Reckless GE, Nobrega JN, Fletcher PJ, Kapur S (2006). Dissociation between in vivo occupancy and functional antagonism of dopamine D2 receptors: comparing aripiprazole to other antipsychotics in animal models. *Neuropsychopharmacology.* **31**(9):1854-63.

Natesan S, Reckless GE, Barlow KB, Nobrega JN, Kapur S (2008). Amisulpride the 'atypical' atypical antipsychotic--comparison to haloperidol, risperidone and clozapine. *Schizophr Res.* **105**(1-3):224-35.

Natesan S, Reckless GE, Barlow KB, Nobrega JN, Kapur S (2011). Partial agonists in schizophrenia--why some work and others do not: insights from preclinical animal models. *Int J Neuropsychopharmacol.* **14**(9):1165-78.

Nederpelt I, Georgi V, Schiele F, Nowak-Reppel K, Fernández-Montalván AE, IJzerman AP, Heitman LH (2016). Characterization of 12 GnRH peptide agonists - a kinetic perspective. *Br J Pharmacol.* **173**(1):128-41.

Neve KA, Cox BA, Henningsen RA, Spanoyannis A, Neve RL (1991). Pivotal role for aspartate-80 in the regulation of dopamine D2 receptor affinity for drugs and inhibition of adenylyl cyclase. *Mol Pharmacol*. **39**(6):733-9.

Newman-Tancredi A, Martel JC, Assié MB, Buritova J, Lauressergues E, Cosi C, Heusler P, Bruins Slot L, Colpaert FC, Vacher B, Cussac D (2009). Signal transduction and functional selectivity of F15599, a preferential post-synaptic 5-HT1A receptor agonist. *Br J Pharmacol.* **156**(2):338-53.

Newman-Tancredi A, Kleven MS (2011). Comparative pharmacology of antipsychotics possessing combined dopamine D2 and serotonin 5-HT1A receptor properties. *Psychopharmacology (Berl).* **216**(4):451-73.

Newton CL, Wood MD, Strange PG (2016). Examining the Effects of Sodium Ions on the Binding of Antagonists to Dopamine D2 and D3 Receptors. *PLoS One.***11**(7):e0158808.

Nicholson C. & Rice M.E. (1991) Diffusion of ions and transmitters in the brain cell microenvironment, in Volume Transmission in the Brain (Fuxe K. and Agnati L. F., eds), pp. 279–294. Raven Press, New York.

Nord M, Farde L (2011). Antipsychotic occupancy of dopamine receptors in schizophrenia. *CNS Neurosci Ther.* **17**(2):97-103.

Núñez S, Venhorst J, Kruse CG (2012). Target-drug interactions: first principles and their application to drug discovery. *Drug Discov Today.* **17**(1-2):10-22.

Nusser Z, Cull-Candy S, Farrant M (1997). Differences in synaptic GABA(A) receptor number underlie variation in GABA mini amplitude. *Neuron.* **19**(3):697-709.

Nyberg S, Eriksson B, Oxenstierna G, Halldin C, Farde L (1999). Suggested minimal effective dose of risperidone based on PET-measured D2 and 5-HT2A receptor occupancy in schizophrenic patients. *Am J Psychiatry.* **156**(6):869-75.

Ohno Y, Shimizu S, Tokudome K (2013). Pathophysiological roles of serotonergic system in regulating extrapyramidal motor functions. *Biol Pharm Bull.* **36**(9):1396-400. Review.

Pan AC, Borhani DW, Dror RO, Shaw DE (2013). Molecular determinants of drug-receptor binding kinetics. *Drug Discov Today.* **18**(13-14):667-73.

Park SY, Kang UG (2013). Hypothetical dopamine dynamics in mania and psychosis--its pharmacokinetic implications. *Prog Neuropsychopharmacol Biol Psychiatry.* **43**:89-95.

Parker MA, Kurrasch DM, Nichols DE (2008). The role of lipophilicity in determining binding affinity and functional activity for 5-HT2A receptor ligands. *Bioorg Med Chem.* **16**(8):4661-9.

Patching SG (2014). Surface plasmon resonance spectroscopy for characterisation of membrane protein-ligand interactions and its potential for drug discovery. *Biochim Biophys Acta*. **1838**(1 Pt A):43-55.

Paton WD, Rang HP (1965). The uptake of atropine and related drugs by intestinal smooth muscle of the guinea-pig in relation to acetylcholine receptors. *Proc R Soc Lond B Biol Sci.* **163**:1-44.

Pazos A, Probst A, Palacios JM (1987a). Serotonin receptors in the human brain--IV. Autoradiographic mapping of serotonin-2 receptors. *Neuroscience.* **21**(1):123-39

Pazos A, Probst A, Palacios JM (1987b). Serotonin receptors in the human brain--III. Autoradiographic mapping of serotonin-1 receptors. *Neuroscience.* **21**(1):97-122.

Pehek EA, McFarlane HG, Maguschak K, Price B, Pluto CP (2001). M100,907, a selective 5-HT(2A) antagonist, attenuates dopamine release in the rat medial prefrontal cortex. *Brain Res* **888**: 51-9.

Perez de la Mora M, Hernandez-Mondragon C, Crespo-Ramirez M, Rejon-Orantes J, Borroto-Escuela DO, Fuxe K (2019). Conventional and Novel Pharmacological Approaches to Treat Dopamine-Related Disorders: Focus on Parkinson's Disease and Schizophrenia. Neuroscience. pii: S0306-4522(19)30510-X. doi: 10.1016/j.neuroscience.2019.07.026. [Epub ahead of print] Review

Perkins DO (2002). Predictors of noncompliance in patients with schizophrenia. *J Clin Psychiatry.* **63**(12):1121-8. Review.

Pike VW, Halldin C, McCarron JA, Lundkvist C, Hirani E, Olsson H, Hume SP, Karlsson P, Osman S, Swahn CG, Hall H, Wikström H, Mensonidas M, Poole KG, Farde L (1998). [carbonyl-11C]Desmethyl-WAY-100635 (DWAY) is a potent and selective radioligand for central 5-HT1A receptors in vitro and in vivo. *Eur J Nucl Med.* **25**(4):338-46.

Pilowsky LS, Mulligan RS, Acton PD, Ell PJ, Costa DC, Kerwin RW (1997). Limbic selectivity of clozapine. *Lancet.* **350**(9076):490-1.

Pompeu TE, Monteiro do Monte F, Bosier B, Fraga CA, Barreiro EJ, Menegatti R, Hermans E, Noël F (2015). Partial agonism and fast dissociation of LASSBio-579 at dopamine D2 receptor*. Prog Neuropsychopharmacol Biol Psychiatry.* **62**:1-6.

Pycock CJ, Kerwin RW, Carter CJ (1980). Effect of lesion of cortical dopamine terminals on subcortical dopamine receptors in rats. *Nature.* **286**(5768):74-6.

Radić Z, Kirchhof PD, Quinn DM, McCammon JA, Taylor P (1997). Electrostatic influence on the kinetics of ligand binding to acetylcholinesterase distinctions between active center ligands and fasciculin. *J Biol Chem* **272**:23265–23277.

Ramos I, Aparici M, Letosa M, Puig C, Gavaldà A, Huerta JM, Espinosa S, Vilella D, Miralpeix M (2018). Abediterol (LAS100977), an inhaled long-acting β2-adrenoceptor agonist, has a fast association rate and long residence time at receptor. *Eur J Pharmacol*. **819**:89-97.

Rang HP (1966). The kinetics of action of acetylcholine antagonists in smooth muscle. *Proc R Soc Lond B Biol Sci.* **164**(996):488-510.

Reavill C, Kettle A, Holland V, Riley G, Blackburn TP (1999). Attenuation of haloperidol-induced catalepsy by a 5-HT2C receptor antagonist. *Br J Pharmacol.* **126**(3):572-4.

Pilla Reddy V, Petersson KJ, Suleiman AA, Vermeulen A, Proost JH, Friberg LE (2012). Pharmacokinetic-pharmacodynamic modeling of severity levels of extrapyramidal side effects with markov elements. *CPT Pharmacometrics Syst Pharmacol*. 1:e1.

Reynolds CH, Tounge BA, Bembenek SD (2008). Ligand binding efficiency: trends, physical basis, and implications. *J Med Chem.* **51**(8):2432-8.

Richelson E, Souder T (2000). Binding of antipsychotic drugs to human brain receptors focus on newer generation compounds. *Life Sci.* **68**(1):29-39.

Richtand NM, Welge JA, Logue AD, Keck PE Jr, Strakowski SM, McNamara RK (2007). Dopamine and serotonin receptor binding and antipsychotic efficacy. Neuropsychopharmacology. **32**(8):1715-26.

Riddy DM, Valant C, Rueda P, Charman WN, Sexton PM, Summers RJ, Christopoulos A, Langmead CJ (2015). Label-Free Kinetics: Exploiting Functional Hemi-Equilibrium to Derive Rate Constants for Muscarinic Receptor Antagonists. *Mol Pharmacol.* **588**(4):779-90.

Rosethorne EM, Charlton SJ (2011). Agonist-biased signaling at the histamine H4 receptor: JNJ7777120 recruits β-arrestin without activating G proteins. *Mol Pharmacol.* **79**(4):749-57.

Roth BL, Sheffler D, & Potkin SG. (2003). Atypical antipsychotic drug actions: unitary or multiple mechanisms for “atypicality”? *Clinical Neuroscience Research*, **3**(1-2), 108–117.

Roth BL, Sheffler DJ, Kroeze WK (2004). Magic shotguns versus magic bullets: selectively non-selective drugs for mood disorders and schizophrenia. *Nat Rev Drug Discov.* **3**(4):353-9.

Sahlholm K, Marcellino D, Nilsson J, Ögren SO, Fuxe K, Århem P (2014). Typical and atypical antipsychotics do not differ markedly in their reversibility of antagonism of the dopamine D2 receptor. *Int J Neuropsychopharmacol.* **17**(1):149-55.

Sahlholm K, Zeberg H, Nilsson J, Ögren SO, Fuxe K, Århem P (2016). The fast-off hypothesis revisited: A functional kinetic study of antipsychotic antagonism of the dopamine D2 receptor. *Eur Neuropsychopharmacol.* **26**(3):467-76.

Sanchez C, Amt J, Dragsted N, Hyttel J, Lembol HL, Meier E, et al (1991). Neurochemical and in vivo pharmacological profile of sertindole, a limbic-selective neuroleptic compound. *Drug Dev Res* **22**:239-50.

Sánchez C, Arnt J (2000). In-vivo assessment of 5-HT2A and 5-HT2C antagonistic properties of newer antipsychotics. *Behav Pharmacol.* **11**(3-4):291-8.

Schiele F, Ayaz P, Fernández-Montalván A (2015). A universal homogeneous assay for high-throughput determination of binding kinetics. *Anal Biochem.* **468C**:42-49.

Schmidtke P, Luque FJ, Murray JB, Barril X (2011) Shielded hydrogen bonds as structural determinants of binding kinetics: application in drug design. *J Am Chem Soc* **133**:18903-18910.

Schotte A, Maloteaux JM, Laduron PM (1983). Characterization and regional distribution of serotonin S2-receptors in human brain. *Brain Res.* **276**(2):231-5.

Schotte A, Bonaventure P, Janssen PF, Leysen JE (1995). In vitro receptor binding and in vivo receptor occupancy in rat and guinea pig brain: risperidone compared with antipsychotics hitherto used. *Jpn J Pharmacol.* **69**(4):399-412.

Schotte A, Janssen PF, Gommeren W, Luyten WH, Van Gompel P, Lesage AS, De Loore K, Leysen JE (1996). Risperidone compared with new and reference antipsychotic drugs: in vitro and in vivo receptor binding. *Psychopharmacology (Berl*). **124**(1-2):57-73.

Seamans JK, Yang CR (2004). The principal features and mechanisms of dopamine modulation in the prefrontal cortex. *Prog Neurobiol.* **74**(1):1-58.

Seeman P, Lee T (1975). Antipsychotic drugs: direct correlation between clinical potency and presynaptic action on dopamine neurons. *Science.* **188**(4194):1217-9.

Seeman P, Lee T, Chau-Wong M, Wong K (1976). Antipsychotic drug doses and neuroleptic/dopamine receptors. *Nature.;***261**(5562):717-9.

Seeman P (1995). Therapeutic receptor-blocking concentrations of neuroleptics. *Int Clin Psychopharmacol.* **10** Suppl 3:5-13. Review.

Seeman P, Corbett R, Nam D, Van Tol HH (1996). Dopamine and serotonin receptors: amino acid sequences, and clinical role in neuroleptic parkinsonism. *Jpn J Pharmacol.* **71**(3):187-204.

Seeman P, Corbett R, Van Tol HH (1997a). Atypical neuroleptics have low affinity for dopamine D2 receptors or are selective for D4 receptors. *Neuropsychopharmacology.* **16**(2):93-110.

Seeman P, Tallerico T, Corbett R, Van Tol HH, Kamboj RK (1997b). Role of dopamine D2, D4 and serotonin(2A) receptors in antipsychotic and anticataleptic action. *J Psychopharmacol.* **11**(1):15-7.

Seeman P, Tallerico T (1998). Antipsychotic drugs which elicit little or no parkinsonism bind more loosely than dopamine to brain D2 receptors, yet occupy high levels of these receptors. *Mol Psychiatry.* **3**(2):123-34. Review.

Seeman P, Tallerico T (1999). Rapid release of antipsychotic drugs from dopamine D2 receptors: an explanation for low receptor occupancy and early clinical relapse upon withdrawal of clozapine or quetiapine. *Am J Psychiatry*. **156**(6):876-84.

Seeman P (2002). Atypical antipsychotics: mechanism of action. *Can J Psychiatry.* **47**(1):27-38. Review.

Seeman P (2005). An update of fast-off dopamine D2 atypical antipsychotics. *Am J Psychiatry*. **162**(10):1984-5.

Seeman P (2010). Dopamine D2 receptors as treatment targets in schizophrenia. *Clin Schizophr Relat Psychoses.* **4**(1):56-73.

Seeman P (2013). Schizophrenia thalamus imaging: low benzamide binding to dopamine D2 receptors suggests fewer D2Short receptors and fewer presynaptic terminals. *Psychiatry Res.* **214**(3):175-80.

Selvin PR (2002). Principles and biophysical applications of lanthanide-based probes. *Annu Rev Biophys Biomol Struct.* **31**:275-302.

Senogles SE (1994). The D2 dopamine receptor isoforms signal through distinct Gi alpha proteins to inhibit adenylyl cyclase. A study with site-directed mutant Gi alpha proteins. *Biol Chem.* **269**(37):23120-7.

Senogles SE (2000). The D2s dopamine receptor stimulates phospholipase D activity: a novel signaling pathway for dopamine. *Mol Pharmacol.* **58**(2):455-62.

Shepherd CA, Hopkins AL, Navratilova I (2014). Fragment screening by SPR and advanced application to GPCRs. *Prog Biophys Mol Biol.* 116(2-3):113-23.

Shimizu S, Tatara A, Imaki J, Ohno Y (2010). Role of cortical and striatal 5-HT1A receptors in alleviating antipsychotic-induced extrapyramidal disorders. Prog *Neuropsychopharmacol Biol Psychiatry.* **34**(6):877-81.

Shimizu S, Mizuguchi Y, Ohno Y (2013). Improving the treatment of schizophrenia: role of 5-HT receptors in modulating cognitive and extrapyramidal motor functions. *CNS Neurol Disord Drug Targets* **12**(6):861-9. Review.

Slack RJ, Russell LJ, Hall DA, Luttmann MA, Ford AJ, Saunders KA, Hodgson ST, Connor HE, Browning C, Clark KL (2011). Pharmacological characterization of GSK1004723, a novel, long-acting antagonist at histamine H(1) and H(3) receptors. *Br J Pharmacol.* **164**(6):1627-41.

D'Souza RS, Hooten WM. Extrapyramidal Symptoms (EPS) [Updated 2019 Jan 9]. In: StatPearls [Internet]. Treasure Island (FL): StatPearls Publishing; 2019 Jan-. Available from: https://www.ncbi.nlm.nih.gov/books/NBK534115/

Sridharan R, Zuber J, Connelly SM, Mathew E, Dumont ME (2014). Fluorescent approaches for understanding interactions of ligands with G protein coupled receptors. *Biochim Biophys Acta.* **1838**(1 Pt A):15-33.

Stahl SM (2008). Antipsychotics and Mood Stabilizers: Stahl's Essential Psychopharmacology, 3rd Edition. Publisher Cambridge University Press.

Stahl SM (2013). Role of α1 adrenergic antagonism in the mechanism of action of iloperidone: reducing extrapyramidal symptoms. *CNS Spectr.* **18**(6):285-8.

Stawarz RJ, Hill H, Robinson SE, Setler P, Dingell JV, Sulser F (1975). On the significance of the increase in homovanillic acid (HVA) caused by antipsychotic drugs in corpus striatum and limbic forebrain. *Psychopharmacologia*. **43**(2):125-30.

Stoddart LA, Kilpatrick LE, Briddon SJ, Hill SJ (2015). Probing the pharmacology of G protein-coupled receptors with fluorescent ligands. *Neuropharmacology.* **98**:48-57.

Stoddart LA, Kilpatrick LE, Hill SJ (2018). NanoBRET Approaches to Study Ligand Binding to GPCRs and RTKs. *Trends Pharmacol Sci.* **39**(2):136-147.

Stone JM, Bressan RA, Erlandsson K, Ell PJ, Pilowsky LS (2005). Non-uniform blockade of intrastriatal D2/D3 receptors by risperidone and amisulpride. *Psychopharmacology (Berl).* **180**(4):664-9.

Strange PG (2001). Antipsychotic drugs: importance of dopamine receptors for mechanisms of therapeutic actions and side effects. *Pharmacol Rev.* **53(**1):119-33.

Strange PG (2010). Use of the GTPγS ([35S]GTPγS and Eu-GTPγS) binding assay for analysis of ligand potency and efficacy at G protein-coupled receptors. *Br J Pharmacol.* **161**(6):1238-49. Review.

Sullivan SK, Hoare SR, Fleck BA, Zhu YF, Heise CE, Struthers RS, Crowe PD (2006). Kinetics of nonpeptide antagonist binding to the human gonadotropin-releasing hormone receptor: Implications for structure-activity relationships and insurmountable antagonism. *Biochem Pharmacol.* **72**(7):838-49.

Sulpizio A, Fowler PJ, Macko E (1978). Antagonism of fenfluramine-induced hyperthermia: a measure of central serotonin inhibition. *Life Sci.* **22**(16):1439-46.

Sulzer D, Cragg SJ, Rice ME (2016). Striatal dopamine neurotransmission: regulation of release and uptake. *Basal Ganglia.* **6**(3):123-148.

Swinney DC (2004). Biochemical mechanisms of drug action: what does it take for success? *Nat Rev Drug Discov.* **3**(9):801-8.

Swinney DC (2008). Applications of Binding Kinetics to Drug Discovery. *Pharmaceutical Medicine.* **22**(1):23-34.

Sykes DA, Dowling MR, Charlton SJ (2009). Exploring the mechanism of agonist efficacy: a relationship between efficacy and agonist dissociation-rate at the muscarinic M3 receptor. *Mol Pharmacol*. **76**(3):543-51.

Sykes DA, Dowling MR, Charlton SJ (2010). Measuring receptor target coverage: a radioligand competition binding protocol for assessing the association and dissociation rates of unlabeled compounds. *Curr Protoc Pharmacol*. Chapter 9:Unit 9.14.

Sykes DA, Charlton SJ (2012). Slow receptor dissociation is not a key factor in the duration of action of inhaled long-acting β2-adrenoceptor agonists. *Br J Pharmacol*. **165**(8):2672-83.

Sykes DA, Parry C, Reilly J, Wright P, Fairhurst RA, Charlton SJ (2014). Observed drug-receptor association-rates are governed by membrane affinity: the importance of establishing "micro-pharmacokinetic/pharmacodynamic relationships" at the β2-adrenoceptor. *Mol Pharmacol* **85**: 608-617.

Sykes DA, Bradley ME, Riddy DM, Willard E, Reilly J, Miah A, Bauer C, Watson SJ, Sandham DA, Dubois G, Charlton SJ (2016). Fevipiprant (QAW039), a Slowly Dissociating CRTh2 Antagonist with the Potential for Improved Clinical Efficacy. *Mol Pharmacol.* **89**(5):593-605.

Sykes DA, Moore H, Stott L, Holliday N, Javitch JA, Lane JR, Charlton SJ (2017). Extrapyramidal side effects of antipsychotics are linked to their association kinetics at dopamine D2 receptors .*Nat Commun*. **8**(1):763.

Sykes DA, Charlton SJ (2018). Single Step Determination of Unlabeled Compound Kinetics Using a Competition Association Binding Method Employing Time-Resolved FRET. *Methods Mol Biol.* **1824**:177-194.

Sykes DA, Lane JR, Szabo M, Capuano B, Javitch JA, Charlton SJ (2018). Reply to 'Antipsychotics with similar association kinetics at dopamine D2 receptors differ in extrapyramidal side-effects'. Nat Commun. 9(1):3568.

Sykes DA, Stoddart LA, Kilpatrick LE, Hill SJ (2019). Binding kinetics of ligands acting at GPCRs. *Mol Cell Endocrinol.* **485**:9-19.

Tanaka J, Matsuzaki M, Tarusawa E, Momiyama A, Molnar E, Kasai H, Shigemoto R (2005). Number and density of AMPA receptors in single synapses in immature cerebellum. *J Neurosci*. ***25***(4):799-807.

Tandon R, Jibson MD (2002). Extrapyramidal side effects of antipsychotic treatment: scope of problem and impact on outcome. *Ann Clin Psychiatry.* **14**(2):123-9.

Tauscher J, Küfferle B, Asenbaum S, Fischer P, Pezawas L, Barnas C, Tauscher-Wisniewski S, Brücke T, Kasper S (1999). In vivo 123I IBZM SPECT imaging of striatal dopamine-2 receptor occupancy in schizophrenic patients treated with olanzapine in comparison to clozapine and haloperidol. *Psychopharmacology (Berl).* **141**(2):175-81.

Tauscher J, Kapur S (2001). Choosing the right dose of antipsychotics in schizophrenia: lessons from neuroimaging studies. *CNS Drugs.* **15**(9):671-8. Review.

Tauscher J, Jones C, Remington G, Zipursky RB, Kapur S (2002a). Significant dissociation of brain and plasma kinetics with antipsychotics. *Mol Psychiatry.* **7**(3):317-21.

Tauscher J, Küfferle B, Asenbaum S, Tauscher-Wisniewski S, Kasper S (2002b). Striatal dopamine-2 receptor occupancy as measured with [123I]iodobenzamide and SPECT predicted the occurrence of EPS in patients treated with atypical antipsychotics and haloperidol. *Psychopharmacology (Berl).* **162**(1):42-9.

Tauscher-Wisniewski S, Kapur S, Tauscher J, Jones C, Daskalakis ZJ, Papatheodorou G, Epstein I, Christensen BK, Zipursky RB (2002). Quetiapine: an effective antipsychotic in first-episode schizophrenia despite only transiently high dopamine-2 receptor blockade. *J Clin Psychiatry*. **63**(11):992-7.

Tautermann CS, Kiechle T, Seeliger D, Diehl S, Wex E, Banholzer R, Gantner F, Pieper MP, Casarosa P (2013). Molecular basis for the long duration of action and

kinetic selectivity of tiotropium for the muscarinic M3 receptor. *J Med Chem.* **56**(21):8746-8756.

Traut TW (1994). Physiological concentrations of purines and pyrimidines. *Mol Cell Biochem*. **140**(1):1-22. Review.

Travis MJ, Busatto GF, Pilowsky LS, Kerwin RW, Mulligan R, Gacinovic S, Costa DC, Ell PJ, Mertens J, Terriere D. Serotonin: 5-HT2A receptor occupancy in vivo and response to the new antipsychotics olanzapine and sertindole. *Br J Psychiatry.* **171**:290-1.

Tresadern G, Bartolome JM, Macdonald GJ, Langlois X (2011). Molecular properties affecting fast dissociation from the D2 receptor. *Bioorg Med Chem.* **19**(7):2231-41.

Tummino PJ, Copeland RA (2008). Residence time of receptor-ligand complexes and its effect on biological function. *Biochemistry.* **47**(20):5481-92.

Turner RJ, Charlton SJ (2005). Assessing the minimum number of data points required for accurate IC50 determination. *Assay Drug Dev Technol.* **3**(5):525-531.

Tyrer P, Kendall T (2009). The spurious advance of antipsychotic drug therapy. *Lancet.* **373**(9657):4-5.

Urwyler S, Coward D (1987). Binding of 3H-spiperone and 3H-(-)-sulpiride to dopamine D2 receptors in rat striatal membranes: methodological considerations and demonstration of the identical nature of the binding sites for the two ligands. *Naunyn Schmiedebergs Arch Pharmacol*. **335**(2):115-22.

Varrault A, Journot L, Audigier Y, Bockaert J (1992). Transfection of human 5-hydroxytryptamine1A receptors in NIH-3T3 fibroblasts: effects of increasing receptor density on the coupling of 5-hydroxytryptamine1A receptors to adenylyl cyclase. *Mol Pharmacol.* **41**(6):999-1007.

Vauquelin G (2010). Rebinding: or why drugs may act longer in vivo than expected from their in vitro target residence time. *Expert Opin Drug Discov.* **5**(10):927-41.

Vauquelin, G. & Charlton, S. J (2010). Long-lasting target binding and rebinding as mechanisms to prolong in vivo drug action. *Br J Pharmacol* **161,** 488-508.

Vauquelin G, Bostoen S, Vanderheyden P, Seeman P (2012). Clozapine, atypical antipsychotics, and the benefits of fast-off D2 dopamine receptor antagonism. *Naunyn Schmiedebergs Arch Pharmacol.* **385**(4):337-72.

Vauquelin G, Van Liefde I, Swinney DC (2015). Radioligand binding to intact cells as a tool for extended drug screening in a representative physiological context. *Drug Discov Today Technol*. **17**:28-34.

Vauquelin G (2015). On the 'micro'-pharmacodynamic and pharmacokinetic mechanisms that contribute to long-lasting drug action. *Expert Opin Drug Discov.* **10**(10):1085-98.

Vauquelin G (2016). Impact of target binding kinetics on in vivo drug efficacy: koff, kon and rebinding. *Br J Pharmacol.* **173**(15):2319-34.

Vauquelin G (2018). Link between a high k on for drug binding and a fast clinical action: to be or not to be? *Medchemcomm*. **9**(9):1426-1438.

Verheijen I, Tourlousse D, Vanderheyden PM, Backer JP, Vauquelin G (2004). Effect of saponin and filipin on antagonist binding to AT 1 receptors in intact cells. *Biochem Pharmacol.* **67**(8):1601-6.

Vernaleken I, Siessmeier T, Buchholz HG, Härtter S, Hiemke C, Stoeter P, Rösch F, Bartenstein P, Gründer G (2004). High striatal occupancy of D2-like dopamine receptors by amisulpride in the brain of patients with schizophrenia. Int J *Neuropsychopharmacol.* **7**(4):421-30.

Vernall AJ, Hill SJ, Kellam B (2014). The evolving small-molecule fluorescent-conjugate toolbox for Class A GPCRs. *Br J Pharmacol.* **171**(5): 1073–1084.

Wang Y, Xu R, Sasaoka T, Tonegawa S, Kung MP, Sankoorikal EB (2000). Dopamine D2 long receptor-deficient mice display alterations in striatum-dependent functions. *J Neurosci.* **20**(22):8305-14.

Ward RJ, Milligan G (2014). Structural and biophysical characterisation of G protein-coupled receptor ligand binding using resonance energy transfer and fluorescent labelling techniques. *Biochim Biophys Acta.* **1838**(1 Pt A):3-14.

Weiden PJ (2007). EPS profiles: the atypical antipsychotics are not all the same. *J Psychiatr Pract*. **13**(1):13-24. Review.

Wiciński M, Węclewicz MM (2018). Clozapine-induced agranulocytosis/granulocytopenia: mechanisms and monitoring. *Curr Opin Hematol.* **25**(1):22-28.

Wolf MA, Yassa R, Llorca PM (1993). Neuroleptic-induced movement disorders: historical perspectives. *Encephale.* **19**(6):657-61.

Wong DF, Kuwabara H, Brašić JR, Stock T, Maini A, Gean EG, Loebel A (2013). Determination of dopamine D_2 receptor occupancy by lurasidone using positron emission tomography in healthy male subjects. *Psychopharmacology (Berl).* **229**(2):245-52.

Xia L, de Vries H, IJzerman AP, Heitman LH (2016). Scintillation proximity assay (SPA) as a new approach to determine a ligand's kinetic profile. A case in point for the adenosine A1 receptor. *Purinergic Signal.* **12**(1):115-26.

Xiberas X, Martinot JL, Mallet L, Artiges E, Loc'H C, Mazière B, Paillère-Martinot ML (2001). Extrastriatal and striatal D(2) dopamine receptor blockade with haloperidol or new antipsychotic drugs in patients with schizophrenia. *Br J Psychiatry.* **179**:503-8.

Yap BK, Buckle MJ, Doughty SW (2012). Homology modeling of the human 5-HT1A, 5-HT 2A, D1, and D2 receptors: model refinement with molecular dynamics simulations and docking evaluation. *J Mol Model.* **18**(8):3639-55.

Ye N, Song Z, Zhang A (2014). Dual ligands targeting dopamine D2 and serotonin 5-HT1A receptors as new antipsychotical or anti-Parkinsonian agents. *Curr Med Chem.* **21**(4):437-57.

Yokoi F, Gründer G, Biziere K, Stephane M, Dogan AS, Dannals RF, Ravert H, Suri A, Bramer S, Wong DF (2002). Dopamine D2 and D3 receptor occupancy in normal humans treated with the antipsychotic drug aripiprazole (OPC 14597): a study using positron emission tomography and [11C]raclopride. *Neuropsychopharmacology.* **27**(2):248-59.

Yoshida K, Sugita T, Higuchi H, Hishikawa Y (1998). Effect of tandospirone on tardive dyskinesia and parkinsonian symptoms. *Eur Psychiatry.* **13**(8):421-2.

Yu Z, IJzerman AP, Heitman LH (2015). Kv 11.1 (hERG)-induced cardiotoxicity: a molecular insight from a binding kinetics study of prototypical Kv 11.1 (hERG) inhibitors. *Br J Pharmacol.* **172**(3):940-55.

Zivkovic B, Guidotti A, Revuelta A, Costa E (1975). Effect of thioridazine, clozapine and other antipsychotics on the kinetic state of tyrosine hydroxylase and on the turnover rate of dopamine in striatum and nucleus accumbens. *J Pharmacol Exp Ther.* **194**(1):37-46.